

DISSERTAZIONE PRESENTATA PER IL CONSEGUIMENTO DEL TITOLO
DI DOTTORE DI RICERCA IN INGEGNERIA DELLE STRUTTURE

**EXPERIMENTAL TESTING AND
NONLINEAR VISCOELASTIC MODELING
OF FILLED RUBBER**

JACOPO CIAMBELLA

ROMA, MARZO 2010

CICLO XXII

SUPERVISORE

PROF. ACHILLE PAOLONE

IL COORDINATORE DEL DOTTORATO

PROF. GIUSEPPE REGA

Contents

Summary	v
1 Rubber Phenomenology	1
1.1 Material Description	3
1.2 Standard Phenomenology	5
1.2.1 Quasi-static	5
1.2.2 Dynamic	8
1.3 Other Nonlinear Effects	13
1.3.1 Mullins effect	13
1.3.2 Payne effect	14
1.4 Experimental Techniques	16
1.4.1 Testing Procedures	16
1.4.2 Specimen Geometry	17
1.5 Experimental Evidences	21
1.5.1 Specimen Preconditioning	21
1.5.2 Quasi-static	23
1.5.3 Dynamic	28
1.5.4 Payne Effect	31
2 Nonlinear Elasticity	35
2.1 Kinematics	37
2.2 Strain Energy Function	38
2.3 Restrictions on the Strain Energy Function	39
2.4 Compressibility	40
2.5 Incompressibility	42
2.6 Homogeneous deformations	43
2.6.1 Simple Tension	43
2.6.2 Simple Shear	45
3 Nonlinear Viscoelasticity	47
3.1 Nonlinear Theory of Viscoelasticity	49
3.2 State of the Art	50
3.3 Quasi-Linear Viscoelasticity	57
3.3.1 Fung's Model	57
3.3.2 Fosdick and Yu's model	59
3.3.3 Abaqus FEA model	60
3.4 Linear Viscoelasticity	61

3.4.1	Reduction from nonlinear theory	61
3.4.2	Dynamic Moduli	63
3.4.3	Some Remarks on Energy Dissipation	64
3.5	Nonlinear Dynamic Moduli	65
3.5.1	Definitions	68
3.5.2	One-dimensional model	73
4	Model Identification	77
4.1	Position of the Problem	79
4.2	Standard Identification Procedure	79
4.2.1	Instantaneous Response	79
4.2.2	Viscoelastic Kernel	82
4.2.3	Fitting of the Prony Series	84
4.2.4	Identification Results	85
4.3	Joint Identification	90
4.3.1	Constitutive models under consideration	94
4.3.2	Experimental Set-up	95
4.3.3	Identification of Material Parameters	99
4.3.4	Results and Discussion	101
4.3.5	Conclusions and perspectives	108
5	Numerical Applications	111
5.1	Hyperelastic Material Simulation	113
5.2	Implicit vs. Explicit Formulation	113
5.3	Static Analysis	114
5.3.1	Uniaxial Extension	114
5.3.2	Simple Shear	118
5.4	Dynamic Simulations	118
5.4.1	Uniaxial Extension	120
5.4.2	Simple Shear	121
	References	137
	Acknowledgements	139

Summary

Background and Motivations

Owing to its unique physical properties, rubber plays a key role in countless industrial applications. Tires, vibration absorbers and shoe soles are only but a few of the myriad uses of natural and synthetic rubber in an industry which in 2009 had an estimated market value of 2 billion euro.

Despite a peculiar internal structure, the macroscopic behavior of filled-rubber is reminiscent of several biological soft tissues. While rubber is internally constituted by flexible long chain molecules that intertwine with each other, a similar role is played, in soft-tissues, by collagen fiber bundles. As a consequence, both classes of materials are able to sustain large strains and exhibit the characteristics of a viscous fluid and an elastic solid.

In industry, the requirement to model complex geometrical structures made of materials exhibiting a nonlinear constitutive behavior is a compelling reason to use Finite Element Analysis (FEA) software. The predictive capabilities of these numerical tools strongly rely upon the capabilities of the underlying model to describe the material's rheological properties. The possibility of simulating accurately the material behavior over the entire working range avoids the use of excessive number of prototypes, thereby reducing the need for expensive and difficult experimental tests; consequently, development costs can be drastically reduced.

The theory of viscoelasticity is crucial in describing materials, such as filled rubber, which exhibit time dependent stress-strain behavior. In many engineering applications, such as the estimate of the rolling resistance of tires and hysteretic losses in soft biological tissues, the energy dissipation is a primary feature to be predicted (Fig. 1). In addition, in the usual operative range, tires, shock absorbers and other rubber components bear finite dynamic deformations. Therefore, a reliable constitutive equation must be assessed within the theory of nonlinear viscoelasticity.

A review of the literature revealed significantly more well-established studies dealing with hyperelastic constitutive models, than those dealing with finite viscoelasticity.

Over the years, many hyperelastic models able to describe all the relevant aspects of the quasi-static response have been introduced. Furthermore, the American norms (ASTM D412, ASTM D575, ASTM D945, ASTM D6147, ASTM D1456) establish all the experimental techniques to identify the material constitutive parameters. In this context, many authors have recently addressed the problem of finite amplitude wave propagation or focused their interest upon particular boundary value problems.

On the other hand, there is a lack of well-established nonlinear viscoelastic models capable of describing all the relevant effects in the material response. Moreover, a standardization similar to that concerning the static norms is yet to be achieved. The usual methodology provides for small harmonic deformations superimposed on a large static displacement. However, such a prescription does not allow the capture of many of the relevant nonlinear phenomena. In the literature, experimental evidence concerning finite dynamic deformations is rarely reported.

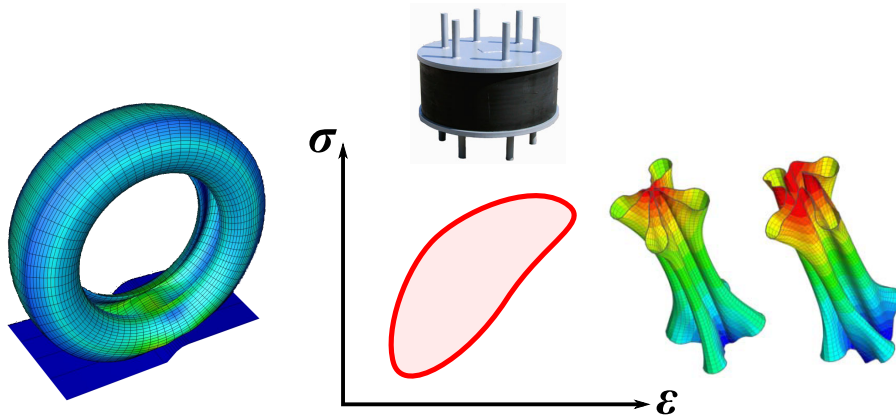


Figure 1 The energy dissipation is a primary feature to be predicted in many engineering applications such as the estimate of the rolling resistance of tires and hysteretic losses in biological tissues and the design of vibration absorbers.

Outline

In this work, the behavior of carbon black-filled rubber is thoroughly analyzed with the intention of developing a constitutive model able to reproduce both static and dynamic material responses. However, due to the similarities between rubber and biological tissues, most of the results presented can be applied in a wider context.

The objectives of this thesis can be summarized as follows:

- to define ad-hoc experimental procedures for the evaluation of viscoelastic constitutive parameters;
- to formulate a constitutive model able to predict hysteresis losses at finite strain and low frequencies;
- to solve the numerical problems related to the identification of viscoelastic constitutive parameters.

Several nonlinear viscoelastic models have been examined thoroughly and for each of them advantages and disadvantages are highlighted.

A series of experiments concerning both static and dynamic tests were performed aimed at measuring all the relevant nonlinear effects. Temperature and strain rate dependencies were investigated and discussed. The standard methodology was applied to perform both tensile and compressive quasi-static tests. Some shortcomings of this procedure, resulting in a unreliable stress-strain constitutive curve around the undeformed configuration, were identified. This led to the design of a non-standard cylindrical specimen able to bear both tensile and compressive loadings. Consequently, the influence of the shape factor was removed and the same boundary conditions, in tension and compression, was applied. This allowed the stiffness around the undeformed configuration to be evaluated in detail.

The quasi-static experimental results also allowed the influence of the Mullins effect on the quasi-static response to be investigated: during the loading cycles, there is a significant reduction in the stress at a given level of strain, which is a consequence of the internal material rearrangement, i.e., the Mullins effect. This damage phenomenon is sometimes reported to induce transverse isotropy in the material, which is usually assumed to be isotropic. The results of the experiments have clarified this issue.

To measure the dynamic properties of the rubber compound, creep, relaxation and cyclic tests at different strain rates were performed. While relaxation and creep experiments incorporate the long-term material response, the stress arising from loading/unloading cycles at different strain-rates involves the shortest characteristic times, thus the highest characteristic frequencies. This methodology allows the accurate reproduction of the actual material operative range. In addition, the incorporation of creep tests into loading/unloading cycles proved to be the most effective methodology to evaluate nonlinear viscoelastic parameters.

Finally, to allow a comparison with the literature results, the usual harmonic testing procedure was also applied.

Thereafter, all the constitutive equations under consideration have been analyzed thoroughly in terms of their capabilities of describing the collated experimental data.

The material coefficients were initially identified by a procedure which relies on the separate identification of the “instantaneous” (elastic) term and of the “dissipative” (inelastic) part. By means of high strain rate loading path, the elastic moduli of the material were identified. Thereafter, relaxation and oscillatory data was used to obtain the characteristic times and the dissipative moduli. It has been proved that, to guarantee the well-conditioning of the resulting least-squares problem, i.e., to avoid relevant numerical error, relaxation tests should be applied for the viscoelastic kernel identification rather than the standard oscillatory tests. However, the results of this procedure were unsatisfactory for some of the models.

To overcome these limitations, a joint identification of the elastic and dissipative terms was introduced. A common choice to deal with the numerical difficulties, related to the transcendental dependence of the constitutive function upon the characteristic times, is to fix them a-priori, e.g., one or two per decades of the experimental time range. This choice, while often used by many authors, led to unsatisfactory results when dealing with filled rubber. As a matter of fact, it does not account for the well-known property of carbon black-filled elastomers of having characteristic times very close to each other. As a consequence, an enhanced iterative scheme, which actually allows a more accurate estimate of the characteristic times clusters, has been introduced. Moreover, this iterative scheme deals with the requirement of keeping the number of constitutive parameters to a minimum in order to avoid non-uniqueness of their determination and to provide a clear physical interpretation for each of them.

The resulting identification problem requires the minimization of a nonlinear functional, which was solved numerically. The penchant of local optimization algorithms to become trapped in local minima on such landscapes required the adoption of a non-local optimization strategy based on a Pattern search algorithm.

Although all the models under consideration were able to reproduce the relaxation or the cyclic test, they failed to extrapolate the material behavior under different kinds of deformation. Furthermore, they encounter difficulties in the prediction of the dynamic response especially at low frequencies and low strain rates. This should be considered an important drawback as the frequencies up to 10-15 Hz are often the most significant in many applications, e.g., rolling tire at 100 km/h or human heart rate.

The extension of the definition of dynamic moduli to the nonlinear case provided new insights into the dynamic response of a broad class of constitutive equations. In view of the novel definition, it has been possible to prove that every nonlinear viscoelastic equation cannot account for the linear frequency dependence of the storage modulus observed at low frequencies. Therefore, a one-dimensional constitutive model, based on hysteretic damping and formulated in the frequency domain, has been proposed. The corresponding time-domain representation of the model required the introduction of the Hilbert transform.

Original Contributions

The main original contributions to the existing literature could be summarized as follows.

- New experimental evidence concerning the deformation of filled rubber at finite strain and finite strain rate.
- New experimental evidence concerning the transverse isotropy induced by the Mullins effect.
- A critical analysis of the literature proposals for nonlinear viscoelastic models.
- A study of the numerical conditioning of the minimization problem resulting from the identification of nonlinear viscoelastic constitutive equations.
- A novel iterative identification technique, which has allowed the characteristic times of the material to be evaluated more accurately.
- An experimental/numerical comparison of the different nonlinear viscoelastic models through the proposed identification technique.
- The extension of the definition of dynamic moduli to the nonlinear case.
- The proof of the incapability of most literature proposals to describe the dynamic moduli at low frequencies.
- A one-dimensional constitutive model based on hysteretic damping able to fit the dynamic behavior of filled rubber at low frequencies.

Further Developments

Having considered all the outlined results, the following points are still under development.

- The extension of the one-dimensional model proposed to the three-dimensional case.
- The introduction of a constitutive equation in the time domain, able to reproduce the low frequency behavior of the dynamic moduli.
- The introduction of transversely isotropic and anisotropic nonlinear viscoelastic constitutive models.
- Experimental procedures to identify the anisotropic viscoelastic models.

Fiber reinforced polymer, collagen fiber bundles, and human ligaments are materials which, nowadays, play a significant role in numerous engineering applications. All of them display strong anisotropic response due to fiber orientation. While the constitutive theory of isotropic materials has reached a certain level of completion, substantial effort must be made to develop viscoelastic models for anisotropic materials at finite strain and to place them within a consistent thermodynamic framework.

Further complications arise from the identification of these anisotropic nonlinear viscoelastic models, since a number of independent quasi-static and dynamic tests are necessary to identify separately the material coefficients. Very often, these experiments are difficult to perform, particularly for *in vivo* soft-tissues. Therefore, the problem of identifying correctly the material parameters is still a challenging engineering task.

Finally, finite element multiscale codes are increasingly used to simulate complex biological tissues and rubber structures. In view of the significant computational effort required by

the simulation of an entire human organ or a vehicle tire, the computational efficiency of these numerical tools must be a primary requirement. Parallel computing techniques should be considered and new parallel algorithms based on GPU computing investigated.

Structure of the Thesis

- **Chapter 1.** The behavior of carbon black filled-rubber in relation to quasi-static and dynamic responses is examined in detail. New insights regarding the material behavior are provided by examining the results from the performed experiments.
- **Chapter 2.** The main aspects of the nonlinear theory of elasticity are discussed.
- **Chapter 3.** The main approaches followed to model nonlinear viscoelastic solids during isothermal deformation are thoroughly described. Some of the most common integral models are reviewed and advantages and disadvantages of each are highlighted. The concept of *dynamic moduli*, introduced in linear viscoelasticity and referred to as *storage* and *loss moduli*, is extended, in a consistent manner, to the nonlinear case. Finally, a one-dimensional model based on hysteretic damping is introduced.
- **Chapter 4.** The standard identification procedure of the material parameters for a nonlinear viscoelastic (NLV) constitutive equation is analyzed in view of the collated experimental results. The main features of this approach are evaluated by considering Fung's constitutive model. Thereafter, a joint identification of the elastic and of the dissipative term is introduced.
- **Chapter 5.** The behavior of isotropic, almost-incompressible, nonlinear elastic and viscoelastic materials is simulated by means of the ABAQUS FEA code. Simple deformations are considered and the numerical results are compared with the analytical solutions. Finally, shortcomings of the ABAQUS finite viscoelasticity model are highlighted and discussed.

Chapter 1

Rubber Phenomenology

Chapter Outline. In this chapter the behavior of carbon black-filled rubber in relation to quasi-static and dynamic responses is examined in detail. In particular, the main features of the micro-structure of the material and their influence on the macro-mechanical response are highlighted. The effects of strain, strain-rate and temperature on the constitutive response are discussed. New insights regarding the material phenomenological behavior are provided by examining the results of the experiments carried out in this work. Mullins and Payne effects, which are peculiar in the behavior of filled elastomers, are reviewed and new results are shown.

1.1 Material Description

Owing to its unique physical properties, rubber plays a keyrole in countless industrial applications. Tires, vibration absorbers and shoe soles are only but a few of the myriad uses of rubber in an industry which in 2009 had an estimated market value of two billion euro.

The term *rubber* is actually misleading: it is used both to indicate the material, technically referred to as *natural rubber*, and the broad class of synthetic elastomers which share with natural rubber some fundamental chemical properties. Indeed, the majority of rubber used for industrial applications are synthetically produced and derived from petroleum ¹.

Rubber, or elastomer, has an internal structure which consists of flexible, long chain molecules that intertwine with each other and continually change contour due to thermal agitation. Elastomers are polymers with long chains (Ferry, 1980). The morphology of an elastomer can be described in terms of convolution, curls and kinks. Convolutions represent the long-range contour of an entire molecular chain, which forms entanglements (knots). Curls are shorter range molecular contours that develop between entanglements and crosslinks, and kinks are molecular bonds within a curl. Each molecular bond has rotational freedom that allows the direction of the chain molecule to change at every bond. Thus the entire molecular chain can twist, spiral and tangle with itself or with adjacent chains. This basic morphology is shared among all the fifty thousand compounds used in the market today and generically referred to by the term rubber. Despite this intricate internal structure, the random orientation of the molecular chains results in a material which is externally isotropic and homogeneous.

Prior of using, the neat elastomer is subjected to physical/chemical treatments to enhance its mechanical properties. One of these treatments consists of the addition, through heating, of sulfur-based curatives which create crosslinks among the macromolecules chains; this process is commonly called *vulcanization* (see, e.g., Callister, 2007).

Figure 1.1 highlights the different behavior of a vulcanized and a non-vulcanized rubber specimen subjected to a tensile loading. Initially, both of the elastomers have a similar intertwined internal structure. When stretched, the macromolecules of the non-vulcanized compound disentangle themselves according to the direction of the applied force. This microstructural change results in a more ordered internal state with a subsequent reduction in entropy. Thereafter, the macro-brownian motions of the macromolecules cause the chains to slide back, one onto each other, to the disordered state. Finally, once the external load is removed (step d in the figure), each macromolecule maintains its state of maximum entropy. Therefore, the initial overall shape is not recovered: all the energy externally supplied to stretch the specimen is dissipated by the viscous friction among the macromolecules.

A different microstructural response occur during the deformation of the vulcanized specimen. Indeed, when subjected to an external traction, the molecular chains dispose parallel to the macro-displacement and, because of the crosslinks introduced

by the vulcanization, they cannot slide back to the initial disordered state. By removing the external loading, the system tends towards the initial state of maximum entropy and the specimen recover the initial length. In this case, the external supplied energy is totally recovered.

The behavior of a real elastomer slightly differs from this simplified description. Indeed, even if the elastomer is vulcanized, the macromolecules can partially slide one onto each other with a dissipation of the mechanical energy.

At the end of the vulcanization process for some specific applications, such as in tires, reinforcing filler, usually carbon black, is added to the compound. This carbon based curative

¹The uncontrolled growth of the petroleum price in 2008 has forced many producers to substitute partially the synthetically produced compounds with natural rubber.

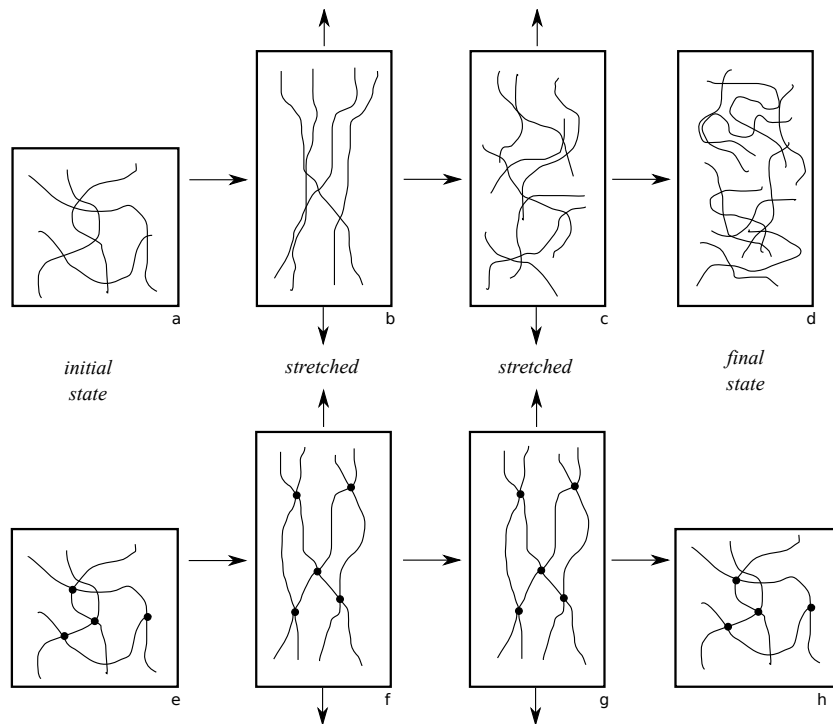


Figure 1.1 Effects of stretching on a non-vulcanized (above) and a vulcanized (below) elastomer.

leads to the material the black color typical of tires.

The tensile strength of rubber increases with increasing filler content up to a certain level. Beyond this level, the tensile strength decreases with higher filler concentrations. [Goldberg *et al.* \(1989\)](#) suggested that this is because high amounts of carbon black fillers cause the carbon black to agglomerate into large clusters and these clusters impart flaws that can easily create cracks and lead to a catastrophic failure. The quantity of filler present in the elastomer is measured in *phr*, parts per hundred by weight of elastomer; the concentration at which maximum tensile strength is obtained, varies with the type of carbon black. For carbon black fillers with smaller particle size, the maximum tensile strength is attained at lower concentrations than those for large particle sized carbon black fillers.

The resulting mechanical characteristics such as strength, tear and abrasion resistance, along with stiffness, considerably increase with respect to the neat elastomer. The addition of filler contributes also to alter greatly the viscous behavior and temperature dependence. For example, unfilled elastomers exhibit a linear viscoelastic behavior for shear strains up to 20% or more, while a carbon black-filled elastomer shows a pronounced nonlinear behavior at shear strains as low as 0.5% ([Chazeau *et al.*, 2000](#)).

In the next section the standard phenomenology of carbon black-filled rubber will be presented and the influence on the constitutive response of temperature and filler concentration will be discussed. Although the focus is on traditional vulcanized rubber, other thermoplastic elastomers show similar mechanical properties even if their chemical composition is quite different. Moreover, from a macroscopic point of view, the behavior of such materials is very close to the behavior of some biological soft tissues, such as ligaments and tendons, for what concerns both their static and dynamic responses.

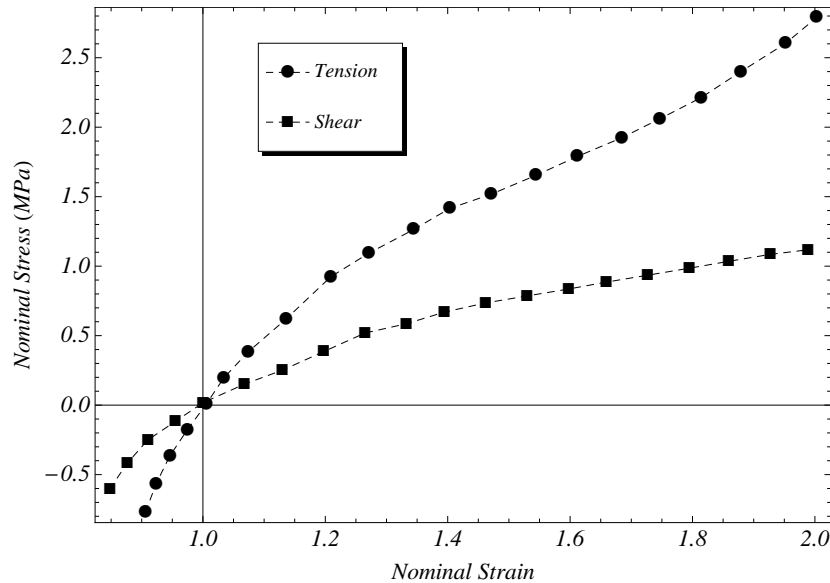


Figure 1.2 Experimental data on carbon black-reinforced styrene butadiene rubber for tensile (circle) and pure shear (square) tests (Drozdov, 2007). The ratio of the tangent stiffness around the undeformed configuration, i.e., nominal strain equal to 1, is approximately equal to 3.

1.2 Standard Phenomenology

1.2.1 Quasi-static

The behavior of carbon black-filled elastomers can be primarily described as *hyperelastic*: under static or quasi-static loading dissipative effects are negligible.

There have been numerous experimental studies addressing the response of rubber under quasi-static loading conditions, including uniaxial tension/compression, shear, equibiaxial tension (Drozdov & Dorfmann, 2003; Laraba-Abbes *et al.*, 2003; Przybylo & Arruda, 1998; Treloar, 2005). In all these experimental conditions, the resulting constitutive curves are strongly nonlinear. However, constitutive nonlinearities coupled with heterogeneous strain field could lead to experimental results which are very difficult to analyze¹. Thus, displacement fields leading to homogeneous deformation should be opted for. A typical example is the equibiaxial (two-dimensional) extension test which is preferred to the equivalent uniaxial compression, because the difficulties related to the bulging of the specimen under compressive loading are avoided (Treloar, 2005).

The typical stress-strain constitutive curves of a carbon black-filled elastomer are shown in Fig. 1.2 (Drozdov, 2007). The material is subjected to uniaxial tension/compression, and pure shear. In the typical working range ($0.8 \leq \lambda \leq 2.0$) the constitutive nonlinearities are evident; indeed, as the breaking point is approached, the material stiffness rapidly increases so that the slope of the experimental curves begins to rise. As a consequence of the intertwining internal structure, during compression, high levels of loading force are suddenly reached, i.e., the material is much stiffer with a non-symmetric behavior between tensile and compressive stresses.

From Fig. 1.2, it is evident that the shear modulus G around the undeformed configuration,

¹In recent years the use of digital image correlation techniques to evaluate heterogeneous strain fields has spread rapidly (see, e.g., Chevalier *et al.*, 2001; Sasso *et al.*, 2008). However, for technical reasons, these techniques are limited to experiments involving very low strain rate.

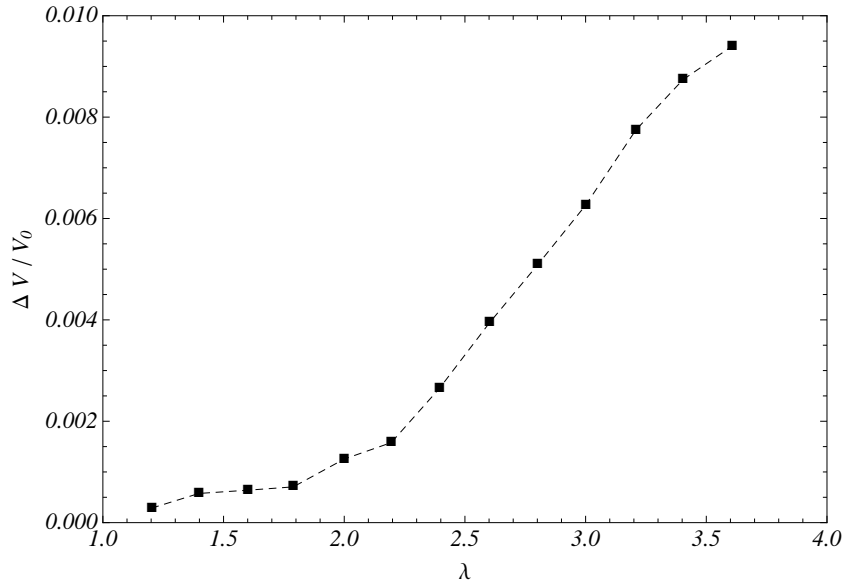


Figure 1.3 Volume dilatation for a rubber specimen undergoing a uniaxial tensile experiment (results provided by Reichert *et al.*, 1987). The volume change remains limited over a wide strain range.

i.e., nominal strain equal to 1, has a lower value compared to the Young modulus E in tensile experiments. The ratio E/G is approximately equal to 3, which corresponds to a Poisson function in the undeformed configuration equal to $\nu = 0.5$, meaning that the material is incompressible.

The incompressibility of carbon black-filled rubber has been confirmed by a number of different researchers over the years (Bischoff *et al.*, 2001; MacKnight, 1966; Ogden, 1976; Penn, 1970; Reichert *et al.*, 1987). Experiments by Reichert *et al.* (1987) in Fig. 1.3 show a limited volume variation ($\Delta V/V_0 \approx 0.01$) at large strain ($\lambda \approx 4$) corroborating the incompressibility constraint introduced in many constitutive equations (see also Mott & Roland, 2010; Mott *et al.*, 2008; Voinovich, 2010).

The effects upon the quasi-static response of an increasing quantity of reinforcing filler have been studied and results have been provided in (Yeoh & Fleming, 1997) for pure shear tests (see Fig. 1.4). The addition of carbon black produces higher value of the initial stiffness (i.e., tangent modulus around the undeformed configuration) with respect to the neat elastomer, while it makes the compound more sensitive to temperature variations. Indeed, the same qualitative behavior has been reported whatever the loading conditions.

The influence of the temperature on the stress-strain curve is shown in Fig. 1.5. At very low temperatures, the polymer will behave like glass and exhibit a high modulus. As the temperature is increased, the polymer will undergo a transition from a hard “glassy” state to a soft “rubbery” state in which the modulus can be several orders of magnitude lower than it was in the glassy state. The transition from glassy to rubbery behavior is continuous and the transition zone is often referred to as the *leathery zone*. The onset temperature of the transition zone, moving from glassy to rubbery, is known as the *glass transition temperature*, or T_g .

The stiffness reduction produced by the temperature is strongly affected by the amount of filler. Results in Fig. 1.6 by Chanliau-Blanot *et al.* (1989) show that a compound with filler content of 45 phr has a percentage variation of the stiffness with the temperature higher than a compound with 0 phr of filler.

The majority of rubber compounds currently used in industry have a glass transition temperature T_g much less than 0 °C. Hence, within the common operative range the material

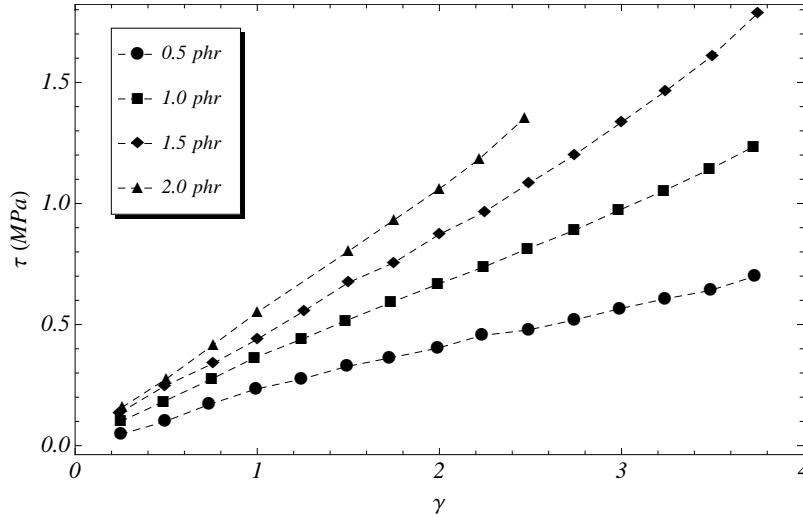


Figure 1.4 Results of shear tests on rubber specimens with an increasing filler concentration (Yeoh & Fleming, 1997). The initial material stiffness shows a monotonic growth for higher value of filler content in the range $\phi \in \{0.5, 1.0, 1.5, 2.0\}$ phr.

behaves as elastic and the effects due to a glassy state are avoided.

1.2.2 Dynamic

The material behavior above-described refers to the quasi-static response. However, elastomers subjected to real world loading conditions possess fluid-like characteristics typical of a viscoelastic material. When loaded by means of a stepwise strain, they *stress-relax*, i.e., the reaction force resulting from the application of an initial peak falls to an asymptotic value, which is theoretically reached after an infinite time (see the experiments by Khan *et al.*, 2006, shown in Fig. 4.8). Moreover, if an external force is suddenly applied, *creep* is observed and the strain begins to change slowly towards a limiting value.

Both these phenomena are caused by the complex geometrical entanglements between chains, which produce a local enhancement of the residual (Van der Waals) force. Under prolonged loading, such “entanglement-cohesion” will slowly breakdown, giving rise to the phenomena of stress-relaxation and creep described above (Treloar, 2005). For shorter times of stressing, these effects are limited and the elastic contribution is predominant.

This behavior provides evidences of the *fading memory* property of the material. Therefore, the entire strain (and temperature) history must affect the constitutive behavior of filled rubber elastomers. While the strain-rate sensitivity and the failure time dependency are recognized and well-documented in the case of other materials such metals, the incorporation of history-dependent properties of elastomers requires further clarification.

A frequently employed characterization of elastomers is achieved through sinusoidal strain histories of frequency ω . This type of material characterization is frequently referred to as *dynamic* meaning that it implicates moving parts, differing from methods leading to quasi-static response. Therefore, in this context, the adjective “dynamic” is not reserved to phenomena involving inertia (e.g., wave propagation) which can be neglected in most of the experimental conditions.

Under the action of dynamic loading, the deformation of rubber, like other viscoelastic solids, occurs with a certain delay owing to viscous friction inside the material. Under harmonic deformation, this delay manifests itself by a phase shift between the applied dis-

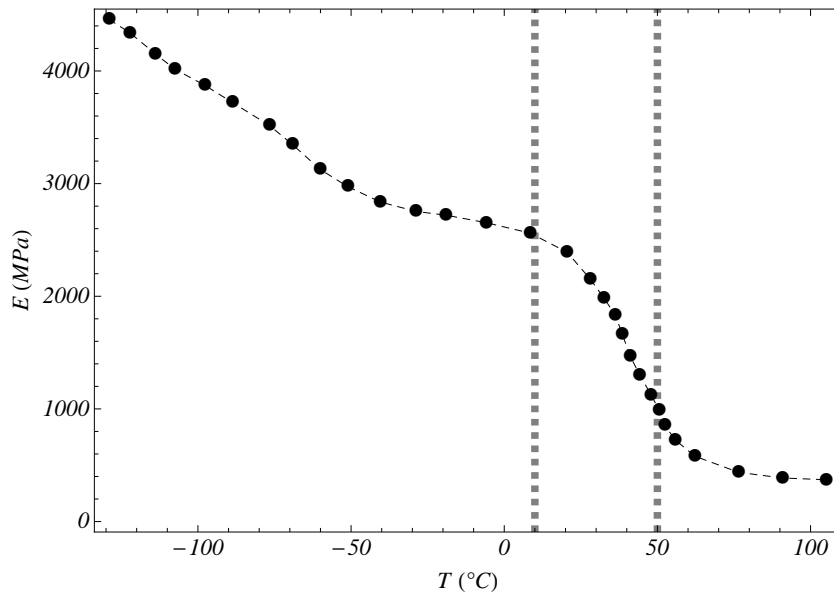


Figure 1.5 Young modulus as function of temperature for polyamide-6. The thick dashed lines indicate the transition *leathery zone* (Shan *et al.*, 2007).

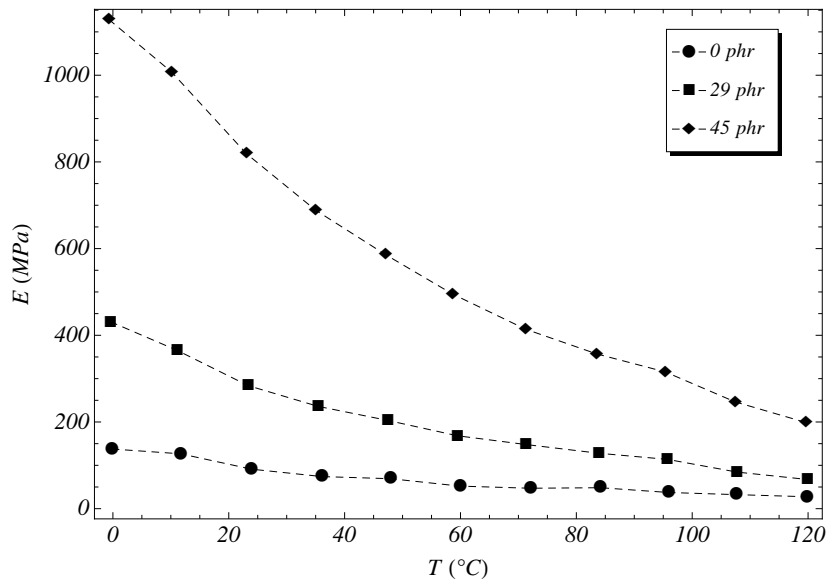


Figure 1.6 Young modulus temperature dependence of a rubber-polyethylene blend for a filler content in the range $\{0, 29, 45\}$ phr (Chanliau-Blanot *et al.*, 1989).

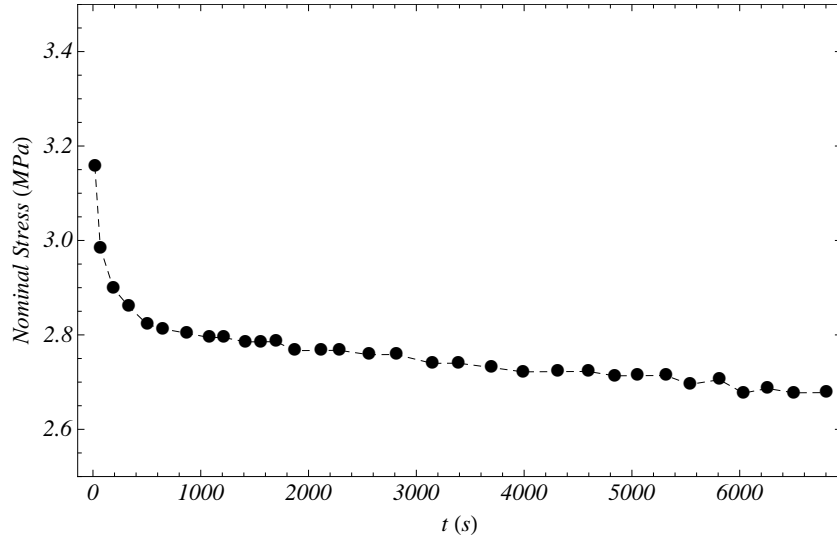


Figure 1.7 Nominal stress as function of time for a relaxation experiment on Adiprene-L100 (Khan *et al.*, 2006).

placement and the load (Boiko *et al.*, 2010). This shift is proportional to the viscous losses.

In order to explain thoroughly elastomers behavior under oscillatory deformation, let

$$u(t) = u_0 + \Delta u \sin(\omega t) \quad (1.1)$$

be the longitudinal displacement in an uniaxial deformation from which the nonlinear Lagrangian strain follows as

$$\epsilon(t) = \epsilon_0 + \Delta \epsilon_1 \sin(\omega t) \quad (1.2)$$

obtained by dividing u by the length l_0 of the undeformed specimen. The imposed strain function (1.2) implies, in the nonlinear case, the time-dependent *nominal stress* response $\sigma(t)$, i.e., force applied to the specimen divided by the initial area, whose steady state response is assumed to have the Fourier series

$$\sigma(t) = \frac{b_0}{2} + \sum_{k=1}^{\infty} [a_k \sin(k\omega t) + b_k \cos(k\omega t)]. \quad (1.3)$$

Here,

$$S(\epsilon_0, \omega, \Delta \epsilon_1) := \frac{1}{\Delta \epsilon_1} a_1(\epsilon_0, \omega, \Delta \epsilon_1), \quad (1.4)$$

$$L(\epsilon_0, \omega, \Delta \epsilon_1) := \frac{1}{\Delta \epsilon_1} b_1(\epsilon_0, \omega, \Delta \epsilon_1) \quad (1.5)$$

are the *storage* and *loss* moduli, also generically referred to as *complex* moduli. In general, neither S nor L depend on $\Delta \epsilon_1$, if $|\Delta \epsilon_1|$ is small (small strain). On the contrary, the aforementioned moduli for carbon black-reinforced rubber show a rather strong dependence on $\Delta \epsilon_1$ in the case $|\Delta \epsilon_1|$ is large. This nonlinear amplitude dependence is called the Payne effect (see Sec. 1.3).

The storage and loss moduli frequency dependence bears no special name, but it is of fundamental importance to understand the dynamic behavior of elastomers.

Figure 1.8 outlines the dynamic moduli as function of the frequency ω for different values of static prestrain ϵ_0 (Lee & Kim, 2001). At lower frequencies ($\omega \rightarrow 0$) the storage modulus tends to a finite nonzero value with a nonzero derivative. As it will be shown in a following chapter,

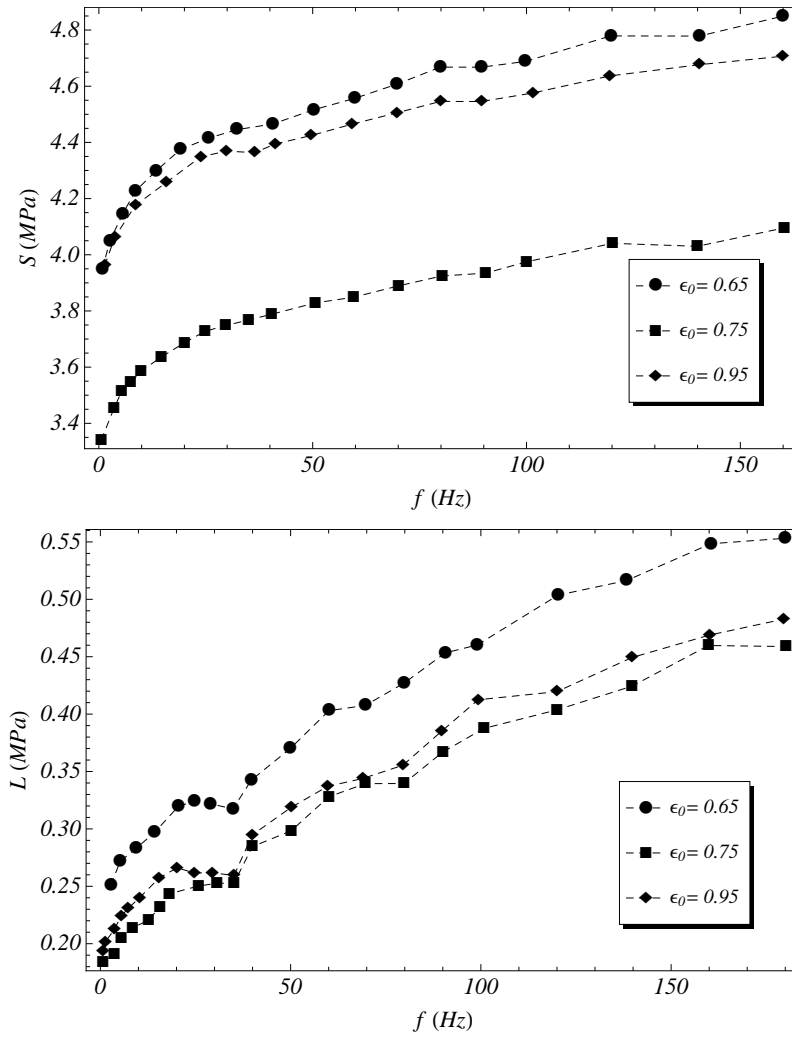


Figure 1.8 Storage S and loss L moduli as functions of the frequency ω in the range $\omega \in [0, 1200]$ Hz for different values of static prestrain $\epsilon_0 \in \{0.65, 0.75, 0.95\}$. The amplitude value was $\Delta\epsilon_1 = 0.63$ for all the experiments (Lee & Kim, 2001).

this behavior cannot be described by (linear or nonlinear) standard viscoelastic constitutive equations. The data collated by Lee & Kim (2001) suggest a non-monotonic dependence of the storage modulus upon the static prestrain ϵ_0 : from $\epsilon_0 = 0.65$ to $\epsilon_0 = 0.75$, the storage modulus S considerably decreases, but it increases again at $\epsilon_0 = 0.95$. A similar, but less accentuated, trend is shown by the loss modulus. Experiments collated in (Gottenberg & Christensen, 1972; Osanaiye, 1996) and more recently in (Luo *et al.*, 2010) are in agreement with Lee & Kim's results.

As in the static case, the dynamic behavior of elastomers also exhibits a very strong temperature dependence. This effect is much more pronounced than in the comparable types of tests conducted upon metals, where the mechanical properties could reasonably be taken as temperature independent within the common working range.

A standard assumption made in the modeling of filled elastomers, which can be corroborated by experimental data, is the so-called thermorheologically simple behavior. Within this context, the basic postulate is that a viscoelastic mechanical property - relaxation function, creep function or complex moduli - at a series of different temperatures, when plotted against the logarithm of time or frequency can be superimposed to form a single curve (Pipkin, 1986;

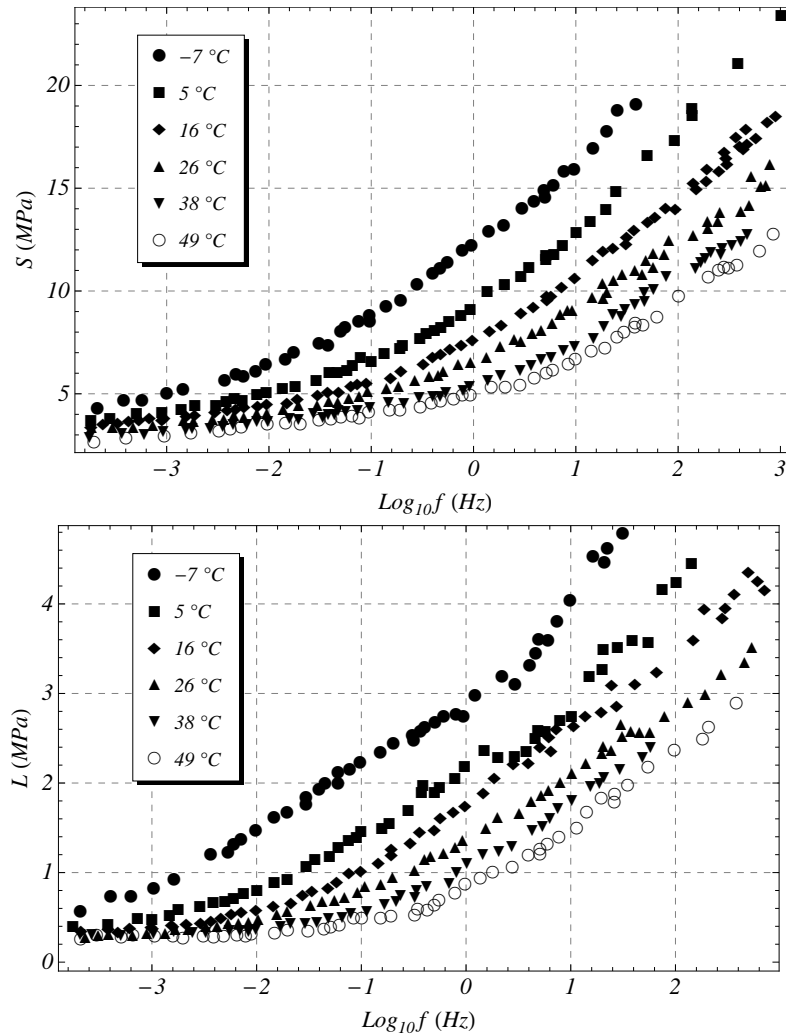


Figure 1.9 Storage S and loss L moduli plotted against logarithmic frequency ($\log_{10} f$) for six different temperatures $T \in \{-7, 5, 16, 26, 38, 49\}$ °C (Gottenberg & Christensen, 1972). The same results are shown in a linear frequency scale in Fig. 1.10.

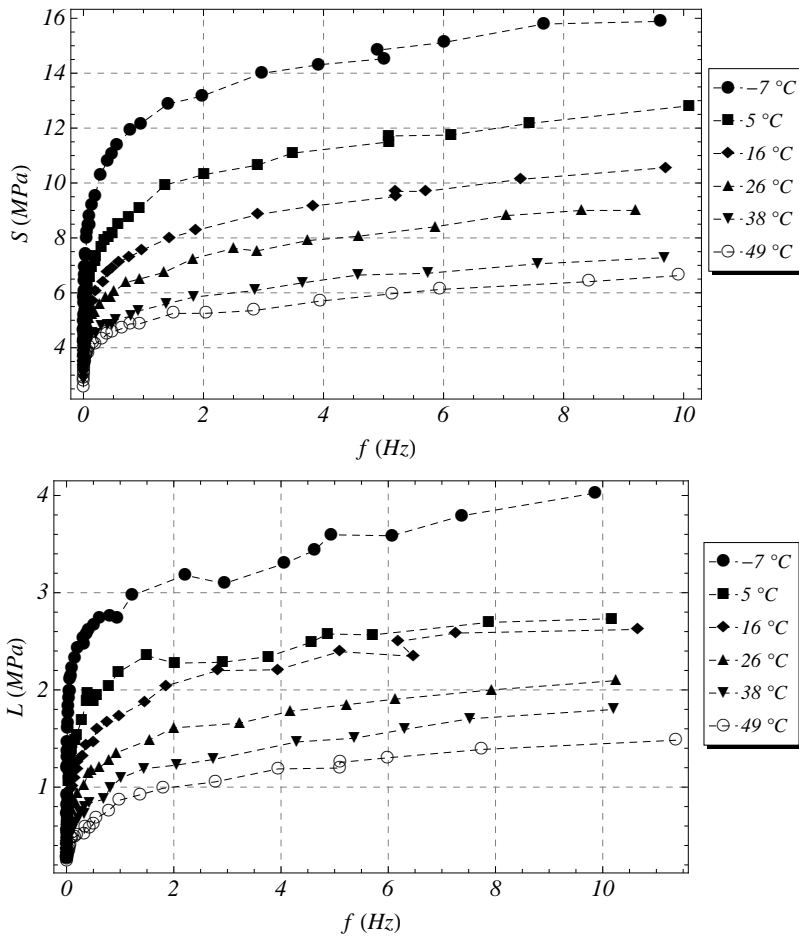


Figure 1.10 Storage S and loss L moduli plotted against frequency in the range $f \in [0, 15]$ Hz for six different temperatures $T \in \{-7, 5, 16, 26, 38, 49\}^\circ\text{C}$ (Gottenberg & Christensen, 1972).

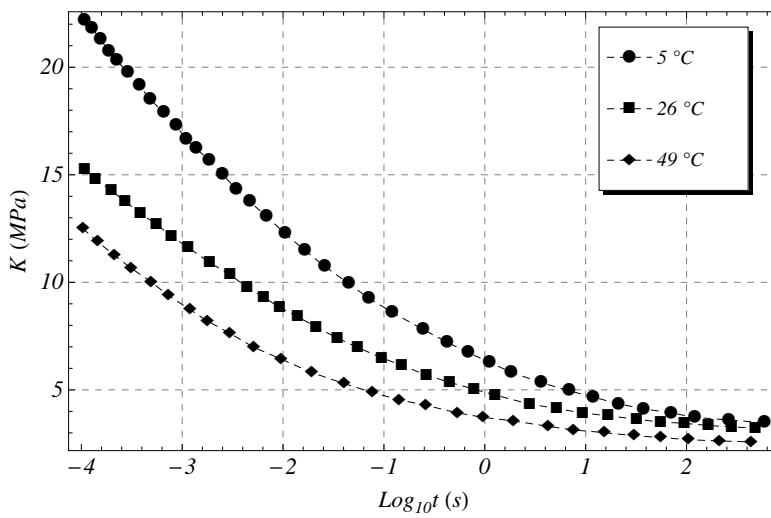


Figure 1.11 Relaxation function plotted against logarithmic time ($\text{log}_{10} t$) for three different temperatures $T \in \{5, 26, 49\}^\circ\text{C}$ (Christensen, 2003).

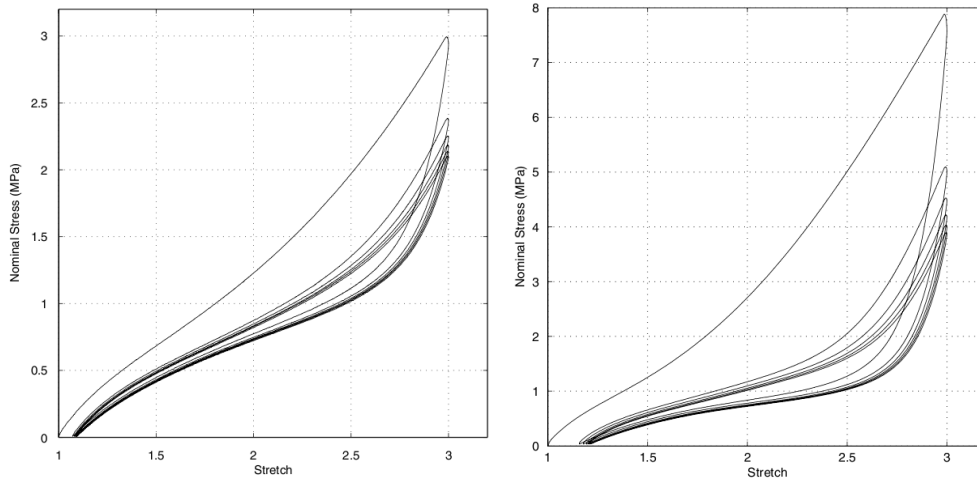


Figure 1.12 Pre-conditioning cycles of a particle-reinforced dumbbell specimen with 20 phr (left) and 60 phr (right) of carbon black with maximum stretch $\lambda := \ell/\ell_0 = 3$ (Dorfmann & Ogden, 2004).

Williams *et al.*, 1955), shifting the various curves at different temperatures along the time or frequency axis. Such a temperature dependence is schematically shown in Fig. 1.9 for the storage S and loss L moduli. Similar temperature dependence is shown for the relaxation function in Fig. 1.11 (Christensen, 2003). Materials obeying this empirical principle are called *thermorehological simple*. Even for thermorehological simple materials such a procedure can be expected to be valid only over a limited time and temperature range, primarily above the glass transition temperature (see, e.g., Singh *et al.*, 2006).

1.3 Other Nonlinear Effects

Apart from the standard phenomenology described in the previous section, carbon black-filled elastomers present some effects peculiar of this class of materials. These effects are the Mullins effect, which concerns the quasi-static behavior, and the Payne effect, dealing with the dynamic response.

1.3.1 Mullins effect

The Mullins effect (Mullins, 1947) is a strain induced softening phenomenon, which is associated mainly with a significant reduction in the stress at a given level of strain during the unloading path as compared with the stress on initial loading in stress-strain cyclic tests (Dorfmann & Ogden, 2003).

In filled rubber this phenomenon is due to the mechanical hysteresis from filler particles debonding from each other or from the polymer chains caused by the stretching. Owing to this, highly reinforced elastomers suffer a more pronounced stiffness reduction than those with low filler content. After the first few loading/unloading cycles the internal microstructure reaches a permanent state and changes in stiffness become no more significant. Figure 1.12 represents typical loading/unloading curves for a rubber specimen subjected to multiple cycles of uniaxial stretching (Dorfmann & Ogden, 2004). Although this anelastic effect is irreversible for a fixed temperature, an increase in the temperature of the specimen could result in a partial recovery of the previously broken bonds and, consequently, on a recovery of the material stiffness.

For the sake of completeness, in the following the main approaches used to describe the Mullins effect will be reviewed (see, e.g. [Ouyang, 2006](#); [Vakada, 2005](#), and references therein).

The first attempt to develop a quantitative theory to account for the softening resulting from rubber stretching was developed by [Blanchard & Parkinson \(1952\)](#). They considered that value of the shear modulus G is a measure of the total number of cross-links within rubber and a reflection of the chemical cross-links produced within vulcanization as well as linkages between rubber and filler. They suggested that the decrease in G was due to the breakdown of linkages between filler and rubber. Their interpretation has provided a useful starting point for the work of other researchers.

One of the other early investigations was done by [Mullins & Tobin \(1957\)](#) who considered the filled rubber as a heterogeneous system comprising hard and soft phases. The hard phase was considered to be inextensible and the soft phase to have the characteristics of gum rubber. During deformation, hard regions are broken down and transformed into soft regions. Then the fraction of the soft region becomes greater with the increasing tension which in turn is responsible for the reduced material stiffness. However, [Mullins & Tobin](#) did not provide a direct physical interpretation for their model.

More recently, new insights into Mullin's effect have been obtained and many researchers proposed their own constitutive model ([Dorfmann & Ogden, 2004](#); [Govindjee & Simo, 1992](#); [Horgan *et al.*, 2004](#); [Ogden & Roxburgh, 1999](#); [Qi & Boyce, 2004](#)).

In [Govindjee & Simo \(1992\)](#) a micromechanically based continuum damage model for carbon-black filled elastomers was introduced. The keypoint of the paper was to incorporate both a damage induced phenomenon such as Mullin's effect and the viscous behavior of a theory of viscoelasticity. Within the framework of damage elasticity, relaxation processes in the material are described via stress-like convected internal variables, governed by dissipative evolution equations (see Chap. 3); they are interpreted as the nonequilibrium interaction stresses between the polymer chains in the network.

[Ogden & Roxburgh \(1999\)](#) proposed to account for the Mullins effect with a phenomenological model based on the theory of incompressible isotropic elasticity amended by the incorporation of a single continuous damage parameter. The dissipation is measured by a damage function which depends only on the damage parameter and on the point of the primary loading path from which unloading begins. A specific form of this function with two adjustable material constants, coupled with standard forms of the (incompressible, isotropic) strain-energy function, was used to illustrate the qualitative features of the Mullins effect in both simple tension and pure shear. However any effects of residual strain were not incorporated.

[Dorfmann & Ogden \(2004\)](#) introduced a constitutive model for the Mullins effect with permanent set in particle-reinforced rubber. The theory of pseudoelasticity has been used for this model, the basis of which is the inclusion of two variables in the energy function in order to capture separately the stress softening and residual strain effects. The dissipation of energy i.e. the difference between the energy input during loading and the energy returned on unloading is also accounted for in the model by the use of a dissipation function, which evolves with deformation history.

A phenomenological model based on the limiting chain extensibility associated with the Gent model of rubber elasticity has been proposed by [Horgan *et al.* \(2004\)](#). The Gent strain energy function ([Gent, 1996](#)) was modified to incorporate stress softening characteristics typical of the Mullins effect. Although the Gent model is phenomenological in nature, a microscopically based interpretation was given to all of its constitutive parameters. In this way, it has been possible to develop a model for the Mullins effect based on the alteration of the polymeric network. Indeed they showed that their approach is a particular case of the more general framework of pseudo-elasticity developed in ([Ogden & Roxburgh, 1999](#)).

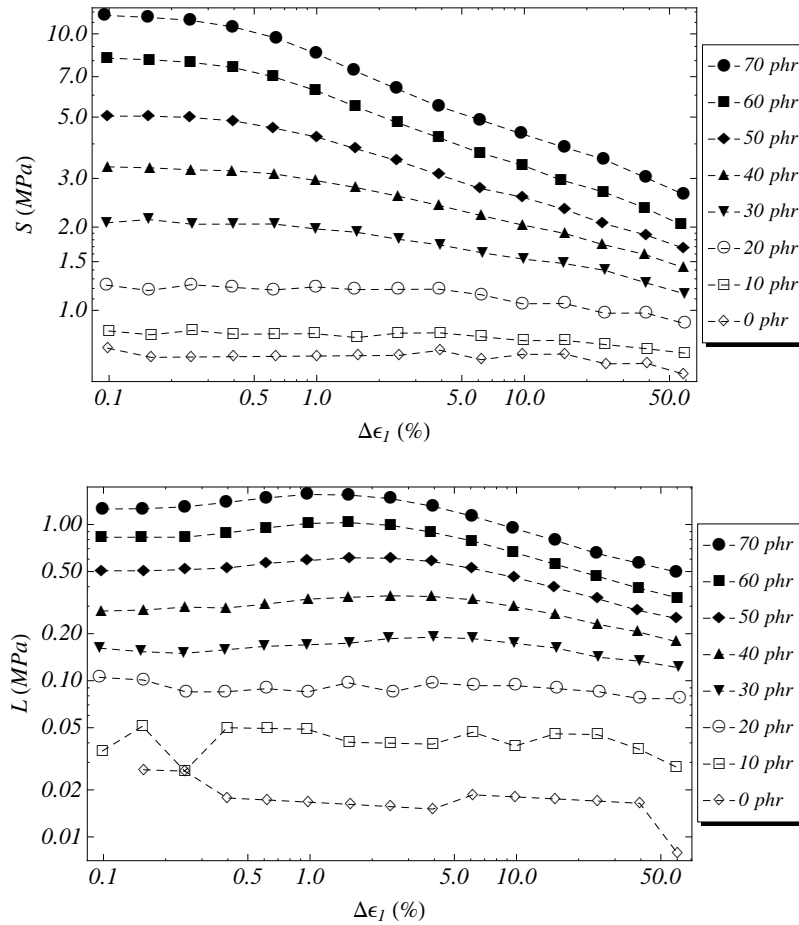


Figure 1.13 Strain dependence of the storage and loss moduli (Payne effect) at 70 °C and 10 Hz for a rubber compound with different concentration of carbon black filler (Wang, 1999). The graphs suggest a monotonic dependence of the dynamic moduli on the filler content in the range $\phi \in [0, 70]$ phr. The Payne effect becomes unnoticeable for low reinforced elastomers ($\phi \in \{0, 10\}$ phr).

1.3.2 Payne effect

Another softening phenomena which manifests the dependence of the stress upon the entire history of deformation is the so-called Payne effect. Like the Mullins effect, this is a softening phenomena but it concerns the behavior of carbon black-filled rubber subjected to oscillatory displacement. Indeed, the dynamic part of the stress response presents a rather strong non-linear amplitude dependence, which is actually the Payne effect (Chazeau *et al.*, 2000; Huber *et al.*, 1996; Payne, 1962).

For a dynamic strain arising from a harmonic displacement (1.1), the storage and loss moduli depends nonlinearly upon the strain amplitude $\Delta\epsilon_1$ as shown in Fig. 1.13 for a strain amplitude in the range $\Delta\epsilon \in [0.1, 0.6]$ and a frequency $f = 2\pi/\omega = 10$ Hz.

There have been several attempts to explain the Payne effect by macroscale mechanism based models. Chazeau *et al.* (2000) classify them as (i) filler-structure models, (ii) matrix filler bonding and debonding models and (iii) phenomenological or nonlinear network models. They also state: “Payne himself suggested qualitatively that the amplitude dependence of the storage and loss moduli were due to a filler network in which the filler contacts depended on the strain amplitude. At lower amplitudes, he argued that the filler contacts are largely intact

and contribute to the high value of the modulus [moduli, the author]. Conversely, at higher amplitudes the filler structure has broken down and does not have time to reform". Therefore, Payne's explanation is of class (ii).

Following the work of Payne, Kraus (1984) proposed an empirical model based on the agglomeration/deagglomeration kinetics of filler aggregates, assuming a Van der Waals type interaction between the particles. In a paper addressing universal properties in the dynamic deformation of filled rubbers, Huber *et al.* (1996) introduced the rheological model of Zener with a nonlinear and linear spring and a dashpot to corroborate the phenomenologically based formula

$$\frac{G' - G'_\infty}{G'_0 - G'_\infty} = \frac{1}{1 + (\Delta\epsilon_1/a_c)^{2m}}, \quad (1.6)$$

where G' is the storage modulus, G'_∞ its value at very large strain and G'_0 the corresponding value at very small strain. Moreover, a_c is a constant and $m \approx 0.6$ is nearly universal, i.e. to a large extent independent of temperature, frequency, filler content and type of carbon. Whilst Huber *et al.* (1996) call (1.6) a theoretical result, it is still based on a rheological model. Chazeau *et al.* (2000) stress this effect in their paper, and so it qualifies no, or no much, better than the phenomenological approach of continuum mechanicians (see Lion & Kardelky, 2004, for references) who postulate nonlinear stress strain behavior. In those approaches the matrix-filler bonding and debonding is formulated considering the dependence upon the entire stress history with the debonding modeled by the appropriate irreversibility properties.

In 1999 Wang (Wang, 1999) investigated the impact of the filler network, both its strength and architecture on the dynamic modulus and hysteresis during dynamic strain. It was found that the filler network can substantially increase the effective volume of the filler due to rubber trapped in the agglomerates, leading to high elastic modulus. During the cyclic strain, while the stable filler network can reduce the hysteresis of the filled rubber, the breakdown and reformation of the filler network would cause an additional energy dissipation resulting in the higher hysteresis. The experiments, shown in Fig. 1.13, were done at strain amplitudes $\Delta\epsilon_1 \in [0.1, 60]$ % with a frequency of 10 Hz under a constant temperature of 70°C. The results show that the dependence of the storage and loss moduli upon $\Delta\epsilon_1$ is strongly influenced by the quantity of carbon black filler used in the compound, vanishing for low reinforced elastomers. Therefore, higher hysteresis at low temperature and low hysteresis at high temperature could be achieved by depressing filler network formation.

Even though the Payne effect has been known for more than 40 years, a model able to describe such a phenomenon in the relevant frequency and amplitude range is still missing ¹.

1.4 Experimental Techniques

1.4.1 Testing Procedures

The constitutive nonlinearities of carbon black-filled elastomers must be treated warily by any experimenter in his exploration of the material properties. Indeed, nonlinearities coupled with non-uniform strain fields could lead to experimental results very difficult to analyze because the strain nonuniformities can easily mask the actual nonlinear behavior of the material (Beatty, 1996). Moreover, the ability of filled rubber to undergo finite strains is a compelling reason to characterize the material through displacement fields for which the relation between stress components and the position vector is known at any point of the body.

¹Recently Höfer & Lion (2009) have proposed a new model which seems able to describe the Payne effect; their constitutive relationship is based on Volterra-type fading memory scalar internal variables, but they need a lot of them to obtain a convincing match of the storage and loss moduli with the experiments.

Among the solutions of the balance equation, every deformation, in equilibrium with zero body force and supported by suitable surface traction alone, is called a *controllable solution*. A *universal solution*, or *universal relation*, is a controllable solution valid for all the materials in a given class (Ericksen, 1954; Pucci & Saccomandi, 1997; Saccomandi, 2001).

Among universal solutions, homogeneous strain are the preferred way to test the behavior of nonlinear homogeneous isotropic materials (Beatty & Hayes, 1992a). Since the strain field is uniform, conducting and measuring displacement and forces are equivalent to control and measure strains and stresses (Haupt, 2002).

In solid mechanics the testing procedures usually rely upon tension/compression, torsion and shear experiments.

Thin specimens with a constant cross-section are the preferred way to test the material behavior under tensile loadings. Indeed, a homogeneous uniaxial state of stress prevails in the central thin shaft. Thick cylinders are commonly employed either for compressive loading or torsion testing. In the first case, barrel deformation of the lateral mantle is avoided by a proper lubrication of the platelets, while torsion test can be interpreted in terms of a universal relation. A torsion test carried out on a cylindrical tube produces a homogeneous shear stress distribution if the wall is thin enough. Shear of a short cylindrical specimen results in a homogeneous strain field, as far as the height-to-diameter ratio remains limited and the bulging of the lateral surface can be ignored.

Non-uniform strain field could also be used (Beatty & Hayes, 1992b). However, two different situations could occur: nonhomogeneities of the deformation field are ignored and the stress field is interpreted as homogeneous (Przybylo & Arruda, 1998), while combined mechanical-optical techniques are used to decouple constitutive nonlinearities and strain inhomogeneities (Chevalier *et al.*, 2001; Sasso *et al.*, 2008). The first solution could lead to an approximation error which could become relevant depending upon the testing conditions. The latter requires hard data processing and its applicability is limited to low strain rate processes.

1.4.2 Specimen Geometry

The material properties inferred from an experiment can be strongly influenced by the specimen geometry. Therefore, a lot of care should be taken to ensure that strain fields within the specimen reflect the ideal homogeneous deformation state. Owing to this, the study of new specimens and clamps is an active research area (Castellucci *et al.*, 2008; Rittel *et al.*, 2002; Zhao *et al.*, 2009).

In Tables 1.1 and 1.2 several specimens commonly employed to characterize the stress-strain properties of filled rubber are reviewed. These include: cylindrical specimen for compression / tension (e.g., Bergström & Boyce, 1998; Lion, 1998), dumbbell (e.g., Drozdov & Dorfmann, 2003; Kar & Bhowmick, 1997; Yoshida *et al.*, 2004), rubber strip (e.g., Przybylo & Arruda, 1998; Ramorino *et al.*, 2003), cylindrical (or rectangular) double shear specimen (e.g., Chazeau *et al.*, 2000; Dorfmann *et al.*, 2002) and compression tension hourglass (e.g., Haupt & Sedlan, 2001). In particular, Tab. 1.1 shows those specimen actually employed for the material characterization carried out in this work, while Tab. 1.2 presents some new literature proposals.

A Dumbbell specimen is represented in Tab. 1.1a. Its typical dog-bone shape is standardized together with molding techniques and dimensions in the ASTM D412 norm (ASTM, 1998, 2003). The proper size of the specimen depends upon the load cell equipped in the testing machine. The enlarged boundaries are intended to increase the contact area between the holders and the material, allowing a wider range of strains to be imposed. Moreover, this particular shape contributes to the prevention of the onset of a fracture near the clamps where

the maximum stress is located. Even if a heterogeneous strain field is present, the deformation could reasonably be assumed as homogeneous in the middle of the shaft. Therefore, while the displacement is exerted controlling the distance between the clamps, the deformation is monitored in the central region. External measurement equipments such as strain-gauges, extensometers or fast cameras are commonly employed.

All these devices can accurately measure displacement fields arising from low strain rate processes. At higher frequencies, however, the additional inertia due to strain gauges and extensometers can overcome the inertia of the specimen resulting in incorrect measurements. Moreover, fast cameras produce a large amount of data, which is difficult to handle and analyze.

Because of these limitations, dumbbell specimens are rarely used for high frequency testing, while thin rubber strips (tension) or thick cylindrical specimens (compression) are preferred¹. In both cases, the deformation is assumed as proportional to the distance between the platelets by neglecting nonhomogeneities of the deformation field.

The length of the rubber strips used in dynamic tests is chosen according to the physical dimensions of the DMA load cell (*Dynamic Mechanical Analyzer*). Based on this, very small specimens are also used (e.g., $L = 2$ mm and $H = 2$ cm), requiring very careful handling of the interfaces between the specimen and the load device. Pressure controlled holders can avoid slipping, but for technical reasons, they are rarely used in testing machines. An alternative solution could be gluing the specimen into the clamps.

Cylindrical shaped specimens are commonly employed for compression experiments. During the test, the displacement is exerted controlling the distance between the platelets. If the plates are accurately lubricated, the bulging of the lateral surface is avoided and the nonhomogeneities of the strain field can be considered negligible. To this end temperature inert silicon or graphite based lubricants are commonly employed.

Dimensions and shapes of cylindrical specimens are standardized in the ASTM D575 norm (ASTM, 2003). Indeed, the diameter-to-height ratio is limited by the occurrence of buckling instabilities. In particular, by considering a hinged-hinged isotropic homogeneous beam subjected to a compressive load, the critical value of the stretch λ_c can be calculated in terms of the beam shape factor (Fig. 1.14). Based on this, a tall cylindrical specimen, with $H = 54$ mm and diameter $D = 18$ mm, was engineered. Our intention was to use a unique specimen for both compressive and tensile loads avoiding any effects due to the different shape factors and clamping conditions. Although the chosen height-to-diameter ratio results in $\lambda_c = 0.7$, to safely avoid any buckling instabilities, the deformation was limited to $\lambda = 0.8$. A knife extensometer was used to monitor the strain in the central shaft, while the edges were glued to the plates for the transmission of the tensile force. An epoxy adhesive, capable of resisting high temperatures, allowed us to reach tensile stresses of the order of 10 MPa.

The results of these tension/compression tests will be discussed in the next section.

1.5 Experimental Evidences

The experiments presented in this section were conducted by the author at the Bridgestone Technical Center Europe s.p.a. in Rome and at Dipartimento di Ingegneria Chimica e Materiali di Sapienza Università di Roma. The material tested was a carbon black-filled rubber. Three different compounds were used: a weakly, a medium and a heavily reinforced compound, which are indicated, respectively, as A, B and C in the following. Further details on

¹At higher frequencies, specimen geometry and clamping conditions become critical and different set-up are used (ASTM, 2003; Lakes, 2004).

Table 1.1 Schematic representation of the rubber specimens used in this work.

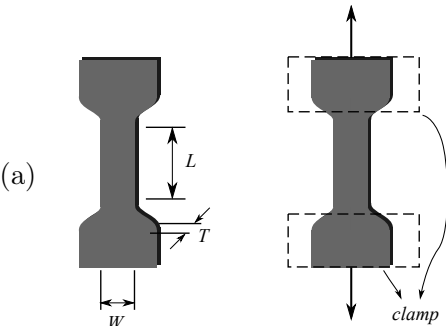
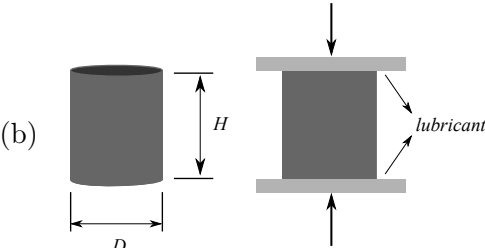
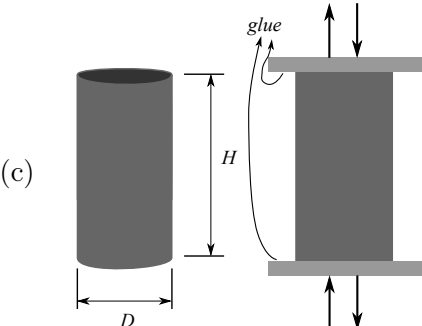
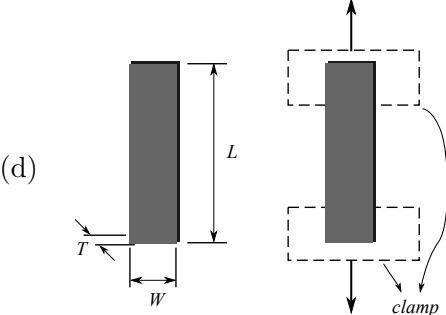
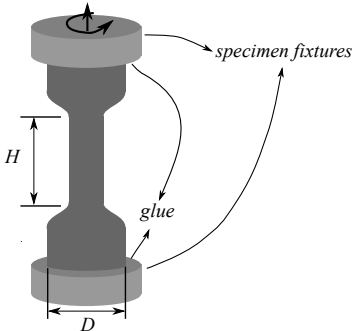
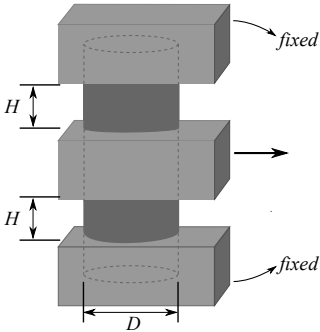
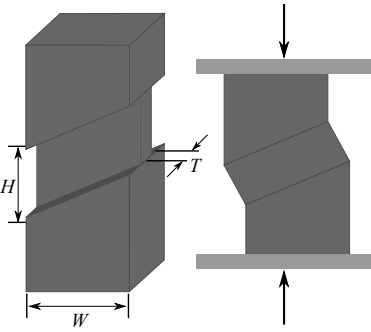
Shape	Remarks
	<p>Test: Tension. Shape, size and molding techniques are standardized in the ASTM D412 norm (ASTM, 2003). Dimensions: $W = 7$ mm, $L = 30$ mm, $T = 2$ mm.</p>
	<p>Test: Compression. Dimensions: $H = 25$ mm, $D = 19$ mm (ASTM D575 norm, ASTM, 2003). Boundary Conditions: platelets lubricated with graphite.</p>
	<p>Test: Tension-Compression. Dimensions: $H = 54$ mm, $D = 19$ mm. Boundary Conditions: specimen glued to the platelets.</p>
	<p>Test: Tension. Dimensions: $L = 50$ mm, $W = 5$ mm. Boundary Conditions: in absence of pressure controlled clamps, the specimen could be glued to the grips to avoid slipping at the interface.</p>

Table 1.2 Schematic representation of specimens used in the literature for elastomers testing.

Shape	Remarks
<p>(a) </p>	<p>Test: Tension - Compression - Torsion. Typical dimensions: $H = 20$ mm, $D = 30$ mm. Boundary Conditions: the specimen is molded directly into the grips (see, e.g., Haupt & Sedlan, 2001).</p>
<p>(b) </p>	<p>Test: (double) Shear. Typical dimensions: $H = 2.5$ mm, $D = 19$ mm. For low strain, the state of deformation can be reasonably interpreted as a pure shear state (see, e.g., Castellucci et al., 2008).</p>
<p>(c) </p>	<p>Test: Shear. Typical dimensions: $H = 2$ mm, $W = 12$ mm, $T = 2$ mm. The specimen can sustain larger strain than the standard double shear specimen. Moreover, this test does not necessitate of any special holders (see, e.g., Zhao et al., 2009).</p>

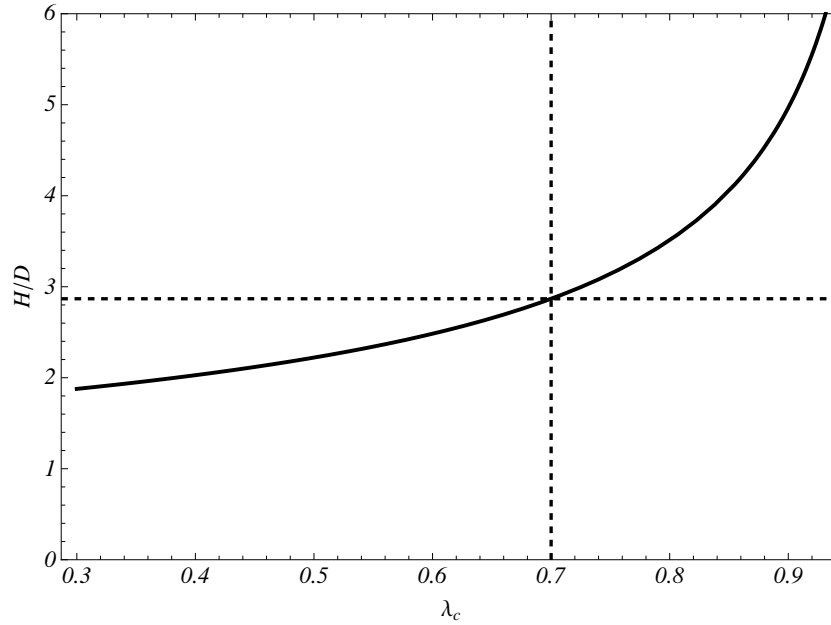


Figure 1.14 Height-to-diameter ratio, H/D , as function of the critical strain λ_c .

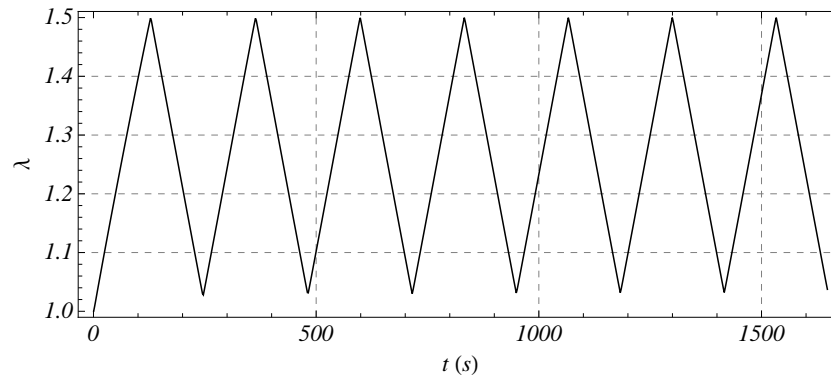


Figure 1.15 Stretch ($\lambda := \ell/\ell_0$) plotted against time for the preconditioning cycles to account for the Mullins effect. The experiment was monitored exerting a displacement with a constant strain rate leading to a constant velocity of the crossing bar of 50 mm/min.

the chemical composition and the specific content and type of carbon black-filler unfortunately can not be given as they are not known to the author.

Both static and dynamic tests were performed. Static tests were conducted with a Zwick/Roell z010 machine with cylindrical and dumbbell specimens; for dynamic tests a GABO Eplexor 500N testing machine for tension and an MTS 825 Elastomer Testing System for compression were used.

1.5.1 Specimen Preconditioning

To eliminate the influence of the Mullins effect, before any experiments, all samples were subjected to a cyclic strain.

For dumbbell specimen, the preconditioning cycles were monitored by exerting a displacement from the undeformed configuration ($\lambda = 1$) up to the strain $\lambda = 1.5$. The loading-unloading path was repeated seven times with a constant strain rate corresponding

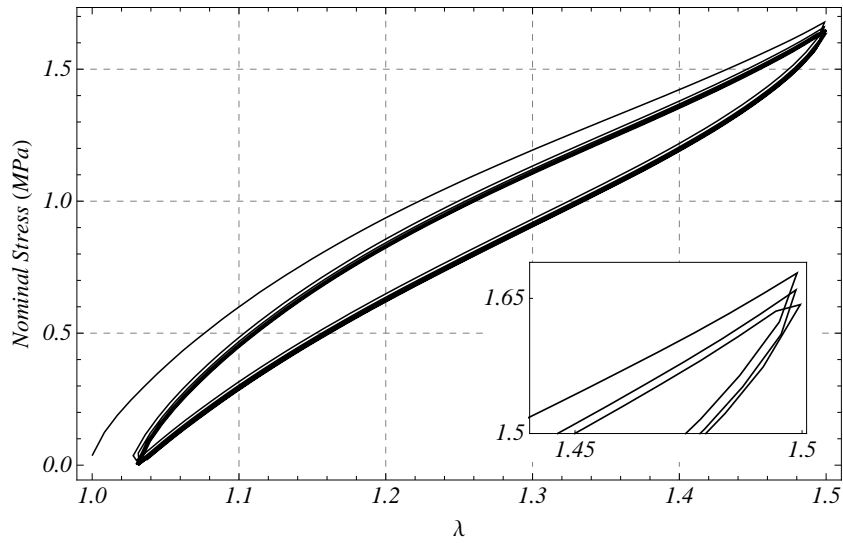


Figure 1.16 Nominal stress plotted against stretch (λ) for the preconditioning cycles performed on a dumbbell specimen. The inset shows the left-drift of the first three cycles of the constitutive curve which is actually a manifestation of the Mullins effect. The sixth and seventh repetitions overlap.

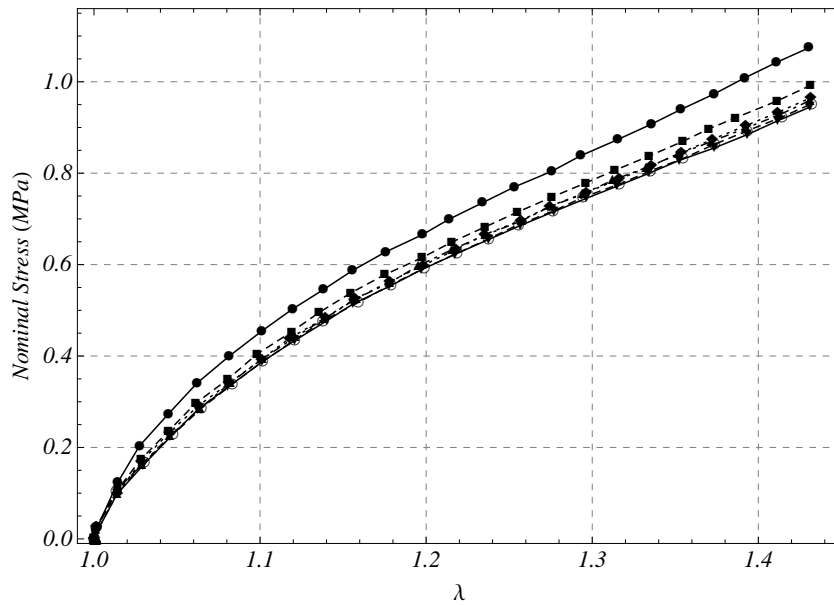


Figure 1.17 Nominal stress plotted against stretch (λ) for the preconditioning cycles performed on a rubber strip (only the loading paths are shown). The stiffness reduction caused by the Mullins effect is evident.

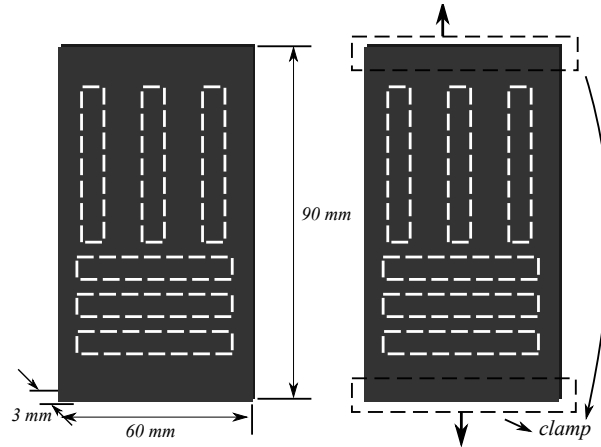


Figure 1.18 Rubber pad used to investigate the transverse isotropy induced by the Mullins effect. 6 different specimens, 3 in the direction of the displacement, 3 in the orthogonal direction, were cut after the preconditioning procedure.

to a velocity of the crossing bar of 50 mm/min (Figs. 1.15 and 1.16). The number of repetitions was established by observing that after seven deformation cycles, the material reached a permanent state and the Mullins effect is no longer significant. This behavior was observed for all the compounds.

The softening phenomenon manifestation of the Mullins effect is due to the change in the microstructure caused by deformation. This internal “damage” could induce a preferred direction resulting in a different material symmetry with respect to the neat elastomer (Dorfmann & Ogden, 2004; Horgan *et al.*, 2004).

In order to provide new insights into this phenomenon, a thin pad of rubber with dimensions $W = 60$ mm, $L = 90$ mm and $T = 3$ mm was subjected to an uniaxial displacement leading to the strain shown in Fig. 1.15. Thereafter, six specimens were cut, three in the direction of the displacement (Specimen V in Fig. 1.18) and three in the orthogonal direction (Specimen H). If the transverse isotropy induced by the Mullins effect were relevant, the two classes of specimens would have different preferred directions, thus different uniaxial behavior.

However, experiments in Fig. 1.19 show that the stress-strain curves of the vertical and horizontal preconditioned specimens are sufficiently close to one another. Moreover, after the first few loading/unloading cycles the differences between the experimental curves become negligible.

In view of these results, the microstructural changes caused by the preconditioning can be ignored and the material can be assumed reasonably as isotropic.

In the following, all the results have been obtained with preconditioned specimens.

1.5.2 Quasi-static

The quasi-static tests were conducted with a Zwick/Roell z010 for both tensile and compressive loads.

A dumbbell specimen (Tab. 1.1a) with size $L = 30$ mm, $W = 7$ mm and $T = 2$ mm, clamped at the upper and lower ends for the transmission of the tensile force was used. The experiment was monitored by exerting a displacement with a static load corresponding to tension up to the stretch $\lambda = 1.5$. The corresponding strain was obtained from the displacement measured in the thin shaft of the specimen, through a contact extensometer equipped with knife edges.

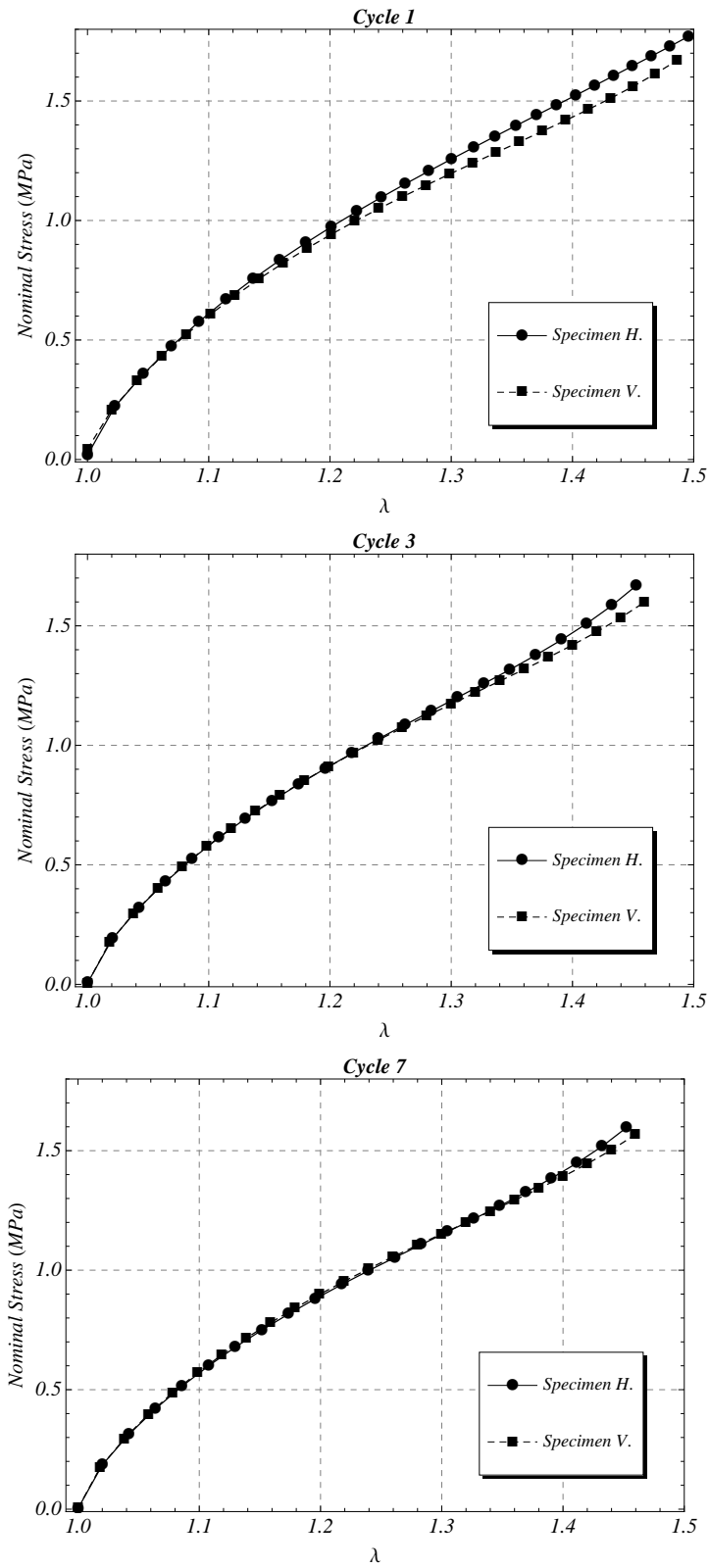


Figure 1.19 Nominal stress plotted against stretch (λ) in the range $\lambda \in [1.0, 1.5]$ for the horizontally H and vertically V prestretched specimens. After few loading-unloading cycles the two curves overlap.

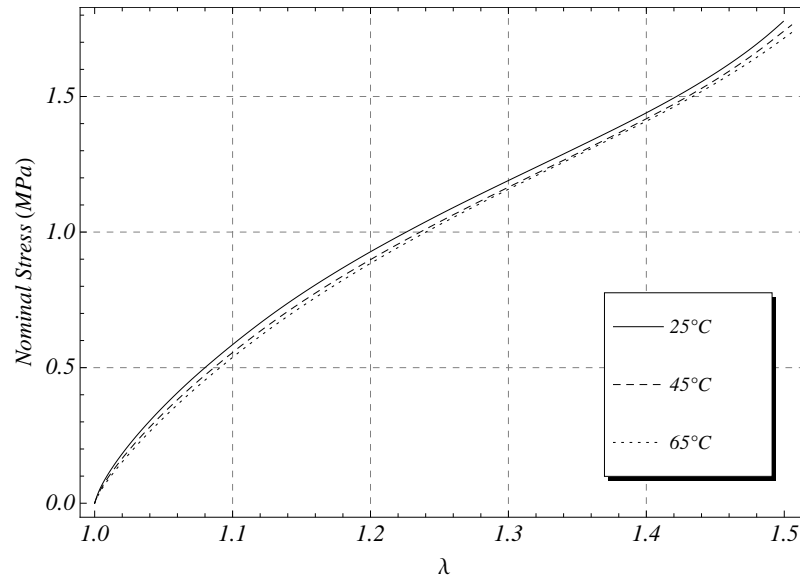


Figure 1.20 Nominal stress plotted against stretch in the range $\lambda \in [1.0, 1.5]$. The experiment was repeated for three different temperatures $T \in \{25, 45, 65\}$ °C. The velocity of the crossbar for the force transmission was 10 mm/min.

For the compression tests, cylindrical specimens with diameter-to-height ratio $D/H = 0.76$ (Tab. 1.1b) were used. The top and bottom surfaces of the cylinder were lubricated with graphite to guarantee uniform lateral displacement over the height and, consequently, avoid bulging of the mantle surface. Central transfer of the load was very accurate so that bending and torsional deformations, if present, were negligible. Both tension and compression tests were repeated for three temperatures in the range $T \in \{25, 45, 65\}$ °C and three velocities of the crossbar $v \in \{10, 30, 50\}$ mm/min. To ensure the homogeneity of the temperature field inside the sample, each specimen was kept at a constant temperature for one hour. Moreover, after this heating process, the preconditioning procedure was repeated to take account of the rebonded physical cross-links, responsible for the Mullins effect, caused by the temperature increase.

The tensile and compressive stress-strain constitutive curves are shown in Figs. 1.20 - 1.23. Strain rate effects on the material stiffness are very limited and the loading curves almost overlap (Figs. 1.22 and 1.23). Moreover, as seen in Figs. 1.20 and 1.21, the changes in the compound stiffness for a temperature range of 25 °C - 65 °C are negligible.

All the results up to this point, have dealt with quasi-static compression and tension tests. They have revealed a very different material response to tensile and compressive loads. In particular, at lower strains, the stress-strain curve shows an inflection point and, consequently, a change of the tangent stiffness around the undeformed configuration (Figs. 1.22 - 1.23 and 1.20 - 1.21). This behavior could be interpreted in terms of the different micromechanical phenomena undergoing compression, e.g., macromolecules entanglement grows, and tension, e.g., macromolecular chains disentangle themselves. However, for very low strain, a much smoother change of the stiffness has been reported (Mott & Roland, 1995, 1996; Roland *et al.*, 1999). Therefore, the reliability of the measurements in the initial region of the constitutive curves can be questioned, e.g., a non accurate transmission of the load may result in an overestimate of the initial stiffness.

To investigate thoroughly this point, a tall cylindrical specimen with sizes and shape reported in Tab. 1.1c was molded. This non-standard specimen was used for both tensile and

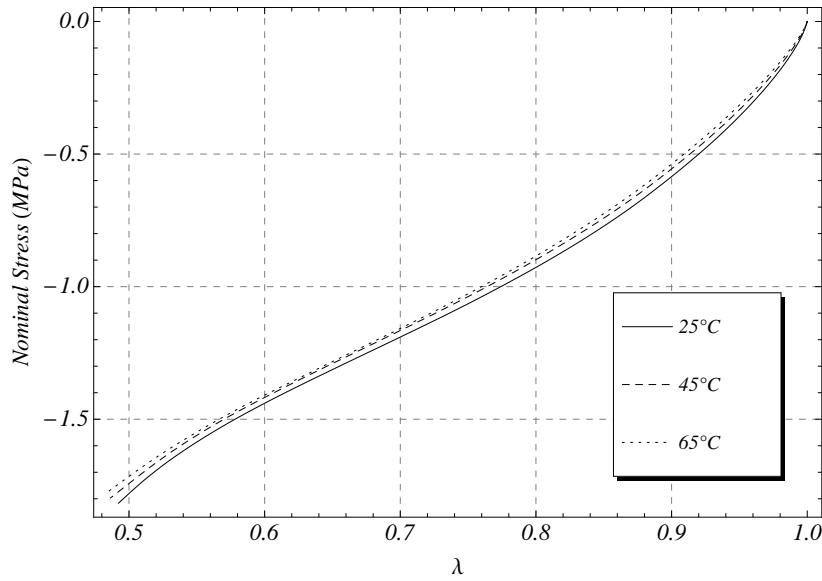


Figure 1.21 Nominal stress plotted against stretch in the range $\lambda \in [0.4, 1.0]$ for a cylindrical specimen. The experiment was repeated for three different temperatures $T \in \{25, 45, 65\}$ °C. The velocity of the crossbar for the force transmission was 10 mm/min.

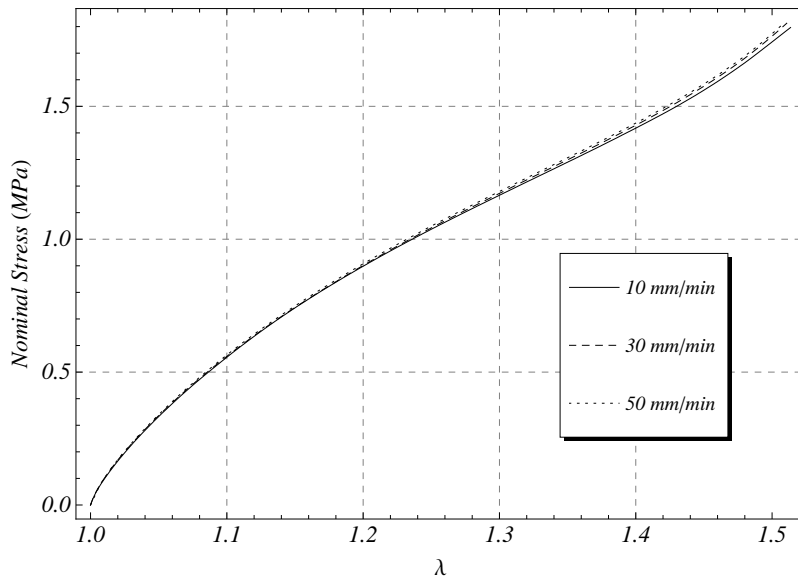


Figure 1.22 Nominal stress plotted against stretch in the range $\lambda \in [1.0, 1.5]$. The experiment was repeated for three velocities of the crossbar $v \in \{10, 30, 50\}$ mm/min. The temperature was held constant at 25 °C.

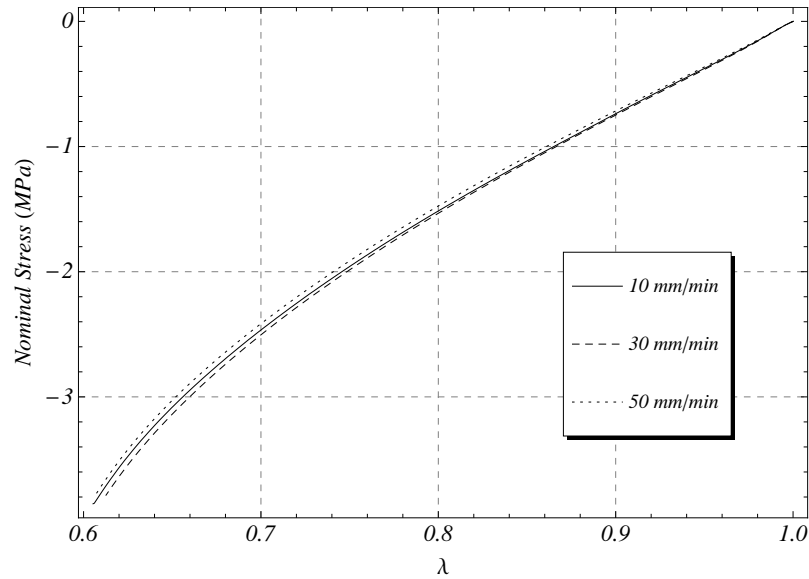


Figure 1.23 Nominal stress plotted against stretch in the range $\lambda \in [0.6, 1.0]$ for cylindrical specimen. The experiment was repeated for three velocities of the crossing bar $v \in \{10, 30, 50\}$ mm/min. The temperature was held constant at 25 °C.

compressive loading, avoiding the influence on the measurements of the clamping conditions and of the shape factor.

The results of these non-standard tests are shown in Fig. 1.24. The change in the tangent stiffness between compression (thick cylinder) and tension (dumbbell) is noticeable, while a much smoother change is observed with the tall cylindrical specimen. Moreover, the material stiffness measured with dumbbell and tall cylindrical specimens is comparable, while it differs considerably from that measured with the thick cylindrical shape. This suggests a low reliability at lower strains of the measurements, in particular during compression, owing to both an inaccurate transfer of the load and an improper lubrication. By using a unique specimen, these experimental difficulties have been overcome and the material behavior in the range $\lambda \in [0.8, 1.2]$, i.e., the actual working range, have been properly described.

1.5.3 Dynamic

The carbon black-filled rubber behavior cannot be inferred by means of static experiments only. Indeed, real world loading conditions imply loading rates which are outside the range of quasi-static tests ($v \leq 10$ mm/min). Dynamic tests for elastomers are usually conducted by statically stretching the specimen to a large value of strain and then making it oscillate with a small amplitude sinusoidal time law (Cho & Youn, 2006; Darvish & Crandall, 2001; Knauss *et al.*, 2008; White *et al.*, 2000). However, this procedure does not allow the triggering of all the nonlinearities of the dynamic response.

In this work, with the intention of reproducing loading conditions in agreement with the actual operative range, oscillatory tests at finite strain, relaxation, creep and cyclic experiments were conducted. While the oscillatory tests require a very precise Dynamic Mechanical Analyzer (DMA) to reach higher frequencies, the other experiments do not require expensive testing machinery. Therefore, apart from the material characterization itself, the intention was to investigate the possibility of inferring dynamic material properties through relaxation and creep rather than loading and unloading cycles at finite strain or standard harmonic tests.

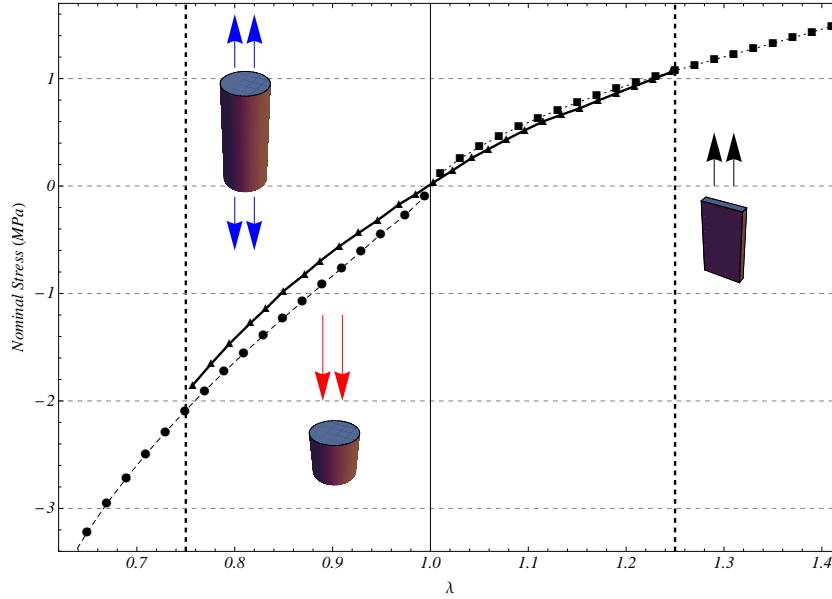


Figure 1.24 Nominal stress as functions of strain in the range $\lambda \in [0.7, 1.4]$ for three different specimen shapes: dumbbell, thick cylinder and tall cylinder. The results show a different value of the tangent stiffness around the undeformed configuration ($\lambda = 1$) in tension with respect to compression, probably caused by the lubrication of the platelets. These differences disappear by using the same specimen for both tensile and compressive loads.

The stress relaxation tests were performed on both cylindrical and dumbbell specimens (Tab. 1.1 a and b).

The cylindrical specimen was compressed, starting from the initial undeformed configuration, $\lambda = 1$, up to the final strain $\lambda = 0.83$ (17 %) in $\Delta t = 0.7$ s with a constant strain rate. Thereafter, the deformation was held fixed for 100 s. In particular, the strain rate of the initial ramp was $\dot{\lambda} \approx 0.24 \text{ s}^{-1}$, corresponding to a velocity of the crossbar for the transmission of the load $v \approx 370 \text{ mm/min}$. The resulting stress relaxation curves are shown in Fig. 1.25 for three temperatures in the range $T \in \{0, 25, 65\} \text{ }^\circ\text{C}$. It can be seen from the graphs that an increase in temperature results in a reduction of the material stiffness and, consequently, in a lower (absolute) value of the maximum force.

Theoretically, the same deformation history with an infinite strain rate, i.e., $\Delta t \rightarrow 0$, would have allowed the direct measurement of the viscoelastic properties. However, this is not possible when dealing with laboratory equipment. Indeed, not accounting for the finite strain rate of the initial ramp would result in an underestimate of the material characteristic times (Antonakakis *et al.*, 2006).

The laboratory environments normally imposes a range for the observable time scales. The highest sampling rate the acquisition channel can reach determines the shortest achievable time; besides the duration of the experiment is an upper bound for time scales. The Zwick/Roell z010 equipment is able to acquire data up to the frequency 10 kHz; 1 kHz was used, whereas the experiments lasts 30 s. This choice was a compromise between the minimum observable time scale and number of data samples recorded.

Relaxation tests permit the capturing of the material behavior involving larger characteristic times. Since in many engineering applications (e.g., tires, shock absorbers, etc.), the shortest intrinsic times are also significant, loading/unloading cycles at high strain rate were performed. As shown in Figs. 1.26 and 1.27, the loading/unloading path was repeated for four different speeds of the rising ramp in the range $\dot{\lambda}_{min} = 0.14 \text{ s}^{-1}$ to $\dot{\lambda}_{max} = 1.09 \text{ s}^{-1}$. All

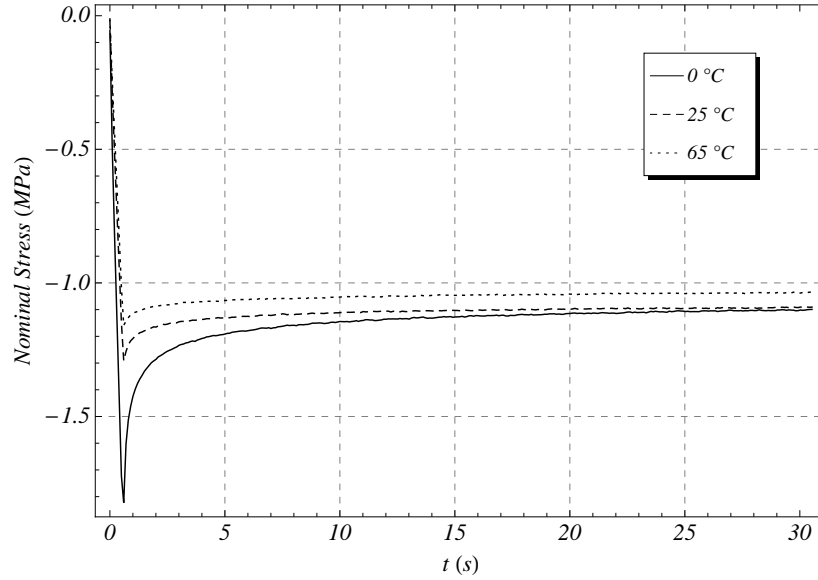


Figure 1.25 Nominal stress plotted against time in the range $t \in [0, 30]$ for the relaxation experiment repeated for three different temperatures $T \in \{0, 25, 65\}$. The strain rate during the initial ramp was $\dot{\lambda} \cong 0.24 \text{ s}^{-1}$, corresponding to a velocity of the crossbar for the transmission of the load $v \cong 370 \text{ mm/min}$.

the loading paths from the undeformed configuration, $\lambda = 1$, to the maximum strain $\lambda = 0.83$ were displacement controlled; all the unloading paths were force controlled up to the zero force. This has allowed us to perform after each cycle a three seconds creep test to recover the undeformed, stress-free initial configuration. The time-rate of the force controlled unloading paths were proportional to those of the loading ramps.

Figure 1.27 outlines the stress-strain constitutive curves related to the strain history represented in Fig. 1.26. The stiffness growth for increasing values of the strain rate $\dot{\lambda}$ is evident. Moreover, the dissipated energy over a cycle, which is proportional to the area of the cycle, shows a monotonic dependence upon the strain rate. Indeed, this behavior is shown by all the viscoelastic materials either solids or fluids.

Standard oscillatory test, both in tension and in compression, were also performed. They were obtained through a sinusoidal displacement of amplitude $\Delta\epsilon_1$ overimposed on a static stretch ϵ_0 as outlined in Fig. 1.28a in the case of a compression test with $\epsilon_0 = -0.17$, $\Delta\epsilon_1 = 0.1$ and $f_1 = 5 \text{ Hz}$. The experiment was repeated for $\Delta\epsilon_1$ ranging in $\{0.01, 0.05, 0.1\}$ and frequency $f_1 \in [0, 70] \text{ Hz}$.

The time history of the stress is shown in Fig. 1.28b. It is evident from the graph that the material response involves both short and long-term contributions. In particular, the relaxation phenomenon associated with larger characteristic times is evident for $t < 4 \text{ s}$, while the stress settles for $t > 5 \text{ s}$. The steady state response, corresponding to the last few cycles in Fig. 1.28, was used to extract the dynamic moduli through Eqs. (1.4) and (1.5). Figures 1.30, 1.31 and 1.32 outline the variation of the dynamic moduli with the frequency f_1 and their dependence upon the temperature, the compound type and the dynamic amplitude. In particular, Fig. 1.32 displays a much stronger frequency dependence of a heavily reinforced compound (Compound C) with respect to a weakly reinforced one (Compound A).

Dynamic tension tests were conducted with a GABO Eplexor 500N testing machine on the rubber strip represented in Tab. 1.1d. Two prestrain were used, $\epsilon_0 = 0.20$ and $\epsilon_0 = 0.40$ respectively and the strain amplitude $\Delta\epsilon_1$ ranges from 0.01 to 0.13. It is seen from Fig. 1.29

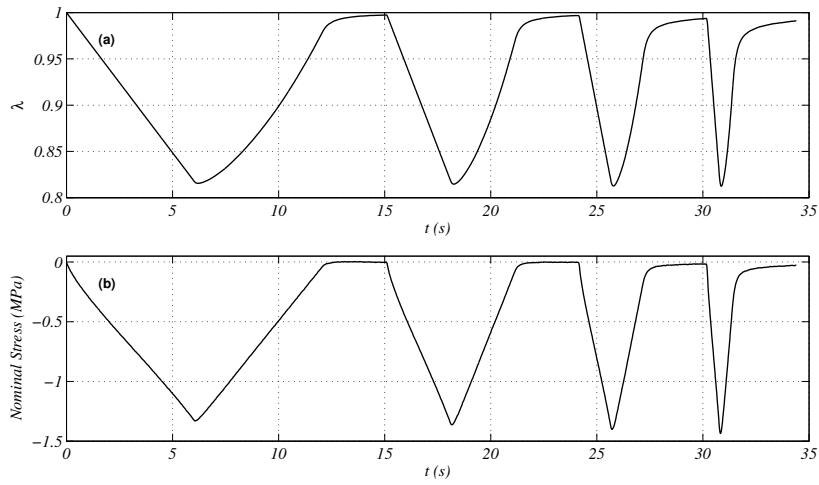


Figure 1.26 (a) Strain, λ , and (b) nominal stress plotted against time in the range $t \in [0, 35]$ for the loading-unloading experiment. The loading path was repeated for four strain rate $\dot{\lambda}$ in the range $\dot{\lambda} \in [0.03, 0.3]$.

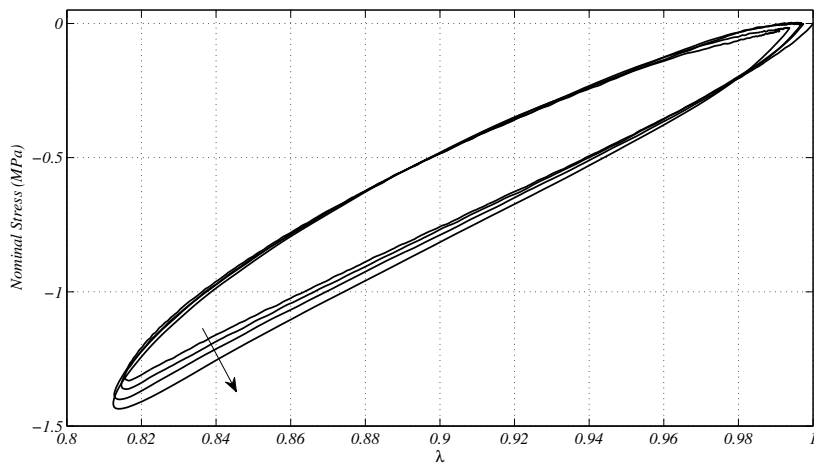


Figure 1.27 Nominal stress plotted against strain, λ , for four different strain rate $\dot{\lambda}$ in the range $\dot{\lambda} \in [0.03, 0.3]$. The arrow highlights the stiffness increase due to the increasing strain rate.

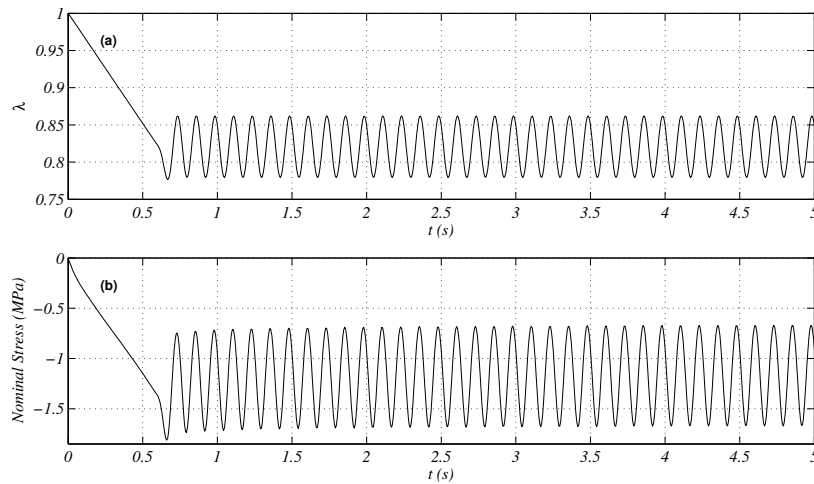


Figure 1.28 Nominal stress plotted against time in the range $t \in [0, 30]$ for $\epsilon_0 = -0.17$, $\Delta\epsilon_1 = 0.10$ and $f_1 = 8$ Hz.

that, for larger $\Delta\epsilon_1$, the stress-strain curve is no more elliptic, meaning that the nonlinearities become relevant. The slope variation of the ellipse major axes, which indicates a reduction of the Storage modulus, is a manifestation of the Payne effect.

The tests were repeated for three frequencies as shown in Figs. 1.33 and 1.34.

1.5.4 Payne Effect

Figure 1.34 shows storage (panel (a)) and loss (panel (b)) moduli as functions of $\Delta\epsilon_1$ for three different driving frequencies as shown in the insets. Symbols represent measured values, and solid, dashed and dotted lines are linear interpolations between these. In the linear case, these graphs would reduce to values independent of $\Delta\epsilon_1$; so, the $\Delta\epsilon_1$ -dependence, is a manifestation of the nonlinear response (Payne effect). It is seen that the storage modulus is a monotonically decreasing function of $\Delta\epsilon_1$ with a maximum value for $\Delta\epsilon_1 \rightarrow 0$ and likely approaching an asymptotic value for large $\Delta\epsilon_1$. The loss modulus also shows a monotonic decay but only for $\Delta\epsilon_1 \gtrsim 0.002$. Below this value the graphs indicate a peak value at positive $\Delta\epsilon_1$ and a small drop for even smaller $\Delta\epsilon_1$. Such behavior has also been measured by Höfer & Lion (2009).

Figure 1.33 displays storage, S , and loss, L , moduli plotted against $\Delta\epsilon_1$ for different values of static prestrain ϵ_0 as indicated in the insets. It is evident that both moduli react to the static prestress and that, in the considered range ($\epsilon_0 \in \{0.2, 0.4\}$), S and L increase with growing ϵ_0 . This results partially confirmed the measurements of (Lee & Kim, 2001), even if in those results a clear monotonic dependence upon ϵ_0 was absent at lower strain.

Figure 1.30 shows the analogous behavior of the storage and loss moduli as functions of frequency for different values of $\Delta\epsilon_1$. These graphs show a monotonic growth of the storage and loss moduli and give no hint that the values for S and L would saturate at larger frequencies.

To see whether the dependencies of storage and loss moduli of Figs. 1.30 and 1.34 are reliably secured experimental results, the experiments of Fig. 1.34 were repeated several times under the same conditions. We would be able to show the results by reproducing the graph of Fig. 1.34, but in order to “amplify” the difference between several curves we produced Fig. 1.35, in which the storage and loss moduli are shown in doubly logarithmic representation for $0.0005 \leq \Delta\epsilon_1 \leq 0.2$. Figure 1.35 shows results for the storage and loss moduli of five-fold repetitions of the experiments as shown in Figs. 1.30 and 1.34. It is clearly seen that

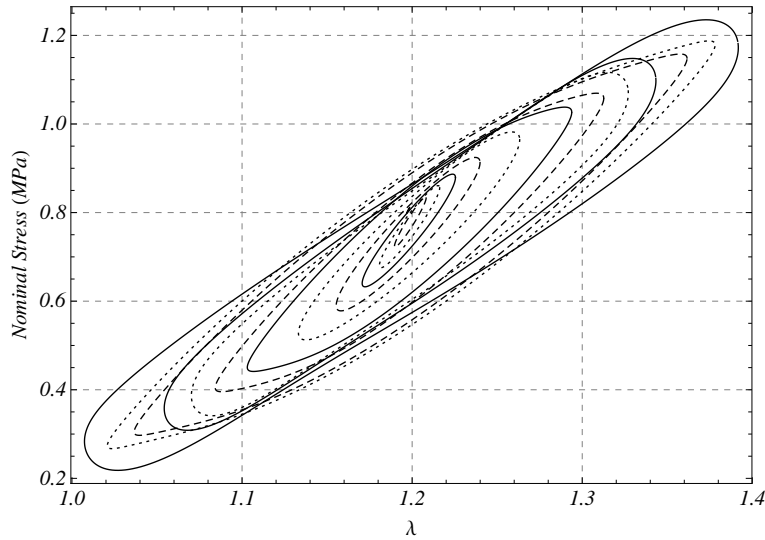


Figure 1.29 Nominal stress as function of the stretch λ for different values of the dynamic strain amplitudes $\Delta\epsilon_1 \in [0.01, 0.13]$ in the case of a tensile test ($\epsilon_0 = 0.2$, $f_1 = 15$ Hz) on a rubber strip. For the largest $\Delta\epsilon_1$, the stress-strain curve is no more elliptic, meaning that the nonlinearities become relevant. The slope variation of the ellipse major axis, which indicates a reduction of the Storage modulus, is a manifestation of the Payne effect.

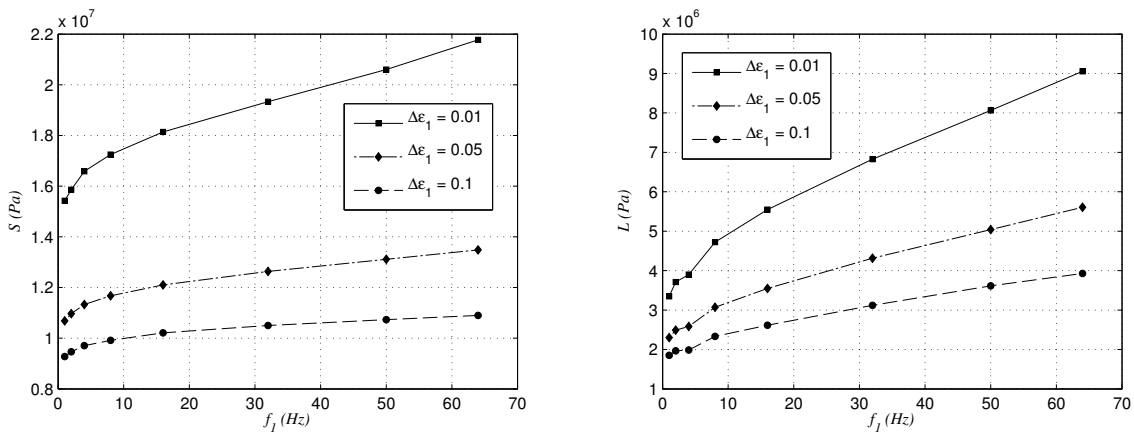


Figure 1.30 Storage, S , and loss, L , moduli, plotted against the frequency f_1 in the range $f_1 \in [0, 70]$ Hz for three different strain amplitude $\Delta\epsilon_1 \in \{0.01, 0.05, 0.1\}$. The temperature was $T = 25$ °C and prestrain was $\epsilon_0 = -0.15$ (compression) for all the frequencies. The reduction of the dynamic moduli with increasing dynamic amplitudes is a manifestation of the Payne effect.

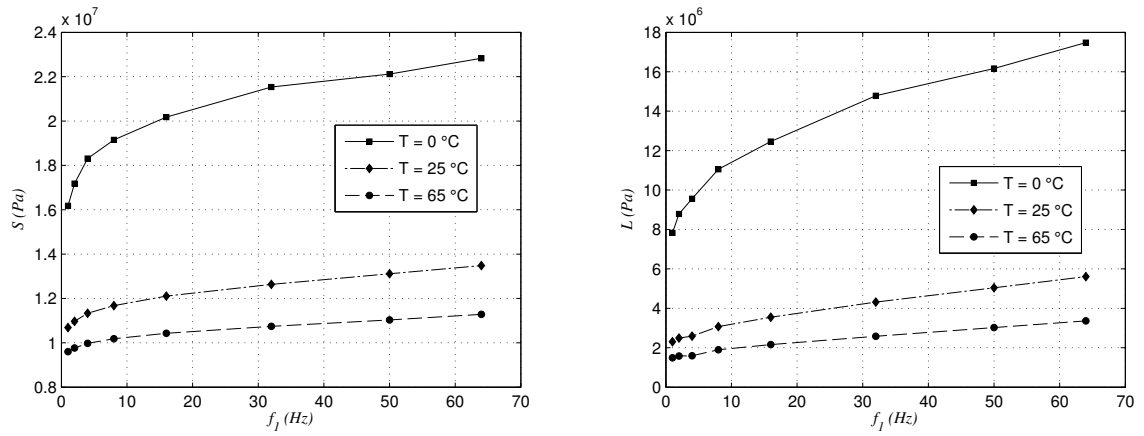


Figure 1.31 Storage, S , and loss, L , moduli, plotted against the frequency f_1 in the range $f_1 \in [0, 70]$ Hz for three different temperature $T \in \{0, 25, 65\}^\circ\text{C}$. The dynamic amplitude was $\Delta\epsilon_1 = 0.05$ and prestrain was $\epsilon_0 = -0.15$ (compression) for all the frequencies.

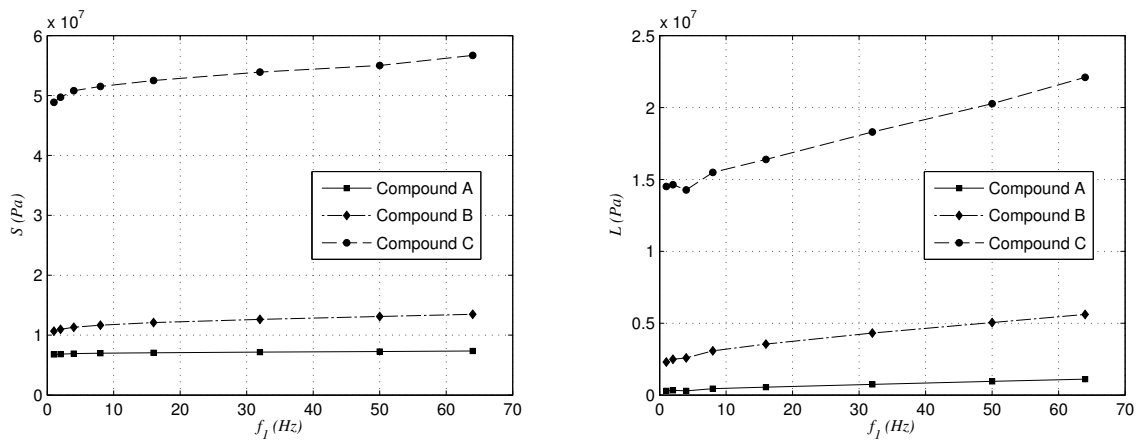


Figure 1.32 Storage, S , and loss, L , moduli, as functions of the frequency f_1 in the range $f_1 \in [0, 70]$ Hz for the three different compounds tested. The content of filler monotonically increases from compound A to C. The dynamic amplitude was $\Delta\epsilon_1 = 0.05$, the prestrain $\epsilon_0 = -0.15$ (compression) and the temperature $T = 25^\circ\text{C}$ for all the frequencies.

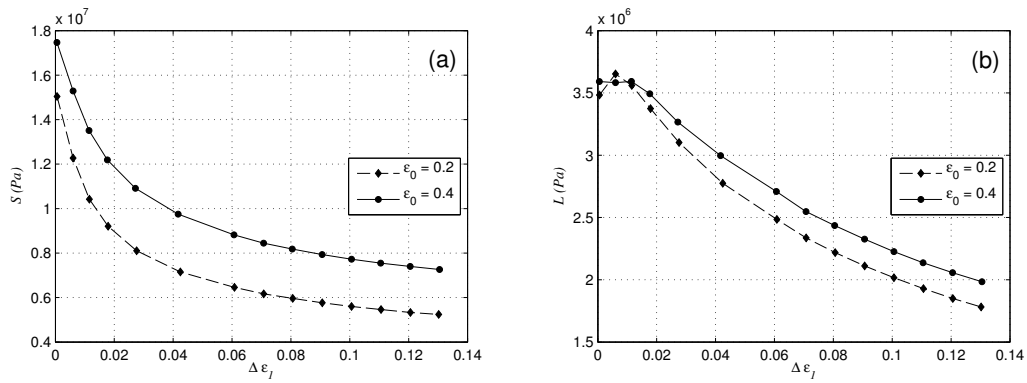


Figure 1.33 (a) Storage, S , and (b) loss, L , moduli, plotted against the strain amplitude $\Delta\epsilon_1$ in the range $\Delta\epsilon_1 \in [0, 0.13]$ for the static prestrains listed in the insets. The graphs suggest a dependence on the static prestrain. The value of the frequency was $f_1 = 10$ Hz.

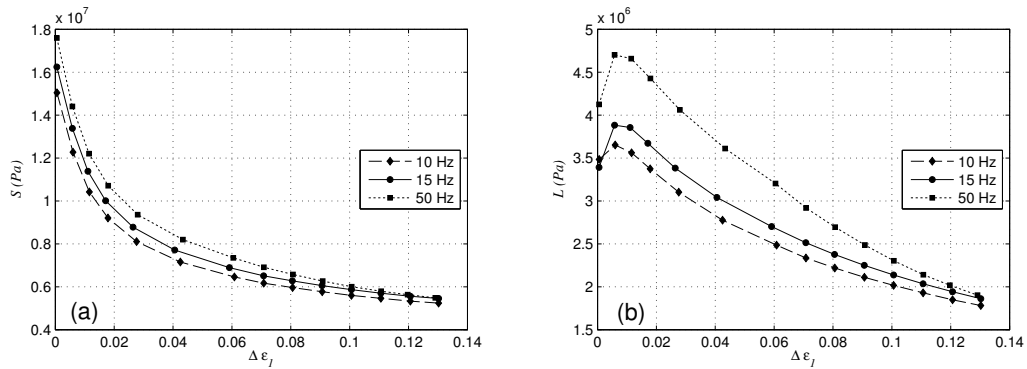


Figure 1.34 (a) Storage, S , and (b) loss, L , moduli, plotted against the strain amplitude $\Delta\epsilon_1$ in the range $\Delta\epsilon_1 \in [0, 0.13]$ for three different driving frequencies $f = 10, 15$ and 50 Hz. The variation of S and L with $\Delta\epsilon_1$ are manifestations of the Payne effect. The prestrain was $\epsilon_0 = 0.2$ (tension) for all the frequencies.

reproducibility for $\Delta\epsilon_1 \geq 0.005$ is excellent. Below this value, the measured points show a somewhat enlarged spreading, more for the loss than for the storage modulus, but still sufficiently close to one another that the robustness of the results can be trusted.

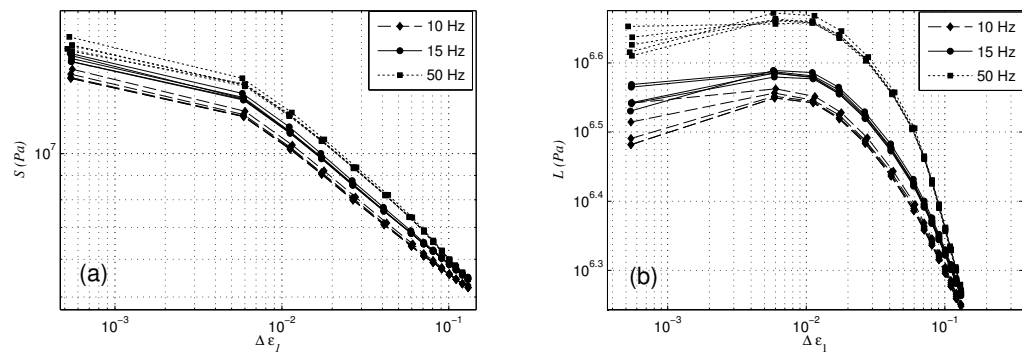


Figure 1.35 Doubly logarithmic representation of (a) storage, S , and (b) loss, L , moduli as function of $\Delta\epsilon_1$ for three different frequencies $f = 10, 15$ and 50 Hz. For each of these, five repetitions of the experiment are shown. The value of the prestrains was $\epsilon_0 = 0.2$ (tension).

Chapter 2

Nonlinear Elasticity

Chapter Outline. In this chapter the main aspects of the nonlinear theory of elasticity are presented. As nonlinear elasticity, and, in particular, hyperelasticity, is such a useful tool in the description of the behavior of carbon black-filled rubber undergoing quasi-static loadings, the main methodologies for describing the behavior of materials subjected to large strains are introduced. Some of the results herein presented will be applied to nonlinear viscoelastic constitutive models and discussed in subsequent chapters.

2.1 Kinematics

In the following section, the basic concepts used to describe the (finite) deformation of a *simple material* are briefly presented. A comprehensive introduction of finite elasticity can be found, for instance, in (Beatty, 1996; Holzapfel, 2000; Ogden, 1997).

We consider a continuous body which occupies a connected open subset of a three-dimensional Euclidean point space, and we refer to such a subset as a *configuration* of the body. We identify an arbitrary configuration as a *reference configuration* and denote this by \mathfrak{B}_r .

Let points in \mathfrak{B}_r be labelled by their position vectors \mathbf{X} relative to an arbitrarily chosen origin and let $\partial\mathfrak{B}_r$ denote the boundary of \mathfrak{B}_r . Now suppose that the body is deformed quasi-statically from \mathfrak{B}_r so that it occupies a new configuration, \mathfrak{B} say, with boundary $\partial\mathfrak{B}$. We refer to \mathfrak{B} as the *current* or *deformed configuration* of the body. The deformation is represented by the mapping $\chi : \mathfrak{B}_r \rightarrow \mathfrak{B}$ which takes points \mathbf{X} in \mathfrak{B}_r to points \mathbf{x} in \mathfrak{B} . Thus,

$$\mathbf{x} = \chi(\mathbf{X}), \quad \mathbf{X} \in \mathfrak{B}_r, \quad (2.1)$$

where \mathbf{x} is the position vector of the point \mathbf{X} in \mathfrak{B} . The mapping χ is called the *deformation* from \mathfrak{B}_r to \mathfrak{B} and is required to be one-to-one. Its inverse χ^{-1} satisfies

$$\mathbf{X} = \chi^{-1}(\mathbf{x}), \quad \mathbf{x} \in \mathfrak{B}. \quad (2.2)$$

Both χ and its inverse are assumed to satisfy proper regularity conditions, e.g., $C^2(\mathfrak{B}_r) \cap C^0(\overline{\mathfrak{B}_r})$.

For simplicity we consider only Cartesian coordinate systems and let \mathbf{X} and \mathbf{x} respectively have coordinates X_α and x_i , where $\alpha, i \in \{1, 2, 3\}$, so that $x_i = \chi_i(X_\alpha)$. Greek and Roman indices refer, respectively, to \mathfrak{B}_r and \mathfrak{B} and the usual summation convention for repeated indices is used.

The *deformation gradient tensor*, denoted \mathbf{F} , is given by

$$\mathbf{F} = \text{Grad} \mathbf{x}, \quad (2.3)$$

and has Cartesian components $F_{i\alpha} = \partial x_i / \partial X_\alpha$, Grad being the gradient operator in \mathfrak{B}_r . Local invertibility of χ requires that \mathbf{F} be non-singular. Similarly, for the inverse deformation gradient

$$\mathbf{F}^{-1} = \text{grad} \mathbf{X}, \quad (\mathbf{F}^{-1})_{\alpha i} = \frac{\partial X_\alpha}{\partial x_i}, \quad (2.4)$$

where grad is the gradient operator in \mathfrak{B} . With the use of the notation defined by

$$J = \det \mathbf{F}. \quad (2.5)$$

The equation

$$d\mathbf{x} = \mathbf{F}d\mathbf{X} \quad (2.6)$$

(in components $dx_i = F_{i\alpha}dX_\alpha$) describes how an infinitesimal line element $d\mathbf{X}$ of material at the point \mathbf{X} transforms linearly under the deformation into the line element $d\mathbf{x}$ at \mathbf{x} .

Following (Ogden, 1997), we can define a tensor measure of strain:

$$\mathbf{G} = \frac{1}{2} (\mathbf{F}^T \mathbf{F} - \mathbf{I}) \quad (2.7)$$

where \mathbf{I} is the identity tensor, and \mathbf{G} is called *Green strain tensor*.

Other suitable strain measures are:

$$\mathbf{C} = \mathbf{F}^T \mathbf{F}, \quad \mathbf{B} = \mathbf{F} \mathbf{F}^T \quad (2.8)$$

which are called, respectively, the *right* and the *left Cauchy-Green* deformation tensors.

2.2 Strain Energy Function

Materials whose constitutive behavior is only a function of the current state of deformation, measured through \mathbf{C} or \mathbf{G} , are generally known as elastic or *Cauchy elastic materials*. In this setting a more useful concept from both theory and applications is *hyperelasticity* (or *Green elasticity*), which is a particular case of Cauchy elasticity. In the case of hyperelastic materials the existence of a strain energy function Ψ defined on the space of deformation gradient is postulated: the work done by the stresses during a deformation process is only dependent on the initial and final body configurations.

For such materials the following stress measure can be introduced:

$$\mathbf{T} = \frac{\partial \Psi(\mathbf{G})}{\partial \mathbf{G}} \quad (2.9)$$

which is called the *second Piola-Kirchhoff* stress tensor: it represents a contact force density measured in the current configuration per unit area of the reference shape.

According to (2.9), we can introduce other well-known stress measures, e.g.,

$$\mathbf{\Pi} = \mathbf{F}\mathbf{T} = \mathbf{F} \frac{\partial \Psi}{\partial \mathbf{G}} \quad (2.10)$$

$$\boldsymbol{\sigma} = J^{-1} \mathbf{\Pi} \mathbf{F}^T = J^{-1} \mathbf{F} \frac{\partial \Psi}{\partial \mathbf{G}} \mathbf{F}^T \quad (2.11)$$

where $J = \det \mathbf{F}$, \mathbf{T} is the so called *nominal* stress tensor and $\boldsymbol{\sigma}$ is the *Cauchy* stress tensor. The mechanical interpretation of these stress measures are:

- the *second Piola-Kirchhoff* stress tensor represents a contact force density measured in the reference configuration per unit of reference area;
- the *Cauchy* stress tensor represents a contact force density measured in the current configuration per unit of current area;
- $\mathbf{\Pi}^T$ is called *first Piola-Kirchhoff*; it expresses the contact force density in the reference frame per unit of current area.

We remark that the only assumption used to introduce definitions (2.9) - (2.11) is that a strain energy density function can be defined in the reference configuration. Indeed, this is the most general way of describing nonlinear elastic simple materials. Moreover, since the function Ψ depends only on the Cauchy-Green strain tensor \mathbf{G} , and it is defined in the reference configuration, it is not affected by any change of observer. The previous requirement is mechanically known as *Principle of Frame Invariance* and for the constitutive relations (2.9) - (2.11) is automatically fulfilled (Liu, 2004; Murdoch, 2005; Rivlin, 2002, 2005; Truesdell & Noll, 1965).

In order to clarify this assertion, let us suppose that a rigid-body motion, i.e.,

$$\mathbf{x}^* = \mathbf{Q} \mathbf{x} + \mathbf{c}$$

is superimposed on the deformation $\mathbf{x} = \boldsymbol{\chi}(\mathbf{X})$, where \mathbf{Q} and \mathbf{c} are constant with respect to the position \mathbf{X} (\mathbf{c} is the translation vector). \mathbf{Q} belongs to the class of the orthogonal tensor, which we will call *Orth*₃. The resulting deformation gradient, say \mathbf{F}^* , is given by

$$\mathbf{F}^* = \mathbf{Q} \mathbf{F}$$

and

$$\mathbf{G}^* := \frac{1}{2} (\mathbf{F}^{*T} \mathbf{F}^* - \mathbf{I}) = \mathbf{G}$$

Therefore, using equation (2.11) the following relation for the Cauchy stress tensor holds for each deformation gradient \mathbf{F} and for all $\mathbf{Q} \in Orth_3$:

$$\boldsymbol{\sigma}^* = \mathbf{Q} \boldsymbol{\sigma} \mathbf{Q}^T. \quad (2.12)$$

Relation (2.12) expresses the fact that the constitutive law (2.11) is *objective*. In essence, it means that the material properties are independent on the superimposed rigid-body motions.

2.3 Restrictions on the Strain Energy Function

The form of the constitutive law can be simplified if the material is characterized by some symmetry properties. From the physical point of view this means that there exist a change in the reference placement such that after this change the material is indistinguishable.

The set of all material symmetry transformations at a material point \mathbf{X} depends on the selected reference configuration and for hyperelastic materials can be defined as

$$g_{R,X} = \{ \mathbf{H} \in Lin^+ \mid \det \mathbf{H} = 1 \wedge \Psi(\mathbf{H}^T \mathbf{G} \mathbf{H}) = \Psi(\mathbf{G}) \} \quad (2.13)$$

where Lin^+ is the space of the positive definite tensor. The set $g_{R,X}$ is a group (see, e.g., Ogden, 1997, for the completed proof) and it is called *material symmetry group*.

Materials which are indistinguishable after every rotation of the reference frame are called *isotropic materials*. In such a case, it results

$$Orth_3^+ \subset g_{R,X} \quad (2.14)$$

i.e., the symmetry group contains the class of all the rotations of the reference frame. Constitutive equations for isotropic materials are, actually, the simplest ones.

According to (2.13), for isotropic materials the energy function Ψ must fulfill the condition:

$$\forall \mathbf{Q} \in Orth_3^+, \quad \Psi(\mathbf{Q}^T \mathbf{G} \mathbf{Q}) = \Psi(\mathbf{G}) \quad (2.15)$$

$Orth_3^+$ being the class of all the rotations.

Every scalar function Ψ of a symmetric tensor \mathbf{G} which satisfies (2.15) is called an *Isotropic Tensor Function* of \mathbf{G} . An isotropic scalar-valued function of \mathbf{G} is also called a *scalar invariant* of \mathbf{G} . It may easily be checked that the principal invariants of \mathbf{G} , defined by

$$\widehat{I}_1(\mathbf{G}) = \text{tr} \mathbf{G}, \quad (2.16)$$

$$\widehat{I}_2(\mathbf{G}) = \frac{1}{2} [I_1^2(\mathbf{G}) - \text{tr} \mathbf{G}^2], \quad (2.17)$$

$$\widehat{I}_3(\mathbf{G}) = \det \mathbf{G} \quad (2.18)$$

are scalar invariants in accordance with definition (2.15).

Rivlin & Ericksen (1955) showed that a scalar-valued function of a symmetric tensor \mathbf{G} is isotropic if and only if it is expressible as a function of $I_1(\mathbf{G})$, $I_2(\mathbf{G})$ and $I_3(\mathbf{G})$. Hence, for isotropic materials the strain energy density function takes the form:

$$\Psi(\mathbf{G}) = \widetilde{\Psi}(\widehat{I}_1(\mathbf{G}), \widehat{I}_2(\mathbf{G}), \widehat{I}_3(\mathbf{G})) \quad (2.19)$$

or, since

$$\mathbf{G} = \frac{1}{2} (\mathbf{C} - \mathbf{I}), \quad (2.20)$$

it is natural to express the strain energy density function in terms of the invariants of the strain tensor \mathbf{C} , i.e.,

$$\Psi(\mathbf{C}) = \widehat{\Psi}(I_1, I_2, I_3), \quad (2.21)$$

where

$$I_1 = \widehat{I}_1(\mathbf{C}), \quad I_2 = \widehat{I}_2(\mathbf{C}), \quad I_3 = \widehat{I}_3(\mathbf{C}). \quad (2.22)$$

According to equation (2.19) and definitions (2.16) - (2.18), the most general form of the second Piola-Kirchhoff stress tensor for an isotropic and hyperelastic material is:

$$\begin{aligned} \mathbf{T} &= 2 \frac{\partial \Psi}{\partial \mathbf{C}} \\ &= 2 \left(\frac{\partial \Psi}{\partial I_1} + I_1 \frac{\partial \Psi}{\partial I_2} \right) \mathbf{I} - 2 \frac{\partial \Psi}{\partial I_2} \mathbf{C} + 2 I_3 \frac{\partial \Psi}{\partial I_3} \mathbf{C}^{-1}, \end{aligned} \quad (2.23)$$

where the following equalities have been used:

$$\frac{\partial I_1}{\partial \mathbf{C}} = \mathbf{I}, \quad \frac{\partial I_2}{\partial \mathbf{C}} = I_1 \mathbf{I} - \mathbf{C}, \quad \frac{\partial I_3}{\partial \mathbf{C}} = I_3 \mathbf{C}^{-1}. \quad (2.24)$$

From equation (2.11), the relation between the Cauchy stress and the strain invariants follows

$$\begin{aligned} \boldsymbol{\sigma} &= 2 I_3^{1/2} \frac{\partial \Psi}{\partial I_3} \mathbf{I} + 2 I_3^{-1/2} \left(\frac{\partial \Psi}{\partial I_1} + I_1 \frac{\partial \Psi}{\partial I_2} \right) \mathbf{B} - 2 I_3^{-1/2} \frac{\partial \Psi}{\partial I_2} \mathbf{B}^2 \\ &= \theta_0(I_1, I_2, I_3) \mathbf{I} + \theta_1(I_1, I_2, I_3) \mathbf{B} + \theta_2(I_1, I_2, I_3) \mathbf{B}^2. \end{aligned} \quad (2.25)$$

By applying the Cayley-Hamilton theorem, the previous equation can be rewritten as

$$\boldsymbol{\sigma} = \alpha_0(I_1, I_2, I_3) \mathbf{I} + \alpha_1(I_1, I_2, I_3) \mathbf{B} + \alpha_{-1}(I_1, I_2, I_3) \mathbf{B}^{-1}, \quad (2.26)$$

being

$$\begin{cases} \alpha_0 = \theta_0 - I_2 \theta_2, \\ \alpha_1 = \theta_1 + I_1 \theta_2, \\ \alpha_{-1} = I_3 \theta_2 \end{cases} \quad (2.27)$$

Assuming that the stress vanishes in the reference configuration ($T(\mathbf{I}) = 0$), one gets the following restriction on the strain energy Ψ :

$$\left. \frac{\partial \Psi}{\partial I_1} \right|_{\mathbf{C}=\mathbf{I}} + 2 \left. \frac{\partial \Psi}{\partial I_2} \right|_{\mathbf{C}=\mathbf{I}} + \left. \frac{\partial \Psi}{\partial I_3} \right|_{\mathbf{C}=\mathbf{I}} = 0 \quad (2.28)$$

A stress-free reference configuration is commonly called a *natural state*.

2.4 Compressibility

A typical choice to model compressible materials is to decompose the left Cauchy-Green strain tensor into a pure *isochoric* and a pure *volumetric* part (Flory, 1961; Sansour, 2008):

$$\mathbf{C} = \overline{\mathbf{C}} (I_3^{1/3} \mathbf{I}) \quad (2.29)$$

so that $\det \overline{\mathbf{C}} = 1$.

Furthermore, the first and the second *modified* invariants are introduced as the invariants of $\overline{\mathbf{C}}$ in the same manner of those of \mathbf{C} in (2.16)-(2.17):

$$\overline{I}_1 = I_1(\overline{\mathbf{C}}) = I_3^{-1/3} I_1, \quad \overline{I}_2 = I_2(\overline{\mathbf{C}}) = I_3^{-2/3} I_2. \quad (2.30)$$

According to (2.29), the relation $\overline{I}_3 = 1$ holds for all deformations.

In the field of nonlinear mechanics, an *ansatz* assumed by several researchers is that the strain energy function Ψ is additively decomposed as

$$\Psi(I_1, I_2, I_3) = \Psi_I(\bar{I}_1, \bar{I}_2) + \Psi_V(I_3), \quad (2.31)$$

where Ψ_I depends only upon the isochoric part of the deformation and Ψ_V depends on changes in volume (Ogden, 1997; Sansour, 2008; Simo *et al.*, 1985). This choice could eventually leads to a non-physical behavior at large strains (Ehlers & Eppers, 1998). From equation (2.25), the Cauchy stress tensor becomes

$$\begin{aligned} \boldsymbol{\sigma} = & 2I_3^{1/2} \left(\frac{\partial \Psi_I}{\partial I_3} + \frac{\partial \Psi_V}{\partial I_3} \right) \mathbf{I} + 2I_3^{-1/2} \left(\frac{\partial \Psi_I}{\partial I_1} + I_1 \frac{\partial \Psi_I}{\partial I_2} \right) \mathbf{B} \\ & - 2I_3^{-1/2} \frac{\partial \Psi_I}{\partial I_2} \mathbf{B}^2 \end{aligned} \quad (2.32)$$

and from definitions (2.30) one gets the following derivatives of the the strain energy function Ψ with respect to the modified invariants \bar{I}_1 , \bar{I}_2 and \bar{I}_3 ,

$$\begin{aligned} \frac{\partial \Psi_I}{\partial I_1} &= I_3^{-1/3} \frac{\partial \Psi_I}{\partial \bar{I}_1}, \\ \frac{\partial \Psi_I}{\partial I_2} &= I_3^{-2/3} \frac{\partial \Psi_I}{\partial \bar{I}_2}, \\ \frac{\partial \Psi_I}{\partial I_3} &= -\frac{1}{3} I_3^{-1} \left[\frac{\partial \Psi_I}{\partial \bar{I}_1} \bar{I}_1 + 2 \frac{\partial \Psi_I}{\partial \bar{I}_2} \bar{I}_2 \right]. \end{aligned} \quad (2.33)$$

By substituting equations (2.33) into (2.32), one gets:

$$\boldsymbol{\sigma}_D(\bar{\mathbf{B}}_D) = 2I_3^{-1/2} \left(\frac{\partial \Psi_I}{\partial \bar{I}_1} + \bar{I}_1 \frac{\partial \Psi_I}{\partial \bar{I}_2} \right) \bar{\mathbf{B}}_D - 2I_3^{-1/2} \frac{\partial \Psi_I}{\partial \bar{I}_2} (\bar{\mathbf{B}}^2)_D \quad (2.34)$$

$$\boldsymbol{\sigma}_V(I_3 \mathbf{I}) = 2I_3^{1/2} \frac{\partial \Psi_V}{\partial I_3} \mathbf{I}. \quad (2.35)$$

in which the subscripts D and V represent the *deviatoric* and the *volumetric* part of the tensor.

Equations (2.34)-(2.35) state that:

1. a superimposed deviatoric stress doesn't produce any volume changes, but only shape changes ($\text{tr} \boldsymbol{\sigma}_D = 0$);
2. a superimposed pressure uniquely produces a volume change.

Points 1 and 2 are the extension to the nonlinear case of the deviatoric/volumetric stress decomposition introduced in the framework of linear elasticity (and are consistent with that).

Equation (2.35) implies that the reference configuration is stress-free if the following restriction on the function Ψ_V is valid:

$$\left. \frac{\partial \Psi_V}{\partial I_3} \right|_{I_3=1} = 0. \quad (2.36)$$

Therefore, assuming a sufficient regularity for the function Ψ_V , expression (2.31) can be expanded by Taylor series around the undeformed configuration ($I_3 = 1$) as:

$$\Psi_V(I_3) = \sum_{i=2}^{\infty} \frac{1}{D_i} (I_3 - 1)^i \quad (2.37)$$

where

$$(D_i)^{-1} = \frac{1}{i!} \left. \frac{\partial^i \Psi_V}{\partial I_3^i} \right|_{I_3=1}. \quad (2.38)$$

With similar assumptions, one obtains the following expansion around the reference configuration ($I_1 = 3$, $I_2 = 3$) for the function Ψ_I :

$$\Psi_I(\bar{I}_1, \bar{I}_2) = \sum_{i,j=0}^{\infty} c_{ij} (\bar{I}_1 - 3)^i (\bar{I}_2 - 3)^j \quad (2.39)$$

where

$$c_{ij} = \begin{cases} 0, & \text{if } (i, j) = (0, 0), \\ \frac{1}{i!j!} \left. \frac{\partial^{i+j} \Psi}{\partial I_1^i \partial I_2^j} \right|_{I_1=3, I_2=3}, & \text{otherwise.} \end{cases} \quad (2.40)$$

2.5 Incompressibility

Experimental evidences shown in Chapter 1 have revealed a negligible change in volume occurring during the deformation. This behavior allows the modeling of rubber as an incompressible material. From one hand, this assumption simplifies the determination of equilibrium solutions, but, on the other hand, it makes the constitutive relation hard to implement in a numerical code. Therefore, both near-incompressible and incompressible materials will be considered in the following.

Every deformation allowed in a hyperelastic incompressible material must satisfy:

$$I_3 = \det \mathbf{C} = 1 \quad (2.41)$$

The constraint (2.41) defines an hypersurface in the space of the deformation gradients. Any stress normal to this surface, i.e., in the direction $\partial \det \mathbf{C} / \partial \mathbf{F}$, does not expend work on any (virtual) incremental deformation $\delta \mathbf{x}$ compatible with the constraint. The stress is, hence, determined by the constitutive law unless a vector parallel to $\partial \det \mathbf{C} / \partial \mathbf{F}$. From an energetic point of view this is tantamount to assume the strain energy function as

$$\Psi(I_1, I_2, I_3) = \Psi(I_1, I_2, 1) - p (I_3 - 1), \quad (2.42)$$

where $p(I_1, I_2)$ is the Lagrange multiplier associated to the constraint (2.41) which depends upon boundary conditions.

Once more, assuming a sufficient regularity of the function Ψ_I , one obtains the following Taylor expansion around the reference configuration

$$\Psi_I(I_1, I_2) = \sum_{i,j=1}^N c_{ij} (I_1 - 3)^i (I_2 - 3)^j. \quad (2.43)$$

Equation (2.43) was firstly introduced by Rivlin & Saunders (1952), and for this reason it is sometimes called *Rivlin-Saunders's expansion*. Some of the most used material models and the respective parameters c_{ij} are reported in table 2.1.

The following expression of the Cauchy stress for an incompressible material follows from equations (2.25) and (2.42):

$$\boldsymbol{\sigma} = -p \mathbf{I} + 2 \left(\frac{\partial \Psi}{\partial I_1} + I_1 \frac{\partial \Psi}{\partial I_2} \right) \mathbf{B} - 2 \frac{\partial \Psi}{\partial I_2} \mathbf{B}^2. \quad (2.44)$$

In order to verify the stress-free condition ($\boldsymbol{\sigma}(\mathbf{I}) = 0$) in the reference configuration, the unknown pressure field p must satisfy:

$$p(I_1, I_2)|_{\mathbf{C}=\mathbf{I}} = p(3, 3) = 2 \left. \frac{\partial \Psi}{\partial I_1} \right|_{\mathbf{C}=\mathbf{I}} + 4 \left. \frac{\partial \Psi}{\partial I_2} \right|_{\mathbf{C}=\mathbf{I}} \quad (2.45)$$

Table 2.1 Material models based on Rivlin's expansion (Hartmann, 2001a).

Author/Model						
Mooney Rivlin	c_{10}	c_{01}				
Isihara et al.	c_{10}	c_{01}		c_{20}		
Neo-Hooke	c_{10}					
Yeoh	c_{10}			c_{20}		c_{30}
James et al.	c_{10}	c_{01}	c_{11}	c_{20}		c_{30}
Biderman	c_{10}	c_{01}		c_{20}		c_{30}
Tschoegl	c_{10}	c_{01}	c_{11}			
Tschoegl	c_{10}	c_{01}			c_{22}	
Lion	c_{10}	c_{01}				c_{50}
Haupt/Sedlan	c_{10}	c_{01}	c_{11}	c_{02}		c_{30}

2.6 Homogeneous deformations

In the following we analyze some elementary problems in which the deformation is *homogeneous*, i.e. the deformation gradient \mathbf{F} is constant in whole body. Homogeneous deformations are equilibrium solution for all the class of hyperelastic materials; for this reason they are called *universal solutions* (see, e.g., Pucci & Saccomandi, 1997).

2.6.1 Simple Tension

In the case of *simple tension* or *simple compression* the deformation is given by

$$x_1 = \lambda_1 X_1, \quad x_2 = \lambda_2 X_2, \quad x_3 = \lambda_2 X_3, \quad (2.46)$$

hence the deformation gradient is a diagonal matrix

$$\mathbf{F} = \text{Diag} \{ \lambda_1, \lambda_2, \lambda_2 \}, \quad (2.47)$$

where λ_1, λ_2 are called *principal stretches*, which are constant because the deformation is homogeneous. Here the λ_1 -direction is the direction of the external load. Since in a simple tension test, the lateral surfaces of the specimen are supposed to be unloaded, the principal stresses corresponding to the directions 2 and 3 vanish.

For deformation (2.47) the strain invariants become:

$$\tilde{I}_1 = \lambda_1^2 + 2\lambda_2^2, \quad \tilde{I}_2 = \lambda_1^{-2} + 2\lambda_2^{-2}. \quad (2.48)$$

Incompressible Materials

In the case of incompressibility, the constraint (2.41) must be satisfied, and the following relation between the stretches must hold:

$$\lambda_1 \lambda_2^2 = 1 \iff \lambda_2 = \lambda_1^{-1/2}, \quad (2.49)$$

Table 2.2 Uniaxial Cauchy stress arising from a stretch λ for some of the most used incompressible material models.

Model	σ_{11}
Neo-Hooke	$\sigma_{11} = 2c_{10} (\lambda^2 - \lambda^{-1})$
Mooney-Rivlin	$\sigma_{11} = 2(c_{10}\lambda + c_{01}) (\lambda - \lambda^{-2})$
Yeoh ($c_{30} = 0$)	$\sigma_{11} = 2(\lambda - \lambda^{-2}) [c_{10}\lambda + 2c_{20}(\lambda^2 - 3\lambda + 2)]$

hence the strain invariants depend only upon λ_1 , e.g.,

$$\tilde{I}_1 = \lambda_1^2 + 2\lambda_1^{-1}, \quad \tilde{I}_2 = \lambda_1^{-2} + 2\lambda_1 \quad (2.50)$$

The unknown pressure field can be determined from the condition that the stresses σ_{22} and σ_{33} vanish

$$p = 2 \left[\frac{\partial \Psi}{\partial I_1} + I_1 \frac{\partial \Psi}{\partial I_2} \right]_{I_1=\tilde{I}_1, I_2=\tilde{I}_2} \lambda_1^{-1/2} - 2 \left[\frac{\partial \Psi}{\partial I_2} \right]_{I_1=\tilde{I}_1, I_2=\tilde{I}_2} \lambda_1^{-1}. \quad (2.51)$$

In the following the solution of the simple tension problem will be presented for three of the most used nonlinear elastic models, viz. Neo-Hooke, Mooney-Rivlin and Yeoh model.

The strain energy function in the Neo-Hookean model is

$$\Psi_I = c_{10}(I_1 - 3) \quad (2.52)$$

thus, from equation (2.44):

$$\boldsymbol{\sigma} = -p\mathbf{I} + \mu_0\mathbf{B}, \quad (2.53)$$

where $\mu_0 = 2c_{10}$ is the so called *initial shear modulus* (shear modulus in the reference configuration).

From equation (2.51), the expression of the pressure field follows:

$$p = \mu_0 \frac{1}{\lambda} \quad (2.54)$$

and the stress in the direction 1 becomes:

$$\sigma_{11} = \mu_0 \left(\lambda^2 - \frac{1}{\lambda} \right). \quad (2.55)$$

In the same manner by means of equation (2.44) the unidimensional stress-strain relation can be obtained for Mooney-Rivlin and Yeoh model. These results are shown in table 2.2.

Compressible Materials

In the compressible case the relation (2.49) is not anymore valid, thus the orthogonal stretch λ_2 must be derived from the implicit relation:

$$\sigma_{22}(\lambda_1, \lambda_2) = 0 \quad (2.56)$$

or equivalently $\sigma_{33}(\lambda_1, \lambda_2) = 0$, which follows from the condition that the components of the stress σ_{22} and σ_{33} vanish. Equation (2.56) has to be solved numerically for each λ_1 .

Numerical results in the cases of Neo-Hooke, Mooney-Rivlin and Yeoh models will be discussed in Chapter 5.

Model	σ_{12}
Neo-Hooke	$\sigma_{12} = 2c_{10}\gamma$
Mooney-Rivlin	$\sigma_{12} = 2(c_{10} - c_{01})\gamma$
Yeoh ($c_{30} = 0$)	$\sigma_{12} = 2[c_{10} + 2c_{20}(I_1 - 3)]\gamma$

Table 2.3 Simple shear test results for some of the most used material models.

2.6.2 Simple Shear

Another example of a homogeneous deformation state is a *simple shear* defined by

$$x_1 = X_1 + \gamma X_2, \quad x_2 = X_2, \quad x_3 = X_3, \quad (2.57)$$

where γ is the amount of shear strain. Thus,

$$\mathbf{F} = \begin{bmatrix} 1 & \gamma & 0 \\ 0 & 1 & 0 \\ 0 & 0 & 1 \end{bmatrix}, \quad \mathbf{B} = \begin{bmatrix} 1 + \gamma^2 & \gamma & 0 \\ \gamma & 1 & 0 \\ 0 & 0 & 1 \end{bmatrix}, \quad \mathbf{C} = \begin{bmatrix} 1 & \gamma & 0 \\ \gamma & 1 + \gamma^2 & 0 \\ 0 & 0 & 1 \end{bmatrix} \quad (2.58)$$

and

$$I_1(\mathbf{C}) = 3 + \gamma^2, \quad I_2(\mathbf{C}) = 3 + \gamma^2, \quad I_3(\mathbf{C}) = 1. \quad (2.59)$$

that is the strain invariants are even function of the shear strain.

The simple shear is an isochoric deformation that is possible in every compressible, homogeneous, and isotropic hyperelastic material. The constitutive relation (2.26) shows that the shear stress related to the shear strain γ is given by:

$$\sigma_{12} = \gamma \alpha(I_1, I_2, 1), \quad (2.60)$$

wherein the generalized shear response function is defined by

$$\alpha(I_1, I_2, 1) = \alpha_1(I_1, I_2, 1) - \alpha_{-1}(I_1, I_2, 1) \quad (2.61)$$

From (2.26) one gets

$$\begin{cases} \alpha_0(I_1, I_2, 1) = 2 \frac{\partial \Psi}{\partial I_3} - 2 I_2 \frac{\partial \Psi}{\partial I_2} \\ \alpha_1(I_1, I_2, 1) = 2 \frac{\partial \Psi}{\partial I_1} \\ \alpha_{-1}(I_1, I_2, 1) = -2 \frac{\partial \Psi}{\partial I_2} \end{cases} \quad (2.62)$$

thus,

$$\sigma_{12} = 2 \left(\frac{\partial \Psi}{\partial I_1} - \frac{\partial \Psi}{\partial I_2} \right) \gamma \quad (2.63)$$

It is seen that the shear stress is an odd function of the amount of shear.

Furthermore notice that the shear stress is in the direction of the shear if and only if $\alpha(I_1, I_2, 1) > 0$. However, the only presence of shear stress cannot produce a simple shear state.

It also follows from (2.32) that the scalar function α_1 and α_{-1} are determined by the normal stress differences; we have:

$$\sigma_{11} - \sigma_{33} = \alpha_1 \gamma^2, \quad (2.64)$$

$$\sigma_{22} - \sigma_{33} = \alpha_{-1} \gamma^2, \quad (2.65)$$

where

$$\sigma_{33} = \alpha_0 + \alpha_1 + \alpha_{-1} = \tau(\gamma^2) \gamma^2 \quad (2.66)$$

where since α_i are even function of γ , this dependence has been explicitly shown in the last term. Moreover the last relation allows to determine $\tau(\gamma^2)$, hence α_0 . We highlight that the normal stresses are unchanged if the shear is reverted. If these are not furnished, the block will tend to contract or to expand. Such normal stress effects are typical of problems in finite elasticity.

The most striking feature of the simple shear problem is that the results (2.64)-(2.66) do not involve the shear stress. On the contrary, the shear stress is determined by the difference of the normal stresses:

$$\gamma \sigma_{12} = \sigma_{11} - \sigma_{22}, \quad (2.67)$$

and it is determined in the same way for every homogeneous, isotropic hyperelastic material, regardless of the form of the response functions. The formula (2.67) is an example of an universal relation in the finite elasticity theory.

Chapter 3

Nonlinear Viscoelasticity

Chapter Outline. In the first section of this chapter the main approaches followed in modeling nonlinear viscoelastic solids during isothermal deformation are thoroughly described. Since filled rubber can reasonably be assumed isotropic, only isotropic constitutive relations are considered. Thereafter, the attention is focused on integral viscoelastic models. In particular, some of the most common integral models are reviewed and advantages and disadvantages of each of them are highlighted. Uniaxial stretch histories are investigated by reducing the general three-dimensional model to the one-dimensional case. In this context, the concept of dynamic moduli, introduced in linear viscoelasticity and referred to as storage and loss moduli, is extended, in a consistent manner, to the nonlinear case. Moreover, for some of the constitutive equations examined, the analytical value of the storage and loss moduli is computed and their frequency behavior discussed with reference to the collated experiments on carbon black-filled rubber. Finally the predicting capabilities of the classical linear integral viscoelastic model and of a new model based on hysteretic damping are analyzed.

3.1 Nonlinear Theory of Viscoelasticity

The theory of viscoelasticity is crucial when describing materials, such as rubber, which exhibit time dependent stress-strain behavior.

Indeed, carbon black-filled rubber, when loaded with time-dependent external forces, suffers a state of stress which is the superposition of two different aspects: a time independent, *long-term*, behavior (sometimes improperly called “hyperelastic”) opposed to a time dependent, *short-term*, response. Step-strain relaxation tests suggest that short term stresses are larger than the long term or quasi-static ones (Johnson *et al.*, 1995). Moreover, oscillatory (sinusoidal) tests indicate that dissipative anelastic effects are significant, which leads to the consideration of a constitutive relation which depends not only on the current value of the strain but on the entire strain history. This assumption must be in accordance with some principles which restrict the class of reliable constitutive equations. These restrictions can be classified as “physical” and “constitutive”. The former are restrictions to which every rational physical theory must be subjected to, e.g., frame indifference. The latter, on the other hand, depends upon the material under consideration, e.g., internal symmetries.

The principle of determinism (Truesdell & Noll, 1965) belongs to the first class. It states that: the stress at a given material point is determined by the entire past history of the motion in a neighborhood of the considered point.

Another basic assumption in every rational constitutive theory is the principle of *frame indifference*: the response of the system must be the same for all observers (Liu, 2004; Murdoch, 2005; Rivlin, 2002, 2005; Truesdell & Noll, 1965).

Then one is lead to consider constitutive restrictions. One important assumption, proposed by Noll (1958), postulates that the material is *simple*, which means that the stress at a given material point depends only on the history of the first order spatial gradient of the deformation, in a small neighborhood of the material point. Therefore, the influence of the higher order spatial gradients is ignored. Although this assumption is usually considered non-constitutive, it legitimately belongs to the class of constitutive restrictions because there exist materials, e.g., porous media and functionally graded, leading to an unacceptable approximation if higher order spatial gradients are ignored¹.

Other simplifications of the constitutive laws are obtained by assuming that the material is non-aging, which means that the microscopic changes at the time-scale of experimental test can be ignored, which indeed, complies with the experimental observations discussed in Sec. 1.2 (see, e.g., Wineman, 2009). An additional assumption, which is also corroborated by the experimental data, is the isotropy of the material, i.e., the material at a given point in one reference configuration is indistinguishable in its response from the same material after it has been statically rotated into another reference configuration. Then, the constitutive equation is simplified accordingly. As expected, the constitutive laws for isotropic materials are, by far, the simplest ones. Finally, the internal material constraints of incompressibility is yet another way to restrict and simplify the constitutive laws.

All the results presented are consistent with these principles.

In the following, we are motivated to develop a general nonlinear theory of viscoelasticity because, in the practical application of tire industry, rubber materials are used under conditions which do not comply with the infinitesimal deformation assumptions of the linear theory. For these materials, the range of deformation beyond which superposition and thereby linearity holds is extremely limited. Anyway, one of the first requirements for a nonlinear constitutive law is that, for a very small deformation, the model reduces to the corresponding

¹ The dependence upon higher order spatial gradient may have significant applications in the modeling of solids subjected to concentrated strains and fractured. As this, the applications on rubber modeling are forthcoming (see, e.g., dell’Isola *et al.*, 2009).

linear model (see, e.g., [Quintanilla & Saccomandi, 2007](#)).

In the following section a review of the constitutive equations used to model nonlinear viscoelastic solids undergoing isothermal deformation is provided.

3.2 State of the Art

Pioneering Works

Polymeric materials, such as rubber, exhibit a mechanical response which can not be properly described by means of elastic and viscous effects. In particular, elastic effects account for materials which are able to store mechanical energy with no dissipation. On the other hand, a viscous fluid in a hydrostatic stress state dissipates energy, but is unable to store it. As the experimental results reported in Chapter 1 have shown, filled rubber present both the characteristics of a viscous fluid and of an elastic solid. Viscoelastic constitutive relations have been introduced with the intent of describing the behavior of materials able to both store and dissipate mechanical energy.

The origin of the theory of viscoelasticity may be traced to various isolated researchers in the last decades of the 19th Century. This early stage of development is essentially due to the work of Maxwell, Kelvin and Voigt who independently studied the one dimensional response of such materials. The linear constitutive relationships introduced therein are the base of rheological models which are still used in many applications (see, e.g., [Malkin, 1995](#)). Their works led to Boltzmann's ([Boltzmann, 1874](#)) first formulation of three dimensional theory for the isotropic medium, which was generalized later to the anisotropic case by [Volterra \(1912\)](#).

However, in filled rubber, constitutive nonlinearities turn out to be significant even at small strains because of their internal entangled structure. In addition, when the material is able to bear large strains, geometrical nonlinearities also become relevant. Therefore an approach considering both constitutive and geometrical nonlinearities must be pursued.

The early stage of development, following the works of Maxwell, Kelvin and Voigt, has constituted the starting point for many other researchers. In particular in the mid 40s different modeling strategies have actually been used to describe nonlinear viscoelastic solids.

Internal-variables Formulations

A general approach, introduced by [Coleman & Noll \(1961\)](#), is to formulate the constitutive equation in terms of thermodynamic state-variables: the internal energy is expressed as function of both the current values of strain (stress) and the so-called internal state variables ([Coleman, 1964](#); [Coleman & Gurtin, 1967](#); [Coleman & Noll, 1963](#))¹. The latter may be identified with local micro-structural quantities, e.g., filler content ([Schapery, 1997](#)), or suitably defined averages ([Lion, 1997](#)). Rate effects are introduced through evolution equations, which usually relate time rates-of-change of internal variables to thermodynamic forces, which are the derivatives of the internal energy with respect to each internal variable.

[Simo \(1987\)](#) proposed a constitutive equation based on an internal variables formulation which has provided a starting point for many successive works ([Govindjee & Simo, 1992](#); [Holzapfel, 1996](#); [Holzapfel & Gasser, 2001](#); [Yoshida *et al.*, 2004](#)). In Simo's approach, the internal energy is split according to the multiplicative decomposition of the deformation gra-

¹In the isothermal and adiabatic context considered here, the internal energy coincides with the Helmholtz free energy; furthermore, the Clausius-Duhem inequality reduces to the Clausius-Planck inequality.

dient into dilatational and volume-preserving parts ²

Even though this choice might lead to non-physical results at finite strains (Eihlers & Eppers, 1998), Simo's model is able to reproduce the hysteretic behaviors of carbon-filled rubber, incorporating also the Mullins effect. In this case the internal energy is split as the sum of three different parts: (i) a volumetric term depending upon the volume change $J = \det \mathbf{F}$, (ii) a term depending upon the isochoric deformation $\bar{\mathbf{F}} = J^{-1}\mathbf{F}$ and (iii) a term relying on the internal variable \mathbf{q} representing the nonequilibrium part of the stress. The evolution equation of \mathbf{q} is postulated assuming the generalized force is proportional to the derivative of the internal energy with respect to the isochoric strain. This approach is found to be computationally very efficient, and thus adopted in many commercial finite element codes. However, Simo's model has not been conclusively proven to satisfy the second law of thermodynamics for all the admissible processes. Hence, it is essentially restricted to viscoelastic response for strain states near the elastic equilibrium.

Govindjee & Simo (1992) developed a similar model on the basis of the micromechanical structures of the carbon black particles and rubber matrices: the relaxation processes in the material were described through stress-like internal variables. These variables are governed by dissipative evolution equations, and interpreted as the nonequilibrium stresses due to the interaction between the polymer chains. Holzapfel (1996) proposed a model in which the internal energy is additively partitioned in the standard volumetric term plus an isochoric part. The latter depends both on the isochoric strain and a set of internal variables Γ_α that can be regarded as an internal strain tensor. This approach generalizes the additive decomposition introduced by Simo.

An advantage of the state-variable formulations is that, in contrast to the other approaches, it is not restricted to isotropic responses. Anisotropic effects could be easily taken into account, e.g., by introducing state variables depending upon fiber orientations as in Holzapfel & Gasser (2001). Moreover physical theories, such as dislocation models, may be introduced directly in the formulation of the evolution equations. However, it has been reported that the viscosity alone is not enough to reproduce the large hysteretic energy behavior of high-damping rubber, used in vibration absorbers. Thus, Yoshida *et al.* (2004) proposed a constitutive model consisting of two parts: an elastoplastic term with a strain-dependent isotropic hardening law, representing the energy dissipation of the material, and a second part consisting of a hyperelastic body with a damage model, which expresses the evolutionary direction of the stress tensor.

Additive Decomposition of Ψ

A decomposition of the deformation gradient into elastic and inelastic terms leads to alternative formulations of the strain energy function (Meggyes, 2001). This decomposition was first proposed by (Sidoroff, 1974) and later by Lubliner (1985) who extended the pioneering work of Green & Tobolsky (1946). Although in the framework of elastoplasticity the decomposition of the deformation gradient, into elastic and plastic terms, relies on clear physical assumptions, there is a lack of evidence in the context of viscoelasticity. However, it has been successfully applied in many nonlinear constitutive equations (e.g., Bonet, 2001; Hasanpour *et al.*, 2009; Haupt & Sedlan, 2001; Hoo Fatt & Al-Quraishi, 2008; Huber & Tsakmakis, 2000; Lion, 1997, and many others).

In this context, it is assumed that the deformation gradient can be decomposed as

$$\mathbf{F} = \mathbf{F}_e \mathbf{F}_i . \quad (3.1)$$

²The multiplicative decomposition of the deformation gradient into volumetric and isochoric parts was first introduced by Flory (1961) (see, e.g., Sansour, 2008).

The inelastic term \mathbf{F}_i , sometimes called viscous term \mathbf{F}_v , introduces an intermediate configuration. However, the decomposition (3.1) is a conceptual one, and cannot generally be determined experimentally since neither \mathbf{F}_e nor \mathbf{F}_i are observable quantities (Vidoli & Sciarra, 2002). The inelastic term in (3.1) was also extended to three, four or more deformation parts

$$\mathbf{F}_i = \mathbf{F}_i^{(1)} \dots \mathbf{F}_i^{(N)} \quad (3.2)$$

and was adopted and studied, for example, in elastoplasticity and viscoelasticity (see, e.g., Bonet, 2001; Haupt, 1985; Haupt & Sedlan, 2001; Meggyes, 2001, and references therein).

The decomposition (3.1) is generally followed by the *ansatz* on the internal energy for which Ψ is split as the sum of an equilibrium part and an overstress term, i.e.,

$$\Psi = \Psi_e(\mathbf{C}) + \Psi_o(\mathbf{C}_e). \quad (3.3)$$

Here \mathbf{C} is the right-Cauchy-Green strain tensor and $\mathbf{C}_e = \mathbf{F}_e^T \mathbf{F}_e$ is the elastic strain in the intermediate configuration. This form of the internal energy has been postulated by several researchers (Hasanpour *et al.*, 2009; Haupt & Sedlan, 2001; Hoo Fatt & Al-Quraishi, 2008; Lion, 1997).

Bonet (2001) proposed a more general equation for Ψ , e.g.,

$$\Psi = \Psi_e(\mathbf{C}) + \Psi_o(\mathbf{C}, \mathbf{C}_i), \quad (3.4)$$

in which the overstress term depends both on the whole strain tensor \mathbf{C} and on the inelastic (viscous) strain $\mathbf{C}_i = \mathbf{F}_i^T \mathbf{F}_i$; assuming that the viscous components is proportional to the long term expression, e.g.,

$$\Psi_o(\mathbf{C}, \mathbf{C}_i) = \alpha \Psi_e(\mathbf{C}_e), \quad (3.5)$$

equation (3.4) reduces to (3.3).

All these constitutive choices for the free energy Ψ lead to different expressions of the stress in terms of the deformation gradient. By applying the Coleman and Noll procedure (Coleman & Noll, 1963), i.e., by restricting the form of the stress tensor in such a way that the Clausius-Planck inequality is verified for every admissible process, the Piola symmetric stress tensor is shown below

$$\mathbf{T} = \mathbf{T}_e + \mathbf{T}_i, \quad (3.6)$$

where \mathbf{T}_e is the equilibrium stress and \mathbf{T}_i the overstress. In particular, for an internal energy of the form (3.3), the following relations between Ψ_e , Ψ_o and \mathbf{T}_e , \mathbf{T}_i are valid:

$$\mathbf{T}_e = \frac{\partial \Psi_e}{\partial \mathbf{C}}, \quad \mathbf{T}_i = \frac{\partial \Psi_o}{\partial \mathbf{C}_i}. \quad (3.7)$$

Equation (3.7) is not sufficient to determine the behavior of the material. In order to complete the description, the evolution equations (or flow rules) of the internal variables \mathbf{F}_e and/or \mathbf{F}_i , which determine the way viscoelastic processes evolve, must be defined. Often the evolution equations are suitably defined to be efficient with respect to time integration algorithms (Holzapfel & Gasser, 2001). A common choice for the flow rule is to apply a generalization of the one-dimensional linear Maxwell-model to the three-dimensional and nonlinear regime. In this case the evolution equations are assumed to be linear, and the overstress term arising from them is the generalization of the extra-stress arising in Maxwell element (see, e.g. Holzapfel, 2000; Huber *et al.*, 1996). Lion (1997) proposed nonlinear evolution equations based on strain, time and temperature. Bonet (2001) also used nonlinear evolution equations of rate type for the internal variables. These are based on a particular linear relaxation form of the Maxwell model which leads to a viscoelastic formulation that can be seen as a particular case of a large strain viscoplastic model. A variational formulation of Bonet's model has been developed in (Fancellò *et al.*, 2008).

Integral Formulation

The internal-variables formulation is not the only way to define the internal energy. Following the seminal work of Boltzmann (1874), Green & Rivlin (1957) and successively Coleman & Noll (1961) proposed constitutive relations for which the stress at time t depends upon the entire history of deformation up to the current time instant. However, the definition of the internal energy was developed accordingly and in agreement with the *fading memory* properties, i.e., strains which occurred in the distant past have less influence on the present value of Ψ than those which occurred in the more recent past.

To mathematically express the fading memory property, Coleman & Noll (1961) introduced the following inner product in the space of deformation histories

$$\mathbf{C}_1^t(s) : \mathbf{C}_2^t(s) := \int_0^\infty \text{tr} \{ \mathbf{C}_1^t(s) \mathbf{C}_2^t(s) \} h^2(s) ds, \quad (3.8)$$

which induces the norm

$$\| \mathbf{C}^t(s) \|_{\mathcal{H}^t} := (\mathbf{C}^t(s) : \mathbf{C}^t(s))^{1/2}. \quad (3.9)$$

Here, \mathbf{C}^t represents the history of the right-Green strain tensor up to time t , i.e.,

$$\mathbf{C}^t(s) = \mathbf{C}(t-s) \quad , s \in [0, \infty). \quad (3.10)$$

Moreover $h(t)$ is called *obliviator* of order r and it satisfies the following conditions (Truesdell & Noll, 1965):

1. $h(s)$ is defined for $0 \leq s < \infty$ and has a positive real value: $h(s) > 0$;
2. $h(s)$ is normalized by the condition $h(0) = 1$;
3. $h(s)$ decays to zero monotonically for large s in such a way that

$$\lim_{s \rightarrow \infty} s^r h(s) = 0. \quad (3.11)$$

The norm (3.9) equipped with a function h satisfying properties 1, 2 and 3 is called fading memory norm; in this topology, two deformation histories are distant if they are distant in the recent past, i.e., deformations which occur in the recent past have more weight than those which occurred in the distant past.

Fichera (1979) was the first to point out that in order to assure the existence of equilibrium solutions the influence function has to satisfy the decreasing condition (3.11) (see the contribution of Fichera in Carroll & Hayes, 1996).

The mathematical assumptions behind the theory of fading memory have been recently reviewed by Drapaca *et al.* (2007). Definition (3.9) leads to the so-called Strong Principle of Fading Memory (Truesdell & Noll, 1965) (SPFM)¹, which defines the class of admissible internal energy functionals:

There exists an obliviator $h(t)$ of order greater than $n+1/2$ such that the constitutive function Ψ is defined and n -times Fréchet-differentiable in a neighborhood of the zero strain history.

The SPFM alone is not sufficient to define properly an internal energy, but rather restrictive conditions must be satisfied to assure the existence of a stationary point of Ψ (see, e.g., Fabrizio *et al.*, 1995).

Over the years, many researchers have dealt with a proper definition of internal energy accounting for deformation histories (Del Piero & Deseri, 1997; Fabrizio & Morro, 1992;

¹Less restrictive conditions on Ψ are stated in the so-called Weak Principle of Fading Memory (WPFM) (Drapaca *et al.*, 2007).

Golden, 2005, and references therein). It is well known that the internal energy and entropy of a material with memory is generally not uniquely defined (Golden, 2001). A fundamental result in this area is due to Gurtin & Hrusa (1988) who obtained a necessary and sufficient condition for the existence of the internal energy arising from a stress-strain constitutive relation of single integral type. Moreover they were able to develop the following explicit formula for Ψ ,

$$\Psi(\mathbf{C}^t) = \Psi_1(\mathbf{C}(t)) + \int_0^\infty \psi(\tau, \mathbf{C}(\tau), \mathbf{C}(t - \tau)) d\tau. \quad (3.12)$$

The majority of models obtained from an a priori internal energy fits within this single hereditary framework (Haupt & Lion, 2002; Höfer & Lion, 2009; Lion & Kardelky, 2004). The stress arising from the constitutive assumption (3.12) involves a single hereditary integral of a nonlinear function of the strain. In this wide sense, single integral constitutive relations encompass a class of viscoelastic models equivalent to differential and fractional differential models (Adolfsson *et al.*, 2005; Hanyga, 2007; Hanyga & Sredynska, 2007).

The theory of single integral constitutive equations developed by Gurtin & Hrusa was extended to multiple integral functionals by Hanyga & Sredynska (2007). In this context, the internal energy Ψ reads as

$$\begin{aligned} \Psi(\mathbf{C}^t) = & \Psi_1(\mathbf{C}(t)) + \\ & + \sum_{n=1}^N \int_0^\infty \dots \int_0^\infty \psi(\tau, \mathbf{C}(\tau), \mathbf{C}(t - \tau_1), \dots, \mathbf{C}(t - \tau_n)) d\tau_1 \dots d\tau_n, \end{aligned} \quad (3.13)$$

where N is a positive integer. The models introduced by Green & Rivlin (1957), Pipkin & Rogers (1968), and Hassani *et al.* (1998) fit into this enlarged framework¹. However, in general, their applicability to describe the behavior of real materials is questioned since many parameters are necessary to fit the experimental data (see Chap. 5 of Lockett, 1972).

Single Integral Formulation

In applied viscoelasticity not all the constitutive equations are formulated by an a-priori defined internal energy Ψ , but the constitutive model is expressed directly by the functional relation between the stress and the strain through an hereditary integral. In rheology this class of constitutive models is called Rivlin-Sawyers models; Fung's (Fung, 1972), Fosdick and Yu's (Fosdick & Yu, 1998) and many other models currently used belong to this constitutive class. Because Rivlin-Sawyers models are not obtained with the Coleman and Noll's procedure, their thermodynamic consistency must be verified a posteriori.

Single hereditary formulation has proven to reproduce all the crucial aspects of rubber behavior (hysteresis, relaxation and creep). In the simplest situation, the current value of the stress is the sum of two different contributions: a purely elastic term depending on the current value of the strain and a hereditary integral depending on the whole strain history. In the linear model of viscoelasticity, introduced by Bernstein *et al.* (1963), the stress dependence on the strain history is assumed to be linear, i.e.,

$$\begin{aligned} \boldsymbol{\sigma}(t) = & 2\mu \mathbf{G}(t) + \lambda \operatorname{tr} \{ \mathbf{G}(t) \} \mathbf{I} \\ & + \int_0^t \dot{k}(s) [2\mu \mathbf{G}(t - s) + \lambda \operatorname{tr} \{ \mathbf{G}(t - s) \} \mathbf{I}] ds \end{aligned}$$

¹Multiple integral theory might be obtained by a proper Taylor-like series approximation of the functional Ψ on the space of deformation histories. In this sense, single integral models are obtained by the former expansion truncated at the first term (Drapaca *et al.*, 2007; Wineman, 2009).

where $k(t)$ is the so-called *viscoelastic kernel* (or relaxation function), λ and μ the Lamé moduli and \mathbf{E} the Green-Lagrangian strain tensor. A common choice for the relaxation function is to assume $k(0) = 1$, thus k is referred to as *reduced* relaxation function.

A suitable kernel in the integral can account for both the short and long term strain contributions to the current stress value. To be consistent with the second principle of thermodynamics, $k(t)$ must be a completely monotonic function of t (see, e.g., [Hanyga, 2005](#)), i.e., it must be infinitely differentiable and satisfy

$$\forall n \in \mathbb{N}, \quad \forall t > 0, \quad (-1)^n \frac{\partial^n k}{\partial t^n} \geq 0, \quad (3.14)$$

The condition of infinite differentiability can be dropped obtaining a much weaker requirements for k (see, e.g., [Lion & Kardelky, 2004](#)),

$$k(t) \geq 0, \quad k'(t) \leq 0, \quad k''(t) \geq 0. \quad (3.15)$$

In order to express the reduced relaxation function $k(t)$, a discrete relaxation spectrum, whose form was derived by various molecular models ([Pipkin, 1986](#)), is generally used. Formally,

$$k(t) = \sum_{i=1}^N k_i + \sum_{i=1}^N (1 - k_i) e^{-\frac{t}{\tau_i}}, \quad \sum_{i=1}^N k_i < 1. \quad (3.16)$$

Equation (3.16) is commonly referred to as Prony's series.

Recently fractional calculus has started to play an increasing role in polymer rheology ([Adolfsson & Enelund, 2003](#); [Adolfsson et al., 2005](#); [Gil-Negrete et al., 2009](#); [Hanyga, 2007](#); [Haupt & Lion, 2002](#); [Haupt et al., 2000](#); [Lion & Kardelky, 2004](#)). This is due to the fact that the frequency dependence of the dynamic moduli of filler-reinforced rubber is fairly weak and essentially of the power-law type ([Lion & Kardelky, 2004](#)). As shown in the literature such behavior can be represented with a minimum of material constants using the fractional calculus.

In terms of fractional derivatives, the relaxation function can be defined as

$$k(t) = 1 + \frac{1}{\Gamma(1 - \alpha)} \int_0^t (t - s)^{-\alpha} \eta(s) ds, \quad (3.17)$$

where $0 < \alpha < 1$, $\Gamma(x) = \int_0^\infty z^{x-1} e^{-z} dz$ is the Eulerian Gamma function and $\eta(s)$ is a suitable function such that $\lim_{t \rightarrow \infty} k(t) < \infty$. The time derivative of k becomes the left-sided Riemann-Liouville fractional derivative, i.e.,

$${}_0D_t^\alpha \eta(t) = \frac{1}{\Gamma(1 - \alpha)} \frac{d}{dt} \int_0^t (t - s)^{-\alpha} \eta(s) ds. \quad (3.18)$$

The behavior of the dynamic moduli arising from a fractional order viscoelastic kernel, like (3.17), has been studied in ([Rogers, 1983](#)).

Another way to introduce fractional derivatives is through rheological models of fractional order. In particular, the fractional Maxwell element corresponds to a spring in series with a fractional damper. The one-dimensional linear stress, σ , versus strain, ϵ , relation of a spring in parallel with the fractional Maxwell element can expressed in terms of fractional derivatives ([Metzler & Nonnenmacher, 2003](#)), e.g.,

$$\sigma(t) = \int_0^t \left[\mu_{eq} + \mu_{0v} E_\beta \left(-\frac{(t-s)^\beta}{\zeta^\beta} \right) \right] \dot{\epsilon}(s) ds \quad (3.19)$$

where the kernel

$$E_\beta(t) = \sum_{i=0}^{\infty} \frac{t^i}{\Gamma(1 + \beta i)}, \quad (3.20)$$

is the Mittag-Leffler function (see Haupt *et al.*, 2000; Metzler & Nonnenmacher, 2003, and references therein). Since $E_1(t)$ equals the exponential function, the Mittag Leffler function is also known as the fractional exponential function.

Fractional order models present a relevant drawback due to the difficulty in handling numerically constitutive equations of fractional order, in particular of differential type (Adolfsson *et al.*, 2005). Moreover, the identification of the constitutive parameters relies on a strongly ill-conditioned minimization problem (see Chapter 4). For this reason, they are rarely implemented in commercial codes and therefore their use is very limited.

Quasi-Linear Viscoelasticity

Because of the inherent nonlinear behavior exhibited by most of carbon black-filled rubber, the linear formulation is not applicable in general.

In the context of nonlinear viscoelasticity, one of the simplest model is the Quasi-Linear viscoelastic model proposed by Fung (Fung, 1972). In one dimension, he suggested the following relationship for the second Piola-Kirchhoff stress T in terms of the stretch $\lambda := \ell/\ell_0$,

$$T(t) = \int_{-\infty}^t k(t-s) \frac{\partial T^e[\lambda(s)]}{\partial \lambda} \frac{\partial \lambda}{\partial s} ds, \quad (3.21)$$

that is, the tensile stress at time t is the sum of contributions of all the past changes, each governed by the same relaxation function. $T^e(\lambda)$, a function of λ alone, is the nonlinearly elastic response.

Rewriting Eq. (3.21) in the form

$$T(t) = \int_{-\infty}^t k(t-s) \dot{T}^e(s) ds, \quad (3.22)$$

we see that the stress response depends linearly upon the nonlinear function of the strain $T^e(\lambda)$, from which the name ‘‘Quasi-Linear’’ derives. If the material is in the natural state for $t < 0$, Eq. (3.22) reduces to

$$T(t) = T^e[\lambda(t)] + \int_0^t \frac{\partial k(t-s)}{\partial t-s} T^e[\lambda(s)] ds, \quad (3.23)$$

since $k(0) = 1$ and all the functions are smooth in $0 \leq t < \infty$. Equation (3.23) states that the tensile stress at time t is equal to the instantaneous elastic response T^e decreased by an amount depending on the past history, since $\dot{k}(t)$ is negative.

Recently many investigators have proposed their own nonlinear viscoelastic constitutive relationship. Among them, the predictive capabilities of the models introduced in (Fosdick & Yu, 1998; Hallquist, 1998; Hibbit *et al.*, 2007; Shim *et al.*, 2004; Yang *et al.*, 2000) will be analyzed in Chap. 4 with respect to the experimental data shown in Chap. 1.

There are several applications of the viscoelastic theory concerning the behavior of carbon black-filled elastomers at high strain rates ($10^2 - 10^3 \text{ s}^{-1}$) (Hoo Fatt & Ouyang, 2007; Shim *et al.*, 2004; Yang *et al.*, 2000). In all these models the time derivative of the strain explicitly appears in the hereditary term. Hoo Fatt & Ouyang’s model is developed from the BKZ constitutive equation (Bernstein *et al.*, 1963) and is reported to be able to capture the high modulus due to high strain rates. However, it shows some shortcomings owing to a zero Young’s modulus in the undeformed configuration and, hence, it will not be considered in the comparison addressed in Chap. 4.

In particular, for this model, the Cauchy stress σ arising from a constant strain rate test, say $\dot{\epsilon}_0$, such that $\lambda = 1 + \dot{\epsilon}_0 t$, is

$$\sigma = 2\alpha_1(I_1 - 3)^{\alpha_2} \left(\lambda^2 - \frac{1}{\lambda} \right) - \left(\lambda^2 - \frac{1}{\lambda} \right) \int_1^\lambda \left[2\beta_1 \dot{k} \left(\frac{\lambda - \zeta}{\dot{\epsilon}_0} \right) \left(\zeta^2 + \frac{2}{\zeta} - 3 \right) \left(\zeta - \frac{1}{\zeta^2} \right) \right] d\zeta$$

and, hence, the Young's modulus around the undeformed configuration is zero ($[\partial\sigma/\partial\lambda]_{\lambda=1} = 0$), which contrasts with the experimental evidences.

Advanced finite element codes are often called upon to simulate tires and biological soft tissues because of the complex behavior of these NLV materials. Among many, two of the most used FEA codes, which includes a finite viscoelasticity model, are the Abaqus FEA and the LS-Dyna code. Both of these numerical tools are used in different branches of engineering (e.g. aeronautical, automotive, structural).

In particular, the LS-Dyna finite viscoelastic relationship (Hallquist, 1998) takes into account rate effects through linear viscoelasticity by a convolution integral. The model corresponds to a Maxwell fluid consisting of dampers and springs in series. The Abaqus FEA model is reminiscent of, and similar to, a well-established model of finite viscoelasticity, namely the Pipkin–Rogers model (Pipkin & Rogers, 1968). This model, with an appropriate choice of the constitutive parameters, reduces to the Fung (QLV) model (Ciambella *et al.*, 2009; Hibbit *et al.*, 2007).

Differential Viscoelasticity

Finally, it is worth mentioning another approach used to describe nonlinear viscoelastic solids: nonlinear differential viscoelasticity (Biot, 1954; Schapery, 1997; Tvedt, 2008). This theory has been successfully applied to model finite amplitude waves propagation (Destrade & Saccomandi, 2004; Destrade *et al.*, 2009; Hayes & Saccomandi, 2000). It is the generalization to the three-dimensional nonlinear case of the rheological element composed by a dashpot in series with a spring. Thus in the simplest case, the stress depends upon the current values of strain and strain rate only. In this sense, it can account for the nonlinear short-term response and the creep behavior, but it fails to reproduce the long-term material response (e.g., relaxation tests). The so-called Mooney-Rivlin viscoelastic material (Beatty & Zhou, 1991) and the incompressible version of the model proposed by Landau & Lifshitz (1986) belong to this class.

The substantive “grade 1” is generally used referring to such models for remarking the dependence of stress on the strain rate only (see Truesdell & Noll, 1965). Constitutive equations with higher order time derivatives are also used (see, e.g., Fosdick & Yu, 1996).

3.3 Quasi-Linear Viscoelasticity

3.3.1 Fung's Model

A quite general integral series representation of the internal energy Ψ was proposed by Pipkin & Rogers (1968). Dai *et al.* (1992) used the first term of such an integral series to describe the nonhomogeneous deformation of a nonlinearly viscoelastic slab. The constitutive relation they obtained is

$$\mathbf{T}(t) = \mathbf{R}[\mathbf{C}(t), 0] + \int_0^t \frac{\partial}{\partial(t-s)} (\mathbf{R}[\mathbf{C}(s), t-s]) ds. \quad (3.24)$$

Here $\mathbf{R}[\mathbf{C}(t), 0]$ represents the stress due to an instantaneous deformation occurring at time $t = 0$, while $\mathbf{R}[\mathbf{C}(s), \xi]$ is a strain dependent tensorial relaxation function which in the case of isotropy has the form

$$\mathbf{R}[\mathbf{C}(\tau), \xi] = \phi_0(\tau, I_i(\xi))\mathbf{I} + \phi_1(\tau, I_i(\xi))\mathbf{C}(\tau) + \phi_{-1}(\tau, I_i(\xi))\mathbf{C}^{-1}(\tau), \quad (3.25)$$

where $\phi_0, \phi_1, \phi_{-1}$ are scalar functions of time ξ and of the principal strain invariants I_1, I_2 and I_3 (2.16)-(2.18) at time τ . The expression given by eq. (3.24) incorporates the assumption that there has been no deformation prior to time $t = 0$.

Johnson *et al.* (1996a) have shown that, if the relaxation property can be described by a scalar function $k(t)$, the single integral representation (3.24) is equivalent to the *Quasi-Linear Viscoelastic (QLV)* model first introduced by Fung (1972), i.e.,

$$\begin{aligned} \mathbf{T}(t) = & \widehat{\theta}_0(t)\mathbf{I} + \widehat{\theta}_1(t)\mathbf{C}(t) + \widehat{\theta}_{-1}(t)\mathbf{C}^{-1}(t) \\ & + \int_0^t \dot{k}(t-s) \left\{ \widehat{\theta}_0(s)\mathbf{I} + \widehat{\theta}_1(s)\mathbf{C}(s) + \widehat{\theta}_{-1}(s)\mathbf{C}^{-1}(s) \right\} ds \end{aligned} \quad (3.26)$$

which follows from (3.24)-(3.25) with the identification

$$\phi_i(\tau, I_i(\xi)) = k(\xi)\widehat{\theta}_i(I_1(\tau), I_2(\tau), I_3(\tau)), \quad i \in \{1, -1, 0\} \quad (3.27)$$

where $k(t)$ is the reduced viscoelastic kernel. In the next, the dependence of θ_i upon the strain invariants I_1, I_2, I_3 will be specified only when necessary.

The Quasi-Linear Viscoelastic (QLV) model has proven to be a successful phenomenological model for describing the nonlinear viscoelastic behavior of solids (see references in Johnson *et al.*, 1996b; Rajagopal & Wineman, 2008).

If the reference configuration is stress free, the coefficients $\theta_0, \theta_1, \theta_{-1}$ cannot be arbitrary assigned, but the following restriction

$$\theta_0(3, 3, 1) + \theta_1(3, 3, 1) + \theta_{-1}(3, 3, 1) = 0 \quad (3.28)$$

must hold.

In the case of incompressibility Fung's model reads as

$$\begin{aligned} \mathbf{T}(t) = & p(t)\mathbf{C}^{-1}(t) + \theta_0(t)\mathbf{I} + \theta_1(t)\mathbf{C}(t) \\ & + \int_0^t \dot{k}(t-s) \left\{ \theta_0(s)\mathbf{I} + \theta_1(s)\mathbf{C}(s) \right\} ds, \end{aligned} \quad (3.29)$$

where $p(t)$ is the Lagrange multiplier associated to the incompressibility constraint, which in the dynamic case reads as

$$\forall t, \quad \det \mathbf{C}(t) = 1. \quad (3.30)$$

As in the static case, $p(t)$ must be determined from equilibrium equations and boundary conditions.

Equation (3.29) states that the stress at time t is equal to the instantaneous response decreased by an amount depending on the past history, since $\dot{k}(t)$ is generally negative valued. In other words, the *QLV* model reflects strain history dependent stress and fading memory.

In order to express relaxation properties, Prony's series (3.16) might be used, i.e.,

$$k(t) = \sum_{i=1}^N \frac{\mu_i}{\mu_0} + \sum_{i=1}^N \left(1 - \frac{\mu_i}{\mu_0} \right) e^{-\frac{t}{\tau_i}}, \quad \sum_{i=1}^N \mu_i = \mu_\infty, \quad (3.31)$$

where μ_0 is a real constant representing the shear modulus in the reference configuration, μ_∞ is the ultimate value to which the shear modulus settles after an infinite time and τ_i are the characteristic time constants.

To emphasize some limits of Fung's model, we henceforth focus on an incompressible viscoelastic solid for which the instantaneous response is modeled by a Neo-Hookean stress-strain relationship, i.e.,

$$\mathbf{T}_e = p\mathbf{C}^{-1} + \mu_0\mathbf{I} \quad (3.32)$$

Then from (3.29) we have the identification $\theta_0 = \mu_0$, $\theta_1 = \theta_{-1} = 0$, that yields:

$$\mathbf{T}(t) = p(t)\mathbf{C}^{-1}(t) + \mu_0 k(t)\mathbf{I}, \quad (3.33)$$

since $k(0) = 1$, or for the Cauchy stress tensor:

$$\boldsymbol{\sigma}(t) = p(t)\mathbf{I} + \mu_0 k(t)\mathbf{B}(t). \quad (3.34)$$

Let us consider an uniaxial deformation described by

$$x_1 = \lambda(t)X_1, \quad x_2 = \lambda(t)^{-1/2}X_2, \quad x_3 = \lambda(t)^{-1/2}X_3, \quad (3.35)$$

where $\lambda(t)$ is the stretch ratio in the direction of the extension. The resulting deformation gradient has the diagonal form

$$\mathbf{F}(t) = \text{Diag} \left[\lambda(t), \lambda(t)^{-1/2}, \lambda(t)^{-1/2} \right]. \quad (3.36)$$

Assuming that the uniaxial deformation arises from a *uniaxial tension* with $\sigma_{11} \neq 0$, $\sigma_{22} = \sigma_{33} = 0$ enables us to compute the Lagrange multiplier $p(t)$. The resulting non-zero component of the Cauchy stress is

$$\sigma_{11}(t) = \left[\mu_\infty + \sum_{i=1}^N (\mu_0 - \mu_i) \exp^{-t/\tau_i} \right] [\lambda^2(t) - \lambda^{-1}(t)], \quad (3.37)$$

hence, system response in the steady state ($t \gg \max \{\tau_1, \dots, \tau_N\}$) is

$$\sigma_{11}^{SS}(t) = \mu_\infty [\lambda^2(t) - \lambda^{-1}(t)], \quad (3.38)$$

which is the response of a purely elastic non-dissipative material.

3.3.2 Fosdick and Yu's model

In the framework of nonlinear viscoelasticity, Fosdick & Yu (1998) proposed their own constitutive equation.

They assumed that the second Piola-Kirchhoff stress tensor is given by

$$\begin{aligned} \mathbf{T}(t) = & \theta_0(t)\mathbf{I} + \theta_1(t)\mathbf{C}(t) + \theta_{-1}(t)\mathbf{C}^{-1}(t) \\ & + J(t)\mathbf{F}^{-1}(t) \left\{ \int_0^\infty \dot{k}(s) [\mathbf{C}_t(t-s) - \mathbf{I}] ds \right\} \mathbf{F}^{-T}(t), \end{aligned} \quad (3.39)$$

where $\mathbf{C}_t(s)$ is the relative right Cauchy-Green strain tensor:

$$\mathbf{C}_t(s) = \mathbf{F}_t^T(s)\mathbf{F}_t(s) = \mathbf{F}^{-T}(s)\mathbf{F}^T(s)\mathbf{F}(s)\mathbf{F}^{-1}(t), \quad (3.40)$$

being $\mathbf{F}_t(s) = \mathbf{F}(s)\mathbf{F}^{-1}(t)$.

If a strain $\mathbf{C}(t)$ is suddenly applied at time $t = 0$, e.g.,

$$\mathbf{C}(t) = \begin{cases} \mathbf{I}, & \text{if } t \leq 0 \\ \mathbf{C}^+(t) \neq \mathbf{I}, & \text{if } t > 0 \end{cases} \quad (3.41)$$

equation (3.39) takes the following form

$$\mathbf{T}(t) = \mathbf{T}^e(t) + J(t)\mathbf{F}^{-1}(t)\mathbf{F}^{-T}(t) \left\{ \int_0^t \dot{k}(t-s) [\mathbf{C}(s) - \mathbf{C}(t)] ds \right\} \mathbf{F}^{-1}(t)\mathbf{F}^{-T}(t) \quad (3.42)$$

where

$$\mathbf{T}^e(t) = \theta_0(t)\mathbf{I} + \theta_1(t)\mathbf{C}(t) + \theta_{-1}(t)\mathbf{C}^{-1}(t) \quad (3.43)$$

is the instantaneous part of the stress.

For an incompressible material, a Lagrangian multiplier accounting for the constraint $\det \mathbf{C} = 1$ must be introduced and, hence, equation (3.39) becomes

$$\begin{aligned} \mathbf{T}(t) = & q(t)\mathbf{C}^{-1}(t) + \theta_0(t)\mathbf{I} + \theta_1(t)\mathbf{C}(t) \\ & + \mathbf{F}^{-1}(t)\mathbf{F}^{-T}(t) \left\{ \int_0^t \dot{k}(t-s)\mathbf{C}(s)ds \right\} \mathbf{F}^{-1}(t)\mathbf{F}^{-T}(t), \end{aligned} \quad (3.44)$$

or in terms of Cauchy stress,

$$\boldsymbol{\sigma}(t) = \tilde{q}(t)\mathbf{I} + \tilde{\theta}_0(t)\mathbf{B}(t) + \tilde{\theta}_1(t)\mathbf{B}^2(t) + \mathbf{F}^{-T}(t) \left\{ \int_0^t \dot{k}(t-s)\mathbf{C}(s)ds \right\} \mathbf{F}^{-1}(t). \quad (3.45)$$

Fosdick and Yu's model has been successfully applied to describe finite amplitude wave propagation (Destrade & Saccomandi, 2006; Hayes & Saccomandi, 2000; Salvatori & Sanchini, 2005).

By comparing (3.44) with Fung's constitutive equation (3.29), the differences between the two models appear:

- the "instantaneous" part of the stress is the same in the two models;
- the "dissipative" term of Fosdick's model differs from that of the QLV model (3.29) since it represents the history of the symmetric Piola-Kirchhoff stress transformed by push-forward and pull-back deformations.

To investigate thoroughly the behavior of Fosdick and Yu's model, let us consider a simple shear deformation of amount $\gamma(t)$ in the plane 12, e.g,

$$\mathbf{F}(t) = \begin{bmatrix} 1 & \gamma(t) & 0 \\ 0 & 1 & 0 \\ 0 & 0 & 1 \end{bmatrix}. \quad (3.46)$$

Hence, the right-Cauchy-Green strain tensor reads as

$$\mathbf{C}(t) = \begin{bmatrix} 1 & \gamma(t) & 0 \\ \gamma(t) & 1 + \gamma^2(t) & 0 \\ 0 & 0 & 1 \end{bmatrix}. \quad (3.47)$$

If there is no traction acting on the lateral surfaces, it results $\sigma_{33}(t) = 0$, then the Lagrangian multiplier $p(t)$ into (3.45) can be computed. The Cauchy stress resulting from Eq. (3.39) has the following components:

$$\begin{aligned} \sigma_{11}(t) &= \gamma^2(t)[\tilde{\theta}_0(t) + 3\tilde{\theta}_1(t) + \tilde{\theta}_1(t)\gamma^2(t)], \\ \sigma_{12}(t) &= \gamma(t)[\tilde{\theta}_0(t) + 2\tilde{\theta}_1(t) + \tilde{\theta}_1(t)\gamma^2(t)] + \int_0^\infty \dot{k}(t-s)[\gamma(s) - \gamma(t)] ds, \\ \sigma_{22}(t) &= \tilde{\theta}_1(t)\gamma^2(t) + \int_0^\infty \dot{k}(t-s)[\gamma(s) - \gamma(t)]^2 ds. \end{aligned}$$

While the stresses σ_{12} and σ_{22} consist of an elastic term plus a dissipative integral as the standard one-dimensional model of linear viscoelasticity, σ_{11} is a purely elastic force distribution, i.e., there is no stress-relaxation. This behavior seems in contrast to the assumed isotropy of the material.

3.3.3 Abaqus FEA model

Commercial finite element codes are often called upon to simulate the behaviour of tyres in real-world applications. These numerical codes are mostly used as “black-boxes”, and the validity of the results is rarely questioned, even though they might provide a decisive argument in favour of, or against, the viability of a given tyre model.

With this aim we introduce the ABAQUS FEA finite viscoelasticity constitutive relation¹ and we investigate the resulting material behavior by means of two prototype experiments.

Section 4.8.2 of the ABAQUS Theory Manual (Hibbit *et al.*, 2007) gives the constitutive relation for modeling nonlinear viscoelastic effects in the form:

$$\boldsymbol{\sigma}(t) = \boldsymbol{\sigma}_e(t) + \text{SYM} \left\{ \mathbf{F}(t) \left[\int_0^t \frac{J(s)}{J(t)} \dot{k}(t-s) \mathbf{F}^{-1}(s) \boldsymbol{\sigma}_e(s) \mathbf{F}(s) ds \right] \mathbf{F}^{-1}(t) \right\}, \quad (3.48)$$

where $\boldsymbol{\sigma}_e$ is the instantaneous elastic Cauchy stress response (elastic response at very short times), k is the so-called viscoelastic kernel, which characterizes the stress relaxation and satisfies $k(0) = 1$.

Also, “SYM” represents the symmetric part of the bracketed term. The constitutive relation (3.48) is valid for compressible as well as incompressible solids. In the latter case the hydrostatic term $-\hat{p}\mathbf{I}$ in $\boldsymbol{\sigma}_e$ (where \hat{p} is a Lagrange multiplier) is a workless constraint stress in both the instantaneous response and in the history term, as expected. Indeed, for an incompressible solid, it results $J(t) = 1$, for each t , and $\boldsymbol{\sigma}_e$ has the general form:

$$\boldsymbol{\sigma}_e = -\hat{p}\mathbf{I} + \psi_1\mathbf{B} + \psi_2\mathbf{B}^2, \quad (3.49)$$

where ψ_1, ψ_2 are scalar functions of time and of the first and second principal invariants, I_1, I_2 , of \mathbf{C} .

Then (3.48) reduces to

$$\begin{aligned} \boldsymbol{\sigma}(t) = & -p(t)\mathbf{I} + \psi_1(t)\mathbf{B}(t) + \psi_2(t)\mathbf{B}(t)^2 \\ & + \sum_{i=1}^2 \text{SYM} \left\{ \mathbf{F}(t) \left[\int_0^t \dot{k}(t-s) \psi_i(s) \mathbf{C}(s)^i ds \right] \mathbf{F}^{-1}(t) \right\}, \end{aligned} \quad (3.50)$$

where $p(t) = \hat{p}(t) + \int_0^t \dot{k}(t-s)\hat{p}(s)ds$ is arbitrary and remains to be determined from initial/boundary conditions.

On inspection of equations (3.29) and (3.50), it can be seen that there are two main differences between the models. First, the integral term in equation (3.50) is generally non-symmetric, in contrast to the integral term in equation (3.29). This is taken care of in an ad hoc manner by using the “SYM” operator. Also, the history (time integral) term in the ABAQUS model terminates with $\mathbf{F}(t)^{-1}$ in contrast to the history term in the the QLV model, which terminates with $\mathbf{F}(t)^T$. The latter fits more naturally with the usual expression for the traction $\boldsymbol{\sigma}nda$ via Nanson’s formula $\mathbf{F}^Tnda = JNdA$ connecting reference and deformed area elements ($J = 1$ here). In fact, the ‘push-forward’ to the configuration at time t from that at time s of the (symmetric) Cauchy stress $\boldsymbol{\sigma}_e(s)$ should involve $\mathbf{F}(t)\mathbf{F}^{-1}(s)\boldsymbol{\sigma}_e(s)\mathbf{F}^{-T}(s)\mathbf{F}^T(t)$ rather than the $\mathbf{F}(t)\mathbf{F}^{-1}(s)\boldsymbol{\sigma}_e(s)\mathbf{F}(s)\mathbf{F}^{-1}(t)$ that appears in (3.50). This change would remove the need to apply the SYM operation. However, for an incompressible material use of (3.49) then leads to a term in p that doesn’t give a workless constraint stress. This can be corrected by, for example, dropping this term from (3.49) in the integral, in which case (3.50) would be

¹A new version of the Abaqus Finite Element Analysis package has recently been released (June 2009) and the finite viscoelasticity model has been replaced

replaced by

$$\begin{aligned} \boldsymbol{\sigma}(t) = & -p(t)\mathbf{I} + \psi_1(t)\mathbf{B}(t) + \psi_2(t)\mathbf{B}(t)^2 \\ & + \mathbf{F}(t) \left[\int_0^t \dot{k}(t-s)\psi_i(s)\mathbf{C}(s)^i ds \right] \mathbf{F}^T(t), \end{aligned} \quad (3.51)$$

with $p(t)$ the arbitrary pressure. This is then a special case within the model (3.29).

A numerical comparison between the QLV and the Abaqus FEA model for the simple shear and uniaxial extension case has been performed to further highlight the differences between the two models. The results of the simulations are reported in Section 5.4.

3.4 Linear Viscoelasticity

3.4.1 Reduction from nonlinear theory

In order to prove the compatibility of Fung's QLV model with the linear theory of infinitesimal viscoelasticity (see, e.g., Coleman & Noll, 1961; Gurtin & Sternberg, 1962) we will reduce the QLV constitutive equation to (3.14) by ignoring higher order terms in the deformation gradient.

The base assumption of linear elasticity, thus viscoelasticity, is that the second order term in a formal series expansion (with respect to a small scalar evolution parameter ε) of the displacement gradient can be ignored.

To make the meaning of "small" precise, let assume that $\mathbf{F} = \mathbf{F}(\tau)$ is the deformation gradient at time τ , and let put

$$\mathbf{H} = \mathbf{F} - \mathbf{I}. \quad (3.52)$$

The tensor \mathbf{H} is the gradient of the vector $\mathbf{u} = \mathbf{u}(\tau)$ of the displacement from the reference configuration.

We put

$$\mathbf{H}_\varepsilon = \varepsilon \mathbf{H} \quad (3.53)$$

where $\varepsilon = \|\mathbf{H}_\varepsilon\|$ and $\|\mathbf{H}\| = 1$. We regard ε as the measure of "smallness" of the deformation history. The linearized strain tensors, hence, follow

$$\begin{aligned} \mathbf{F}_\varepsilon &= \mathbf{I} + \varepsilon \mathbf{H} + o(\varepsilon^2) \\ \mathbf{C}_\varepsilon &= \mathbf{F}_\varepsilon^T \mathbf{F}_\varepsilon = \mathbf{I} + 2\varepsilon \mathbf{E} + o(\varepsilon^2) \\ \mathbf{C}_\varepsilon^{-1} &= \mathbf{I} - 2\varepsilon \mathbf{E} + o(\varepsilon^2) \end{aligned} \quad (3.54)$$

where $\mathbf{E} = (\mathbf{H} + \mathbf{H}^T)/2$ is the symmetric part of the displacement gradient, while the linearized strain invariants are

$$I_1^\varepsilon = 3 + 2\varepsilon \text{tr}\{\mathbf{E}\} + o(\varepsilon^2), \quad (3.55)$$

$$I_2^\varepsilon = 3 + 4\varepsilon \text{tr}\{\mathbf{E}\} + o(\varepsilon^2), \quad (3.56)$$

$$I_3^\varepsilon = 1 + 2\varepsilon \text{tr}\{\mathbf{E}\} + o(\varepsilon^2). \quad (3.57)$$

Let recall the QLV model introduced by Fung

$$\mathbf{T}(t) = \mathbf{T}_e(t) + \int_0^t \dot{k}(t-s)\mathbf{T}_e(s)ds, \quad (3.58)$$

$$\mathbf{T}_e(t) = \theta_0(t)\mathbf{I} + \theta_1(t)\mathbf{C}(t) + \theta_{-1}(t)\mathbf{C}^{-1}(t),$$

where $\theta_\Gamma(I_1, I_2, I_3)$, $\Gamma = -1, 0, 1$, is a function of the strain invariants I_1 , I_2 and I_3 at time t . For small strains, the coefficients θ_Γ can be expanded in Taylor's series as

$$\theta_\Gamma(I_1^\varepsilon, I_2^\varepsilon, I_3^\varepsilon) = \theta_\Gamma^0 + 2\varepsilon \operatorname{tr}\{\mathbf{E}\} \left[\frac{\partial \theta_\Gamma}{\partial I_1^\varepsilon} + 2 \frac{\partial \theta_\Gamma}{\partial I_2^\varepsilon} + \frac{\partial \theta_\Gamma}{\partial I_3^\varepsilon} \right]_{\varepsilon=0}, \quad \theta_\Gamma^0 = \theta_\Gamma(3, 3, 1), \quad (3.59)$$

where higher order terms in ε^2 have been neglected. Therefore the constitutive equation for the instantaneous stress $\mathbf{T}_e(t)$ becomes

$$\begin{aligned} \mathbf{T}_e^\varepsilon(t) &= [\theta_{-1}^0 + \theta_0^0 + \theta_1^0] \mathbf{I} + 2\varepsilon [\theta_1^0 - \theta_{-1}^0] \mathbf{E} + \\ &+ 2\varepsilon \operatorname{tr}\{\mathbf{E}\} \mathbf{I} \sum_{\Gamma=-1,0,1} \left[\frac{\partial \theta_\Gamma}{\partial I_1^\varepsilon} + 2 \frac{\partial \theta_\Gamma}{\partial I_2^\varepsilon} + \frac{\partial \theta_\Gamma}{\partial I_3^\varepsilon} \right]_{\varepsilon=0}. \end{aligned} \quad (3.60)$$

If the reference configuration is a *natural state*, then $\theta_{-1}^0 + \theta_0^0 + \theta_1^0 = 0$ and the QLV constitutive equation reduces to the linear viscoelastic model, i.e.,

$$\begin{aligned} \boldsymbol{\sigma}(t) &= 2\mu \mathbf{E}(t) + \lambda \operatorname{tr}\{\mathbf{E}(t)\} \mathbf{I} + \\ &+ \int_0^t \dot{k}(t-s) [2\mu \mathbf{E}(s) + \lambda \operatorname{tr}\{\mathbf{E}(s)\} \mathbf{I}] ds \end{aligned} \quad (3.61)$$

where λ and μ are called *Lamé moduli*.

From equations (3.60) and (3.61) the relation between the Lamé parameters and the coefficients θ_Γ follows, e.g.,

$$\begin{aligned} \mu &= \theta_1^0 - \theta_{-1}^0 \\ \lambda &= 2 \sum_{\Gamma=-1,0,1} \left[\frac{\partial \theta_\Gamma}{\partial I_1^\varepsilon} + 2 \frac{\partial \theta_\Gamma}{\partial I_2^\varepsilon} + \frac{\partial \theta_\Gamma}{\partial I_3^\varepsilon} \right]_{\varepsilon=0} \end{aligned} \quad (3.62)$$

An improved model in linear viscoelasticity can be obtained from equation (3.61) in the hypothesis of different relaxation properties for the deviatoric and spheric parts of the strain. It means that the previous equation can be rewritten as:

$$\boldsymbol{\sigma}_D(t) = G(0) \mathbf{E}_D(t) + \int_0^t \mathbf{E}_D(t-s) \dot{G}(s) ds \quad (3.63)$$

$$\boldsymbol{\sigma}_V(t) = H(0) \operatorname{tr}\mathbf{E}(t) \mathbf{I} + \int_0^t \operatorname{tr}\mathbf{E}(t-s) \mathbf{I} \dot{H}(s) ds \quad (3.64)$$

where a subscript $(\cdot)_D$ represents the deviatoric part of a tensor, $G(t)$ and $H(t)$ are the viscoelastic kernels of the deviatoric and volumetric part of the stress, respectively. They are usually called *shear* and *bulk* modulus.

3.4.2 Dynamic Moduli

There are practical situations in which viscoelastic bodies may be subjected to steady state oscillatory conditions. The fading memory property guarantees that, for such displacement law, the stress gets into a steady state, hence, it is reasonable to expect that a special form of the stress might arise (see, e.g., [Christensen, 2003](#)). This situation will here be analyzed.

Let us consider the case of isotropic materials subjected to an uniaxial deformation, and let the stress-strain relation

$$\sigma(t) = k_\alpha(0) \epsilon(t) + \int_0^t \epsilon(t-s) \dot{k}_\alpha(s) ds \quad (3.65)$$

designate either the deviatoric or the volumetric part of the stress in equations (3.63) and (3.64), depending upon whether $\alpha = 1$ or $\alpha = 2$.

With integration by parts, equation (3.65) becomes

$$\sigma(t) = k_\alpha(t) \epsilon(0) + \int_0^t k_\alpha(t-s) \dot{\epsilon}(s) ds \quad (3.66)$$

We let the strain history be specified as being a harmonic function of time according to:

$$\epsilon(t) = \epsilon_0 + \epsilon_1 \sin(\omega t) \quad (3.67)$$

hence

$$\begin{aligned} \sigma(t) &= k_\alpha(t) \epsilon_0 + \epsilon_1 \int_0^t k_\alpha(t-s) \omega \cos(\omega s) ds \\ &= k_\alpha(t) \epsilon_0 + \epsilon_1 \int_0^t k_\alpha(s) \omega \cos(\omega(t-s)) ds \\ &= k_\alpha(t) \epsilon_0 + \epsilon_1 \cos(\omega t) \int_0^t k_\alpha(s) \omega \cos(\omega s) ds \\ &\quad + \epsilon_1 \sin(\omega t) \int_0^t k_\alpha(s) \omega \sin(\omega s) ds \end{aligned} \quad (3.68)$$

It is useful to decompose the viscoelastic kernel $k_\alpha(t)$ as:

$$k_\alpha(t) = \tilde{k}_\alpha + \hat{k}_\alpha(t) \quad (3.69)$$

where in accordance to fading memory properties, it results:

$$\hat{k}_\alpha(t) \rightarrow 0 \quad \text{as} \quad t \rightarrow \infty \quad (3.70)$$

By means of (3.69) and (3.70), the steady state response of the system ($t \rightarrow \infty$) is:

$$\begin{aligned} \sigma_s(t) &\simeq \tilde{k}_\alpha \epsilon_0 + \epsilon_1 \sin(\omega t) \left[\tilde{k}_\alpha + \int_0^\infty \hat{k}_\alpha(t) \omega \sin(\omega s) ds \right] \\ &\quad + \cos(\omega t) \int_0^\infty \hat{k}_\alpha(t) \omega \cos(\omega s) ds \\ &= \tilde{k}_\alpha \epsilon_0 + \epsilon_1 [S_\alpha(\omega) \sin(\omega t) + L_\alpha(\omega) \cos(\omega t)] \end{aligned} \quad (3.71)$$

The existence of the integrals in previous equation is assured by (3.70) and by the fading memory requirement (3.14).

The quantities

$$\begin{aligned} S_\alpha(\omega) &= \tilde{G}_\alpha + \int_0^\infty \hat{k}_\alpha \omega \sin(\omega s) ds \\ L_\alpha(\omega) &= \int_0^\infty \hat{k}_\alpha \omega \cos(\omega s) ds \end{aligned} \quad (3.72)$$

are generally referred to as the *storage* and the *loss* moduli. Moreover the complex function:

$$k_\alpha^*(\omega) = S_\alpha(\omega) + j L_\alpha(\omega), \quad j = \sqrt{-1} \quad (3.73)$$

is called *dynamic modulus*.

From equation (3.71) we can obtain the inverse relation between the stress and the complex moduli

$$S_\alpha(\omega) := \frac{2}{\epsilon_1} \frac{\omega}{2\pi} \int_0^{\frac{2\pi}{\omega}} \sigma_s(t) \sin(\omega t) dt = -(\pi \epsilon_1^2 \omega)^{-1} \int_0^{\frac{2\pi}{\omega}} \sigma_s(t) \epsilon(t) dt \quad (3.74)$$

$$L_\alpha(\omega) := \frac{2}{\epsilon_1} \frac{\omega}{2\pi} \int_0^{\frac{2\pi}{\omega}} \sigma_{SS}(t) \cos(\omega t) dt = (\pi \epsilon_1^2)^{-1} \int_0^{\frac{2\pi}{\omega}} \sigma_{SS}(t) \dot{\epsilon}(t) dt \quad (3.75)$$

which allows us to calculate these moduli from experimental data.

Prony's series form is generally chosen for the viscoelastic kernels, i.e.

$$\frac{k_\alpha(t)}{k_\alpha^0} = k_\alpha(t) = 1 + \sum_{i=1}^N k_i^\alpha \left(\exp^{-\frac{t}{\tau_i^\alpha}} - 1 \right) \quad (3.76)$$

where k_α^0 is the modulus (shear or bulk) in the reference configuration. The normalized storage and loss moduli become:

$$\frac{S_\alpha(\omega)}{k_\alpha^0} = 1 - \sum_{i=1}^N k_i^\alpha + \sum_{i=1}^N \frac{k_i^\alpha \tau_i^{\alpha 2} \omega^2}{1 + \tau_i^{\alpha 2} \omega^2} \quad (3.77)$$

$$\frac{L_\alpha(\omega)}{k_\alpha^0} = \sum_{i=1}^N \frac{k_i^\alpha \tau_i^\alpha \omega}{1 + \tau_i^{\alpha 2} \omega^2} \quad (3.78)$$

3.4.3 Some Remarks on Energy Dissipation

Dissipation in materials with memory is strictly related to the structure of the viscoelastic kernel.

To investigate more thoroughly this point, let us consider an incompressible isotropic material following the constitutive relation (3.61) subjected to the dynamic oscillation (3.67). For such a material the volumetric part of the stress is not constitutively assigned and the average rate of working per unit volume in the steady state oscillatory condition is:

$$\begin{aligned} E_d(\omega, \epsilon_1) &= \frac{\omega}{2\pi} \int_0^{\frac{2\pi}{\omega}} \sigma_s(t) \dot{\epsilon}(t) dt \\ &= \frac{1}{2} \epsilon_1^2 \omega L(\omega) \end{aligned} \quad (3.79)$$

Equation (3.79) furnishes an alternative definition of loss modulus and contributes to explain better the relation with the dissipation.

Assuming, once more, for the viscoelastic kernel the Prony's series expansion, one gets:

$$E_d(\omega, \epsilon_1) = \frac{1}{2} \epsilon_1^2 k_0 \sum_{i=1}^N \frac{k_i \tau_i \omega^2}{1 + \tau_i^2 \omega^2} \quad (3.80)$$

hence $E_d(\omega, \epsilon_1)$ attains its maximum E_M for $\omega \rightarrow \infty$, that is:

$$E_M = \lim_{\omega \rightarrow \infty} E_d(\omega, \epsilon_1) = \frac{1}{2} \epsilon_1^2 k_0 \sum_{i=1}^N \frac{k_i}{\tau_i} \quad (3.81)$$

The value of the maximum amount of energy is strictly related to the time behavior of the viscoelastic kernel $k(t)$; indeed, since

$$k(t) = k_0 \left[1 + \sum_{i=1}^N k_i \left(\exp^{-\frac{t}{\tau_i}} - 1 \right) \right], \quad (3.82)$$

the time derivative of (3.82) around the initial time instant is:

$$\left. \frac{\partial k(t)}{\partial t} \right|_{t=0} = -G_0 \sum_{i=1}^N \frac{k_i}{\tau_i} \quad (3.83)$$

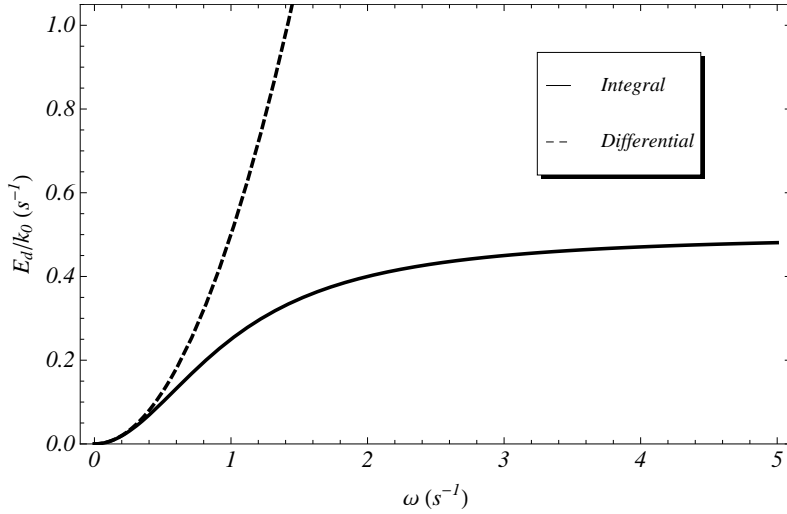


Figure 3.1 Average rate of working per unit volume normalized with respect to k_0 for $k_1 = 1$, $\tau_1 = 1$, $\eta = 1$ and $\epsilon_1 = 1$.

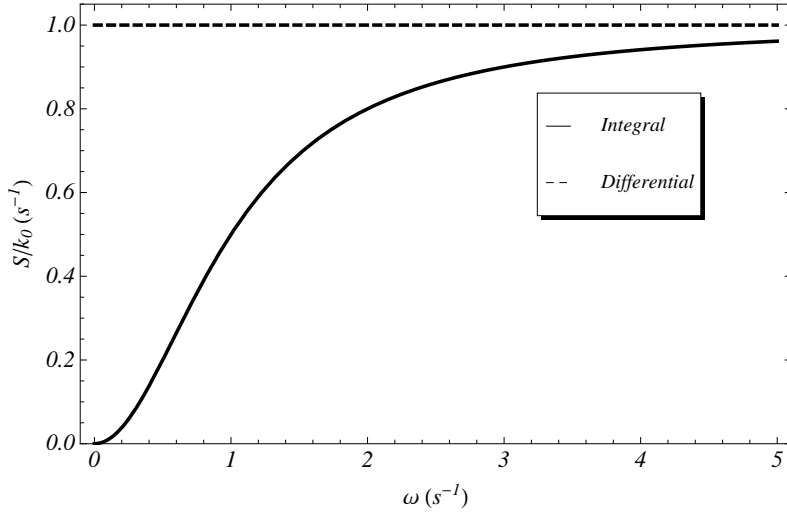


Figure 3.2 Storage modulus normalized with respect to k_0 for $k_1 = 1$, $\tau_1 = 1$ and $\eta = 1$.

Comparison between equation (3.80) and (3.83) shows us that for linear viscoelastic materials the average rate of working increases as fast as the memory fades.

This result can be compared with the case of differential viscoelasticity, which can be considered the limit case of a material with instantaneous memory. The stress-strain constitutive relation is:

$$\sigma(t) = k_0 \epsilon(t) + \eta \dot{\epsilon}(t) \tag{3.84}$$

where k_0 , η ($k_0 > 0$, $\eta > 0$) are material constants. In this case the average rate of working is:

$$E_d(\omega, \epsilon_1) = \frac{\eta}{2} \epsilon_1^2 \omega^2 \tag{3.85}$$

that differs considerably from (3.80), as reported in figure (3.1).

Differences between (3.80) and (3.85) reflect on the different storage and loss moduli behaviors (Figs. (3.2) and (3.3)).

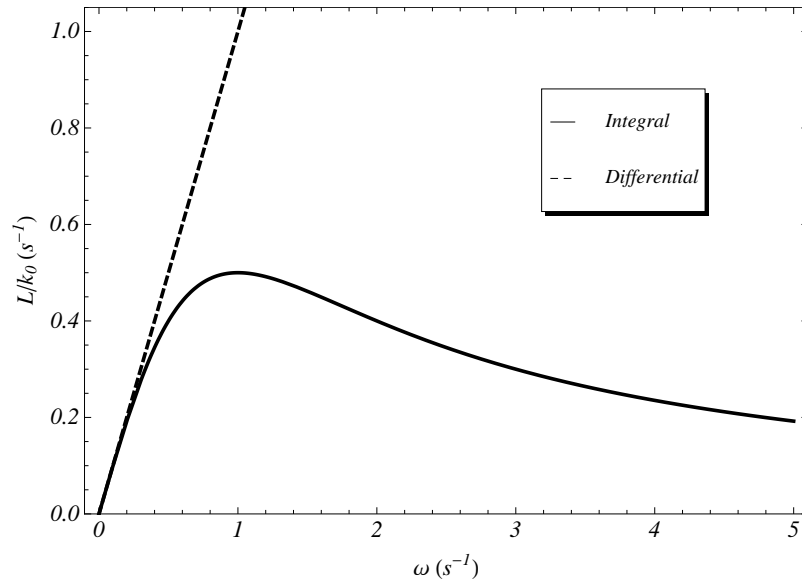


Figure 3.3 Loss modulus normalized with respect to k_0 for $k_1 = 1$, $\tau_1 = 1$ and $\eta = 1$.

3.5 Nonlinear Dynamic Moduli

The relation between loss modulus and dissipated energy indicates how to extend the definitions of dynamic moduli to nonlinear viscoelastic models. For small strain and assumed linear viscoelastic stress-deformation model, the stress response is monochromatic at the same frequency of sinusoidal input. However, real world loading conditions do not comply with this linear assumption, since modes at multiple frequencies are also excited. Therefore, the assumptions underlying equation (3.71) are no longer valid, requiring the introduction of a more general definition.

Experimental evidence showing the variation of the dynamic moduli with respect to the frequency for carbon black-filled rubber (Osanaiye, 1996), a polyurethane matrix (Gottenberg & Christensen, 1964) and mozzarella cheese (Singh *et al.*, 2006) are displayed in Fig. 3.4.

When assessed at the lowest frequencies, both the storage and loss moduli of all the materials considered depend linearly on the frequency. For carbon black-filled rubber this behavior has been reported by a number of different researchers (Lee & Kim, 2001; Luo *et al.*, 2010). In particular, Luo *et al.* use the empirical Kraus model endowed with a set of parameters varying linearly with the frequency, in order to achieve an adequate match with the experimental data. However, such an empirical relation cannot be derived from any known constitutive equation. Consequently, the possibility of introducing a stress-strain constitutive relation able to reproduce the linear dependence of the dynamic moduli at low frequencies has been investigated. Because, the linear viscoelastic model (3.65) is unable to reproduce this behavior, a simple nonlinear model may be appropriate?

In particular, three different classes of nonlinear constitutive equation have been considered: (i) elastic, (ii) differential viscoelastic and (iii) integral viscoelastic. Although (i) cannot account for dissipative effects, the derivation of the dynamic moduli in this case was useful for the calculation involving models (ii) and (iii) which, instead, are generally used to describe materials showing relevant hysteresis losses. Commonly employed constitutive equations belonging to the class (i) are the Neo-Hooke and Mooney-Rivlin hyperelastic models (see, e.g., Hartmann, 2001b). The so-called Mooney-Rivlin viscoelastic material (Beatty & Zhou, 1991) and the incompressible version of the model proposed by Landau & Lifshitz (1986) belong to class (ii). Finally, most of the nonlinear integral viscoelastic models fit within class (iii) (see

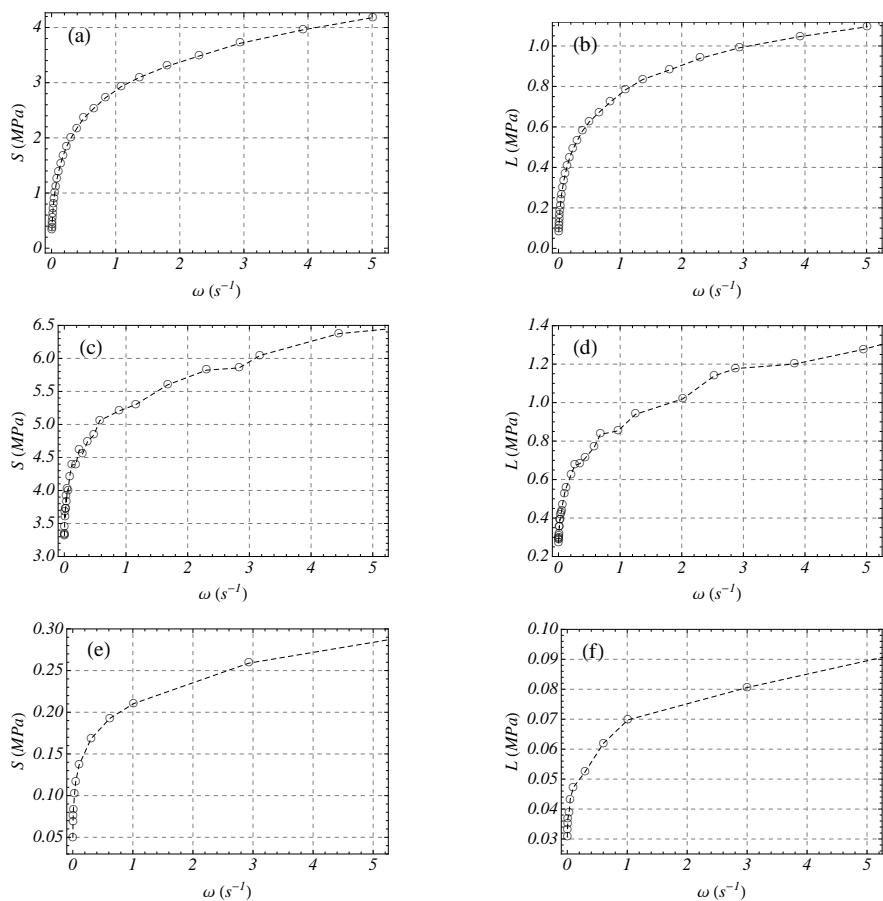


Figure 3.4 Frequency dependence of the storage and loss moduli for different materials: (a)-(b) carbon black-filled rubber (Osanaïye, 1996); (c)-(d) polyurethane matrix containing salt and aluminum powder (Gottenberg & Christensen, 1964); (e)-(f) mozzarella cheese (Singh *et al.*, 2006).

Chap. 4).

3.5.1 Definitions

Most of the solid materials, under a suddenly applied deformation, exhibit a decaying stress as function of time, while they react to a fast load with a time increasing deformation. Both these phenomena are consequences of the fading memory properties of the material.

Fading memory mathematically translates into a constitutive relation for which the stress at time t , say $\sigma(t)$, depends on the deformation history up to time t , say ε^t , i.e.,

$$\sigma(t) = \mathfrak{F}[\varepsilon^t]. \quad (3.86)$$

It should be noted that the function \mathfrak{F} depends upon the time only implicitly through ε . Indeed, this corresponds to the assumption that the material is non-aging.

The idea of fading memory is rendered mathematically through the relaxation property (see, for instance, Fabrizio *et al.*, 1995). If ε_1 and ε_2 are two deformations such that $\varepsilon_1(t) = \varepsilon_2(t)$ for each $t \geq t_0$, then the relaxation property states that

$$\lim_{t \rightarrow \infty} \{ \mathfrak{F}[\varepsilon_1^t] - \mathfrak{F}[\varepsilon_2^t] \} = 0. \quad (3.87)$$

In the case of dynamic motion, let

$$u(t) = u_0 + u_1 \sin(\omega t) \quad (3.88)$$

be the longitudinal displacement in an uniaxial deformation from which the nonlinear Lagrangian strain is as follows

$$\varepsilon(t) = \varepsilon_0 + \varepsilon_1 \sin(\omega t) \quad (3.89)$$

obtained by dividing $u(t)$ by the reference length l_0 . Therefore, by assuming into (3.87) $\varepsilon_1(t) = \varepsilon(t)$ and $\varepsilon_2(t) = \varepsilon(t + T)$, with $T = 2\pi/\omega$, then for each t , $\varepsilon_1(t) = \varepsilon_2(t)$ and Eq. (3.87); thus,

$$\lim_{t \rightarrow \infty} \{ \mathfrak{F}[\varepsilon^t] - \mathfrak{F}[\varepsilon^{t+T}] \} = 0, \quad (3.90)$$

and the steady state stress, say $\sigma_s(t)$, arising from deformation (3.89) is T -periodic.

Therefore, fading memory properties assure that the material response to a harmonic deformation gets into a periodic steady state.

Under weak regularity assumptions, e.g., $\sigma_s(t) \in L^2[-\frac{\pi}{\omega}, \frac{\pi}{\omega}]$, the Fourier series of $\sigma_s(t)$ uniformly converges:

$$\sigma_s(t) = \frac{\sigma_0^C}{2} + \sum_{i=1}^{\infty} [\sigma_i^S \sin(i\omega t) + \sigma_i^C \cos(i\omega t)], \quad (3.91)$$

being σ_i^S and σ_i^C the Fourier coefficients of $\sigma_s(t)$ defined as

$$\begin{aligned} \sigma_i^S &= \frac{\omega}{\pi} \int_{-\pi/\omega}^{\pi/\omega} \sigma_s(t) \sin(i\omega t) dt, & i = 1, 2, \dots, \\ \sigma_i^C &= \frac{\omega}{\pi} \int_{-\pi/\omega}^{\pi/\omega} \sigma_s(t) \cos(i\omega t) dt, & i = 1, 2, \dots. \end{aligned} \quad (3.92)$$

For materials whose constitutive response is linear, only the first coefficients, i.e., $i = 1$, in the series (3.91) are non zero. In the nonlinear case, however, the stress arising from the harmonic displacement (3.88) is no longer monochromatic since components at multiple of the

input frequency are excited. Therefore, by considering the steady state stress response (3.91), the definition of dynamic moduli can be extended to the case of a nonlinear stress-strain relation, viz.

$$\begin{aligned} S &= \widehat{S}(\varepsilon_0, \varepsilon_1, \omega) := \frac{1}{\varepsilon_1} \frac{\omega}{\pi} \int_{-\pi/\omega}^{\pi/\omega} \sigma_s(\tau) \sin(\omega\tau) \, ds = \frac{\sigma_1^S}{\varepsilon_1}, \\ L &= \widehat{L}(\varepsilon_0, \varepsilon_1, \omega) := \frac{1}{\varepsilon_1} \frac{\omega}{\pi} \int_{-\pi/\omega}^{\pi/\omega} \sigma_s(\tau) \cos(\omega\tau) \, ds = \frac{\sigma_1^C}{\varepsilon_1}. \end{aligned} \quad (3.93)$$

The definitions given in Eqs. (3.93) are consistent with those introduced in the linear context and, hence, the same nomenclature of storage and loss moduli has been adopted.

By introducing the stationary average rate of working over a cycle, i.e.,

$$\Psi = \widehat{\Psi}(\varepsilon_0, \varepsilon_1, \omega) := \lim_{t \rightarrow \infty} \frac{\omega}{\pi} \int_t^{t+2\pi/\omega} \sigma(\tau) \dot{\varepsilon}(\tau) \, d\tau, \quad (3.94)$$

the loss modulus can be expressed in terms of Ψ as $L = 2\Psi/(\omega \varepsilon_1^2)$.

Elasticity

In the general framework of materials with memory, nonlinear elasticity can be considered a subset of this theory aimed at describing materials for which memory effects can be ignored. Indeed, stress depends only upon the current value of strain. Although elastic constitutive equations are not used to describe the dynamic behavior of elastomers, since they cannot account for dissipated energy, for the sake of completeness the dynamic moduli have also been derived.

The constitutive equation for a Cauchy elastic material reads as

$$\sigma(t) = f[\varepsilon(t)] \quad (3.95)$$

where f is a nonlinear smooth function of $\varepsilon(t)$.

If $\varepsilon(t)$ is T -periodic, i.e., periodic of period T , then $\sigma(t)$ is also T -periodic:

$$\sigma(t+T) = f[\varepsilon(t+T)] = f[\varepsilon(t)] = \sigma(t), \quad (3.96)$$

and, therefore, $\sigma(t) = \sigma_s(t)$ being the Fourier series (3.91) convergent.

Through the change of coordinates $s = \omega\tau/\pi$, the definitions (3.93) become

$$\begin{aligned} S &= \widehat{S}(\varepsilon_0, \varepsilon_1) = \frac{1}{\varepsilon_1} \int_{-1}^1 f[\varepsilon_0 + \varepsilon_1 \sin(\pi s)] \sin(\pi s) \, ds, \\ L &= \widehat{L}(\varepsilon_0, \varepsilon_1) = \frac{1}{\varepsilon_1} \int_{-1}^1 f[\varepsilon_0 + \varepsilon_1 \sin(\pi s)] \cos(\pi s) \, ds, \end{aligned} \quad (3.97)$$

which explicate that, for elastic constitutive equations, both the storage and loss moduli are frequency independent.

Under stronger regularity assumptions on f , e.g., f is an analytic function of ε , the Taylor's series around the prestrained configuration $\varepsilon = \varepsilon_0$ ($\varepsilon_1 = 0$) converges to f , i.e.,

$$\sigma_s(t) = f[\varepsilon_0 + \varepsilon_1 \sin(\omega t)] = \sum_{i=0}^{\infty} \frac{\varepsilon_1^i}{i!} \widetilde{f}_i(\varepsilon_0) \sin^i(\omega t), \quad (3.98)$$

with $\tilde{f}_i(\varepsilon_0) = [\partial^i f / \partial \varepsilon^i]_{\varepsilon_1=0}$. Therefore, Eqs. (3.97) become

$$\begin{aligned} S &= \sum_{i=0}^{\infty} \frac{\varepsilon_1^{i-1}}{i!} \tilde{f}_i(\varepsilon_0) \int_{-1}^1 \sin^{i+1}(\pi s) ds = \sum_{i=0}^{\infty} \tilde{f}_i(\varepsilon_0) \frac{\varepsilon_1^{i-1}}{i!} \frac{1 + (-1)^{i+1}}{\sqrt{\pi}} \frac{\Gamma(1 + \frac{i}{2})}{\Gamma(\frac{3+i}{2})} \\ L &= \sum_{i=0}^{\infty} \frac{\varepsilon_1^{i-1}}{i!} \tilde{f}_i(\varepsilon_0) \int_{-1}^1 \sin^i(\pi s) \cos(\pi s) ds = 0 \end{aligned} \quad (3.99)$$

where $\Gamma(\cdot)$ is the Euler gamma function. It should be noted that to write Eqs. (3.99), the infinite summation has been taken out of the integral since the series (3.98) satisfies the hypothesis of the Dominated Convergence Theorem (see, e.g., Kolmogorov, 1999).

Equations (3.99) state that in the purely elastic case, i.e., for a material described by the constitutive relation (3.95), the loss modulus and the dissipated energy Ψ are zero. Indeed, this result is in accordance with the definition of *hyperelastic* materials for which the work done by body and surface forces is converted into kinetic energy and stored elastic energy, without dissipation.

Equations (3.99) allow the storage modulus to be obtained simply by computing the derivatives of f whatever constitutive equation in the form (3.95) is chosen.

Differential Viscoelasticity

The constitutive relation of a viscoelastic material is:

$$\sigma(t) = g[\varepsilon, \dot{\varepsilon}]. \quad (3.100)$$

Hereafter, a superimposed dot will represent the first-order time derivative.

The constitutive equation (3.100) is generally referred to as differential viscoelasticity to distinguish it from the integral formulation introduced in the following. The substantive “grade 1” is also used referring to (3.100) for emphasizing the dependence of σ on the strain rate only (and not on the higher order time derivatives).

As in the case of a purely elastic material, if $\varepsilon(t)$ is T -periodic, also $\sigma(t)$ is T -periodic, e.g.,

$$\sigma(t+T) = g[\varepsilon(t+T), \dot{\varepsilon}(t+T)] = g[\varepsilon(t), \dot{\varepsilon}(t)] = \sigma(t); \quad (3.101)$$

therefore $\sigma_s(t) = \sigma(t)$.

If the function g is analytic with respect to ε_1 , Taylor’s series around the prestrained configuration $\varepsilon = \varepsilon_0$ ($\varepsilon_1 = 0$) coincides with g (see the Appendix); therefore, the storage and loss modulus become

$$\begin{aligned} S &= \hat{S}(\varepsilon_0, \varepsilon_1, \omega) = \sum_{i=0}^{\infty} \sum_{n=0}^i \frac{\omega^{i-n} \varepsilon_1^i}{n!(i-n)!} \tilde{g}_i(\varepsilon_0) \int_{-1}^1 \sin(\pi s)^{n+1} \cos(\pi s)^{i-n} ds, \\ L &= \hat{L}(\varepsilon_0, \varepsilon_1, \omega) = \sum_{i=0}^{\infty} \sum_{n=0}^i \frac{\omega^{i-n} \varepsilon_1^i}{n!(i-n)!} \tilde{g}_i(\varepsilon_0) \int_{-1}^1 \sin(\pi s)^n \cos(\pi s)^{i-n+1} ds, \end{aligned} \quad (3.102)$$

with $\tilde{g}_i(\varepsilon_0) = [(\partial^n g / \partial \varepsilon^n) (\partial^{i-n} g / \partial \varepsilon^{i-n})]_{\varepsilon_1=0}$.

The derivatives with respect to the frequency for $\omega \rightarrow 0$ are

$$\begin{aligned} \left. \frac{\partial S}{\partial \omega} \right|_{\omega=0} &= \sum_{i=1}^{\infty} \frac{\varepsilon_1^i}{(i-1)!} \tilde{g}_i(\varepsilon_0) \int_{-1}^1 \sin(\pi s)^i \cos(\pi s) ds = 0, \\ \left. \frac{\partial L}{\partial \omega} \right|_{\omega=0} &= \sum_{i=1}^{\infty} \frac{1}{2\sqrt{\pi}} \frac{\varepsilon_1^{2i-1}}{(2i-2)!} \tilde{g}_{2i-1}(\varepsilon_0) \frac{\Gamma(i - \frac{1}{2})}{\Gamma(i+1)}. \end{aligned} \quad (3.103)$$

Integral Viscoelasticity

To take into account the fading memory properties of the material, a hereditary integral should be introduced in the constitutive equation (see, e.g., [Christensen, 2003](#); [Drapaca et al., 2007](#); [Tschoegl, 1989](#)). A convenient formulation to represent most of the nonlinear viscoelastic models used in the literature is

$$\sigma(t) = f[\varepsilon, \dot{\varepsilon}] + l[\varepsilon, \dot{\varepsilon}] \int_{-\infty}^t \dot{k}(t-s) h[\varepsilon, \dot{\varepsilon}] ds \quad (3.104)$$

where $k(t)$ is the viscoelastic kernel. In the linear case, i.e., $f[\varepsilon, \dot{\varepsilon}] = k_0 \varepsilon(t)$, $l[\varepsilon, \dot{\varepsilon}] = 1$ and $h[\varepsilon, \dot{\varepsilon}] = \varepsilon(t)$, the conditions on $k(t)$ to satisfy the principle of thermodynamics are well-known (see, for example, [Hanyga, 2005](#)). They state that

$$\begin{aligned} k(t) &\geq 0, & \dot{k}(t) &\leq 0, & \ddot{k}(t) &\geq 0, \\ \lim_{t \rightarrow \infty} k(t) &= k_\infty < +\infty, & \lim_{t \rightarrow \infty} \dot{k}(t) &= 0 \end{aligned} \quad (3.105)$$

and, hence, $k_\infty < k_0$, with $k_0 = k(0)$.

Constitutive equation (3.104) assures that the stress arising from a T-periodic strain is T-periodic, viz.

$$\begin{aligned} \sigma(t+T) &= f[\varepsilon(t+T), \dot{\varepsilon}(t+T)] \\ &+ l[\varepsilon(t+T), \dot{\varepsilon}(t+T)] \int_0^{+\infty} \dot{k}(\tau) h[\varepsilon(t+T-\tau), \dot{\varepsilon}(t+T-\tau)] d\tau = \\ &= f[\varepsilon(t), \dot{\varepsilon}(t)] + l[\varepsilon(t), \dot{\varepsilon}(t)] \int_0^{+\infty} \dot{k}(\tau) h[\varepsilon(t-\tau), \dot{\varepsilon}(t-\tau)] d\tau = \sigma(t), \end{aligned} \quad (3.106)$$

and, hence, $\sigma_s(t) = \sigma(t)$. Therefore, if the Fourier series of the functions f , g and l are absolutely convergent, then, by means of the Cauchy formula for the product between two series (see, e.g., [Rudin, 1976](#)), the constitutive equation (3.104) can be expressed as

$$\sigma_s(t) = \frac{\tilde{\sigma}_0}{2} + \sum_{i=1}^{+\infty} [\tilde{\sigma}_i^S \sin(i\omega t) + \tilde{\sigma}_i^C \cos(i\omega t)] \quad (3.107)$$

with

$$\begin{aligned} \tilde{\sigma}_0 &= \hat{\sigma}_0(f_0, l_0, H_0), \\ \tilde{\sigma}_i^S &= \hat{\sigma}_i^S(f_i^S, f_i^C, l_i^S, l_i^C, H_i^S, H_i^C; \omega, t), \\ \tilde{\sigma}_i^C &= \hat{\sigma}_i^C(f_i^S, f_i^C, l_i^S, l_i^C, H_i^S, H_i^C; \omega, t), \end{aligned} \quad (3.108)$$

and

$$\begin{aligned} H_0 &= h_0(k_\infty - k_0), & k_0 &< \infty, \\ H_i^S &= h_i^S \int_0^{+\infty} \dot{k}(s) \cos(i\omega s) ds - h_i^C \int_0^{+\infty} \dot{k}(s) \sin(i\omega s) ds, \\ H_i^C &= -h_i^S \int_0^{+\infty} \dot{k}(s) \sin(i\omega s) ds + h_i^C \int_0^{+\infty} \dot{k}(s) \cos(i\omega s) ds. \end{aligned} \quad (3.109)$$

The existence of the integrals in (3.109) is assured by the asymptotic properties (3.105) of the viscoelastic kernel.

In Eqs. (3.108)-(3.109) f_i^S , f_i^C , l_i^S , l_i^C , h_i^S and h_i^C are the Fourier coefficients of the functions f , l and h obtained by Eqs. (3.92); therefore all these coefficients depend on the frequency, but this dependence has been omitted in (3.109) for the sake of brevity.

Equation (3.107) explicates the dependence of the harmonic stress upon the oscillatory strain for the nonlinear constitutive equation (3.104). The dynamic moduli are obtained by a standard projection of (3.107) over $\sin(\omega t)$ and $\cos(\omega t)$. After some manipulations, the result is

$$S = \widehat{S}(\varepsilon_0, \varepsilon_1, \omega) = \frac{1}{\varepsilon_1} \left[f_1^S + \frac{l_0}{2} H_1^S + \frac{l_1^S}{2} H_0 \right] + \frac{1}{2\varepsilon_1} \sum_{i=1}^{+\infty} [-l_i^S H_{i+1}^C + l_{i+1}^S H_i^C] \\ + \frac{1}{2\varepsilon_1} \sum_{i=1}^{+\infty} [l_i^C H_{i+1}^S - l_{i+1}^C H_i^S] \quad (3.110)$$

$$L = \widehat{L}(\varepsilon_0, \varepsilon_1, \omega) = \frac{1}{\varepsilon_1} \left[f_1^C + \frac{l_0}{2} H_1^C + \frac{l_1^C}{2} H_0 \right] + \frac{1}{2\varepsilon_1} \sum_{i=1}^{+\infty} [l_i^S H_{i+1}^S + l_{i+1}^S H_i^C] \\ + \frac{1}{2\varepsilon_1} \sum_{i=1}^{+\infty} [l_i^C H_{i+1}^S + l_{i+1}^C H_i^S]$$

If f , l and h are analytic functions of ε_1 , Equations (3.110) allow the derivative of the storage modulus for $\omega \rightarrow 0$ to be calculated, viz.

$$\left. \frac{\partial S}{\partial \omega} \right|_{\omega=0} = \frac{k_\infty - k_0}{2\varepsilon_1} \sum_{i=1}^{\infty} \left[-\frac{\partial l_i^S}{\partial \omega} h_{i+1}^C - l_i^S \frac{\partial h_{i+1}^C}{\partial \omega} + \frac{\partial l_{i+1}^S}{\partial \omega} h_i^C + l_{i+1}^S \frac{\partial h_i^C}{\partial \omega} \right]_{\omega=0} + \\ \frac{k_\infty - k_0}{2\varepsilon_1} \sum_{i=1}^{\infty} \left[\frac{\partial l_i^C}{\partial \omega} h_{i+1}^S + l_i^C \frac{\partial h_{i+1}^S}{\partial \omega} - \frac{\partial l_{i+1}^C}{\partial \omega} h_i^S - l_{i+1}^C \frac{\partial h_i^S}{\partial \omega} \right]_{\omega=0}. \quad (3.111)$$

It can be easily proven that the coefficients $h_i^S(0)$ and $l_i^S(0)$ ($h_i^C(0)$ and $l_i^C(0)$) are zero if i is even (odd); furthermore, the derivatives $\frac{\partial h_i^S}{\partial \omega}(0)$ and $\frac{\partial l_i^S}{\partial \omega}(0)$ ($\frac{\partial h_i^C}{\partial \omega}(0)$ and $\frac{\partial l_i^C}{\partial \omega}(0)$) are zero if i is odd (even). Therefore, for each i the square bracketed term vanish and $\frac{\partial S}{\partial \omega}(0) = 0$.

3.5.2 One-dimensional model

In the previous paragraph some inconsistencies between the dynamic moduli, following from definitions (3.93), and the experimental data, collated from the literature, were highlighted. In particular, while the results of experiments display a non-zero derivative of the storage modulus for ω which tends to zero, all the constitutive equations considered result in an horizontal tangent at $\omega = 0$. This frequency behavior produces a relevant error in the fitting at lowest frequencies and is an important drawback as in many operative conditions the material is subjected to strain rate corresponding to frequencies lower than 200 s^{-1} .

In order to obtain an accurate match with the experimental data, a constitutive equation not belonging to the classes (i), (ii) and (iii) must be considered.

As the basis for an appropriate constitutive equation, the linear viscoelastic model already introduced in Sec. 3.4 was used, i.e.,

$$\sigma(t) = k_0 \varepsilon(t) + \int_{-\infty}^t \dot{k}(t-s) \varepsilon(s) ds, \quad (3.112)$$

and, as a consequence, the constitutive functions f , h and l are

$$f[\varepsilon, \dot{\varepsilon}] = k_0 \varepsilon(t), \quad l[\varepsilon, \dot{\varepsilon}] = 1, \quad h[\varepsilon, \dot{\varepsilon}] = \varepsilon(t). \quad (3.113)$$

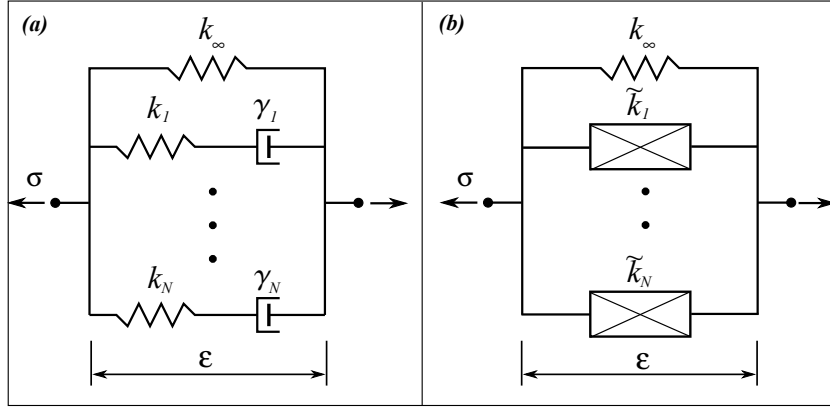


Figure 3.5 Panel (a) displays the N-terms generalized Maxwell element while panel (b) displays the modified Maxwell element with hysteretic dampers.

From Eqs. (3.110), the dynamic moduli are obtained as

$$\begin{aligned} S(\omega) &= k_0 + \int_0^{+\infty} \dot{k}(s) \cos(\omega s) ds, \\ L(\omega) &= - \int_0^{+\infty} \dot{k}(s) \sin(\omega s) ds. \end{aligned} \quad (3.114)$$

If the Prony's series is used to represent the viscoelastic kernel $k(t)$, viz.

$$k(t) = k_0 \left(1 - \sum_{i=1}^N k_i + \sum_{i=1}^N k_i e^{-t/\tau_i} \right), \quad \sum_{i=1}^N k_i < 1, \quad (3.115)$$

Eqs. (3.114) can be expressed in terms of characteristic amplitudes k_i and times τ_i :

$$\begin{aligned} S &= \widehat{S}(\omega, k_0, k_i, \tau_i) = k_0 \left(1 - \sum_{i=1}^N \frac{k_i}{1 + \tau_i^2 \omega^2} \right), \\ L &= \widehat{L}(\omega, k_0, k_i, \tau_i) = k_0 \left(\sum_{i=1}^N \frac{k_i \tau_i \omega}{1 + \tau_i^2 \omega^2} \right), \end{aligned} \quad (3.116)$$

and Eqs. (3.77) and (3.78) are recovered. It should be noted that in the linear case neither moduli depend on ε_0 or on ε_1 , but only on the frequency ω .

Figure 3.6 shows the frequency dependence of the storage and loss moduli for a carbon black-filled elastomer (experiments carried out by the author). In the same figure the results of the fitting obtained with model (3.116) are shown.

In order to match adequately the experimental data, some modifications of the linear model must be considered. To this end it is convenient to reformulate Eq. (3.112) in terms of its equilibrium and overstress parts. The stress can be split into two contributions, i.e.,

$$\sigma(t) = \sigma_{el}(t) + \sigma_{ov}(t) = k_\infty \varepsilon(t) + \sum_{i=1}^N \sigma_{ov}^{(i)}(t), \quad (3.117)$$

with $k_\infty = k_0(1 - \sum_{i=1}^N k_i)$. The evolution equations of the overstress terms are:

$$\dot{\sigma}_{ov}^{(i)}(t) + \frac{1}{\tau_i} \sigma_{ov}^{(i)}(t) = k_0 k_i \dot{\varepsilon}(t) \quad i = 1, \dots, N. \quad (3.118)$$

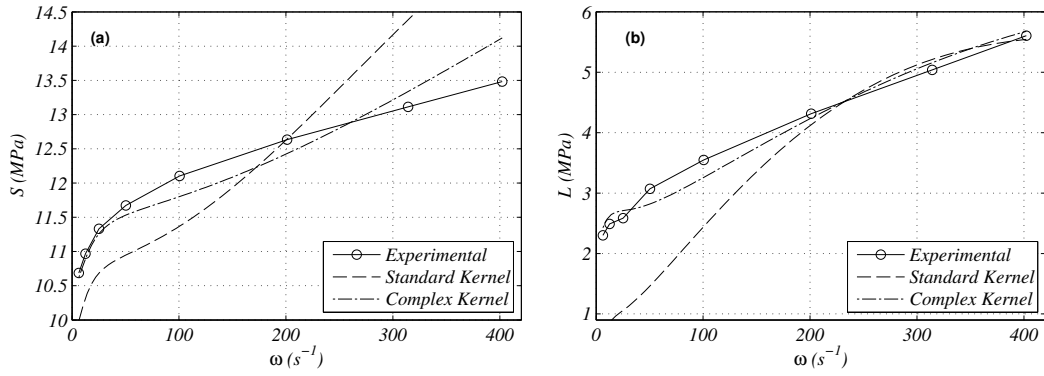


Figure 3.6 Fitting of the storage, (a), and loss, (b), moduli with the standard linear viscoelastic model (*Standard Kernel*) and with the model proposed (*Complex Kernel*).

Equations (3.117) - (3.118) are standard constitutive equations in material rheology. They correspond to a generalized Maxwell element in parallel to a spring (Fig. 3.5a). By integrating (3.118) and substituting into (3.117), the linear viscoelastic model (3.112) is recovered.

Appropriate models to describe the linear frequency dependence of dynamic moduli can be formulated by considering the constitutive equation of a linear hysteretic damper (Inaudi & Makris, 1996), which in Fourier domain reads as

$$\tilde{\sigma}(j\omega) = k [1 - j\eta \text{sign}(\omega)] \tilde{\varepsilon}(j\omega) \quad (3.119)$$

In Eq. (3.119), $\tilde{\sigma}$, $\tilde{\varepsilon}$ are the Fourier transforms of stress and deformation, while $j = \sqrt{-1}$ and η is a frequency independent loss factor; $\text{sign}(\cdot)$ is the signum function, i.e., $\text{sign}(x) = 1$ if $x > 0$, $\text{sign}(x) = -1$ if $x < 0$, $\text{sign}(x) = 0$ if $x = 0$. A time-domain representation of the element (3.119) would involve the Hilbert-transform (Inaudi & Kelly, 1995).

In order to describe the steady state response of mechanical systems subjected to harmonic deformations and, hence, attention has been focused on the frequency domain. The generalized Maxwell model, governed by the evolution equation (3.118), can be modified by introducing N hysteretic blocks in parallel, as shown in Fig. 3.5b. The constitutive equation of the i -th block is given by:

$$\frac{\tilde{\sigma}_{ov}^i(j\omega)}{\tilde{\varepsilon}(j\omega)} = j k_0 (1 + \eta_i \omega \tau_i) \frac{k_i \tau_i \omega}{1 + \omega^2 \tau_i^2} + k_0 (\omega \tau_i + \eta_i) \frac{\omega \tau_i k_i}{1 + \omega^2 \tau_i^2}, \quad (3.120)$$

which arises from the series of a hysteretic spring and dashpot. The constitutive equation of the modified Maxwell element shown in Fig. 3.5 is

$$\tilde{\sigma}(j\omega) = \tilde{\sigma}_{el}(j\omega) + \sum_{i=1}^N \tilde{\sigma}_{ov}^i(j\omega), \quad (3.121)$$

with $k_\infty = k_0 \left(1 - \sum_{i=1}^N k_i\right)$. Indeed, the constitutive assumptions (3.120) are equivalent to introduce a complex stiffness \tilde{k} into Eq. (3.112). As a consequence, the hypotheses underlying Eqs. (3.105) are no longer valid.

In the case of linear stress-strain constitutive model, the storage and loss moduli are obtained as the real and imaginary parts of the frequency response function (Inaudi & Makris,

1996), i.e.,

$$\begin{aligned} S(\omega) &= k_0 \left[1 - \sum_{i=1}^N k_i + \sum_{i=1}^N (\omega \tau_i + \eta_i) \frac{\omega \tau_i k_i}{1 + \omega^2 \tau_i^2} \right], \\ L(\omega) &= k_0 \sum_{i=1}^N \left[(1 + \omega \eta_i \tau_i) \frac{k_i \tau_i \omega}{1 + \omega^2 \tau_i^2} \right], \end{aligned} \tag{3.122}$$

which, for $\eta_i \rightarrow 0$, coincides with the standard dynamic moduli (3.116).

The results of the fitting are shown in Fig. 3.6 for $N = 4$ hysteretic dampers in parallel with a spring. A more accurate match with the experimental data is achieved than with the standard model. Moreover, the initial slope of the storage modulus is reproduced even with a small number of parameters.

Chapter 4

Model Identification

Chapter Outline. In the first section, the standard identification procedure of the material parameters for a nonlinear viscoelastic (NLV) constitutive equation is discussed thoroughly. This routine relies on the separate identification of the “instantaneous” (elastic) and “dissipative” (inelastic) parts. The advantages and disadvantages of this approach are evaluated by considering Fung’s constitutive model. Thereafter, a joint identification of the elastic and dissipative parts is introduced. To this end, the constitutive equation is rewritten in a form suitable for encompassing all the single hereditary models. Therefore, the identification of the constitutive coefficients is reduced to the solution of a nonlinear optimization problem. An iterative technique allowed the refining of the relaxation times around the most significant time constants. The results of the compression tests with cylindrical carbon black-filled rubber specimens, already summarized in Chapter 1, are here used to compare the main features of each model.

4.1 Position of the Problem

Owing to the importance of elastomer components in engineering applications, the accurate prediction of their mechanical behavior under operational conditions is a relevant subject in industry. Often the material is exposed to different short- and long-time loads simultaneously. Thus it is necessary to provide constitutive models able to predict the material response for several loading conditions. Moreover, the models must be endowed with a set of parameters which accurately represents the material behaviour over the entire working range.

Despite the Mullin's effect, in most rubber-like materials no further damage can be observed, even at large deformations. The consideration of pre-damaged materials, which are in a stable stationary state with respect to the Mullin's effect, leads to the choice of a finite viscoelastic constitutive equation.

In the following, the QLV model introduced by Fung (1972) is used to illustrate a possible procedure for the material parameters identification. Fung's model reads as (see Section 3.3.1)

$$\begin{aligned}\mathbf{T}(t) &= \mathbf{T}^e(t) + \int_0^t \dot{k}(t-s)\mathbf{T}^e(s) ds, \\ \mathbf{T}^e(t) &= \phi_0(t)\mathbf{I} + \phi_1(t)\mathbf{C}(t) + \phi_{-1}(t)\mathbf{C}^{-1}(t),\end{aligned}\tag{4.1}$$

where $\phi_\Gamma(t) = \phi_\Gamma(I_1(t), I_2(t), I_3(t))$, $\Gamma = -1, 0, 1$, is a function of the strain invariants I_1 , I_2 and I_3 at time t .

The standard identification algorithm relies on three successive steps:

1. the identification of the "instantaneous" response $\mathbf{T}^e(t)$;
2. the solution of the linear integral equation for $k(t)$;
3. the identification of the viscoelastic kernel parameters, e.g., the coefficients g_i , τ_i in the case of the Prony series for $k(t)$.

In the next sections each of the steps 1, 2 and 3 are discussed thoroughly. However, this procedure requires experimental measurements which are very difficult to perform: a very fast loading ramp is necessary for the identification of the instantaneous stress \mathbf{T}^e , while the viscoelastic kernel necessitates very long relaxation tests. As a consequence of the restrictions imposed by the experimental equipment on the maximum exerting strain rate, the experimental procedure actually employed in the laboratory leads to approximations which are not satisfactory when nonlinear viscoelastic materials are involved.

In order to overcome these limitations, a combined experimental-numerical analysis based on an identification routine, both of the long- and short-time material response, is presented. This procedure actually generalizes the results in Knauss & Zhao (2007) to nonlinear constitutive equations.

4.2 Standard Identification Procedure

4.2.1 Instantaneous Response

The "instantaneous" stress $\mathbf{T}^e(t)$ in equation (4.1) is by definition the tensile stress instantaneously generated when a step function is imposed on the specimen.

Strict laboratory measurements of $\mathbf{T}^e(t)$ according to this definition are difficult, because at a sudden application of the load, transient waves are induced in the specimen and the resulting stress response measurement will be confused by these elastic waves. However, if

the relaxation function $k(t)$ is a continuous function, then $\mathbf{T}^e(t)$ might be estimated by the tensile stress response in a loading experiment with a sufficiently high rate of loading.

In order to justify this procedure, let us consider an uniaxial deformation $\lambda(t)$ produced by an uniaxial stress state ($T_{11}(t) = T(t)$, $T_{22}(t) = T_{33}(t) = 0$). Now, if by some monotonic process, $\lambda(t)$ is increased in a time interval τ from 0 to $\lambda(\tau) = \bar{\lambda}$, then by integrating by parts Eq. (4.1) at time $t = \tau$, the result is:

$$T(\tau) = T^e[\bar{\lambda}] + \int_0^\tau \dot{k}(s) T^e[\lambda(\tau - s)] ds. \quad (4.2)$$

Since the relaxation function $k(t)$ is a continuously varying decreasing function, as s increases from 0 to τ , the integrand never changes sign; by the mean theorem there exists a $\xi \in [0, \tau]$ such that

$$T(\tau) = T^e[\bar{\lambda}] + \tau \dot{k}(\xi) T^e[\lambda(\tau - \xi)]. \quad (4.3)$$

Therefore, being $k(t) \in C^1(\mathbb{R})$ and $\xi \rightarrow 0$ as $\tau \rightarrow 0$, one gets

$$\left| \dot{k}(\xi) \right| \ll \frac{1}{\tau} \Rightarrow T(\tau) \cong T^e[\bar{\lambda}], \quad (4.4)$$

which allows the integral term into (4.2) to be ignored. This result confirms that, in order to model correctly the elastic part T^e , very fast loading/unloading experiments should be preferred to quasi-static tests. Indeed, in the latter case, the material response would involve both elastic and dissipative effects.

If $k(t)$ is represented in terms of the Prony series, e.g.,

$$k(t) = \sum_{i=1}^N k_i + \sum_{i=1}^N (1 - k_i) e^{-\frac{t}{\tau_i}}, \quad \sum_{i=1}^N k_i < 1, \quad (4.5)$$

the inequality in (4.4) yields the maximum value of τ , i.e., the minimum strain rate $\bar{\lambda}/\tau$, for which T^e can be estimated as the tensile stress response T . In particular, since $k(t)$ is a completely monotonic decreasing function, the result is

$$\left| \dot{k}(\xi) \right| \leq \left| \dot{k}(0) \right| = \sum_{i=1}^N \frac{k_i}{\tau_i} < \frac{N}{\tau_{min}}, \quad (4.6)$$

which provides a sufficient condition for the inequality (4.4) to be valid, i.e.,

$$\tau \ll \frac{\tau_{min}}{N}. \quad (4.7)$$

Inequality (4.7) states that the duration in time taken for the ramp to reach the stretch $\bar{\lambda}$ should be much less than the minimum characteristic time of the material. However, since rubber is well-known to have characteristic times of the order of a few milliseconds, or even less, laboratory measurements of T^e are very difficult.

For modeling purposes, a common choice is to assume for T^e an hyperelastic constitutive equation (Hoo Fatt & Ouyang, 2007; Pena *et al.*, 2007; Shim *et al.*, 2004; Yang & Shim, 2004). The relation between the stress and the strain is indirectly specified through the relation between the internal energy and the strain (Rivlin & Saunders, 1952), i.e.,

$$W(I_1, I_2) = \sum_{m=0}^M \sum_{n=0}^N c_{mn} (I_1 - 3)^m (I_2 - 3)^n, \quad (4.8)$$

therefore, specifying the constitutive parameters c_{mn} into (4.8). As a consequence of the incompressibility of rubber, the functional W depends only upon the first and second invariants of the right-Cauchy Green strain tensor.

In the case of uniaxial stretch of a thin sheet of material, the constitutive law for T^e can be expressed in terms of the stretch λ and of the strain energy function W as follows (see Chap. 2),

$$T^e = \lambda^{-1} \frac{\partial W}{\partial \lambda}; \quad (4.9)$$

however, from an experimental point of view, it is more convenient to express (4.9) in terms of the nominal stress, i.e., force over reference area, which is the actual measured quantity, viz.

$$\Pi^e = \frac{\partial W}{\partial \lambda} = \sum_{m=0}^M \sum_{n=0}^N c_{mn} \phi(m, n, \lambda), \quad (4.10)$$

where ϕ is a nonlinear function of λ and of the indices m, n , e.g.,

$$\begin{aligned} \phi(m, n, \lambda) = & 2m \left(\lambda^2 + \frac{2}{\lambda} - 3 \right)^{m-1} \left(\lambda - \frac{1}{\lambda^2} \right) \left(2\lambda + \frac{1}{\lambda^2} - 3 \right)^n + \\ & + 2n \left(\lambda^2 + \frac{2}{\lambda} - 3 \right)^m \left(2\lambda + \frac{1}{\lambda^2} - 3 \right)^{n-1} \left(1 - \frac{1}{\lambda^3} \right). \end{aligned} \quad (4.11)$$

Note that, whatever choice of constitutive parameters used in (4.8), the relation between the stress and the material coefficients c_{mn} is linear.

In order to achieve a more useful form of (4.10) with respect to the identification process, it is possible to introduce the vector $\mathbf{c} \in \mathbb{R}^{mn}$ of the material coefficients, i.e.,

$$\mathbf{c}^T = \{c_{01}, \dots, c_{0n}, c_{10}, \dots, c_{1n}, \dots, c_{m0}, \dots, c_{mn}\}, \quad (4.12)$$

and the matrix $\Phi \in M_{k \times mn}(\mathbb{R})$,

$$\Phi = \begin{bmatrix} \phi(0, 1, \lambda_1) & \phi(0, 2, \lambda_1) & \dots & \dots & \phi(m, 0, \lambda_1) & \dots & \phi(m, n, \lambda_1) \\ \phi(0, 1, \lambda_2) & \phi(0, 2, \lambda_2) & \dots & \dots & \phi(m, 0, \lambda_2) & \dots & \phi(m, n, \lambda_2) \\ \dots & \dots & \dots & \dots & \dots & \dots & \dots \\ \phi(0, 1, \lambda_k) & \phi(0, 2, \lambda_k) & \dots & \dots & \phi(m, 0, \lambda_k) & \dots & \phi(m, n, \lambda_k) \end{bmatrix}, \quad (4.13)$$

where $\lambda_i = \lambda(i \Delta)$ is the stretch at time $t = i \Delta$. In the previous equations, the coefficient c_{00} has been set at zero, which implies that the strain energy is zero in the reference configuration.

With the above notation, the constitutive equation (4.10) can be rewritten as the linear system

$$\mathbf{\Pi}^e = \Phi \mathbf{c}, \quad (4.14)$$

where $\mathbf{\Pi}^e = \{\Pi^e(t_1), \dots, \Pi^e(t_k)\}$ is the discrete-time stress vector.

Since the material is assumed to be incompressible, only two stretches can be varied separately and, hence, biaxial tests would suffice to determine the form of the strain energy function (4.14), i.e., the constitutive relation (4.10). However, in the present investigation, only uniaxial tests were carried out, because of the limited availability of biaxial specimens. Consequently, the resulting identification problem is expected to be ill-conditioned (Ogden *et al.*, 2004).

The minimization problem arising from the identification of (4.14) is

$$\min_{\mathbf{c} \in \mathbb{R}^{mn}} \left\| \Phi \mathbf{c} - \tilde{\mathbf{\Pi}}^e \right\|_2^2 \quad (4.15)$$

where $\tilde{\mathbf{\Pi}}^e$ is the vector of the stress as recorded and sampled by the acquisition equipment, while $\|\cdot\|_2$ is the standard l_2 -norm. A Least-Square method (see, e.g., Golub, 1996) has been used to solve (4.15) in Sec. 4.2.4, where results and discussions are reported.

4.2.2 Viscoelastic Kernel

Once the "instantaneous" response $\mathbf{T}^e(t)$ in equation (4.1) has been identified, the problem of determining the (normalized) viscoelastic kernel $k(t)$, i.e., solving the integral equation (4.1), can be addressed.

The one-dimensional constitutive equation (4.2) can be rewritten through integration by parts as

$$T(t) = k(t)T^e(0) + \int_0^t k(s)\dot{T}^e(t-s) ds. \quad (4.16)$$

If $T^e(0) \neq 0$, introducing the normalized quantities $\hat{T}(t) = T(t)/T^e(0)$ and $D(t) = \dot{T}^e(t)/T^e(0)$, one gets

$$k(t) = \hat{T}(t) - \int_0^t k(s)D(t-s) ds, \quad (4.17)$$

which is a Volterra equation of the second kind for $k(t)$ (Linz, 1985).

A more useful form of (4.17) can be achieved by a standard time-discretization. Indeed, during an experiment, the displacement and the force are recorded at uniform time intervals, e.g.,

$$t_i = i \Delta, \quad i = 0, 1, \dots, N, \quad \Delta = \frac{t}{N}. \quad (4.18)$$

Since k and T^e are smooth functions of the time variable t , for small Δ the integral can be estimated by a finite sum through a quadrature rule (see, e.g., Press, 2007). For the uniform mesh (4.18) a simple scheme is the trapezoidal rule, which gives:

$$\int_0^{t_i} D(t_i-s)k(s) ds = \frac{\Delta}{2} D_i k_0 + \Delta \sum_{j=1}^{i-1} D_{i-j} k_j + \frac{\Delta}{2} D_0 k_i; \quad (4.19)$$

therefore equation (4.17) has the following discrete form:

$$\begin{cases} \hat{T}_0 = k_0, \\ \hat{T}_i = \left(1 + \frac{\Delta}{2} D_0\right) k_i + \frac{\Delta}{2} D_i k_0 + \Delta \sum_{j=1}^{i-1} D_{i-j} k_j, \quad i = 1, \dots, N \end{cases} \quad (4.20)$$

Since $k(0) = k_0 = 1$, $\tilde{T}_i = \hat{T}_i - D_i \Delta/2$ and the result is

$$\tilde{T}_i = \left(1 + \frac{\Delta}{2} D_0\right) k_i + \Delta \sum_{j=1}^{i-1} D_{i-j} k_j, \quad i = 1, \dots, N, \quad (4.21)$$

which can be easily expressed in terms of the linear system

$$\tilde{\mathbf{T}} = \mathbf{\Gamma} \mathbf{k}, \quad (4.22)$$

where $\tilde{\mathbf{T}} = \{\tilde{T}_1, \dots, \tilde{T}_N\}$, $\mathbf{k} = \{k_1, \dots, k_N\}$ and

$$\mathbf{\Gamma} = \Delta \begin{bmatrix} 1/\Delta + D_0/2 & 0 & 0 & \dots & \dots & \dots \\ D_1 & 1/\Delta + D_0/2 & 0 & \dots & \dots & \dots \\ D_2 & D_1 & 1/\Delta + D_0/2 & 0 & \dots & \dots \\ \dots & \dots & \dots & \dots & \dots & \dots \\ D_N & D_{N-1} & \dots & D_2 & D_1 & 1/\Delta + D_0/2 \end{bmatrix} \quad (4.23)$$

is a lower triangular matrix.

Through the (4.20), the identification of the viscoelastic kernel $k(t)$ has been reduced to the solution of the linear system (4.22), which requires the inversion of the matrix $\mathbf{\Gamma}$.

The structural properties of $\mathbf{\Gamma}$ strongly depend upon the experimental test performed to measure $T(t)$. In the case of a step-strain relaxation with an infinite speed of the initial ramp, the strain is suddenly increased to the value $\bar{\lambda}$, kept constant thereafter, e.g.,

$$\lambda(t) = \begin{cases} 1, & t < 0 \\ \bar{\lambda}, & t \geq 0 \end{cases} \quad (4.24)$$

In this case, the derivative of instantaneous stress T^e is vanishing for $t \geq 0$,

$$\dot{T}^e(t) = \frac{\partial T^e(\lambda)}{\partial \lambda} \dot{\lambda} = 0, \quad t \geq 0. \quad (4.25)$$

Therefore, for each l $D_l = 0$, and the matrix $\mathbf{\Gamma}$ reduces to the identity matrix. In this ideal situation, measuring the stress response, i.e., measuring \tilde{T} , is equivalent to measuring the viscoelastic kernel $k(t)$. However, to catch the time dependence of k for $t \rightarrow \infty$ it would be necessary to carry out an infinitely long experimental test.

In the case of filled rubber, an accurate prediction of k can be obtained with a relaxation experiment lasting ten minutes or less (see, e.g., [Antonakakis et al., 2006](#)). It should be noted that a premature cut off may give an erroneous limiting value of $k(t)$ for $t \rightarrow \infty$.

In the laboratory the prescription of $\lambda(t)$ in the form (4.24) is necessarily supplanted by a ramp history wherein the strain increases along a constant strain rate until the predetermined value $\bar{\lambda}$ is reached at time t_0 , e.g.,

$$\lambda(t) = \begin{cases} 1, & t < 0 \\ 1 + (\bar{\lambda} - 1) \frac{t}{t_0}, & 0 \leq t < t_0 \\ \bar{\lambda}, & t \geq t_0 \end{cases} \quad (4.26)$$

Thus, if the undeformed configuration is stress-free, then the instantaneous stress T_0^e vanishes and the equation (4.17) becomes

$$T(t) = \int_0^t k(s) \dot{T}^e(t-s) ds, \quad (4.27)$$

which is a Volterra equation of the first kind ([Linz, 1985](#)).

In analogy with the previous case, by using the trapezoidal quadrature rule, the discrete form of (4.27) can be introduced

$$\begin{cases} T_0 = 0, \\ \tilde{T}_i = \frac{\Delta}{2} k_i + \Delta \sum_{j=1}^{i-1} k_j \hat{D}_{i-j}, \quad i = 1, \dots, N \end{cases} \quad (4.28)$$

where $\tilde{T}_i = T_i/\dot{T}_0^e - \Delta/2 \hat{D}_i$ and $\hat{D}_i = \dot{T}_i^e/\dot{T}_0^e$. In matrix notation, the last equation can be rewritten as

$$\tilde{\mathbf{T}} = \mathbf{\Theta} \mathbf{k} \quad (4.29)$$

where $\tilde{\mathbf{T}} = \{\tilde{T}_1, \dots, \tilde{T}_N\}$, $\mathbf{k} = \{k_1, \dots, k_N\}$ and

$$\mathbf{\Theta} = \Delta \begin{bmatrix} 1/2 & 0 & 0 & \dots & \dots & \dots \\ D_1 & 1/2 & 0 & \dots & \dots & \dots \\ D_2 & D_1 & 1/2 & 0 & \dots & \dots \\ \dots & \dots & \dots & \dots & \dots & \dots \\ D_{N-1} & D_{N-2} & \dots & D_2 & D_1 & 1/2 \end{bmatrix}. \quad (4.30)$$

Differentiating Eq. (4.26), the result is

$$\frac{dT^e(t)}{dt} = \frac{\partial T^e(\lambda)}{\partial \lambda} \dot{\lambda} = \begin{cases} 0, & t < 0 \\ \frac{\bar{\lambda} - 1}{t_0} \frac{\partial T^e(\lambda)}{\partial \lambda}, & 0 \leq t < t_0 \\ 0, & t \geq t_0 \end{cases}, \quad (4.31)$$

hence, $\dot{T}^e(t) \neq 0$ if $0 \leq t < t_0$. The bandwidth of the matrix $\mathbf{\Gamma}$ is $\mathbf{b} = \lfloor t_0/\Delta \rfloor$, where $\lfloor \cdot \rfloor$ is the floor function. Therefore, the influence of the history upon the current value of the stress is limited to the previous \mathbf{b} samples.

The 1-norm of the matrix $\mathbf{\Theta}$ is

$$\|\mathbf{\Theta}\|_1 = \max_{1 \leq j \leq N} \sum_{i=1}^N |\{\mathbf{\Theta}\}_{ij}| = \frac{1}{2} + \sum_{i=1}^{\mathbf{b}} |D_i| \quad (4.32)$$

and, hence, its condition number¹ depends upon the bandwidth \mathbf{b} . For a fastly increasing ramp, the resulting matrix $\mathbf{\Theta}$ has a lower condition number and the linear system (4.29) is well-conditioned. On the opposite, a slowly increasing ramp results in a larger condition number of $\mathbf{\Theta}$ and measurement errors on $T(t)$ may propagate to the solution $k(t)$ and eventually invalidate the result (see, e.g., Golub, 1996). In any case, errors due to a wrong fitting of the instantaneous stress $T^e(t)$ will propagate to $k(t)$.

A frequently employed characterization of the viscoelastic kernel is achieved through sinusoidal strain histories of frequency ω overimposed on a static displacement (Lee & Kim, 2001), e.g.,

$$\lambda(t) = \begin{cases} 1, & t < 0 \\ 1 + (\bar{\lambda} - 1) \frac{t}{t_0}, & 0 \leq t < t_0 \\ \bar{\lambda} + \Delta\lambda_1 \sin(\omega(t - t_0)), & t \geq t_0 \end{cases}, \quad (4.33)$$

In analogy with the previous case, the relation between the viscoelastic kernel and the stress is governed by the linear system (4.29); however, the derivative of T^e with respect to the time does not vanish for $t > t_0$, i.e.,

$$\frac{dT^e(t)}{dt} = \frac{\partial T^e(\lambda)}{\partial \lambda} \dot{\lambda} = \begin{cases} 0, & t < 0 \\ \frac{\bar{\lambda} - 1}{t_0} \frac{\partial T^e(\lambda)}{\partial \lambda}, & 0 \leq t < t_0 \\ \Delta\lambda_1 \omega \cos(\omega(t - t_0)) \frac{\partial T^e(\lambda)}{\partial \lambda}, & t \geq t_0 \end{cases}. \quad (4.34)$$

In this case, hence, the matrix $\mathbf{\Theta}$ is a fully lower triangular matrix.

4.2.3 Fitting of the Prony Series

Once the viscoelastic kernel has been obtained by inverting the matrices $\mathbf{\Theta}$ or $\mathbf{\Gamma}$, the functional form of $k(t)$ must be chosen and the constitutive parameters identified accordingly.

A common assumption for k is

$$k(t; \mathbf{k}, \boldsymbol{\tau}) = 1 + \sum_{i=1}^N k_i \left(e^{-t/\tau_i} - 1 \right), \quad \mathbf{k} = \{k_1, \dots, k_N\}, \quad \boldsymbol{\tau} = \{\tau_1, \dots, \tau_N\}, \quad (4.35)$$

¹The condition number of an invertible matrix A is defined as product between the norm of A and the norm of its inverse A^{-1} (see, e.g., Golub, 1996).

which is the well-known Prony series. This functional form, derived from various molecular models, has been successfully applied to model relaxation phenomena in filled rubber (e.g., Antonakakis *et al.*, 2006; Haupt & Lion, 2002; Johnson *et al.*, 1994; Park & Schapery, 1999; Quigley *et al.*, 1995).

The minimization problem arising from the identification of a N-terms Prony series is

$$\min_{(\mathbf{k}, \boldsymbol{\tau}) \in \mathbb{R}^N \times \mathbb{R}^N} \left\| \mathfrak{K}(\mathbf{k}, \boldsymbol{\tau}) - \widehat{\mathbf{K}} \right\|_2^2, \quad (4.36)$$

where $\mathfrak{K}(\mathbf{k}, \boldsymbol{\tau}) = \{k(t_1; \mathbf{k}, \boldsymbol{\tau}), \dots, k(t_M; \mathbf{k}, \boldsymbol{\tau})\}$, $\widehat{\mathbf{K}}$ is the kernel obtained by inverting the matrices Θ or Γ and $\{t_1, \dots, t_M\}$ are the discrete time instants.

Ten, twenty or even more terms in the series (4.35) are sometimes used to increase the accuracy of the fitting model. However, this choice leads to ill-conditioned solutions of the optimization problem, which as a result are strongly affected by the choice of the initial point.

Owing to the transcendental dependence of k upon the characteristic times, the minimization problem (4.36) is nonlinear, thus, nonconvex. A typical procedure, applied in the literature for reducing the computational effort due to the minimization of a nonconvex functional, is to fix a-priori the relaxation times $\bar{\tau}_i$ (see, e.g., Knauss & Zhao, 2007). The result is a linear optimization problem in the reduced set of variables \mathbf{k} .

If $\bar{\boldsymbol{\tau}} = \{\bar{\tau}_1, \dots, \bar{\tau}_N\}$ are the fixed characteristic times, then (4.36) reduces to

$$\min_{\mathbf{k} \in \mathbb{R}^N} \left\| \mathfrak{H} \mathbf{k} - \widetilde{\mathbf{K}} \right\|_2^2, \quad (4.37)$$

where $\{\widetilde{K}\}_m = (\{\widehat{K}\}_m - 1)$ and \mathfrak{H} is the $M \times N$ matrix

$$\mathfrak{H} = \begin{bmatrix} e^{-t_1/\bar{\tau}_1} - 1 & e^{-t_1/\bar{\tau}_2} - 1 & \dots & e^{-t_1/\bar{\tau}_N} - 1 \\ e^{-t_2/\bar{\tau}_1} - 1 & e^{-t_2/\bar{\tau}_2} - 1 & \dots & e^{-t_2/\bar{\tau}_N} - 1 \\ \dots & \dots & \dots & \dots \\ e^{-t_M/\bar{\tau}_1} - 1 & e^{-t_M/\bar{\tau}_2} - 1 & \dots & e^{-t_M/\bar{\tau}_N} - 1 \end{bmatrix}. \quad (4.38)$$

If $\bar{\tau}_i \neq \bar{\tau}_j$ for each $i \neq j$, the functions $\{e^{-t/\bar{\tau}_1}, \dots, e^{-t/\bar{\tau}_N}\}$ are linearly independent. Hence, the matrix \mathfrak{H} is full column rank and $\mathfrak{H}^T \mathfrak{H}$ is invertible. The solution of (4.37) can be achieved with the standard linear Least Squares algorithm, i.e., by inverting the matrix $\mathfrak{H}^T \mathfrak{H}$.

The time interval, within which the characteristic times are initially selected, is chosen according to the duration of the experiment, i.e., the upper limit for $\{\tau_i\}$, and the sampling rate of the acquisition channel, i.e., the lower limit. Within this range, the relaxation times are initially fixed at equal intervals along the logarithmic time scale with one or two increments per decade (Knauss & Zhao, 2007). However, this choice seems to lead to unsatisfactory results especially when nonlinear viscoelastic models are involved. Therefore, an iterative fitting procedure for refining the estimate of the relaxation times is introduced in Section 4.3.

4.2.4 Identification Results

In the following the identification results obtained through the steps 1,2 and 3 of the above-described procedure are reported.

Compression tests on thick cylindrical specimens were used for the fitting (see Section 1.5). In particular, the ‘‘instantaneous’’ response was obtained exerting a displacement with a constant strain rate up to the stretch $\bar{\lambda} \approx 0.8$. The velocity was 500 mm/min which is approximately fifty times the velocity of a standard quasi-static test.

Table 4.1 Identification results of instantaneous term for three different material models (ρ is the condition number of the matrix $\Phi^T \Phi$).

Model Name	c_{10}	c_{01}	c_{20}	c_{30}	ρ
Neo-Hookean	$1.1426 \cdot 10^6$	-	-	-	1
Mooney-Rivlin	$1.1426 \cdot 10^6$	0	-	-	2910
Yeoh	$1.4543 \cdot 10^6$	-	$-0.3987 \cdot 10^7$	$1.3956 \cdot 10^7$	184880
Yeoh 2	$1.3312 \cdot 10^6$	-	$-1.4101 \cdot 10^6$	-	315

Three models were considered for the instantaneous term T^e , respectively with one (c_{10} - Neo-Hookean), two (c_{10}, c_{01} - Mooney-Rivlin) and three (c_{10}, c_{20}, c_{30} - Yeoh) material coefficients respectively.

The function *lsqlin* in the MATLAB Optimization Toolbox was employed to solve numerically the problem (4.15). Actually, to guarantee the physical admissibility of the fitting models, the following constraints have been introduced (see pag. 243 in Hartmann, 2001b; Holzapfel, 2000):

$$c_{10} > 0, \quad c_{01} \geq 0, \quad c_{20} \leq 0, \quad c_{30} > 0. \quad (4.39)$$

The results of the identification of T^e are shown in Fig. 4.1. All the curves can roughly describe the experimental data. However, to allow a comparison among the different models, the relative errors are also plotted in the figure. In order to avoid a division by small values of the force when stretches are close to one, the relative error is computed as proposed in (Ogden *et al.*, 2004), i.e.,

$$err_i := \frac{|(\Phi \mathbf{c})_i - (\tilde{\Pi}^e)_i|}{\max\{0.5, (\tilde{\Pi}^e)_i\}}. \quad (4.40)$$

The optimum values of the coefficients c_{ij} together with the condition numbers ρ of the matrix $\Phi^T \Phi$ are shown in Tab. 4.1.

For Neo-Hooke and Mooney-Rivlin models, the relative error at low strains is larger than 10 %. The Neo-Hookean and Mooney-Rivlin curves coincide because from the optimization problem the result is $c_{01} = 0$. The 3-parameters Yeoh model shows a good agreement with the experimental data with an error less than 20 % for strain lower than 0.95.

It can be seen from Tab. 4.1 that as the number of parameters increases, the condition number increases greatly, meaning that some of the directions in the space of the parameters \mathbf{c} are not significant. In the case of the Yeoh model, by a singular value decomposition of the matrix $\Phi^T \Phi$, the results is that the direction corresponding to the parameter c_{03} is associated with the smallest eigenvalue, meaning that c_{03} is not significant in describing the experimental data.

To confirm this result, a 2 parameters Yeoh model was also considered ($c_{30} = 0$). While the relative error remains limited the condition number is drastically reduced. However, this model with the choice of the coefficients reported in Table 4.1 leads to a non-physical behavior at larger strains. Therefore this solution must be discarded a-posteriori.

After the “instantaneous” response of the material has been estimated, the relaxation kernel k can be evaluated by inverting the matrix Θ in (4.29). As a result of the discussed well-conditioning of Θ , the errors for computing its inverse Θ^{-1} remain limited.

The matrix Θ is assembled from the relaxation tests (see Sec. 1.5). In this case the cylinder was compressed to the stretch $\bar{\lambda} = 0.15$ with a constant strain rate of 100 mm/min. Thereafter

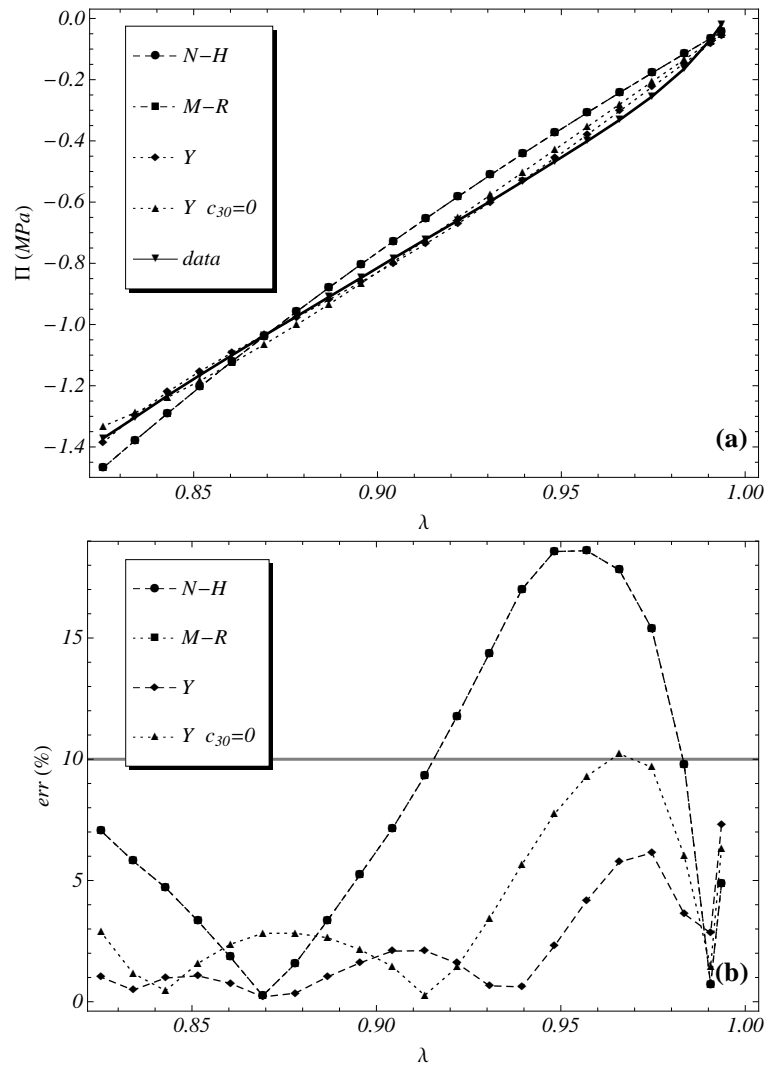


Figure 4.1 Nominal stress, Π , plotted against the stretch λ for Neo-Hookean, Mooney-Rivlin and Yeoh material models (Panel (a)). Since $c_{01} = 0$ in Tab. 4.1, Neo-Hookean and Mooney-Rivlin curves coincide. Panel (b) shows the corresponding relative errors.

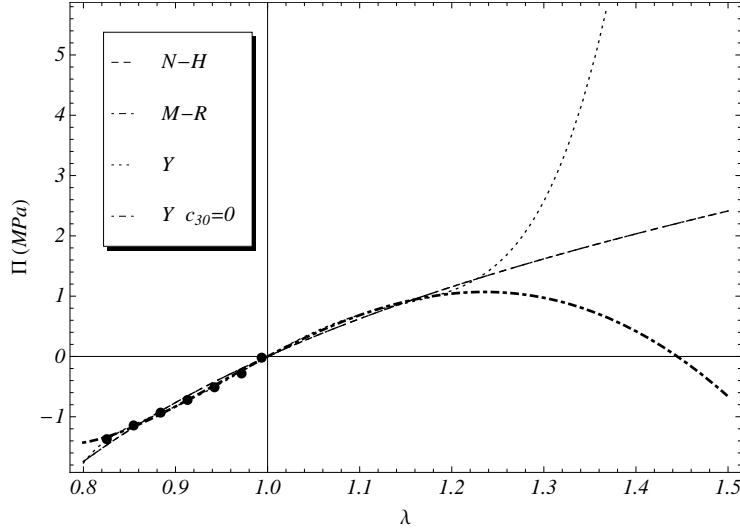


Figure 4.2 Identification results of the instantaneous response for three different material models. A very different behavior is shown outside the range of the experimental data (represented in the figure as big-dots). The 2-parameters Yeoh model exhibits a non-physical behavior.

the strain was held fixed for 100 s. The sampling rate of the external force and displacement was 100 Hz, corresponding to a period $\Delta = 0.01$ s. Therefore the characteristic times in the Prony series were chosen equally spaced in logarithmic scale in the range $\tau_i \in [0.01, 100]$ s.

After k has been calculated, the minimization problem (4.37) can be addressed.

In this case, the identification results are reported in Figure 4.4 for an increasing number of exponential terms in the Prony series. With $N = 10$ coefficients there is a perfect agreement between the fitting model and the experimental curve, with a relative error below 2%. However, the condition number ρ of the matrix $\mathfrak{h}^T \mathfrak{h}$ increases dramatically ($\rho_5 = 127.2$, $\rho_{10} = 2327$ and $\rho_{20} = 4.371 \cdot 10^7$). Therefore, there might be multiple sets of parameters \mathbf{k} resulting in the same value of the objective function, but which produce a very different behavior outside the observed time range.

The robustness of the solution \mathbf{k} has also been investigated. Because of the high values of the condition number, it is expected that a small error either in the experimental data, e.g., \tilde{K} , or in the model, e.g., \mathfrak{h} , produces a large variation in the identified parameters. In particular, by considering the perturbed optimization problem:

$$\min_{\mathbf{k} \in \mathbb{R}^N} \left\| (\mathfrak{h} + d\mathfrak{h}(\gamma_1)) (\mathbf{k} + d\mathbf{k}) - \tilde{K} - d\tilde{K}(\gamma_2) \right\|_2^2, \quad (4.41)$$

the sensitivity of the minimum can be investigated. In (4.41), $d\mathfrak{h}(\gamma_1)$ is the variation in the model matrix induced by a random error of maximum amplitude γ_1 upon the characteristic times $\bar{\tau}_i$, i.e.,

$$\bar{\tau}_1^* = (1 + \gamma_1 r) \bar{\tau}_1, \quad \dots, \quad \bar{\tau}_N^* = (1 + \gamma_1 r) \bar{\tau}_N, \quad (4.42)$$

with $-1 \leq r \leq 1$. Moreover, the vector $d\tilde{K}$ represents the kernel variation produced by a random error of maximum amplitude γ_2 , i.e.,

$$d\tilde{K}_i = \gamma_2 r \tilde{K}_i. \quad (4.43)$$

Table 4.2 outlines the variation of the minimum solution of (4.41) for increasing error amplitudes γ_1 and γ_2 in the range $\{0.01, 0.3\}$. It is evident that the solution is strongly affected by the error amplitudes. Even though the different values of \mathbf{k} correspond to the

Table 4.2 Variation of the minimum solution in the case of $N = 20$ Prony's coefficients for increasing error amplitudes γ_1 and γ_2 in the range $\{0.01, 0.1, 0.3\}$. Only the time constants associated with the largest three coefficients k are shown in the table.

γ_1	γ_2	$\frac{\ d\mathbf{h}\ }{\ \mathbf{h}\ }$	$\frac{\ d\tilde{K}\ }{\ \tilde{K}\ }$	$\frac{\ d\mathbf{k}\ }{\ \mathbf{k}\ }$	k_1	τ_1	k_2	τ_2	k_3	τ_3
[%]	[%]	[%]	[%]	[%]						
0	0	0	0	0	12.9	1.0306	0.0257	12.915	0.0159	8.4743
0	1	0	0.7	11.4	0.1192	1.0306	0.0212	12.915	0.0210	8.4743
0	10	0	7	124.4	0.1035	0.6762	0.0460	5.5603	0.0135	30
0	30	0	21	118.3	0.0627	0.4437	0.0547	0.6762	0.0285	8.4743
1	0	0.1	0	2.6	0.1270	1.0403	0.0257	13.023	0.0158	8.461
1	1	0.1	0.7	13.4	0.1172	1.0403	0.0213	13.023	0.0209	8.461
1	10	0.1	7	123.3	0.1023	0.67155	0.0459	5.5204	0.0139	30.276
1	30	0.1	21	118.3	0.0633	0.44779	0.0540	0.6715	0.0290	8.461
10	0	1	0	18.6	0.1127	1.1275	0.0265	13.989	0.0205	0.6299
10	1	1	0.7	26.1	0.1051	1.1275	0.0269	0.6299	0.0227	13.989
10	10	1	7	106.3	0.0904	0.6299	0.0296	5.1620	0.0264	1.1275
10	30	1	21	118.8	0.0697	0.4849	0.0474	0.6299	0.0336	8.3417
30	0	2.8	0	36.1	0.0998	1.3215	0.0368	0.5674	0.0298	16.137
30	1	2.8	0.7	40.8	0.0942	1.3215	0.0411	0.5674	0.0267	16.137
30	10	2.8	7	92.8	0.0798	0.5674	0.0439	8.0765	0.0435	1.3215
30	30	2.8	21	119.1	0.0650	0.5674	0.0537	0.5373	0.0437	8.0765

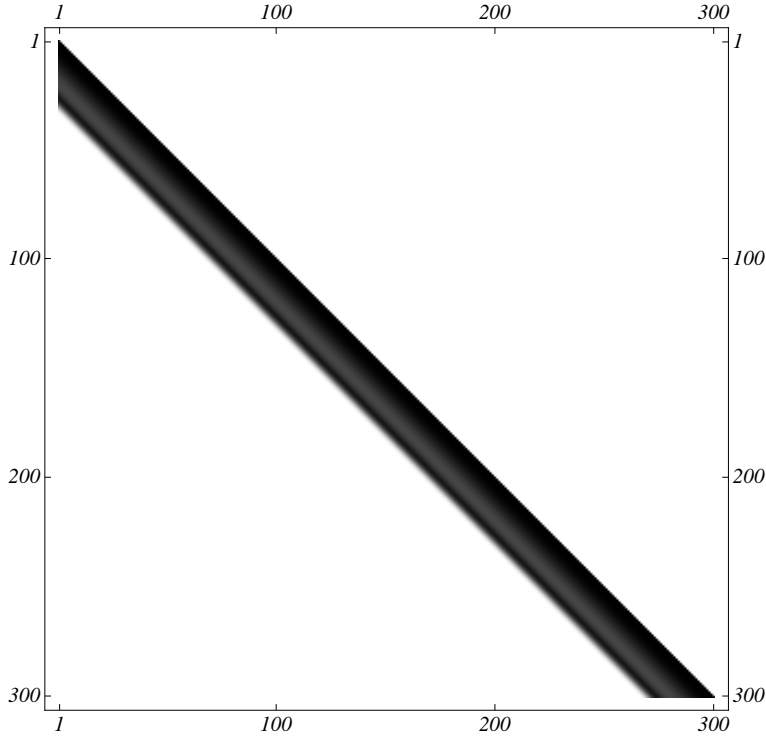


Figure 4.3 Contour plot of matrix Θ_{mn} with $m, n \leq 300$ for the performed relaxation test. The bandwidth of the matrix is evident in the figure and corresponds to a rising time of the initial ramp t_0 approximately equal to 0.5 s.

same value of the objective function, they lead to a completely different frequency behavior, as shown in Fig. 4.5.

The material behavior arising from the identified parameters \mathbf{c} and \mathbf{k} is shown in Fig. 4.6 compared to the experimental data. It is seen that the aforementioned procedure leads to unsatisfactory results because the material stiffness is heavily underestimated and the relaxation behavior around the stress-kink is completely missed. Therefore, in the next section, an alternative identification method for both the instantaneous and dissipative parts of the constitutive equation is introduced.

4.3 Joint Identification

In this section a joint identification of the instantaneous and dissipative terms is presented. To this end a single hereditary formulation for the constitutive equation of a nonlinear viscoelastic solid is introduced which enables us to include also differential and fractional differential models (see for instance [Adolfsson *et al.*, 2005](#); [Lion & Kardelky, 2004](#)).

The hereditary formulation for the current value of the second Piola-Kirchhoff stress $\mathbf{T}(t)$ is introduced as follows:

$$\mathbf{T}(t) = \mathbf{T}^{(e)}(\mathbf{C}(t)) + \mathbf{\Lambda}(\mathbf{C}(t)) \int_0^t \frac{\partial k(t-s)}{\partial(t-s)} \mathbf{\Psi}(\mathbf{C}(s), \mathbf{C}(t)) ds, \quad (4.44)$$

where $\mathbf{T}^{(e)}$ represents the instantaneous stress as a function of the current value of deformation, $\mathbf{\Lambda}$, $\mathbf{\Psi}$ and k account for the memory properties of the material. In particular, $\mathbf{\Lambda}$ is a tensor-valued function of the current strain value $\mathbf{C}(t)$, whilst $\mathbf{\Psi}$ is a tensor-valued function which depends on both the current strain $\mathbf{C}(t)$ and the strain history $\mathbf{C}(s)$.

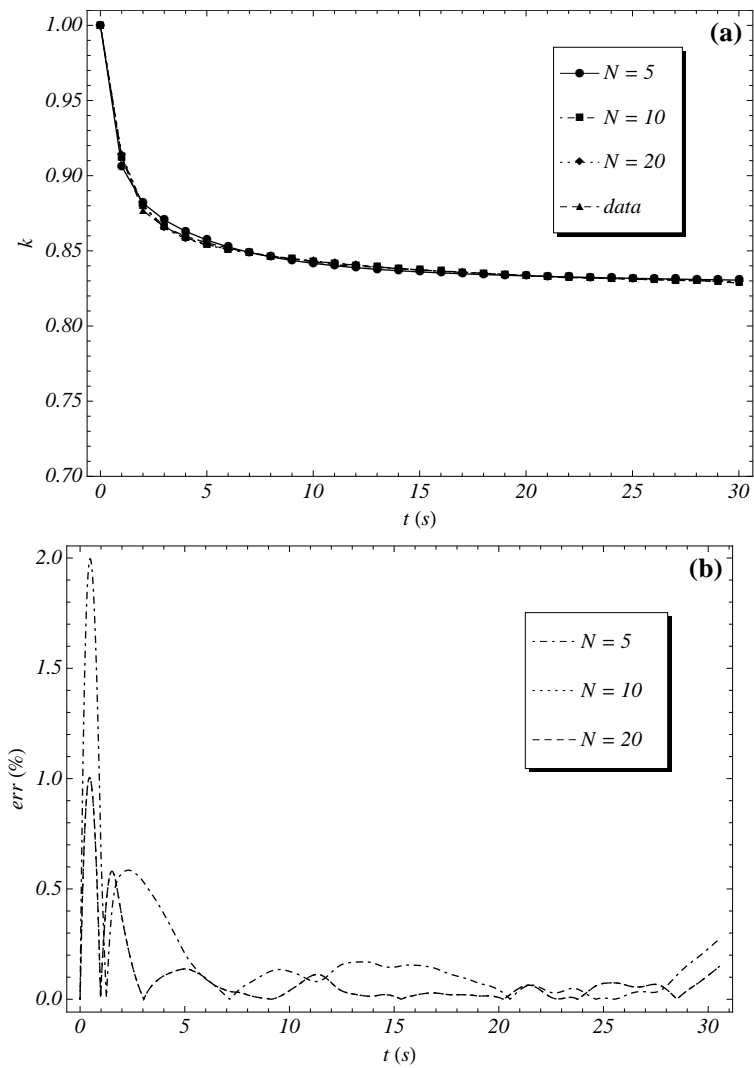


Figure 4.4 Viscoelastic kernel k plotted against time t for an increasing number of exponential terms in the Prony' series (Panel (a)). Even with the lowest number of parameters $N = 5$ the relative error is less than 2% (Panel (b)).

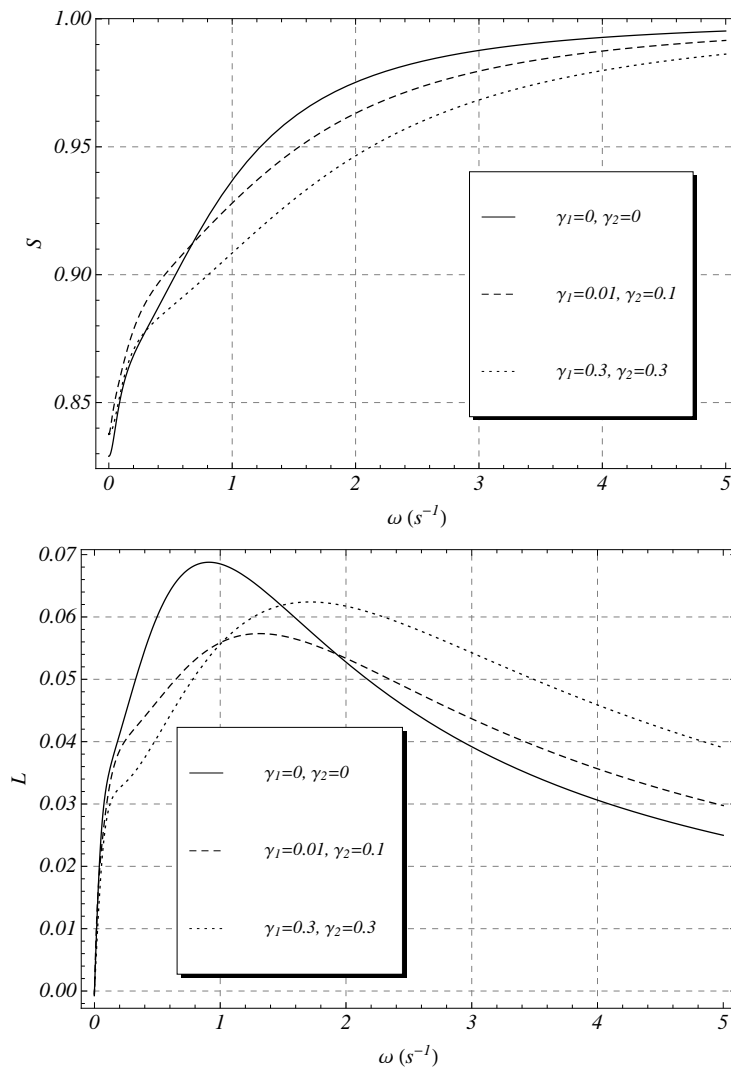


Figure 4.5 Normalized storage, S , and normalized loss, L , moduli plotted against the frequency ω for different values of the error amplitudes γ_1 and γ_2 in the case of $N = 20$ Prony's parameters.

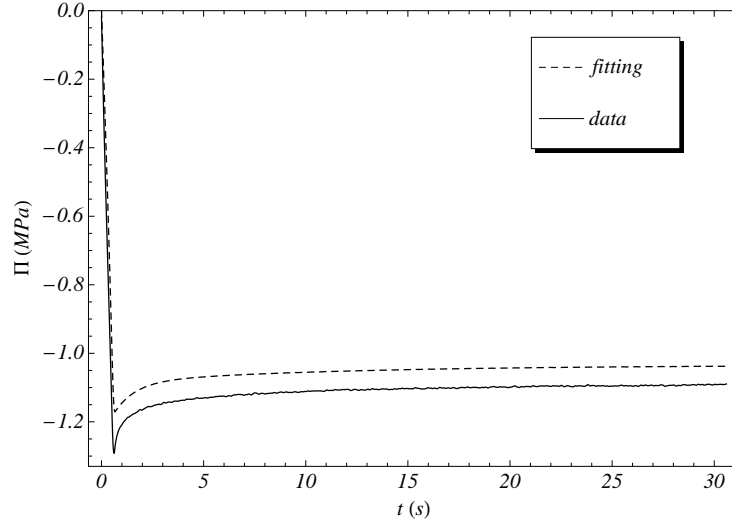


Figure 4.6 Nominal stress plotted against time in the range $t \in [0, 30]$ s for the collected experimental data and the Fung's constitutive equation with a Neo-Hookean elastic part. The model coefficients have been identified through the discussed identification procedure. The material stiffness is heavily underestimated and the relaxation behavior around the stress-kink is completely missed

From an experimental point of view, it is convenient to express the force recorded during the experiment (divided by the reference cross-section area) in terms of the (nominal) strain. To this aim, the previous constitutive relation can be equivalently expressed in terms of the first Piola-Kirchhoff stress tensor:

$$\mathbf{\Pi}(t) = \mathbf{\Pi}^{(e)}(t) + \mathbf{F}(t) \mathbf{\Lambda}(t) \int_0^t \frac{\partial k(t-s)}{\partial(t-s)} \mathbf{\Psi}(s, t) ds, \quad (4.45)$$

with $\mathbf{\Pi} = \mathbf{F}\mathbf{T}$ and $\mathbf{\Pi}^{(e)} = \mathbf{F}\mathbf{T}^{(e)}$.

To express the viscoelastic kernel, the discrete relaxation spectrum, leading to the Prony's series is used:

$$k(t) = 1 + \sum_{i=1}^N k_i (e^{-t/\tau_i} - 1), \quad \sum_i k_i < 1; \quad (4.46)$$

The number N of exponential terms in (4.46) is generally selected to increase the accuracy of the fitting model. In the literature, up to $N = 20$ relaxation times were used (Antonakakis *et al.*, 2006; Knauss & Zhao, 2007); however a large value of N could lead to ill-conditioned identification problems where identified parameters show high sensitivity to errors in the experimental data.

Beside differential viscoelasticity, accounted for with a discontinuous kernel, the constitutive relation (4.44) can also include fractional differential models. In this case the kernel k is expressed as (see for instance Adolfsson *et al.*, 2005; Metzler & Nonnenmacher, 2003):

$$k(t) = 1 + \sum_{i=1}^N k_i (E_{\delta_i}[-(t/\tau_i)^{\delta_i}] - 1), \quad (4.47)$$

with

$$\sum_{i=1}^N k_i < 1, \quad \delta_i > 0, \quad t \geq 0,$$

where E_δ is the δ -order Mittag-Leffler function, which is defined as

$$E_\delta(u) = \sum_{j=0}^{\infty} \frac{u^j}{\Gamma(1+j\delta)}, \quad \delta > 0, \quad (4.48)$$

and Γ is the Eulerian Gamma function. Thermodynamics laws implies the following restrictions for the coefficients δ_i :

$$0 < \delta_i \leq 1, \quad i = 1, \dots, N \quad (4.49)$$

Remark that N additional constitutive parameters δ_i are introduced with respect to the standard Prony series; when $\delta_i \rightarrow 1$, the fractional kernel (4.47) reduces to the standard one (4.46), since $E_1(t)$ equals the exponential function.

The constitutive relation (4.45) is valid for every NLV material bearing no special characteristic. However carbon black-filled elastomers are usually treated as isotropic and incompressible materials. The first property reflects on the constitutive relation (4.45) requiring all the functions, $\mathbf{\Pi}^{(e)}$, $\mathbf{\Lambda}$ and $\mathbf{\Psi}$, to be isotropic tensor functions of \mathbf{C} . In particular, the instantaneous stress, for an incompressible isotropic material, can be expressed as

$$\mathbf{\Pi}^{(e)}(t) = \phi_1(I_1(t), I_2(t))\mathbf{F}(t) + \phi_2(I_1(t), I_2(t))\mathbf{F}(t)\mathbf{C}(t), \quad (4.50)$$

where ϕ_1 and ϕ_2 are functions of the first two invariants of \mathbf{C} at time t , $I_1(t) = \text{tr } \mathbf{C}(t)$ and $I_2(t) = \text{tr } \mathbf{C}^{-1}(t)$.

The incompressibility constraint, $\det \mathbf{F} = 1$, can be easily taken into account by adding to the Cauchy stress a pressure field $p(t)\mathbf{I}$ which is not constitutively assigned, but depends upon the boundary and initial conditions (Ogden, 1997). By adding the unknown pressure in the constitutive equation of the first Piola-Kirchhoff stress, it becomes

$$\mathbf{\Pi}(t) = -p(t)\mathbf{F}^{-T}(t) + \mathbf{\Pi}_{ES}(t); \quad (4.51)$$

therefore, the extra stress term $\mathbf{\Pi}_{ES}(t)$ remains as the only part of the stress-strain relation which is constitutively assigned:

$$\begin{aligned} \mathbf{\Pi}_{ES}(t) &= \mathbf{\Pi}_{ES}^{(e)} + \mathbf{F}(t) \mathbf{\Lambda}(t) \int_0^t \frac{\partial k(t-s)}{\partial(t-s)} \mathbf{\Psi}(s, t) ds, \\ \mathbf{\Pi}_{ES}^{(e)}(t) &= \phi_1(t)\mathbf{F}(t) + \phi_2(t)\mathbf{F}(t)\mathbf{C}(t). \end{aligned} \quad (4.52)$$

A suitable choice of the instantaneous stress $\mathbf{\Pi}_{ES}^{(e)}$, through the functions ϕ_1 and ϕ_2 , of the functions $\mathbf{\Lambda}$, $\mathbf{\Psi}$ and of the viscoelastic kernel k in Eqs. (4.52) allows all the models under investigation to be encompassed. Table 4.3 summarizes such choices for all the considered constitutive equations.

4.3.1 Constitutive models under consideration

To the author knowledge all the major contributions involving hereditary integral viscoelastic models have been here considered (refer to Table 4.3). With the intent of having the same number of parameters for the instantaneous stress $\mathbf{\Pi}_{ES}^{(e)}$ of each model, a Mooney-Rivlin representation has been chosen for the Models 1, 2, 3 and 6, in which the constitutive assumption regarding $\mathbf{\Pi}_{ES}^{(e)}$ were not specified by the respective authors. Moreover, Models 2, 4, 5, in their original versions, had a single relaxation time ($N = 1$), which has revealed unable to fit the experimental data under investigation. A Prony's series with 3, or more, exponential terms was alternatively used.

In particular, we have labeled as number 1 Fung's model (Fung, 1972) which is commonly referred to as the Quasi Linear Viscoelastic (QLV) model. While this represents one of the first major contributions to finite viscoelasticity, its main limit lies in the choice of the function Ψ strictly related to the constitutive function $\Pi_{ES}^{(e)}$, modeling the instantaneous material response.

Recently, based on Fung's seminal work, many investigators have proposed new integral-type nonlinear viscoelastic constitutive relationships. Among them, the equations introduced in (Fosdick & Yu, 1998; Hallquist, 1998; Hibbit *et al.*, 2007; Shim *et al.*, 2004; Yang *et al.*, 2000) are here considered and labeled as 2, 3, 4, 5 and 6 respectively.

In particular we have included several models which were intended to describe the viscoelastic behavior of carbon black-filled rubber at high strain rates (Hoo Fatt & Ouyang, 2007; Shim *et al.*, 2004; Yang *et al.*, 2000). In all these models the time derivative of the strain explicitly appears in the hereditary term. The model by Hoo Fatt & Ouyang (2007) was not considered in the comparison since it has shown some shortcomings owing to a zero Young's modulus in the undeformed configuration. For this model the Cauchy stress σ arising from a constant strain rate test, say $\dot{\epsilon}_0$, such that $\lambda = 1 + \dot{\epsilon}_0 t$, is

$$\begin{aligned} \sigma = & 2\alpha_1(I_1 - 3)^{\alpha_2} \left(\lambda^2 - \frac{1}{\lambda} \right) + \\ & - \left(\lambda^2 - \frac{1}{\lambda} \right) \int_1^\lambda \left[2\beta_1 \dot{k} \left(\frac{\lambda - \zeta}{\dot{\epsilon}_0} \right) \left(\zeta^2 + \frac{2}{\zeta} - 3 \right) \left(\zeta - \frac{1}{\zeta^2} \right) \right] d\zeta, \end{aligned}$$

and, hence, the Young's modulus around the undeformed configuration, that is $[\partial\sigma/\partial\lambda]_{\lambda=1}$, is equal to zero, in contrast with the experimental evidences (see Figs. 4.8 and 4.9).

The comparison includes also the constitutive equations used respectively in the FE commercial codes LS-Dyna (Hallquist, 1998) and Abaqus FEA (Hibbit *et al.*, 2007). The latter are two of the most used FE codes, which include finite viscoelastic effects. In particular, the finite viscoelastic relationship (Hallquist, 1998), used in LS-Dyna, takes into account for rate effects through a convolution integral which is linear with respect to the strain tensor. The model used in Abaqus (Hibbit *et al.*, 2007) is similar to a well-established model of finite viscoelasticity, namely the Pipkin–Rogers model (Pipkin & Rogers, 1968); this constitutive equation, with an appropriate choice of the constitutive parameters, reduces to Fung's QLV relation (Ciambella *et al.*, 2009).

Finally, the fractional derivatives model introduced in (Lion & Kardelky, 2004) is also considered and labeled as number 7 in Tab. 4.3. This model, introduced to describe the amplitude dependence of the storage and loss moduli during dynamic motions, serves here to investigate the effects of the fractional kernel (4.47) upon the prediction of hysteresis losses. Since to define the fractional kernel the additional parameters δ_i must be introduced with respect to the standard Prony's series, to compare properly Lion & Kardelky's model with the others, the fractional coefficients were initially kept fixed, $\delta_i = 1$, leading to the standard Prony's series. Thereafter, they were left free to evolve to further minimize the objective function. The results between the standard and the differential kernel are then compared in terms of predicted energy dissipation.

4.3.2 Experimental Set-up

For the sake of completeness in this section some of the experimental results already discussed in Chap. 1 are here summarized.

The possibility of testing the dynamic behavior of the material through relaxation, creep and fast loading/unloading cycles, that can be performed with a standard tensile machinery. While relaxation and creep experiments incorporate the long-term material response,

Table 4.3 Material models under consideration: 1 - Fung (1972); 2 - Fosdick & Yu (1998); 3 - Hallquist (1998); 4 - Yang *et al.* (2000); 5 - Shim *et al.* (2004); 6 - Hibbit *et al.* (2007); 7 - Lion & Kardelky (2004)

Model	$\mathbf{\Pi}_{ES}^{(e)}$		$\mathbf{\Lambda}$	$\mathbf{\Psi}$
	ϕ_1	ϕ_2		
1	$2[\alpha_1 + \alpha_2 I_1(t)]$	$-2\alpha_2$	\mathbf{I}	$\mathbf{F}^{-1}(s)\mathbf{\Pi}_{ES}^{(e)}(s)$
2	$2[\alpha_1 + \alpha_2 I_1(t)]$	$-2\alpha_2$	$\mathbf{C}^{-1}(t)$	$\beta_1 \mathbf{C}(s)\mathbf{C}^{-1}(t)$
3	$2[\alpha_1 + \alpha_2 I_1(t)]$	$-2\alpha_2$	\mathbf{I}	$-\beta_1 \dot{\mathbf{C}}(s)$
4	α_1	α_2	\mathbf{I}	$-\beta_1 - \beta_2 I_2(s)] \dot{\mathbf{C}}(s)$
5	α_1	α_2	$[1 + \gamma_1 \dot{I}_2(t)] \mathbf{I}$	$-\beta_1 \frac{\dot{I}_1(s)}{I_1(s)} \mathbf{C}(s) + 2\beta_2 \dot{\mathbf{C}}(s)$
6	$2[\alpha_1 + \alpha_2 I_1(t)]$	$-2\alpha_2$	\mathbf{I}	$\mathbf{F}^{-1}(s)\mathbf{\Pi}^{(e)}(s)\mathbf{C}(s)\mathbf{C}^{-1}(t)$
7	α_1	$-$	\mathbf{I}	$-\beta_1 \mathbf{C}^{-1}(s)\dot{\mathbf{C}}(s)\mathbf{C}^{-1}(s)$

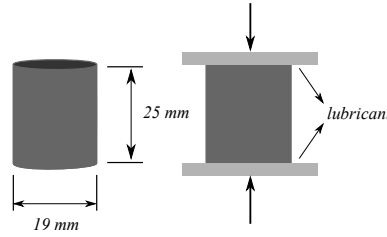


Figure 4.7 Specimen's geometry for compression tests.

the stress arising from loading/unloading cycles at different strain-rates involves the lowest characteristic times, thus the highest characteristic frequencies (in our case of the order of 100 Hz). The identification results reported here, could be complemented with dynamic experimental results at higher frequencies (see Chap. 1). To this aim small harmonic deformations superimposed on large static displacements are sometimes used; however the precision requested to the testing machinery, and its price, sensibly increase as the frequency of interest increases. We have, therefore, limited our analysis to experimental set-ups that can be reproduced in any well-equipped laboratory which does not necessarily have the leading-edge testing machineries.

Experiments were conducted with a Zwick/Roell z010. The specimen was cylindrically shaped with a diameter-to-height ratio $D/H = 0.76$, as shown in Fig. 4.7. During all the experiment the plates were kept lubricated with graphite to guarantee uniform lateral displacement over the height and, consequently, avoid barrel deformation of the mantle. Bending and torsional deformations, if present, were negligible; the strain field could be reasonably assumed uniform along the specimen. This turns out to be particularly important since the material exhibits highly nonlinear behavior: constitutive nonlinearities coupled with nonuniform strain would be difficult, even impossible, to analyze. All the tests were conducted at an average temperature of 25°C. All the samples were subjected to loading/unloading cycles up to 25 % to eliminate the Mullins effect.

Starting from the initial undeformed configuration, $\lambda = 1$, the specimen was compressed up to the final strain $\lambda = 0.83$ in $\Delta t = 0.7$ s with constant strain rate. Thereafter, the deformation was held fixed for 100 s, thus performing the stress relaxation test at a constant stretch $\lambda = 0.83$. Figure 4.8 shows the recorded stretch and stress histories.

Theoretically the same deformation ramp between $\lambda = 1$ and $\lambda = 0.83$ with an infinite strain rate, $\Delta t \rightarrow 0$, would have allowed the direct measurement of the viscoelastic kernel $k(t)$ from the stress response, since, in this case, the nominal stress would have been proportional to the kernel. However, in any actual lab test, to not account for the finite strain rate of the initial ramp results in an underestimate of the material characteristic times (Antonakakis *et al.*, 2006).

Relaxation tests allow the capturing of the material behavior involving larger characteristic times. Since in many engineering applications (e.g., tires, engine mounts, etc.), the shortest intrinsic times are also significant, loading/unloading cycles at high strain rate were also performed. As shown in Fig. 4.9, the loading/unloading path was repeated at four different velocity of the rising ramp in the range $\dot{\lambda}_{min} = 0.14$ s⁻¹ to $\dot{\lambda}_{max} = 1.09$ s⁻¹. All the loading paths from the undeformed configuration, $\lambda = 1$, to the maximum strain $\lambda = 0.83$ were displacement controlled; all the unloading paths were force controlled to the zero force. This has allowed us to perform after each cycle a 3 seconds creep test to recover the undeformed, stress-free initial configuration. The time-rate of the force controlled unloading paths were proportional to those of the loading ramps.

Both relaxation and cyclic tests were repeated several times on different specimens, but under the same environmental conditions. For all the repetitions, a good reproducibility has

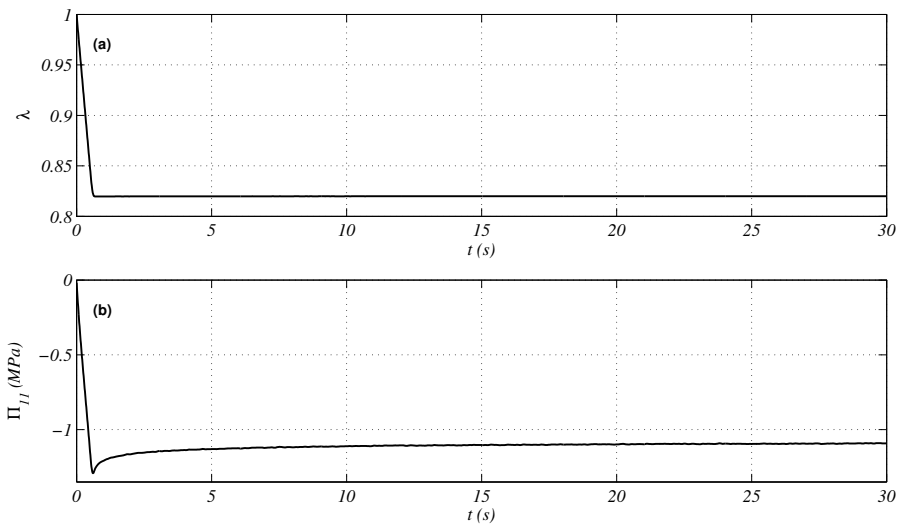


Figure 4.8 Relaxation test: (a) stretch versus time, (b) nominal stress versus time.

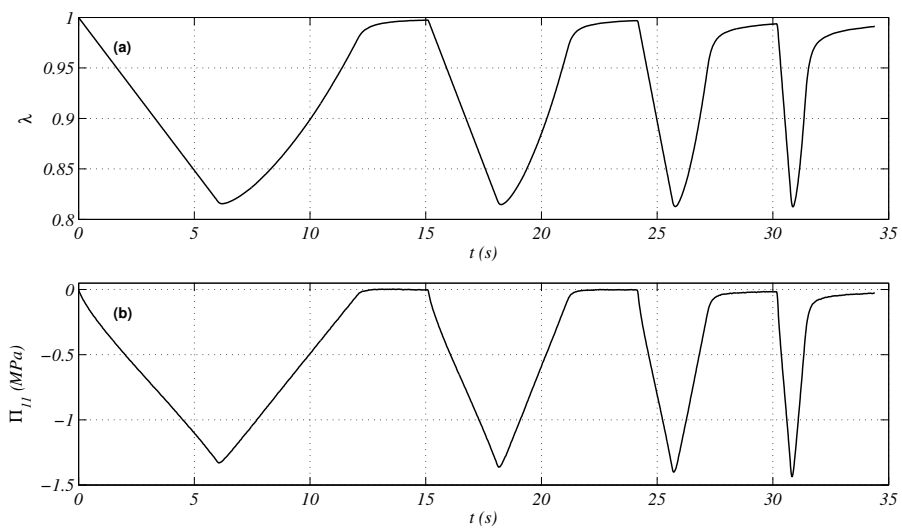


Figure 4.9 Loading/unloading/creep cyclic test at different strain rates: (a) strain versus time, (b) nominal stress versus time. $\dot{\lambda} \in [0.14, 1.09] \text{ s}^{-1}$.

been obtained and the different experimental curves practically overlapped. For the sake of clarity, only one curve is shown in Figs. 4.8 and 4.9.

The experimental results described above can properly be modeled using the standard solution of the extension of an incompressible cylindrical body. Since for all the experiments the strain can reasonably be assumed uniform along the specimen, the deformation is described by

$$x_1 = \lambda(t)X_1, \quad x_2 = \lambda(t)^{-1/2}X_2, \quad x_3 = \lambda(t)^{-1/2}X_3 \quad (4.53)$$

where $\lambda(t)$ (≤ 1) is the stretch ratio in the direction of the uniaxial compression. The resulting deformation gradient has a diagonal form

$$\mathbf{F}(t) = \text{Diag} \left[\lambda(t), \lambda(t)^{-1/2}, \lambda(t)^{-1/2} \right]. \quad (4.54)$$

The condition of a vanishing contact force on the lateral mantle determines the Lagrangian multiplier $p(t)$; eliminating $p(t)$ from Eq. (4.51) and neglecting the inertial forces yields

$$\begin{aligned} \Pi_{11}(t) &= \Pi_{ES11}^{(e)}(t) - \lambda^{-3/2}(t) \Pi_{ES33}^{(e)}(t) \\ &+ \lambda(t) \Lambda_{11}(t) \int_0^t \frac{\partial k(t-s)}{\partial(t-s)} \Psi_{11}(s, t) ds \\ &- \lambda^{-2}(t) \Lambda_{33}(t) \int_0^t \frac{\partial k(t-s)}{\partial(t-s)} \Psi_{33}(s, t) ds, \end{aligned} \quad (4.55)$$

which expresses the relation between the two observable quantities, force per reference area Π_{11} and stretch λ . Equation (4.55) will be used in the next section to identify the constitutive parameters for each of the models under investigation.

4.3.3 Identification of Material Parameters

The standard identification procedure of a linearly viscoelastic model is based on the solution of the static equilibrium equation for the strain history under consideration (see, for instance, [Knauss & Zhao, 2007](#)). This allows the separate identification of the long-term contribution, associated with the stationary stress in a relaxation test, and thereafter of the short-term counterpart.

In the considered nonlinear case, however, the equilibrium equation arising from the constitutive equation (4.55) and the appropriate boundary conditions can only be solved numerically. Moreover, long- and short-term contributions can not be easily decoupled. Therefore, the constitutive parameters are identified by minimizing an error functional which is based on the entire stress history, namely:

$$\min_{\mathbf{p} \in \mathfrak{P}} f(\mathbf{p}) = \min_{\mathbf{p} \in \mathfrak{P}} \left\{ \sum_{i=1}^K w_i^2 \left[\left(\widehat{\Pi}_{11}(\mathbf{p}) \right)_i - \left(\widetilde{\Pi} \right)_i \right]^2 \right\}, \quad (4.56)$$

where $\widetilde{\Pi}$ is the vector of the experimental stress values recorded at the sampling times (t_1, \dots, t_K) , while $\widehat{\Pi}_{11}(\mathbf{p})$ is the vector of the model stress values. The latter depends upon the vector of model parameters \mathbf{p} which spans a subset \mathfrak{P} of \mathbb{R}^P ($P = A + B + 2N$), being constituted by

$$\mathbf{p} = \{\alpha_1, \dots, \alpha_A, \beta_1, \dots, \beta_B, k_1, \dots, k_N, \tau_1, \dots, \tau_N\}, \quad (4.57)$$

with the constraints

$$\alpha_i \geq 0, \quad \beta_i \geq 0, \quad 0 \leq k_i < 1, \quad \sum_{i=1}^N k_i < 1, \quad \tau_i \geq 0. \quad (4.58)$$

The vector $\mathbf{w} = \{w_1, w_2, \dots, w_K\}$ contains the scalar weights used to compare properly the different regions in the experimental curves, e.g., the short- and the long-term responses. From the experimental data, initial estimates for the material stiffnesses α_i have been obtained, whereas the starting point for the material coefficients β_i are chosen to be of the same order of magnitude.

Due to the nonlinear dependence of $\widehat{\Pi}_{11}$ on the constitutive parameters α_i , β_i , k_i and τ_i , the resulting minimization problem (4.56) is generally non-convex. A common choice to overcome the numerical difficulties due to the transcendental dependence of $\widehat{\Pi}_{11}$ upon the τ_i is to fix a-priori the characteristic times, say $\tau_i = \bar{\tau}_i$, inasmuch as one or two per decades of the experimental time range (Knauss & Zhao, 2007). Therefore, the reduced minimization problem becomes

$$\min_{\bar{\mathbf{p}} \in \bar{\mathfrak{P}}} f(\{\alpha_1, \dots, \alpha_A, \beta_1, \dots, \beta_B, k_1, \dots, k_N, \bar{\tau}_1, \dots, \bar{\tau}_N\}). \quad (4.59)$$

with

$$\bar{\mathbf{p}} = \{\alpha_1, \dots, \alpha_A, \beta_1, \dots, \beta_B, k_1, \dots, k_N\} \in \bar{\mathfrak{P}} \subset \mathbb{R}^P.$$

This a-priori choice of the characteristic times, while often used by many authors (Antonakakis *et al.*, 2006; Knauss & Zhao, 2007), has led us to unsatisfactory identification results. As a matter of fact, this choice does not account for the well-known property of carbon black-filled elastomers of having characteristic times very close to each other (Lion, 1997). Therefore, an iterative scheme, which actually allows a better estimate of the characteristic times clusters, is here considered. It consists of the following steps:

1. the minimum characteristic time τ_{min} is chosen according to the acquisition sampling rate, while the maximum characteristic time τ_{max} is dictated by the duration of the experiment;
2. within the range $[\tau_{min}, \tau_{max}]$, N time constants are initially chosen to be equally spaced in logarithmic scale, i.e.,

$$\bar{\tau}_1^{(0)} = \tau_{min}, \quad \dots, \quad \bar{\tau}_i^{(0)} = \tau_{min} 10^{(i-1)\Delta}, \quad \dots, \quad \bar{\tau}_N^{(0)} = \tau_{max} \quad (4.60)$$

where Δ is the logarithmic time step, i.e., $\Delta = [\log_{10}(\tau_{max}/\tau_{min})]/(N-1)$;

3. once the reduced minimization problem

$$\min_{\bar{\mathbf{p}} \in \bar{\mathfrak{P}}} f(\{\alpha_1^{(h)}, \dots, \alpha_A^{(h)}, \beta_B^{(h)}, k_1^{(h)}, \dots, k_N^{(h)}, \bar{\tau}_1^{(h)}, \dots, \bar{\tau}_N^{(h)}\}) \quad (4.61)$$

is solved, a new set $\bar{\tau}_i^{(h+1)}$ of characteristic times is considered. In particular every $\bar{\tau}_i^{(h)}$ is discarded, if the corresponding amplitude $k_i^{(h)}$, minimizing (4.61), is below a given threshold \bar{k} , whereas if $k_i^{(h)}$ overcomes the threshold, the corresponding characteristic time is refined and split into:

$$\bar{\tau}_i^{(h+1)} \leftarrow \bar{\tau}_i^{(h)} \{10^{-(\frac{\Delta}{3})^h}, 1, 10^{(\frac{\Delta}{3})^h}\}. \quad (4.62)$$

The starting point of the minimization (4.61) at step h is taken to be the solution at the previous step $(\alpha_i^{(h-1)}, \beta_i^{(h-1)}, k_i^{(h-1)})$. The initial value of the scalar coefficients $k_i^{(h)}$, corresponding to the newly added time constants, are set to zero. Step 3 is repeated either until all the scalar coefficients k_i exceed \bar{k} , or until the decrement of the objective function between successive steps vanishes.

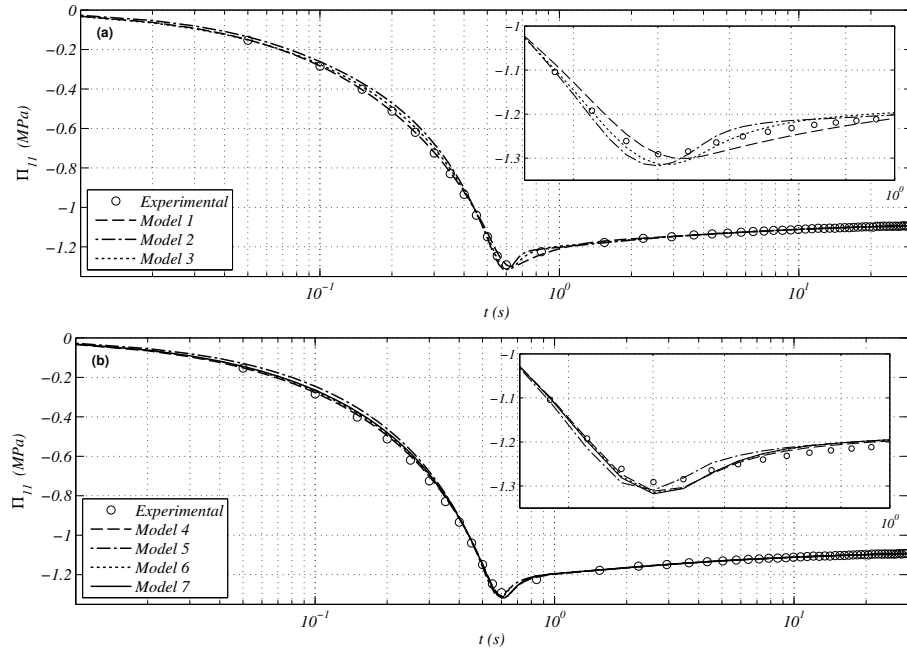


Figure 4.10 Identified nominal stresses Π_{11} versus logarithmic time for the relaxation test: (a) Models 1, 2, 3 and (b) Models 4, 5, 6 and 7. In the nested graph, the fitting models are shown in the range $t \in [0.4, 1]$.

To solve numerically the nonlinear minimization problem (4.61), the combination of the functions *patternsearch* and *fmincon* in the Matlab Optimization Toolbox were used. In particular, the first is a Pattern Search (PS) algorithm (Audet & Dennis, 2003); since it does not require the evaluation of the gradient of the objective function, it turns out to be particularly useful when minimizing high-gradient functions or functions with multiple minima. The latter, instead, is based on a standard Interior Point (IP) algorithm. The combination of PS and IP was needed because the former demonstrated robustness with respect to the choice of the initial points, but poor convergence properties, the latter converged faster, but showed high sensitivity with respect to the starting point. Therefore, at each step, the PS was used to refine the starting point of the IP method.

4.3.4 Results and Discussion

The results of the iterative identification procedure are presented and discussed for all the models under investigation.

We firstly report on the results concerning the relaxation test. In this case the time range of the experimental data is $[0.01 \text{ s}, 30 \text{ s}]$; therefore, at iteration 0 the characteristic times were chosen according to Eq. (4.60):

$$\bar{\tau}_1^{(0)} = 0.01 \text{ s}, \quad \bar{\tau}_2^{(0)} = 0.547 \text{ s}, \quad \bar{\tau}_3^{(0)} = 30 \text{ s}. \quad (4.63)$$

The smallest characteristic time is equal to the sampling rate of the acquisition channel, which in turn was chosen to be 100 Hz.

The results of the optimization algorithm are shown in Fig. 4.10. For almost all the models three steps of the outlined iterative procedure were generally sufficient to reach the stationarity of the objective function. All the models are able to describe the overall behavior of the material also with a low number of initial time constants, $N = 3$ in Eq. (4.63). Fung's

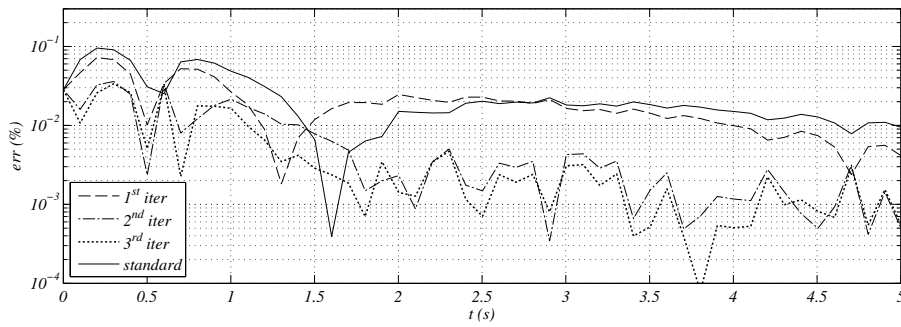


Figure 4.11 Relative error versus time as identified by the standard procedure with $N = 27$ characteristic times and by each of the three steps of the proposed iterative procedure starting with $N = 3$ (Model 4).

Table 4.4 Material parameters as identified through the relaxation test. Only the most significant characteristic times $\bar{\tau}_i$, associated with the highest amplitudes k_i , are reported. In the last column, the corresponding value of the objective function is shown.

Model	α_1	α_2	β_1	β_2	k_I	τ_I	k_{II}	τ_{II}	k_{III}	τ_{III}	f_{val}
	[MPa]	[MPa]	[MPa]	[MPa]	—	[s]	—	[s]	—	[s]	—
1	1.787	0	1.787	0	0.2941	0.312	0.1984	0.252	0.0280	3.646	7.76
2	0.818	0	9.671	—	0.3523	0.038	0.2165	7.9	0.1557	0.005	19.04
3	0.674	0	89.73	—	0.9922	246.9	0.0043	3.646	0.0016	0.082	8.86
4	0	0.731	79.09	0	0.9924	246.9	0.0032	4.507	0.0025	3.646	7.52
5	0	0.865	0	1.946	0.2001	7.9	0.0301	2.08	0.0219	0.082	29.39
6	1.859	0.175	1.859	0.175	0.4777	0.083	0.0249	2.08	0.0156	246.9	9.82
7	1.591	—	7.036	—	0.8589	113.9	0.0486	13.84	0.0445	7.9	12.16

model (Model 1) underestimates the slope and the curvature of the relaxation curve around the kink; this fact is actually related to an under-estimate of the lowest characteristic times.

Figure 4.11 shows the effects of the iterative procedure on the fitting results of Model 4. In order to avoid a division by small values of the force when the stretches are close to one, the relative error is computed as proposed in (Ogden *et al.*, 2004), i.e.,

$$err_i := \frac{\left| \left(\widehat{\Pi}_{11}(\mathbf{p}) \right)_i - \left(\widetilde{\Pi} \right)_i \right|}{\max \left\{ 0.5, \left(\widetilde{\Pi} \right)_i \right\}}, \quad (4.64)$$

and is plotted versus time in Fig. 4.11 for four different cases. The final outcome of the standard procedure with $N = 27$ characteristic times, chosen as suggested in (Knauss & Zhao, 2007), is reported as a solid black line: correspondingly the final value of the objective function was 85.87. The outcomes of all the three steps of the proposed iterative procedure, starting with $N = 3$, are reported as dashed, dotted-dashed and dotted lines, respectively; the final value of the objective function in the third step drops to 7.52. It is evident a monotone reduction of the relative error from the first to the third iteration. Similar results, not shown here, has been obtained for all the other models, proving the effectiveness of the proposed procedure to estimate the characteristic time constants.

Table 4.4 lists the material parameters identified from the relaxation data. On inspection, it is evident that different models are able to fit correctly the same data by different modalities, which in turn call for different stress patterns. Concerning the characteristic times and amplitudes, modeling the material fading memory, we observe that the identification of Prony's series is sensibly ill-conditioned, since several set of characteristic constants are able to produce a good agreement with the experimental data. We remark that for Models 3 and 4, the optimal constitutive parameters are characterized by a factor $\max(\beta_i)/\max(\alpha_i) \approx 100$ between the α - and β -stiffnesses. This happens despite we have chosen the same set of initial data for all the models which is characterized by $\max(\beta_i)/\max(\alpha_i) \approx 1$, as deduced from the experimental curves. Moreover, the optimal values reported in Table 4.4 for Models 3 and 4 happen to be almost insensitive to variations of the initial point in $\overline{\mathfrak{P}}$. We note that, in these two models, the increase of the β -stiffness values corresponds to $\sum k_i \approx 1$. This circumstance can perhaps be explained as in the Fung's model, the only one in which we could obtain some closed-form results, the limit stress value $\Pi_{11}^\infty := \Pi_{11}(t \rightarrow \infty)$ is proportional to $(\beta_1 + \beta_2)(\sum k_i - 1)$. Our guess is that the relaxation data are not sufficient to avoid the spurious behavior of Models 3 and 4, which tends to enlarge the stiffnesses β_i , while letting $\sum k_i \rightarrow 1$.

The results of the iterative fitting for the loading/unloading cyclic tests at different strain rates are shown in Figs. 4.12 and 4.13. While in Fig. 4.12 the whole stress responses are plotted against time, the first and fourth cycles of the same responses are plotted against the stretch in Fig. 4.13a, b and Fig. 4.13c, d, respectively. The latter figure allows the visualization of the error in the energy dissipation for all the considered models. Indeed, a small phase shift in Fig. 4.12 might result in a bad prediction of the dissipated energy along the cycle.

We observe a relevant error for the energy dissipation prediction at low frequencies for all the models; as soon as the strain rate of the loading path increases, and the highest time constants become more significant, a considerable improvement in the fitting is obtained. Figure 4.14 summarizes these results: while, for all the models, the percentage error in the energy dissipation is about 50% for the first cycle at the smallest strain rate, Models 3, 4, 6 and 7 are able to predict the exact dissipated energy within a 3% error at high strain rate. The poor performance of Model 1 (Fung's model) could be due to the strict relation between the elastic instantaneous stress $\Pi_{ES}^{(e)}$ and the integrand of the dissipative part Ψ . By modifying Fung's constitutive equation to have different coefficients in the two terms, a slight

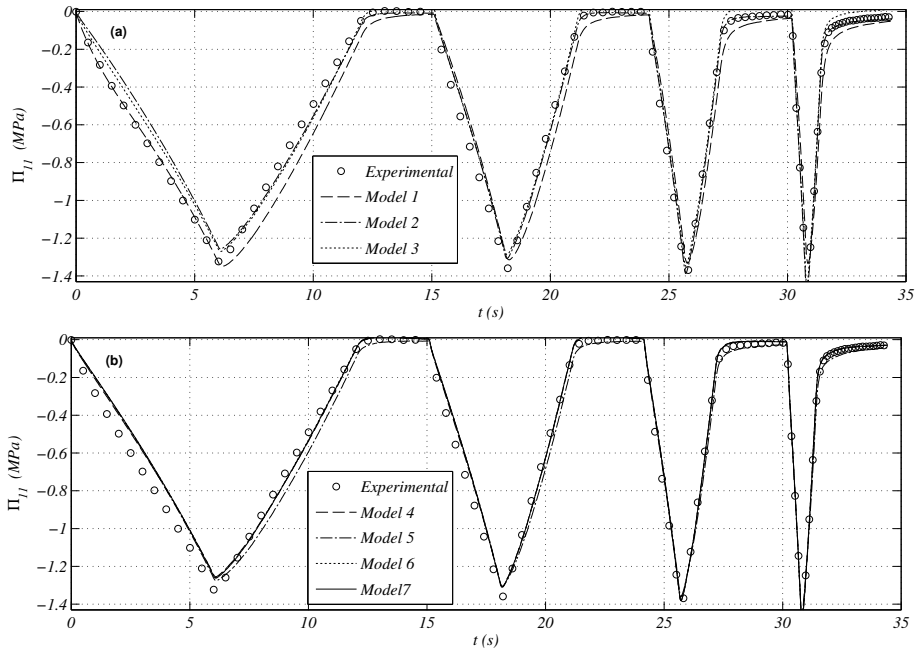


Figure 4.12 Identified nominal stresses Π_{11} versus time t for the loading/unloading cycles: (a) Models 1, 2, 3 and (b) Models 4, 5, 6 and 7.

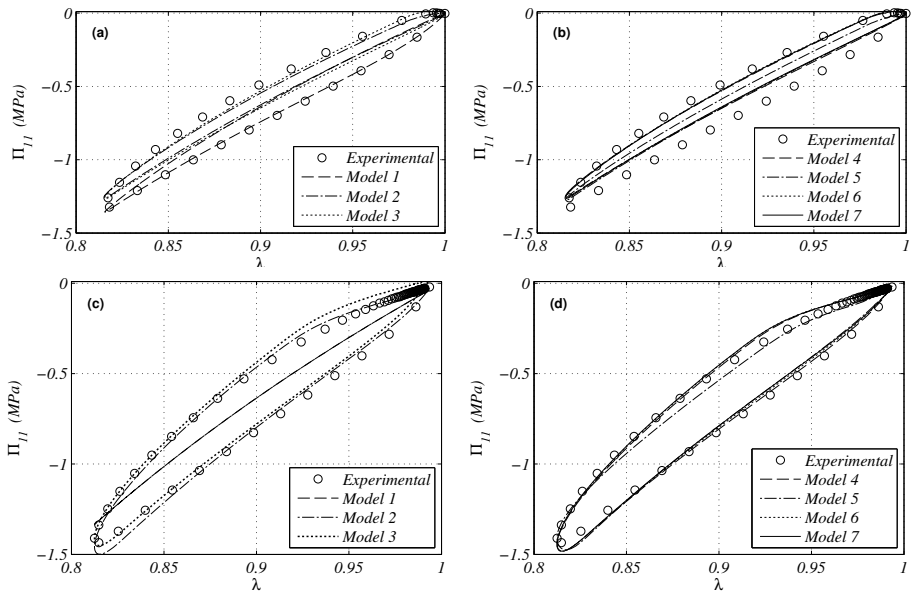


Figure 4.13 Identified nominal stresses Π_{11} versus stretch λ the loading/unloading cycles: (a) Models 1, 2, 3 for $\dot{\lambda} = 0.14 \text{ s}^{-1}$, (b) Models 4, 5, 6, 7 for $\dot{\lambda} = 0.14 \text{ s}^{-1}$ (first cycle), (c) Models 1, 2, 3 for $\dot{\lambda} = 1.09 \text{ s}^{-1}$, (d) Models 4, 5, 6, 7 for $\dot{\lambda} = 1.09 \text{ s}^{-1}$ (fourth cycle).

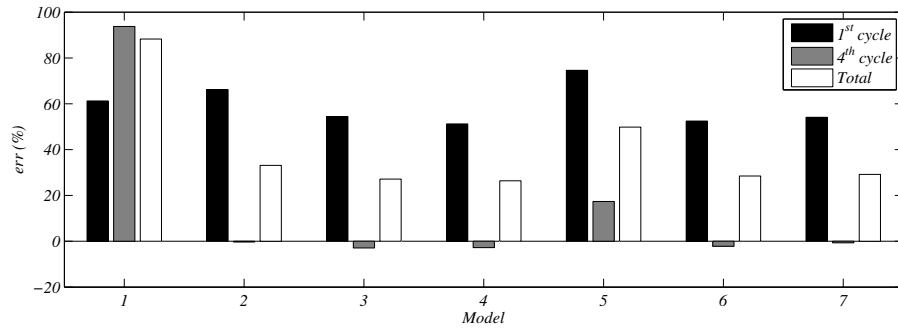


Figure 4.14 Relative error on the dissipated energy for all the considered models in the loading/unloading tests: black, gray and white bars concern the energy dissipation in the first cycle, in the fourth cycle and averaged in the all cycles respectively. A positive error means that the dissipation is underestimated.

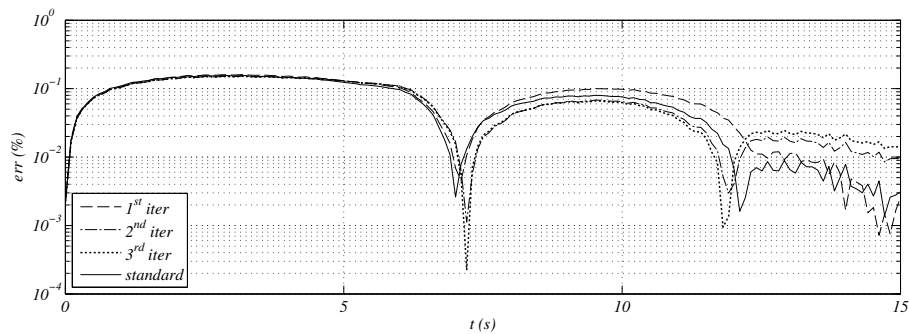


Figure 4.15 Relative errors for the fitting Model 4 through the loading/unloading cyclic tests.

improvement of the fitting model has been obtained. We also recall that when $\alpha_2 \rightarrow 0$, the elastic part of Fung's model reduces to a neo-Hookean constitutive relation and, in this case, it can be proved that its steady-state response is characterized by a vanishing dissipation.

Figure 4.15 shows, for the case of loading/unloading cycles, the advantages of the proposed iterative technique with respect to the standard a-priori choice of the material characteristic times. Again, the solid black curve represents the final outcome of the standard procedure with $N = 27$ Prony's parameters (the final value of the objective function is 2.60), while the dashed, dotted-dashed and dotted lines represent the first three steps of the iterative procedure (the final value of the objective function drops from 3.03 to 2.44). Since the cyclic tests at different strain-rates involve a wide range of characteristic times, the advantages of the iterative procedure are modest, yet its computational effort remains absolutely equivalent to the standard a-priori choice.

Table 4.5 lists the material constants identified from the loading/unloading cyclic tests. For almost all the models, the identified numerical values of the constitutive parameters sensibly differs from the ones listed in Tab. 4.4, which were identified from the relaxation experiment. It is then interesting the following question: is each set of constitutive parameters, identified from one experimental test, able to predict the material response of the other experimental test?

To this aim, Fig. 4.16 shows the material response in loading/unloading cycles as extrapolated by the constitutive parameters identified through the relaxation test. In particular panels *a-b* of Fig. 4.16 refer to the first cycle at low strain rate, while panels *c-d* of the same figure refer to the fourth cycle at high strain-rate. Viceversa, Fig. 4.17 shows the material re-

Table 4.5 Material parameters as identified through the loading/unloading cyclic tests. Only the most significant characteristic times $\bar{\tau}_i$, associated with the highest amplitudes k_i , are reported. In the last column, the corresponding value of the objective function is shown.

Model	α_1	α_2	β_1	β_2	k_I	τ_I	k_{II}	τ_{II}	k_{III}	τ_{III}	f_{val}
	[MPa]	[MPa]	[MPa]	[MPa]	—	[s]	—	[s]	—	[s]	—
1	4.106	0	4.106	0	0.1575	1.187	0.133	0.144	0.1299	2.08	10.11
2	0.881	0	13.08	—	0.3393	0.006	0.2702	0.001	0.0956	0.005	3.15
3	0.003	0	545.9	—	0.9156	246.9	0.0005	0.960	0.0002	0.082	2.48
4	0	0.909	0.934	0.002	0.5002	2.08	0.1485	1.187	0.1234	0.082	2.44
5	0	0.955	0	0.199	0.5569	2.08	0.2678	0.082	0.0624	0.960	4.51
6	9.778	0	9.778	0	0.1249	0.006	0.1151	0.005	0.0757	0.082	2.78
7	1.736	—	0.718	—	0.6025	2.08	0.103	0.960	0.0760	0.082	2.59

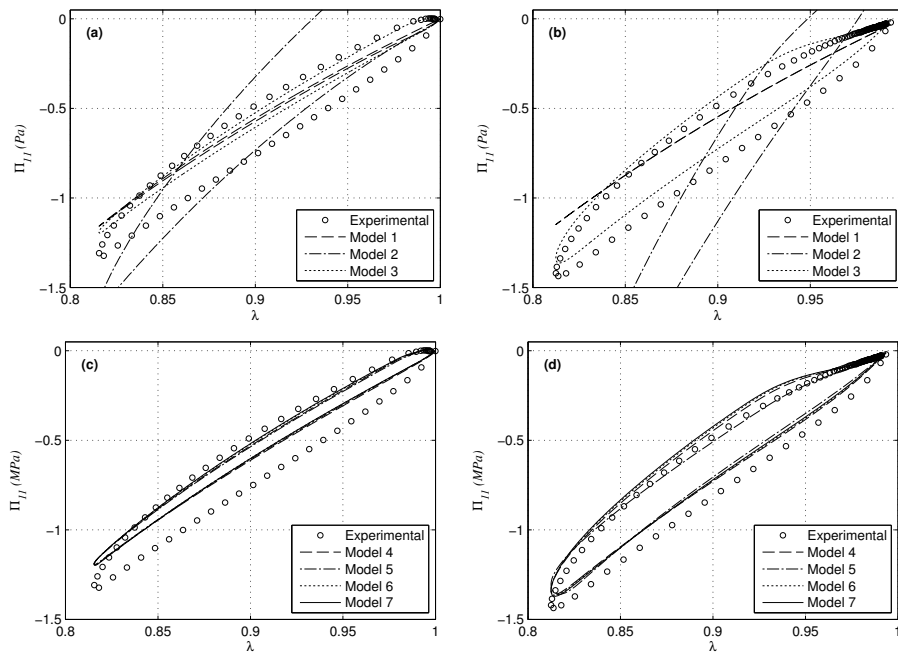


Figure 4.16 Panels (a) and (b) show the hysteresis loop at $\dot{\lambda} = 0.03 \text{ s}^{-1}$ and $\dot{\lambda} = 0.3 \text{ s}^{-1}$, respectively as predicted by the fitting models inferred through the relaxation test.

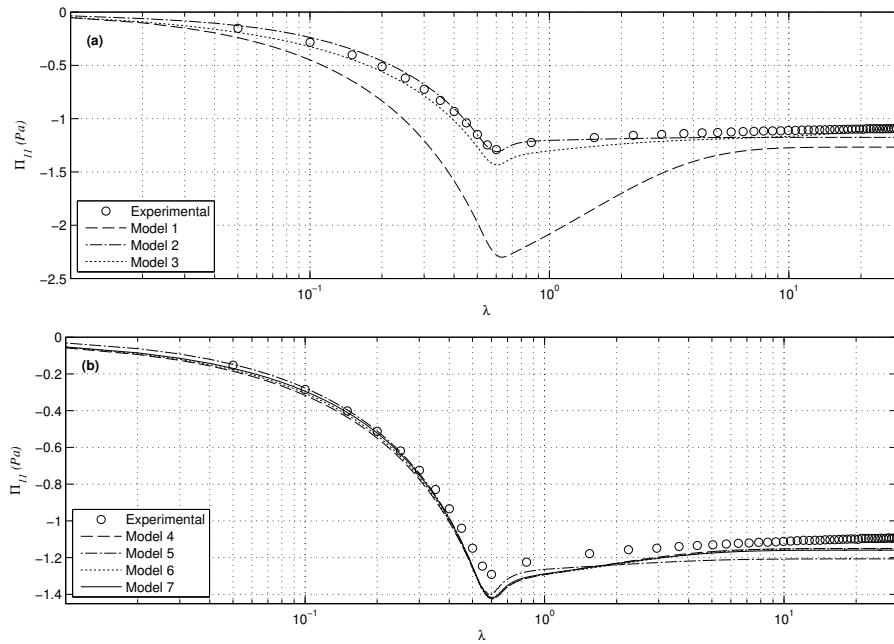


Figure 4.17 Panels (a) and (b) show the relaxation curves as predicted by fitting models inferred through the cyclic test.

sponse in the relaxation test as extrapolated by the constitutive parameters identified through the loading/unloading cycles.

Table 4.6, which refers to the data reported in Fig. 4.16, summarizes the percentage errors in the cross-predictions of the energy dissipation when the material is identified through the relaxation test. Models 1, 2, and 5 show relevant errors at both low and high strain rates. In particular, we observe that i) Model 1 exhibits the already discussed tendency to underestimate significantly the dissipation, ii) Model 2 completely misses the correct material behavior by predicting positive tension stresses under compression strains. On the other hand, Models 3, 4, 6 and 7 perform extremely well by predicting the correct energy dissipation within a percentage error of 67% at low strain rates and within a percentage error of 15% at high strain rates. These two numbers must be compared with the direct prediction errors of Fig. 4.11, i.e., about 50% and 3%, respectively. Models 4, 6 and 7 give also good estimates of the loading and unloading tangent stiffnesses.

Similarly, Tab. 4.7, which refers to the data reported in Fig. 4.17, summarizes the percentage errors in the cross-predictions of maximum and limit stress in the relaxation curve when the material is identified through the cyclic tests. Apart from Model 1, which completely misses the correct behavior, the other models are able to predict the main features of the relaxation test within a 10% error. Model 2 distinguishes by predicting the maximum stress with 1.5% error, while particularly good estimates of the limit stress are given by Models 3, 4, 6 and 7.

Finally, we discuss the fractional kernel (4.47) introduced in (Lion & Kardelky, 2004) (Model 7). As discussed before, up to now the additional parameters δ_i have been kept fixed to allow a fair comparison with the other models. Now these additional parameters are left free to evolve to further minimize the objective function. We remark that in the case of the fractional kernel (4.47), the computational effort in the minimization process considerably increases. Indeed, if the standard viscoelastic kernel is used, since at each step the coefficients τ_i are kept fixed, the resulting objective function is linear with respect to the unknowns α_i and bilinear in β_i and k_i . Instead, when using the fractional model, the kernel function $k(t)$

Table 4.6 Percentage errors in the cross-prediction of energy dissipation when the material is identified through the relaxation test. A positive value means an underestimate.

Model	1 st cycle [%]	4 th cycle [%]	Total [%]
1	93	95	96
2	-79	-48	-56
3	66	13	43
4	66	15	44
5	71	33	56
6	67	12	44
7	66	11	43

Table 4.7 Percentage errors in the cross-predictions of maximum and limit stress when the material is identified through the cyclic tests.

Model	$\max \mathbf{\Pi}_{11} $ [%]	$\mathbf{\Pi}_{11}(t = 30 \text{ s})$ [%]
1	78	16
2	1.5	7.9
3	11	-1.5
4	10	5.5
5	8.4	10
6	10	5.7
7	9.9	6.4

Table 4.8 Percentage errors of Model 7 with $\delta_i = 1$ and $\delta_i = \delta_i^*$. The first two columns show the errors obtained by inferring the material parameters through the cyclic tests, the latter columns refer to the material parameters inferred through the relaxation test.

	$\delta_i = 1$	$\delta_i = \delta_i^*$	$\delta_i = 1$	$\delta_i = \delta_i^*$
	Direct Prediction		Cross-Prediction	
1 st Cycle [%]	54.09	54.03	65.53	65.51
4 th Cycle [%]	-0.67	-0.57	11.4	11.38
Total [%]	29.2	29.08	42.6	42.5
	Cross-Prediction		Direct Prediction	
$\max \mathbf{\Pi}_{11} $ [%]	9.93	9.91	2.04	2.01
$\mathbf{\Pi}_{11}(t = 30 \text{ s})$ [%]	6.41	6.4	0.21	0.19

must be reevaluated for each tentative value of the parameters δ_i , while the resulting objective function depends transcendently on the unknown coefficients. The optimal set $\delta_i = \delta_i^*$ for the fractional kernel is characterized by $0.75 < \delta_i^* \leq 1$; Tab. 4.8 shows the associated results. We observe modest improvements in the direct and cross predictions of Model 7 for what concern both the energy dissipation (at low and high strain rates) and the maximum and limit stresses in relaxation.

4.3.5 Conclusions and perspectives

We have presented a literature survey of the main nonlinear viscoelastic constitutive models and we have identified their parameters on the basis of two different compression tests in the range $\ell/\ell_0 \in [0.83, 1]$. Relaxation and loading/unloading/creep cycles at different strain rates have been performed on a carbon black-filled rubber compound. An iterative identification procedure has been introduced and has led to a better estimate of the characteristic time constants with respect to their a-priori choice used by many authors. The presented results allow us to draw the following conclusions:

- Model 1 (Fung's model), which was firstly introduced to describe the behavior of soft biological tissues, has revealed unable to describe the dissipated energy both at higher and lower strain rates.
- Models 3 (Hallquist, 1998), 4 (Yang *et al.*, 2000), 6 (Hibbit *et al.*, 2007) and 7 (Lion & Kardelky, 2004) have shown the best predicting capabilities: these models are able to predict the dissipated energy in high strain-rate cycles, a crucial quantity in many engineering and bio-medical applications, within a 3% error. The same error raises to 10-15% if their constitutive parameters are identified by the only mean of the relaxation test.
- The relaxation data are not sufficient to resolve both the β_i stiffnesses and the sum of characteristic amplitudes $\sum k_i$ for Models 3 and 4. Thus the limit stress value Π_{11}^∞ is

correctly predicted by the product of a spuriously large stiffness β_i with a spuriously small term $(\sum k_i - 1)$. The cyclic tests eliminate this indetermination for Model 4 but not for Model 3 (cfr. Tabs. 4.4 and 4.5).

- For the purpose of viscoelastic properties identification, the proposed loading/unloading cycles revealed more effective with respect to the simple relaxation test; yet they require the same hardware and the same amount of time to be performed.
- All the considered models sensibly underestimate the energy dissipation in loading/unloading cycles at low strain-rates with 50% errors at least; we recall that the constitutive relations 4 and 5 were specifically aimed at modeling the filled rubber behaviour at high strain rates.
- At least for the presented experimental cases, the use of additional constitutive parameters modeling a fractional derivative viscoelastic kernel does not introduce sensible improvements in the predictions.

Moreover we have observed that different sets of material parameters (as listed in Tabs. 4.4 and 4.5) are able to cross predict the stress response within an acceptable tolerance. Being pretty confident that the described minimization procedure has allowed us to bypass meaningless local minima for the constitutive parameters, we conclude that the presented experimental tests are not sufficient to characterize unequivocally the three-dimensional viscoelastic constitutive relation. In particular tests involving shear deformations, tensile and mixed deformation patterns, yet difficult to perform, could usefully complement the presented data.

Finally we have enlightened a general ill-conditioning in the problem of the identification of the Prony's series modeling the actual material memory. It could be worth curing this difficulty by reducing the description of the viscoelastic kernel to a minimal set of parameters.

Chapter 5

Numerical Applications

Chapter Outline. In this chapter the behavior of isotropic, almost-incompressible, nonlinear elastic and viscoelastic materials is simulated by means of the ABAQUS FEA code. Simple deformations are considered and the numerical results are compared with the analytical solutions. Finally, shortcomings of the ABAQUS finite viscoelasticity model are highlighted and discussed.

5.1 Hyperelastic Material Simulation

When modeling a nonlinear hyperelastic material in ABAQUS, the program makes the following assumptions:

1. the material behavior is *elastic*,
2. the material behavior is *isotropic*,
3. the simulation includes *nonlinear geometrical effects*.

The use of hybrid-type elements is highly recommended when dealing with near-incompressible materials. Such elements are based on mixed-type formulations, where independent interpolations for displacement and stress fields are assumed and two sets of governing equations, both equilibrium and compatibility are enforced in weak form.

As well-known, in the case of incompressible materials, the volumetric strain locking problem appears, if standard displacement-based FE formulations are employed. In order to overcome such numerical drawbacks, various mixed/hybrid FE have been proposed in the literature based on distinct interpolations of displacement and pressure fields. It has been widely demonstrated that such enhanced FE are able to avoid volumetric strain locking. On the other hand, since most of the experimental tests are performed on 2D specimens, where plane stress conditions are satisfied, the use of 2D displacement-based FE together with the plane stress assumption is also justified. In this case the determination of the pressure field is not affected by the volumetric locking problem (see, e.g., [Belytschko, 2000](#)).

In ABAQUS, the identification of the hyperelastic material properties can be performed on the basis of experimental stress-strain curves. Four different tests can be used to get an accurate evaluation of the material parameters. These are uniaxial, planar (pure shear test), equibiaxial and volumetric tests. Clearly, when already known, material parameters can be directly specified in ABAQUS to describe hyperelastic material models. Since the problem of the identification of material parameters has been already addressed in Chap. 4, the second task will be used in this chapter.

In order to investigate ABAQUS performances comparison between analytical and numerical solutions will be carried out. With the aim of investigating how the adopted solution scheme influences the results, standard patch test on single element will be performed and a comparison among different kinds of elements will be addressed (hybrid C3D8H and plane stress CPS4R).

5.2 Implicit vs. Explicit Formulation

Finite Element Analysis (FEA) involving short-time dynamical problems with large deformation, quasi-static problems with large deformations and multiple nonlinearities, or complex contact/impact problems requires the use of either implicit or explicit solution techniques. Examples of these types of simulations are crashworthiness analysis, drop testing, deep drawing, rolling, extruding, pipe whip, bird strike, fan containment and many more.

The ABAQUS FEA program includes the ability to address both implicit as well as explicit solutions. Both the solution procedures are based on a numerical time integration scheme to solve the discrete dynamical equilibrium equations in terms of displacements, velocities and accelerations, then strains and stresses ([Hibbit et al., 2007](#)). Implicit integration schemes (ABAQUS/Standard uses a Hilber-Hughes-Taylor algorithm for implicit integration) assume a constant average acceleration over each time step, $\Delta t = t_{n+1} - t_n$, where t_n and t_{n+1} are the starting and ending points of the time interval Δt . The governing equations are solved and the resulting accelerations and velocities at t_{n+1} are calculated. Then the unknown

displacements at t_{n+1} are determined. Explicit integration schemes (ABAQUS/Explicit uses a Central Difference method) assume a linear change of the displacement in each time step. The governing equations are evaluated and the resulting accelerations and velocities at t_n are calculated. Then, the unknown displacements at t_{n+1} are determined.

There is one major difference between the two techniques in the equations that are used to solve for displacements at t_{n+1} . The implicit solution method requires matrix inversion of the structural stiffness matrix, the explicit solution does not. However, unlike the implicit solution scheme, which is unconditionally stable independently on the time step size, the explicit scheme is stable only for time step size smaller than a critical size evaluated for the analyzed structure. The undamped critical time step size is $2/\omega_n$ (where ω_n is the largest natural circular frequency), which is usually a very small value. This very small time step size requirement for stability thereby makes explicit solutions useful only for very short transient analyses. But, even though the number of time steps in an explicit solution may be orders of magnitude greater than in an implicit solution, it is significantly more efficient than an implicit solution since no matrix inversion is required. Therefore the choice of the integration scheme strongly relies on the problem under investigation.

5.3 Static Analysis

In this section some of the results obtained in Chap. 2 for the simple deformation of hyperelastic materials are recalled. A comparison between analytical and numerical solutions are presented and discussed. The FE analysis was performed using the C3D8R element, which is a general purpose linear brick element, with reduced integration (1 integration point).

5.3.1 Uniaxial Extension

In an uniaxial extension test of an isotropic compressible solid, the (homogeneous) strain tensor is described by

$$\mathbf{F} = \text{Diag} \{ \lambda_1, \lambda_2, \lambda_2 \}, \quad (5.1)$$

where λ_1 and λ_2 are the longitudinal and lateral stretch, respectively. The stretch λ_1 is known, since it depends on the imposed displacement field, but λ_2 has to be determined from the boundary condition. In particular, since $\sigma_{22} = \sigma_{33} = 0$, the stretch λ_2 can be derived from the implicit relation:

$$\sigma_{22}(\lambda_1, \lambda_2) = 0 \quad (5.2)$$

From equations (2.34)-(2.35) the Cauchy stress arising from the deformation (5.1) is

$$\boldsymbol{\sigma} = 2\bar{\phi}_0 \mathbf{I} + 2\bar{\phi}_1 \bar{\mathbf{B}}_D + 2\bar{\phi}_2 (\bar{\mathbf{B}}\bar{\mathbf{B}})_D \quad (5.3)$$

where

$$\bar{\phi}_0 = I_3^{1/2} \frac{\partial \Psi_V}{\partial I_3}, \quad \bar{\phi}_1 = I_3^{-1/2} \left(\frac{\partial \Psi_I}{\partial \bar{I}_1} + \bar{I}_1 \frac{\partial \Psi_I}{\partial \bar{I}_2} \right), \quad \bar{\phi}_2 = -I_3^{-1/2} \frac{\partial \Psi_I}{\partial \bar{I}_2}, \quad (5.4)$$

and $(\cdot)_D$ is the deviatoric part of the tensor.

The dependence of Ψ_{SI} and Ψ_{SV} , i.e., of the isochoric and deviatoric parts of the strain energy function, is known once a constitutive equation is chosen. In the following three different nonlinear models (Neo-Hooke, Mooney-Rivlin, Yeoh) are analyzed.

The Neo-Hookean constitutive law reads as:

$$\begin{aligned} \Psi_I(\bar{I}_1, \bar{I}_2) &= c_{10} (\bar{I}_1 - 3), \\ \Psi_V(I_3) &= \frac{1}{D} \left(I_3^{1/2} - 1 \right)^2, \end{aligned}$$

thus,

$$\boldsymbol{\sigma} = \frac{2}{D}(I_3^{1/2} - 1)\mathbf{I} + 2c_{10}I_3^{-1/2}\bar{\mathbf{B}}_D. \quad (5.5)$$

and the initial shear and bulk moduli (moduli around the reference configuration) are given by:

$$\mu_0 = 2c_{10}, \quad k_0 = 2/D. \quad (5.6)$$

From equation (5.5) one gets the following expression for the Cauchy stress components:

$$\sigma_{11} = \frac{4}{3}(\lambda_1^2 - \lambda_2^2)(\lambda_1 \lambda_2^2)^{-5/3} + \frac{2}{D}(\lambda_1 \lambda_2^2 - 1), \quad (5.7)$$

$$\sigma_{22} = \sigma_{33} = \frac{2}{3}(\lambda_2^2 - \lambda_1^2)(\lambda_1 \lambda_2^2)^{-5/3} + \frac{2}{D}(\lambda_1 \lambda_2^2 - 1), \quad (5.8)$$

Using a numerical root finding method, the lateral strain λ_2 can be obtained from equation (5.2) for a given longitudinal strain λ_1 . We only consider the so-called simple materials, where the implicit relation (5.2) has only one root for a given λ_1 (Ehlers & Eppers, 1998).

In the case of linear elasticity, the Poisson ration ν is known to be a material constant. If a solid is assumed to be incompressible, ν is equal to $1/2$. In what follows, we define a nonlinear Poisson function via the longitudinal and lateral strain (see, e.g., Beatty & Stalnaker, 1986), viz.

$$\nu = -\frac{\lambda_2 - 1}{\lambda_1 - 1}. \quad (5.9)$$

Obviously, ν is not a constant in the case of finite elasticity.

The well-known relation between the initial shear modulus μ_0 , the initial bulk modulus k_0 and the initial Poisson function ν_0 follows from a linearization around the reference configuration of equation (5.3) (Ehlers & Eppers, 1998), i.e.,

$$\nu_0 = \frac{3k_0 - 2\mu_0}{6k_0 + 2\mu_0} \quad (5.10)$$

The values of the nonlinear Poisson function (5.9) have been plotted in figure (5.1) for a Neo-Hookean material and for different values of D and increasing λ_1 .

The same results have been obtained for Mooney-Rivlin and Yeoh models, for which the strain energy functions are:

$$\Psi_I(\bar{I}_1, \bar{I}_2) = c_{10}(\bar{I}_1 - 3) + c_{01}(\bar{I}_2 - 3), \quad (5.11)$$

$$\Psi_V(I_3) = \frac{1}{D} \left(I_3^{1/2} - 1 \right)^2, \quad (5.12)$$

and

$$\Psi_I(\bar{I}_1, \bar{I}_2) = c_{10}(\bar{I}_1 - 3) + c_{20}(\bar{I}_2 - 3), \quad (5.13)$$

$$\Psi_V(I_3) = \frac{1}{D} \left(I_3^{1/2} - 1 \right)^2, \quad (5.14)$$

respectively

From equation (5.3), the following stress-strain relations are valid:

$$\boldsymbol{\sigma} = \frac{2}{D}(I_3^{1/2} - 1)\mathbf{I} + 2I_3^{-1/2}(c_{10} + c_{01}\bar{I}_1)\bar{\mathbf{B}}_D - 2c_{01}I_3^{-1/2}(\bar{\mathbf{B}}^2)_D. \quad (5.15)$$

for a Mooney-Rivlin material, and

$$\boldsymbol{\sigma} = \frac{2}{D}(I_3^{1/2} - 1)\mathbf{I} + 2I_3^{-1/2}[c_{10} + c_{20}(\bar{I}_1 - 3)]\bar{\mathbf{B}}_D. \quad (5.16)$$

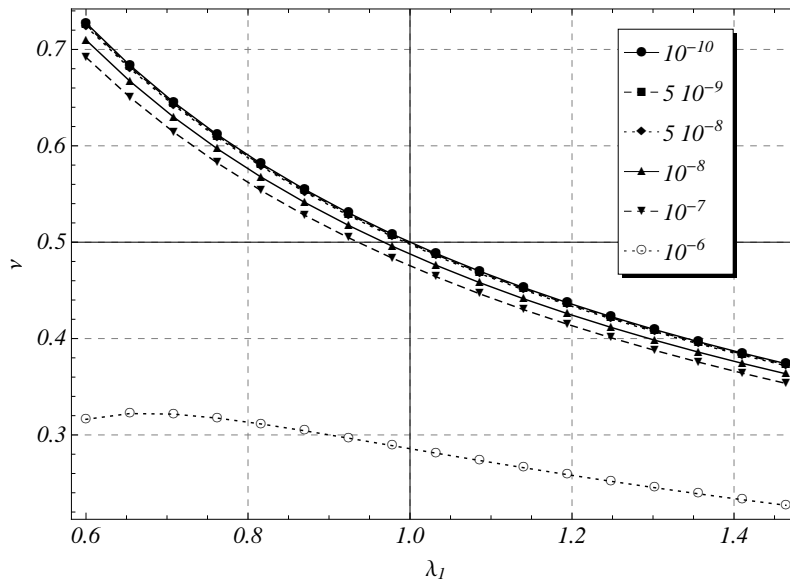


Figure 5.1 Nonlinear Poisson function for a Neo-Hookean material with different values of the compressibility coefficient D for the analytical model (solid curves) and the ABAQUS FEA model (dotted curves). The two curves perfectly overlap.

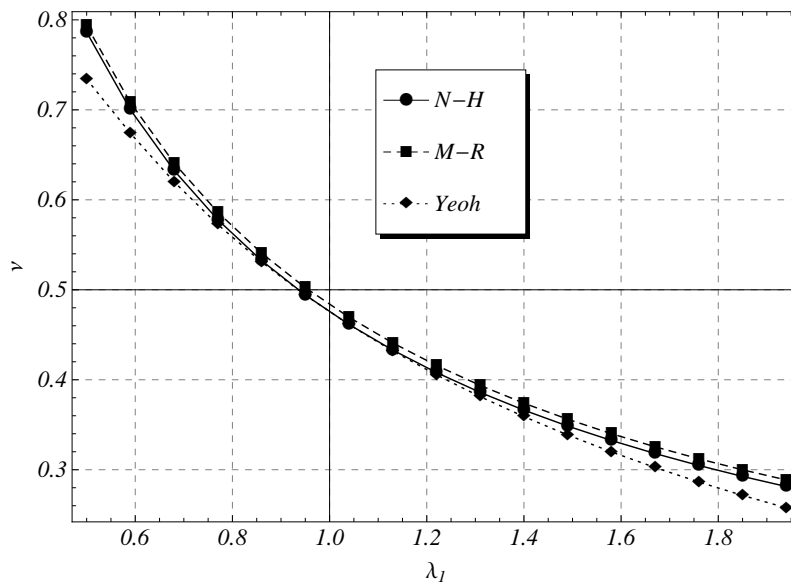


Figure 5.2 Nonlinear Poisson function in the case of different material models for the analytical model (solid curves) and the ABAQUS FEA model (dotted curves) with $D = 10^{-8}$. The analytical and numerical curves perfectly overlap.

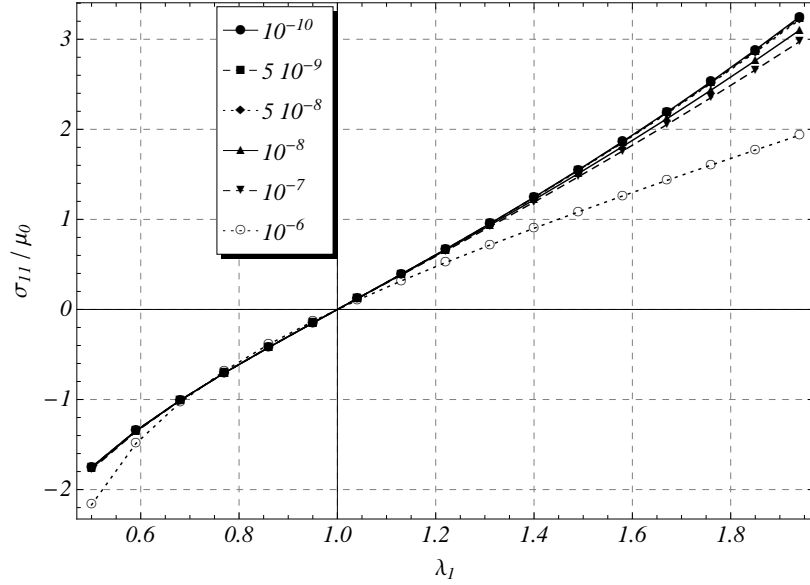


Figure 5.3 Normalized uniaxial stress σ_{11}/μ_0 plotted against stretch λ_1 for a Neo-Hookean material with different values of the compressibility coefficient D for the analytical model (solid curves) and the ABAQUS FEA model (dotted curves). The analytical and numerical curves perfectly overlap.

for a Yeoh material.

Moreover, the initial moduli are:

$$\mu_0 = 2(c_{10} + c_{01}), \quad k_0 = 2/D \quad (5.17)$$

from equations (5.15), and

$$\mu_0 = 2c_{10}, \quad k_0 = 2/D \quad (5.18)$$

from (5.16).

The results of the combined numerical/analytical simulations are shown in Figs. (5.1)-(5.4). The constitutive parameters were chosen as

$$c_{10} = c_{01} = \mu_0/4, \quad (5.19)$$

for Mooney-Rivlin model and

$$c_{20} = \mu_0/4 \quad (5.20)$$

for Yeoh model. In all the cases the volumetric constant was $D = 10^{-8}$.

Figure 5.1 shows the nonlinear Poisson's function in terms of the stretch λ_1 in the case of a Neo-Hookean material model. For every value of the compressibility constraint D in the range $D \in [10^{-10}, 10^{-6}]$, the analytical and (ABAQUS) numerical models predict the same Poisson's function. For $D = 10^{-6}$, ν displays a non-monotonic behavior for smaller stretches, which means that for very high compression ratios the lateral displacement diminishes while the material is being compressed. This non-physical behavior is a consequence of the volumetric/isochoric split of the strain energy function and it is well documented in the literature (Ehlers & Eppers, 1998).

The different nonlinear Poisson's function arising from the material models considered are shown in Fig. 5.2. Figure 5.3 displays the uniaxial behavior of the models.

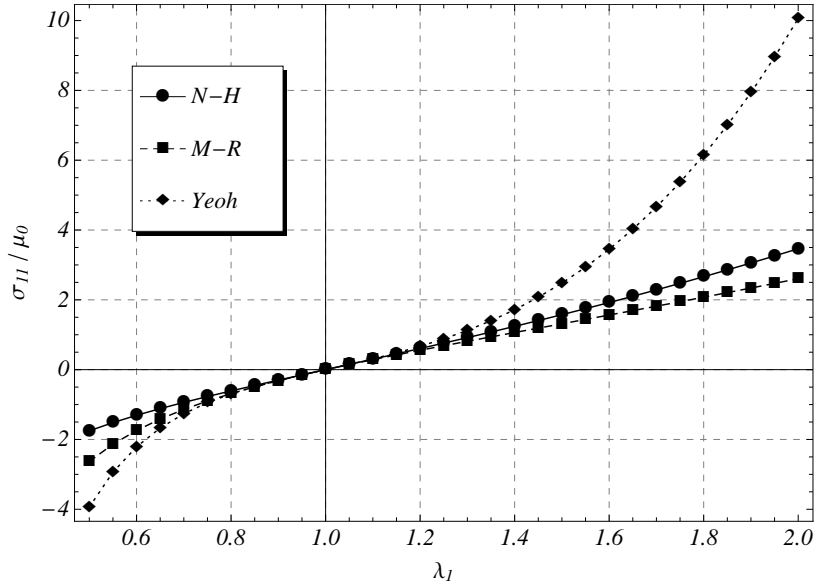


Figure 5.4 Normalized uniaxial stress σ_{11}/μ_0 plotted against stretch λ_1 for different analytical models (solid curves) and the corresponding ABAQUS FEA models (dotted curves) in the simple tension case. The two curves perfectly overlap.

5.3.2 Simple Shear

A simple shear deformation has been described in Chap. 2. Recalling those results, the deformation gradient is given by:

$$\mathbf{F} = \begin{bmatrix} 1 & \gamma & 0 \\ 0 & 1 & 0 \\ 0 & 0 & 1 \end{bmatrix} \quad (5.21)$$

thus, $\det \mathbf{F} = 1$.

The boundary conditions applied to subject a solid to a simple shear deformation state are such that the deformation (5.21) is volume-preserving, independently on the assumed constitutive equation.

We refer here and henceforth to the analytical solutions reported in table (2.2). The comparison between numerical and analytical results are plotted in figures (5.5) and (5.6). The material parameters are the same as in the uniaxial extension case. The volumetric constant D has been set to $D = 10^{-8}$, which for $\mu_0 = 10^6$ corresponds to $\nu = 0.495$.

5.4 Dynamic Simulations

In this section we derive analytical solutions for the two boundary-value problems considered also in the static case: simple shear and uniaxial extension.

We henceforth focus on an incompressible viscoelastic solid for which the instantaneous response is modeled by a two terms Yeoh stress-strain relationship (a standard implementation in ABAQUS):

$$\boldsymbol{\sigma}_e = -p\mathbf{I} + \mu_0(1 - 3\alpha + \alpha I_1) \mathbf{B}, \quad (5.22)$$

where μ_0 and α are positive constants (μ_0 is the shear modulus in the reference configuration) and $I_1(t) = \text{tr}\{\mathbf{B}(t)\}$. Also, for simplicity, the time relaxation of the solid is assumed to be

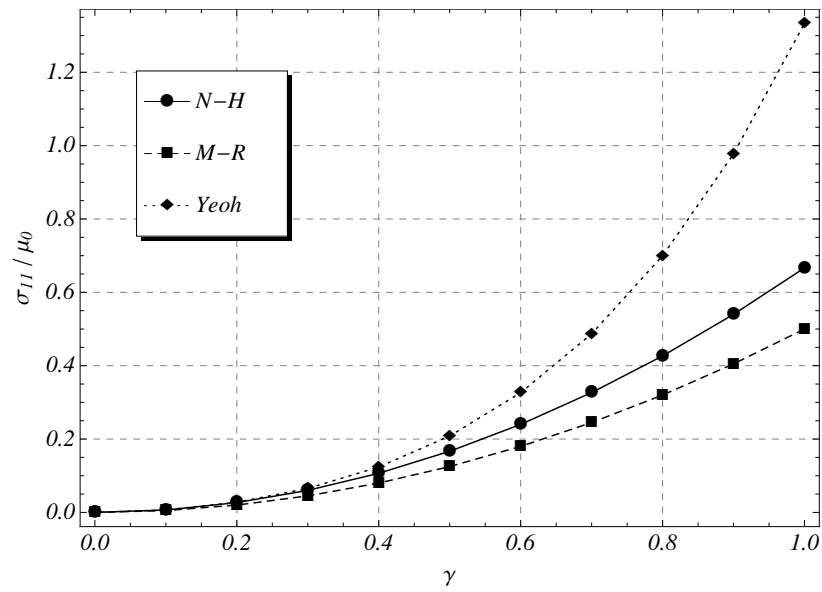


Figure 5.5 Normalized stress σ_{11}/μ_0 plotted against stretch γ for different analytical models (solid curves) and the corresponding ABAQUS FEA models (dotted curves) in the simple shear case.

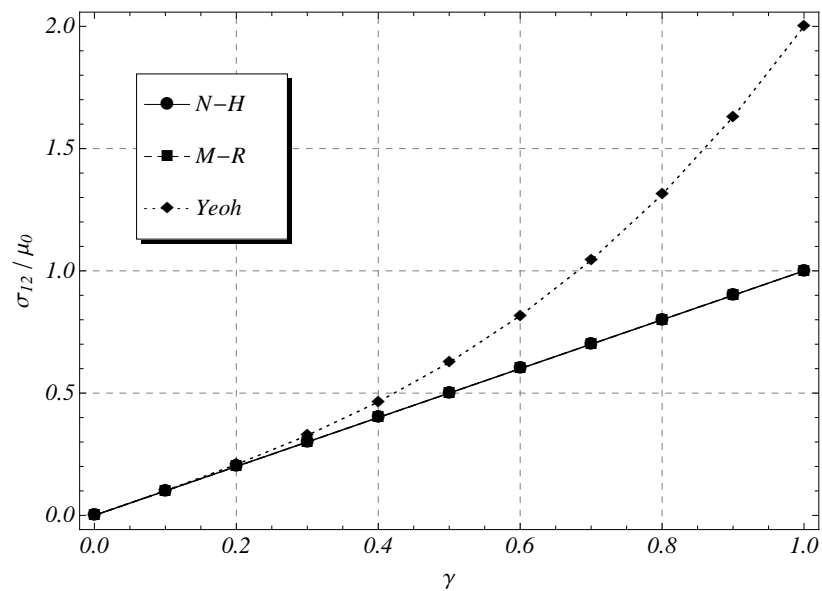


Figure 5.6 Normalized shear stress σ_{12}/μ_0 plotted against stretch γ for different analytical models (solid curves) and the corresponding ABAQUS FEA models (dotted curves) in the simple shear case.

governed by a one-term Prony series expansion given by:

$$G(t) = \frac{\mu_\infty}{\mu_0} + \left(1 - \frac{\mu_\infty}{\mu_0}\right) e^{-t/\tau}, \quad (5.23)$$

where μ_∞ is the asymptotic value to which the shear modulus settles after an infinite time and τ is a characteristic time constant.

For the sake of clarity, let recall the ABAQUS FEA finite viscoelastic model already introduced in Section 3.3.3; for an incompressible solid it reads as

$$\begin{aligned} \boldsymbol{\sigma}(t) = & -p(t)\mathbf{I} + \psi_1(t)\mathbf{B}(t) + \psi_2(t)\mathbf{B}(t)^2 \\ & + \sum_{i=1}^2 \text{SYM} \left\{ \mathbf{F}(t) \left[\int_0^t \dot{G}(t-s)\psi_i(s)\mathbf{C}(s)^i ds \right] \mathbf{F}^{-1}(t) \right\}, \end{aligned} \quad (5.24)$$

where $p(t) = \hat{p}(t) + \int_0^t \dot{G}(t-s)\hat{p}(s)ds$ is arbitrary and remains to be determined from initial/boundary conditions.

Then, for the ABAQUS model we have $\psi_1(t) = \mu_0(1 - 3\alpha + \alpha I_1(t))$, $\psi_2(t) = 0$, and hence (5.24) reduces to:

$$\begin{aligned} \boldsymbol{\sigma}(t) = & -p(t)\mathbf{I} + \mu_0 (1 - 3\alpha + \alpha I_1(t)) \mathbf{B}(t) + \\ & + \frac{(\mu_\infty - \mu_0)}{\tau} \text{SYM} \left\{ \mathbf{F}(t) \left[\int_0^t e^{-(t-s)/\tau} (1 - 3\alpha + \alpha I_1(s)) \mathbf{C}(s) ds \right] \mathbf{F}^{-1}(t) \right\}. \end{aligned} \quad (5.25)$$

By contrast, for the Fung's QLV model introduced in Sec. 3.3.1, the result is

$$\phi_0(s, t-s) = \mu_0 [1 - 3\alpha + \alpha I_1(s)] G(t-s), \quad \phi_1(s, t-s) = 0, \quad \phi_2(s, t-s) = 0, \quad (5.26)$$

yielding

$$\begin{aligned} \boldsymbol{\sigma}(t) = & -p(t)\mathbf{I} + \mu_0 [1 - 3\alpha + \alpha I_1(s)] \mathbf{B}(t) \\ & + \frac{\mu_\infty - \mu_0}{\tau} \int_0^t e^{-(t-s)/\tau} [1 - 3\alpha + \alpha I_1(s)] ds \mathbf{B}(t). \end{aligned} \quad (5.27)$$

In order to further highlight the differences between Abaqus and QLV model, we will compare the average rate of working in the case of the two simple motions considered here. To this end, we define the dissipated energy density E_d over a period T referred to the current configuration.

We recall that the internal rate of working of the stress per unit current volume is $\boldsymbol{\sigma}(t) \cdot \mathbf{D}(t) \equiv \text{tr} \{ \boldsymbol{\sigma}(t) \mathbf{D}(t) \}$. Assuming for $\mathbf{D}(t)$ a periodic time law, the time-averaged work done per unit current volume over a period T starting at time T_0 , is given by

$$E_d = \frac{1}{T} \int_{T_0}^{T_0+T} \boldsymbol{\sigma}(t) \cdot \mathbf{D}(t) dt, \quad (5.28)$$

where T_0 and $T_0 + T$ are the starting and ending time points.

Since the elastic part of the stress does not contribute to this expression (5.28) represents the energy dissipated in a cycle (which depends on T_0 in general).

5.4.1 Uniaxial Extension

When an incompressible isotropic solid is subjected to an uniaxial extension, the (homogeneous) motion is described by:

$$x_1 = \lambda(t)X_1, \quad x_2 = \lambda(t)^{-1/2}X_2, \quad x_3 = \lambda(t)^{-1/2}X_3, \quad (5.29)$$

where $\lambda(t) (\geq 1)$ is the stretch ratio in the direction of the uniaxial tension $\sigma_{11} (\geq 0)$. The resulting deformation gradient has the following diagonal form:

$$\mathbf{F}(t) = \text{Diag} \left[\lambda(t), \lambda(t)^{-1/2}, \lambda(t)^{-1/2} \right]. \quad (5.30)$$

Vanishing of the lateral stresses $\sigma_{22} = \sigma_{33} = 0$ determines the Lagrange multiplier $p(t)$ and elimination of $p(t)$ yields

$$\begin{aligned} \sigma_{11}(t) = & \mu_0 \left[\lambda(t) - \lambda^{-2}(t) \right] \left[2\alpha + (1 - 3\alpha)\lambda(t) + \alpha\lambda^3(t) \right] \\ & + \frac{\mu_\infty - \mu_0}{\tau} \int_0^t e^{-(t-s)/\tau} \left[\lambda(s) - \lambda^{-2}(s) \right] \left[2\alpha + (1 + 3\alpha)\lambda(s) + \alpha\lambda^3(s) \right] ds, \end{aligned} \quad (5.31)$$

for the Abaqus model and

$$\begin{aligned} \sigma_{11}(t) = & \mu_0 \left[\lambda(t) - \lambda^{-2}(t) \right] \left[2\alpha + (1 - 3\alpha)\lambda(t) + \alpha\lambda^3(t) \right] \\ & + \frac{\mu_\infty - \mu_0}{\tau} \left[\lambda^2(t) - \lambda^{-1}(t) \right] \int_0^t e^{-(t-s)/\tau} \lambda^{-1}(s) \left[2\alpha + (1 + 3\alpha)\lambda(s) + \alpha\lambda^3(s) \right] ds, \end{aligned} \quad (5.32)$$

for the QLV model.

The difference between these models is now clear, and it reflects significantly on the rate of working, as we confirm numerically below. From an experimental point of view, it is common practice to employ a dynamic displacement superimposed on a large static deformation. Here we consider a Neo-Hookean solid deformed in tension to a stretch of 1.5 from time $t = 0$ to time $t = 1$, and then made to oscillate with a superimposed amplitude such that the stretch $\lambda(t)$ ranges from 1. to 1.5. Thus,

$$\lambda(t) = \begin{cases} 1 + 0.5t, & 0 \leq t \leq 1, \\ 1.5 + 0.2 \sin \omega(t - 1), & t \geq 1. \end{cases} \quad (5.33)$$

For numerical purposes the stresses are non-dimensionalized by dividing by μ_0 . For the remaining parameters we set

$$\mu_\infty/\mu_0 = 0.5, \quad \tau = 0.01 \text{ s}, \quad \omega = 48\pi \text{ s}^{-1}, \quad (5.34)$$

except when the frequency dependence of the energy dissipation rate is investigated where ω varies.

The numerical results have been obtained with ABAQUS 6.7-1 using a single C3D8H element (brick, 8 nodes, trilinear, hybrid with constant pressure) with an implicit solution scheme. As a check, the same test was done with a 2D plane stress element CPS4 (4 nodes, bilinear, plane stress) and the same results were obtained. Furthermore a comparison among implicit solution scheme, explicit solution scheme and analytical solution has been carried out and the results are shown in Fig. 5.7. In the case of Explicit time integration a C3D8 element has been used.

The results settle very rapidly to the steady state so that the expression (5.28) becomes essentially independent on T_0 . Figure 5.8, in which E_d/μ_0 is plotted against frequency ω in the steady state, shows clearly that the ABAQUS model overestimates the steady state energy dissipation substantially (by a factor of 4 to 5) compared with the QLV model.

5.4.2 Simple Shear

We now consider a simple shear motion of the form:

$$x_1 = X_1 + \gamma(t)X_2, \quad x_2 = X_2, \quad x_3 = X_3, \quad (5.35)$$

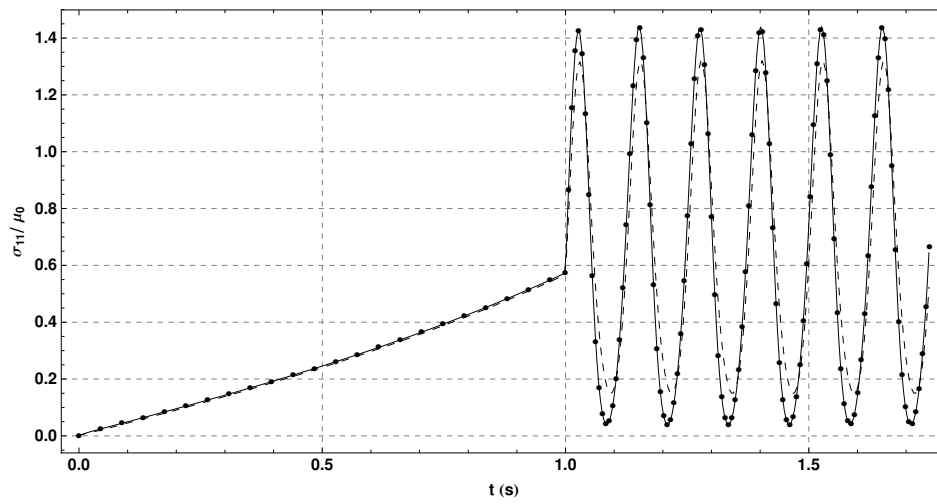


Figure 5.7 Dependence of the dimensionless axial tension σ_{11} on time t for the Abaqus FEA model (solid curve), the ABAQUS output (dotted curve) and the QLV model (dashed curve).

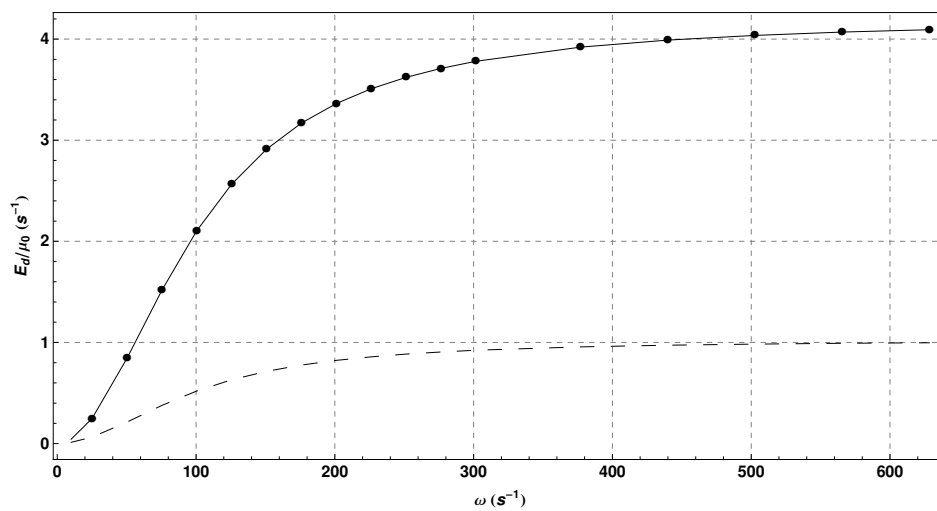


Figure 5.8 Dependence of the rate of working per unit volume in dimensionless form E_d/μ_0 on frequency ω over a single period in the steady state for the ABAQUS model (solid curve), the ABAQUS output (dotted curve) and the QLV model (dashed curve) in the case of uniaxial extension.

where $\gamma(t)$ is the amount of shear strain. The (non-symmetric) deformation gradient results as:

$$\vec{F}(t) = \begin{bmatrix} 1 & \gamma(t) & 0 \\ 0 & 1 & 0 \\ 0 & 0 & 1 \end{bmatrix}. \quad (5.36)$$

Simple calculations reveal that a sheared solid described by the ABAQUS model is in a state of *plane stress* ($\sigma_{ij} \neq 0$ for $i, j \in \{1, 2\}$; $\sigma_{3j} = 0$ for $j = 1, 2, 3$) when the Lagrange multiplier $p(t)$ is taken as

$$p(t) = \mu_\infty - (\mu_\infty - \mu_0)e^{-t/\tau} + \alpha \mu_0 \gamma^2(t) - \alpha \frac{\mu_\infty - \mu_0}{\tau} \int_0^t e^{-(t-s)/\tau} \gamma^2(s) ds. \quad (5.37)$$

Note that the combination of plane strain and plane stress (in the (1, 2) plane) is permissible for an incompressible material provided $p(t)$ (and hence $\sigma_{11}(t)$ and $\sigma_{22}(t)$) is (are) adjusted accordingly. Then, for the ABAQUS model we obtain

$$\begin{aligned} \sigma_{11}(t) &= \mu_0 \gamma^2(t) [1 + \alpha \gamma^2(t)] + \frac{\mu_\infty - \mu_0}{\tau} \gamma(t) \int_0^t e^{-(t-s)/\tau} \gamma(s) [1 + \alpha \gamma^2(s)] ds, \\ \sigma_{12}(t) &= \mu_0 \gamma(t) [1 + \alpha \gamma^2(t)] + \\ &\quad + \frac{(\mu_\infty - \mu_0)}{2\tau} \int_0^t e^{-(t-s)/\tau} \gamma(s) [2 + \gamma(s)\gamma(t) - \gamma^2(t)] [1 + \alpha \gamma^2(s)] ds, \\ \sigma_{22}(t) &= \frac{(\mu_\infty - \mu_0)}{\tau} \int_0^t e^{-(t-s)/\tau} \gamma(s) [\gamma(s) - \gamma(t)] [1 + \alpha \gamma^2(s)] ds, \end{aligned} \quad (5.38)$$

and for the QLV model

$$\begin{aligned} \sigma_{11}(t) &= \mu_0 \gamma^2(t) [1 + \alpha \gamma^2(t)] + \frac{\mu_\infty - \mu_0}{\tau} \gamma^2(t) \int_0^t e^{-(t-s)/\tau} [1 + \alpha \gamma^2(s)] ds, \\ \sigma_{12}(t) &= \mu_0 \gamma(t) [1 + \alpha \gamma^2(t)] + \frac{\mu_\infty - \mu_0}{\tau} \gamma(t) \int_0^t e^{-(t-s)/\tau} [1 + \alpha \gamma^2(s)] ds, \\ \sigma_{22}(t) &= 0. \end{aligned} \quad (5.39)$$

Note that Rivlin's universal relation $\sigma_{11} - \sigma_{22} = \gamma \sigma_{12}$ from isotropic elasticity holds also for the present Yeoh-based viscoelastic model. The expressions in (5.39) are expected intuitively for the Yeoh model because for its instantaneous response at very short times the Cauchy stress has components $\sigma_{e11} = \mu_0 \gamma^2 (1 + \alpha \gamma^2)$, $\sigma_{e12} = \mu_0 \gamma (1 + \alpha \gamma^2)$, $\sigma_{e22} = 0$. By contrast, the ABAQUS model gives rise to a σ_{22} component generated purely by the viscoelastic effects, in which case the relaxation process creates such a component *ex nihilo!* However, since simple shear is a displacement controlled motion the stress components adjust automatically to accommodate the geometry and they are therefore very much dependent on the form of the constitutive law. The difference in the shear stress, however, has serious consequences for the rate of working, and hence the dissipation, because here

$$\mathbf{D}(t) = \begin{bmatrix} 0 & \dot{\gamma}(t)/2 & 0 \\ \dot{\gamma}(t)/2 & 0 & 0 \\ 0 & 0 & 0 \end{bmatrix}, \quad (5.40)$$

and hence $\boldsymbol{\sigma} \cdot \mathbf{D} = \sigma_{12}(t) \dot{\gamma}(t)$, which is obviously not the same for both models.

We confirm these findings by testing the ABAQUS software against the formulas (5.38)-(5.40). We take the amount of shear $\gamma(t)$ to vary as

$$\gamma(t) = \begin{cases} t, & 0 \leq t \leq 1 \\ 1 + 0.2 \sin[\omega(t-1)], & t \geq 1, \end{cases} \quad (5.41)$$

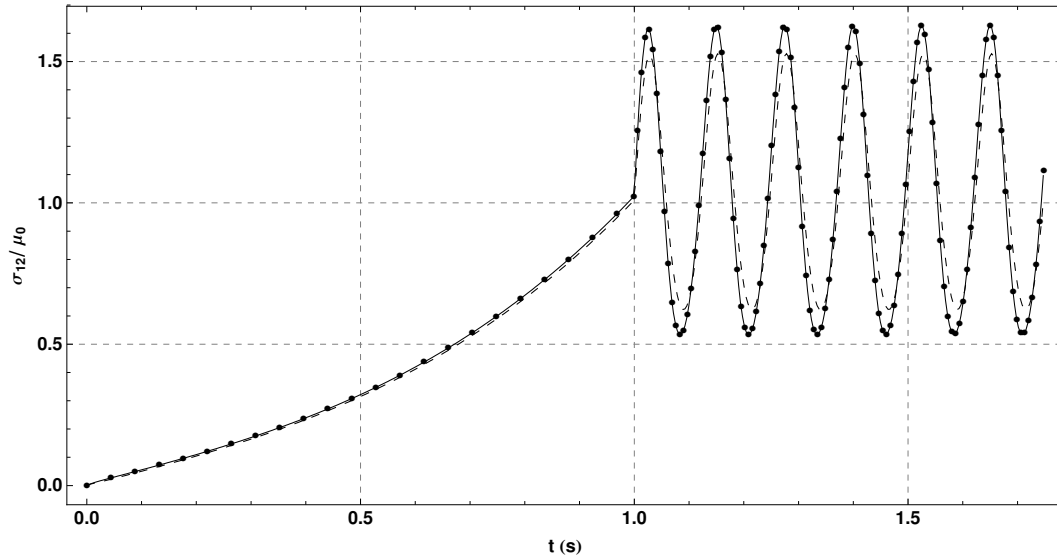


Figure 5.9 Dependence of σ_{12}/μ_0 on time t in simple shear state for the ABAQUS analytical model (solid curve), the ABAQUS output (dotted curve) and the QLV model (dashed curve).

with the other parameters given by (5.34). Figures 5.9 and 5.10 display the variations of the σ_{12} and σ_{22} components computed from (5.38) and (5.39) in dimensionless form. As in the case of simple tension there is not a great difference in the active stress (in this case σ_{12}) between the two models, but the reactive stress σ_{22} is very different. Finally, as also for simple tension, we find that the ABAQUS model overestimates the rate of working with respect to the QLV model (by a factor of 2 to 3), as shown in Fig. 5.11, again in dimensionless form with E_d/μ_0 plotted against frequency ω in the steady state. Using the ABAQUS software, we recovered the thick curves (in Figs. 5.9 and 5.10), which confirms that equation (5.24) is actually implemented in the ABAQUS code.

A comparison between implicit and explicit solution scheme has been performed. In the latter case a C3D8 element has been used (C3D8H is not available in explicit time integration). We find that the explicit solution scheme overestimates the rate of working with respect to the implicit/theoretical model, as shown in Fig. 5.11, again in dimensionless form with E_d/μ_0 plotted against frequency ω in the steady state.

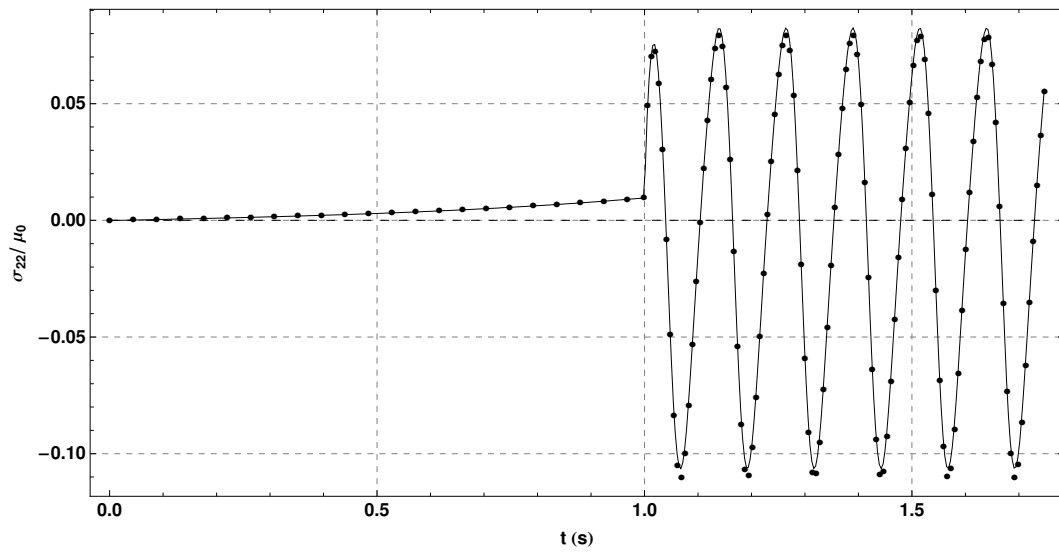


Figure 5.10 Dependence of $\sigma_{22}(t)/\mu_0$ on time t in simple shear for the ABAQUS FEA model (solid curve), the ABAQUS output (dotted curve) and the QLV model (dashed curve). The latter is zero for all times.

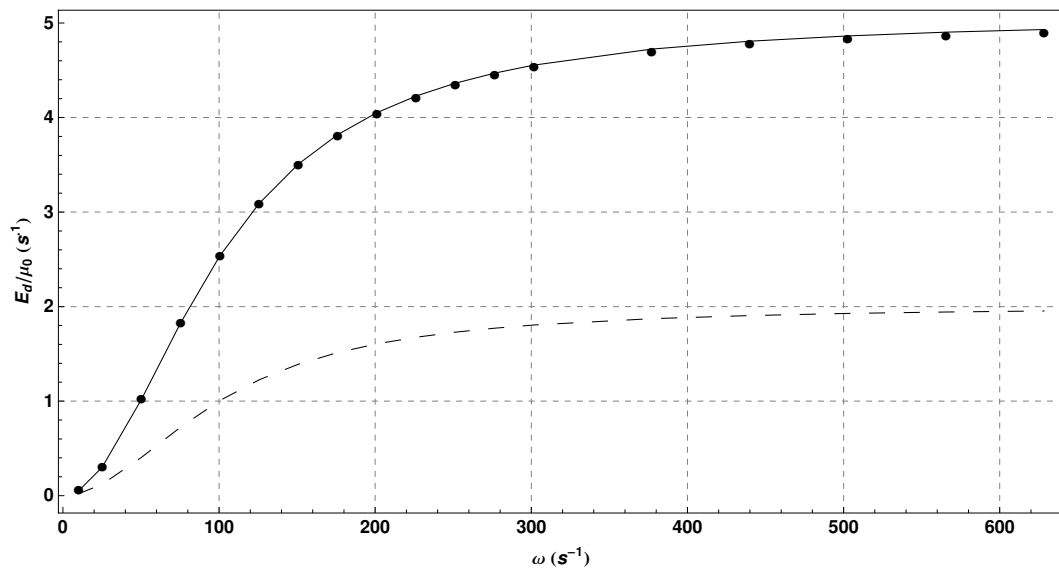


Figure 5.11 Dependence of dissipated energy density in dimensionless form E_d/μ_0 on frequency ω over a single period in the steady state for the ABAQUS model (solid curve), for the ABAQUS output (dotted curve) and for the QLV model (dashed curve) in the case of simple shear.

References

- ADOLFSSON, K. & ENELUND, M. (2003). Fractional Derivative Viscoelasticity at Large Deformations. *Nonlinear Dyn.*, **33**, 301–321.
- ADOLFSSON, K., ENELUND, M. & OLSSON, P. (2005). On the Fractional Order Model of Viscoelasticity. *Mech. Time-Depend. Mat.*, **9**, 15–34.
- ANTONAKAKIS, J.N., BHARGAVA, P., CHUANG, K.C. & ZEHNDER, A.T. (2006). Linear viscoelastic properties of HFPE-II-52 polyimide. *J. Appl. Polym. Sci.*, **100**, 3255–3263.
- ASTM (1998). D412-98a: Standard test methods for vulcanized rubber and thermoplastic rubbers and thermoplastic elastomers - Tension. *Annual Book of ASTM Standards*, cited By (since 1996) 1.
- ASTM (2003). *Basic Rubber Testing*. ASTM International, West Conshohocken.
- AUDET, C. & DENNIS, J.E.J. (2003). Analysis of Generalized Pattern Searches. *SIAM J. Optim.*, **13**, 889–903.
- BEATTY, M. (1996). *Nonlinear Effects in Fluids and Solids*, chap. 2, Introduction to Nonlinear Elasticity, 13–112. Plenum Press, New York.
- BEATTY, M. & HAYES, M. (1992a). Deformations of an elastic, internally constrained material. Part 1: Homogeneous deformations. *J. Elast.*, **29**, 1–84.
- BEATTY, M.F. & HAYES, M.A. (1992b). Deformations of an elastic, internally constrained material. Part 2: Nonhomogeneous deformations. *Q. J. Mech. Appl. Math.*, **45**, 663–709.
- BEATTY, M.F. & STALNAKER, D.O. (1986). The Poisson Function of Finite Elasticity. *J. Appl. Mech.*, **53**, 807–813.
- BEATTY, M.F. & ZHOU, Z. (1991). Universal motions for a class of viscoelastic materials of differential type. *Continuum Mech. Thermodyn.*, **3**, 169–191.
- BELYTSCHKO, T. (2000). *Nonlinear Finite Elements for Continua and Structures*. John Wiley, New York.
- BERGSTRÖM, J.S. & BOYCE, M.C. (1998). Constitutive modeling of the large strain time-dependent behavior of elastomers. *J. Mech. Phys. Solids*, **46**, 931–954.
- BERNSTEIN, B., KEARSLEY, E.A. & ZAPAS, L.J. (1963). A Study of Stress Relaxation with Finite Strain. *J. Rheol.*, **7**, 391–410.
- BIOT, M.A. (1954). Theory of Stress-Strain Relations in Anisotropic Viscoelasticity and Relaxation Phenomena. *J. Appl. Phys.*, **25**, 1385–1391.

- BISCHOFF, J., ARRUDA, E. & GROSH, K. (2001). A new constitutive model for the compressibility of elastomers at finite deformations. *Rubber Chem. Technol.*, **74**, 541–559.
- BLANCHARD, A.F. & PARKINSON, D. (1952). Breakage of Carbon-Rubber Networks by Applied Stress. *J. Ind. Eng. Chem.*, **44**, 799–812.
- BOIKO, A.V., KULIK, V.M., SEOUDI, B.M., CHUN, H. & LEE, I. (2010). Measurement method of complex viscoelastic material properties. *Int. J. Solids Struct.*, **47**, 374–382.
- BOLTZMANN, L. (1874). Zur Theorie der elastischen Nachwirkung. *Sitzungsber. Math. Naturwiss. Kl. Kaiserl. Akad. Wiss.*, **70**, 275–306.
- BONET, J. (2001). Large strain viscoelastic constitutive models. *Int. J. Solids Struct.*, **38**, 2953–2968.
- CALLISTER, W. (2007). *Materials Science and Engineering*. John Wiley & Sons Inc, City.
- CARROLL, M. & HAYES, M.A., eds. (1996). *Nonlinear Effects in Fluids and Solids*. Plenum Press, New York.
- CASTELLUCCI, M., HUGHES, A. & MARS, W. (2008). Comparison of Test Specimens for Characterizing the Dynamic Properties of Rubber. *Exp. Mech.*, **48**, 1–8.
- CHANLIAU-BLANOT, M.T., NARDIIM, M., DONNET, J.B., PAPIRER, E., ROCHE, G., LAURENSEN, P. & ROSSIGNOL, G. (1989). Temperature dependence of the mechanical properties of EPDM rubber-polyethylene blends filled with aluminium hydrate particles. *J. Mater. Sci.*, **24**, 641–648.
- CHAZEAU, L., BROWN, J.D., YANYO, L.C. & STERNSTEIN, S.S. (2000). Modulus recovery kinetics and other insights into the Payne effect for filled elastomers. *Polym. Compos.*, **21**, 202–222.
- CHEVALIER, L., CALLOCH, S., HILD, F. & MARCO, Y. (2001). Digital image correlation used to analyze the multiaxial behavior of rubber-like materials. *Eur. J. Mech. A. Solids*, **20**, 169–187.
- CHO, J.H. & YOUN, S.K. (2006). A viscoelastic constitutive model of rubber under small oscillatory load superimposed on large static deformation considering the Payne effect. *Arch. Appl. Mech.*, **75**, 275–288.
- CHRISTENSEN, R. (2003). *Theory of Viscoelasticity : Second Edition*. Dover Publications, New York.
- CIAMBELLA, J., DESTRADE, M. & OGDEN, R.W. (2009). On the ABAQUS FEA model of finite viscoelasticity. *Rubber Chem. Technol.*, **82**, 184–193.
- COLEMAN, B.D. (1964). Thermodynamics of materials with memory. *Arch. Rational Mech. Anal.*, **17**, 1–46.
- COLEMAN, B.D. & GURTIN, M.E. (1967). Thermodynamics with Internal State Variables. *J. Chem. Phys.*, **47**, 597–613.
- COLEMAN, B.D. & NOLL, W. (1961). Foundations of linear viscoelasticity. *Rev. Modern Phys.*, **33**, 239–249.
- COLEMAN, B.D. & NOLL, W. (1963). The thermodynamics of elastic materials with heat conduction and viscosity. *Arch. Rational Mech. Anal.*, **13**, 167–178.

- DAI, F., RAJAGOPAL, K. & WINEMAN, A. (1992). Non-uniform extension of a non-linear viscoelastic slab. *Int. J. Solids Struct.*, **29**, 911–930.
- DARVISH, K.K. & CRANDALL, J.R. (2001). Nonlinear viscoelastic effects in oscillatory shear deformation of brain tissue. *Med. Eng. Phys.*, **23**, 633–645.
- DEL PIERO, G. & DESERI, L. (1997). On the concepts of state and free energy in linear viscoelasticity. *Arch. Ration. Mech. Anal.*, **138**, 1–35.
- DELL'ISOLA, F., SCIARRA, G. & VIDOLI, S. (2009). Generalized Hooke's law for isotropic second gradient materials. *Proc. R. Soc. A*, **465**, 2177–2196.
- DESTRADE, M. & SACCOMANDI, G. (2004). Finite-amplitude inhomogeneous waves in Mooney-Rivlin viscoelastic solids. *Wave Motion*, **40**, 251–262.
- DESTRADE, M. & SACCOMANDI, G. (2006). Solitary and compactlike shear waves in the bulk of solids. *Phys. Rev. E*, **73**, 065604.
- DESTRADE, M., OGDEN, R. & SACCOMANDI, G. (2009). Small amplitude waves and stability for a pre-stressed viscoelastic solid. *Z. Angew. Math. Phys.*, **60**, 511–528.
- DORFMANN, A. & OGDEN, R.W. (2003). A pseudo-elastic model for loading, partial unloading and reloading of particle-reinforced rubber. *Int. J. Solids Struct.*, **40**, 2699–2714.
- DORFMANN, A. & OGDEN, R.W. (2004). A constitutive model for the Mullins effect with permanent set in particle-reinforced rubber. *Int. J. Solids Struct.*, **41**, 1855–1878.
- DORFMANN, A., FULLER, K.N.G. & OGDEN, R.W. (2002). Shear, compressive and dilatational response of rubberlike solids subject to cavitation damage. *Int. J. Solids Struct.*, **39**, 1845–1861.
- DRAPACA, C.S., SIVALOGANATHAN, S. & TENTI, G. (2007). Nonlinear constitutive laws in viscoelasticity. *Math. Mech. Solids*, **12**, 475–501.
- DROZDOV, A.D. (2007). Constitutive equations in finite elasticity of rubbers. *Int. J. Solids Struct.*, **44**, 272–297.
- DROZDOV, A.D. & DORFMANN, A. (2003). Finite viscoelasticity of filled rubber: experiments and numerical simulation. *Arch. Appl. Mech.*, **72**, 651–672.
- EIHLERS, W. & EPPERS, G. (1998). The simple tension problem at large volumetric strains computed from finite hyperelastic material laws. *Acta Mech.*, **137**, 12–27.
- ERICKSEN, J. (1954). Deformations possible in every isotropic, incompressible, perfectly elastic body. *Z. Angew. Math. Phys.*, **5**, 466–489.
- FABRIZIO, M. & MORRO, A. (1992). *Mathematical Problems in Linear Viscoelasticity*. Society for Industrial and Applied Mathematics, Philadelphia.
- FABRIZIO, M., GIORGI, C. & MORRO, A. (1995). Internal Dissipation, Relaxation Property, And Free-Energy In Materials With Fading Memory. *J. Elasticity*, **40**, 107–122.
- FANCELLO, E., PONTHOT, J. & STAINIER, L. (2008). A variational framework for nonlinear viscoelastic models in finite deformation regime. *J. Comput. Appl. Math.*, **215**, 400–408.
- FERRY, J.D. (1980). *Viscoelasticity Properties of Polymer*. Wiley, 3rd edn.

- FICHERA, G. (1979). Avere una memoria tenace crea gravi problemi. *Arch. Rational Mech. Anal.*, **70**, 101–112.
- FLORY, P. (1961). Thermodynamic relations for high elastic materials. *Trans. Faraday Soc.*, **57**, 829–838.
- FOSDICK, R. & YU, J.H. (1998). Thermodynamics, stability and non-linear oscillations of viscoelastic solids .2. History type solids. *Internat. J. Non-Linear Mech.*, **33**, 165–188.
- FOSDICK, R.L. & YU, J.H. (1996). Thermodynamics, stability and non-linear oscillations of viscoelastic solids .1. Differential type solids of second grade. *Internat. J. Non-Linear Mech.*, **31**, 495–516.
- FUNG, Y.C. (1972). Stress-strain-history relations of soft tissues in simple elongation. In N.P. Y.C. Fung & M. Anliker, eds., *Biomechanics: Its Foundations and Objectives*, 181–208, Prentice Hall, Englewood Cliffs, NJ.
- GENT, A. (1996). A new constitutive relation for rubber. *Rubber Chem. Technol.*, **69**, 59–61.
- GIL-NEGRETE, N., VINOLAS, J. & KARI, L. (2009). A Nonlinear Rubber Material Model Combining Fractional Order Viscoelasticity and Amplitude Dependent Effects. *J. Appl. Mech.*, **76**, 011009.
- GOLDBERG, A., LESUER, D.R. & PATT, J. (1989). Fracture morphologies of carbon-black-loaded SBR subjected to low-cycle, high-stress fatigue. *Rubber Chem. Technol.*, **62**, 272–287.
- GOLDEN, J.M. (2001). Consequences of non-uniqueness in the free energy of materials with memory. *Internat. J. Eng. Sci.*, **39**, 53–70.
- GOLDEN, J.M. (2005). A proposal concerning the physical rate of dissipation in materials with memory. *Q. App. Math.*, **63**, 117–155.
- GOLUB, G. (1996). *Matrix Computations*. Johns Hopkins University Press, Baltimore.
- GOTTENBERG, W. & CHRISTENSEN, R. (1964). An experiment for determination of the mechanical property in shear for a linear, isotropic viscoelastic solid. *Internat. J. Eng. Sci.*, **2**, 45–50, IN1–IN2, 51–57.
- GOTTENBERG, W. & CHRISTENSEN, R. (1972). Prediction of the transient response of a linear viscoelastic solid. *J. Appl. Mech.*, **6**, 448–450.
- GOVINDJEE, S. & SIMO, J.C. (1992). Mullins effect and the strain amplitude dependence of the storage modulus. *Int. J. Solids Struct.*, **29**, 1737–1751.
- GREEN, A.E. & RIVLIN, R.S. (1957). The mechanics of non-linear materials with memory. *Arch. Ration. Mech. Anal.*, **1**, 1–21.
- GREEN, M. & TOBOLSKY, A. (1946). A new approach to the theory of relaxing polymeric media. *J. Chem. Phys.*, **14**, 80–92.
- GURTIN, M. & STERNBERG, E. (1962). On the linear theory of viscoelasticity. *Arch. Ration. Mech. Anal.*, **11**, 291–356.
- GURTIN, M.E. & HRUSA, W.J. (1988). On energies for nonlinear viscoelastic materials of single-integral type. *Q. App. Math.*, **46**, 381–392.

- HALLQUIST, J. (1998). *LS-DYNA theoretical manual*. Livermore Software Technology Corporation.
- HANYGA, A. (2005). Viscous dissipation and completely monotonic relaxation moduli. *Rheol. Acta*, **44**, 614–621.
- HANYGA, A. (2007). Fractional-order relaxation laws in non-linear viscoelasticity. *Continuum Mech. Thermodyn.*, **19**, 25–36.
- HANYGA, A. & SEREDYNSKA, M. (2007). Multiple-integral viscoelastic constitutive equations. *Int. J. Non Linear Mech.*, **42**, 722–732.
- HARTMANN, S. (2001a). Numerical studies on the identification of the material parameters of Rivlin’s hyperelasticity using tension-torsion tests. *Acta Mech.*, **148**, 129–155.
- HARTMANN, S. (2001b). Parameter estimation of hyperelasticity relations of generalized polynomial-type with constraint conditions. *Int. J. Solids Struct.*, **38**, 7999–8018.
- HASANPOUR, K., ZIAEI-RAD, S. & MAHZOON, M. (2009). A large deformation framework for compressible viscoelastic materials: Constitutive equations and finite element implementation. *Int. J. Plast.*, **25**, 1154–1176.
- HASSANI, S., ALAOUI SOULIMANI, A. & EHRLACHER, A. (1998). A nonlinear viscoelastic model: the pseudo-linear model. *Eur. J. Mech. A. Solids*, **17**, 567–598.
- HAUPT, P. (1985). On the concept of an intermediate configuration and its application to a representation of viscoelastic-plastic material behavior. *Int. J. Plast.*, **1**, 303–316.
- HAUPT, P. (2002). *Continuum Mechanics and Theory of Materials*. Springer, Berlin.
- HAUPT, P. & LION, A. (2002). On finite linear viscoelasticity of incompressible isotropic materials. *Acta Mech.*, **159**, 87–124.
- HAUPT, P. & SEDLAN, K. (2001). Viscoplasticity of elastomeric materials: experimental facts and constitutive modelling. *Arch. Appl. Mech.*, **71**, 89–109.
- HAUPT, P., LION, A. & BACKHAUS, E. (2000). On the dynamic behaviour of polymers under finite strains: constitutive modelling and identification of parameters. *Int. J. Solids Struct.*, **37**, 3633–3646.
- HAYES, M.A. & SACCOMANDI, G. (2000). Finite amplitude transverse waves in special incompressible viscoelastic solids. *J. Elast.*, **59**, 213–225.
- HIBBIT, D., KARLSSON, B. & SORENSEN, P. (2007). *ABAQUS/Theory Manual*. Hibbit, Karlsson & Sorensen, Inc., Rhode Island, 6th edn.
- HOLZAPFEL, G. (2000). *Nonlinear Solid Mechanics: A Continuum Approach for Engineering*. Wiley, New York.
- HOLZAPFEL, G.A. (1996). On large strain viscoelasticity: Continuum formulation and finite element applications to elastomeric structures. *Internat. J. Numer. Methods Engrg.*, **39**, 3903–3926.
- HOLZAPFEL, G.A. & GASSER, T.C. (2001). A viscoelastic model for fiber-reinforced composites at finite strains: Continuum basis, computational aspects and applications. *Comput. Meth. Appl. Mech. Eng.*, **190**, 4379–4403.

- HOO FATT, M. & AL-QURAIISHI, A. (2008). High strain rate constitutive modeling for natural rubber. In *Proceedings of the 5th European Conference on Constitutive Models for Rubber, ECCMR 2007*, 53–60, University of Akron, Akron, OH, United States.
- HOO FATT, M.S. & OUYANG, X. (2007). Integral-based constitutive equation for rubber at high strain rates. *Int. J. Solids Struct.*, **44**, 6491–6506.
- HORGAN, C.O., OGDEN, R.W. & SACCOMANDI, G. (2004). A theory of stress softening of elastomers based on finite chain extensibility. *Proc. R. Soc. A*, **460**, 1737–1754.
- HUBER, G., VILGIS, T.A. & HEINRICH, G. (1996). Universal properties in the dynamical deformation of filled rubbers. *J. Phys. Cond. Matter*, **8**, L409–L412.
- HUBER, N. & TSAKMAKIS, C. (2000). Finite deformation viscoelasticity laws. *Mech. Mater.*, **32**, 1–18.
- HÖFER, P. & LION, A. (2009). Modelling of frequency- and amplitude-dependent material properties of filler-reinforced rubber. *J. Mech. Phys. Solids*, **57**, 500–520.
- INAUDI, J.A. & KELLY, J.M. (1995). Linear hysteretic damping and the Hilbert transform. *J. Eng. Mech.*, **121**, 626–632.
- INAUDI, J.A. & MAKRIS, N. (1996). Time-domain Analysis Of Linear Hysteretic Damping. *Earthquake Eng. Struct. Dyn.*, **25**, 529–545.
- JOHNSON, A.R., QUIGLEY, C.J. & MEAD, J.L. (1994). Large-strain Viscoelastic Constitutive Models For Rubber .1. Formulations. *Rubber Chem. Technol.*, **67**, 904–917.
- JOHNSON, A.R., QUIGLEY, C.J. & FREESE, C.E. (1995). A Viscohyperelastic Finite-element Model For Rubber. *Comput. Meth. Appl. Mech. Eng.*, **127**, 163–180.
- JOHNSON, G., LIVESAY, G., WOO, S.Y. & RAJAGOPAL, K. (1996a). A single integral finite strain viscoelastic model of ligaments and tendons. *J. Biomech. Eng.*, **118**, 221–226.
- JOHNSON, G.A., LIVESAY, G.A., WOO, S.L.Y. & RAJAGOPAL, K.R. (1996b). A single integral finite strain viscoelastic model of ligaments and tendons. *J. Biomech. Eng.*, **118**, 221–226.
- KAR, K. & BHOWMICK, A. (1997). Hysteresis loss in filled rubber vulcanizates and its relationship with heat generation. *J. Appl. Polym. Sci.*, **64**, 1541–1555.
- KHAN, A.S., LOPEZ-PAMIES, O. & KAZMI, R. (2006). Thermo-mechanical large deformation response and constitutive modeling of viscoelastic polymers over a wide range of strain rates and temperatures. *Int. J. Plast.*, **22**, 581–601.
- KNAUSS, W., EMRI, I. & LU, H. (2008). *Handbook of Experimental Solid Mechanics*, chap. 3, Mechanics of Polymers: Viscoelasticity, 49–93. Springer.
- KNAUSS, W.G. & ZHAO, J. (2007). Improved relaxation time coverage in ramp-strain histories. *Mech. Time-Depend. Mat.*, **11**, 199–216.
- KOLMOGOROV, A. (1999). *Elements of the Theory of Functions and Functional Analysis*. Dover Pub, New York.
- KRAUS, G. (1984). Mechanical Losses In Carbon-black-filled Rubbers. In *Applied Polymer Symposia*, 75–92, Phillips Petroleum Co, Bartlesville,, OK, USA, Phillips Petroleum Co, Bartlesville, OK, USA.

- LAKES, R.S. (2004). Viscoelastic measurement techniques. *Rev. Sci. Instrum.*, **75**, 797–810.
- LANDAU, L. & LIFSHITZ, E. (1986). *Theory of Elasticity : Volume 7*. Butterworth-Heinemann, Oxford.
- LARABA-ABBES, F., IENNY, P. & PIQUES, R. (2003). A new 'Tailor-made' methodology for the mechanical behaviour analysis of rubber-like materials: II. Application to the hyperelastic behaviour characterization of a carbon-black filled natural rubber vulcanizate. *Polymer*, **44**, 821–840.
- LEE, J.H. & KIM, K.J. (2001). Characterization of complex modulus of viscoelastic materials subject to static compression. *Mech. Time-Depend. Mat.*, **5**, 255–271.
- LINZ, P. (1985). *Analytical and numerical methods for Volterra equations*, vol. XIII of *Studies in Applied Mathematics*. SIAM.
- LION, A. (1997). A physically based method to represent the thermo-mechanical behaviour of elastomers. *Acta Mech.*, **123**, 1–25.
- LION, A. (1998). Thixotropic behaviour of rubber under dynamic loading histories: Experiments and theory. *J. Mech. Phys. Solids*, **46**, 895–930.
- LION, A. & KARDELKY, C. (2004). The Payne effect in finite viscoelasticity: constitutive modelling based on fractional derivatives and intrinsic time scales. *Int. J. Plast.*, **20**, 1313–1345.
- LIU, I.S. (2004). On Euclidean objectivity and the principle of material frame-indifference. *Continuum Mech. Thermodyn.*, **16**, 177.
- LOCKETT, F. (1972). *Nonlinear Viscoelastic Solids*. Academic Press, Boston.
- LUBLINER, J. (1985). A model of rubber viscoelasticity. *Mech. Res. Commun.*, **12**, 93–99.
- LUO, W., HU, X., WANG, C. & LI, Q. (2010). Frequency- and strain-amplitude-dependent dynamical mechanical properties and hysteresis loss of CB-filled vulcanized natural rubber. *Int. J. Mech. Sc.*, **52**, 168–174.
- MACKNIGHT, W. (1966). Volume changes accompanying the extension of rubber-like materials. *J. Appl. Phys.*, **37**, 4587–.
- MALKIN, A. (1995). *Rheology Fundamentals*. ChemTec Publishing, Toronto-Scarborough.
- MEGGYES, A. (2001). Multiple decomposition in finite deformation theory. *Acta Mech.*, **146**, 169–182.
- METZLER, R. & NONNENMACHER, T. (2003). Fractional relaxation processes and fractional rheological models for the description of a class of viscoelastic materials. *Int. J. Plast.*, **19**, 941–959.
- MOTT, P. & ROLAND, C. (2010). Response to "Comment on paper "The bulk modulus and Poisson's ratio of "incompressible" materials". *J. Sound Vib.*, **329**, 368–369.
- MOTT, P., DORGAN, J. & ROLAND, C. (2008). The bulk modulus and Poisson's ratio of "incompressible" materials. *J. Sound Vib.*, **312**, 572–575.
- MOTT, P.H. & ROLAND, C.M. (1995). Uniaxial deformation of rubber cylinders. *Rubber Chem. Technol.*, **68**, 739–745.

- MOTT, P.H. & ROLAND, C.M. (1996). Elasticity of natural rubber networks. *Macromolecules*, **29**, 6941–6945.
- MULLINS, L. (1947). Effect of stretching on the properties of rubber. *J. Rubber Res.*, **16**, 275–289.
- MULLINS, L. & TOBIN, N. (1957). Theoretical model for the elastic behavior of filler-reinforced vulcanized rubbers. *Rubber Chem. Technol.*, **30**, 551–571.
- MURDOCH, A.I. (2005). On criticism of the nature of objectivity in classical continuum physics. *Continuum Mech. Thermodyn.*, **17**, 135–148.
- NOLL, W. (1958). A mathematical theory of the mechanical behavior of continuous media. *Arch. Ration. Mech. Anal.*, **2**, 197–226.
- OGDEN, R., SACCOMANDI & G., I., SGURA (2004). Fitting hyperelastic models to experimental data. *Comput. Mech.*, **34**, 484.
- OGDEN, R.W. (1976). Volume changes associated with the deformation of rubber-like solids. *J. Mech. Phys. Solids*, **24**, 323–338.
- OGDEN, R.W. (1997). *Non-Linear Elastic Deformations*. Dover Publications, New York.
- OGDEN, R.W. & ROXBURGH, D.G. (1999). A pseudo-elastic model for the Mullins effect in filled rubber. *Proc. R. Soc. A*, **455**, 2861–2877.
- OSANAIYE, G.J. (1996). Effects of temperature and strain amplitude on dynamic mechanical properties of EPDM gum and its carbon black compounds. *J. Appl. Polym. Sci.*, **59**, 567–575.
- OUYANG, X. (2006). *Constitutive equations of rubber under large tensile strain and high strain rates*. Master's thesis, University of Akron.
- PARK, S.W. & SCHAPERY, R.A. (1999). Methods of interconversion between linear viscoelastic material functions. Part I - a numerical method based on Prony series. *Int. J. Solids Struct.*, **36**, 1653–1675.
- PAYNE, A.R. (1962). The dynamic properties of carbon black loaded natural rubber vulcanizates. Part II. *J. Appl. Polym. Sci.*, **6**, 368–372.
- PENA, E., CALVO, B., MARTINEZ, M. & DOBLAR, M. (2007). An anisotropic visco-hyperelastic model for ligaments at finite strains. Formulation and computational aspects. *Int. J. Solids Struct.*, **44**, 760–778.
- PENN, R.W. (1970). Volume Changes Accompanying the Extension of Rubber. *J. Rheol.*, **14**, 509–517.
- PIPKIN, A. (1986). *Lectures on Viscoelasticity Theory*. Springer-Verlag, Berlin.
- PIPKIN, A.C. & ROGERS, T.G. (1968). A non-linear integral representation for viscoelastic behaviour. *J. Mech. Phys. Solids*, **16**, 59–72.
- PRESS, W. (2007). *Numerical Recipes*. Cambridge University Press, Cambridge.
- PRZYBYLO, P. & ARRUDA, E. (1998). Experimental investigations and numerical modeling of incompressible elastomers during non-homogeneous deformations. *Rubber Chem. Technol.*, **71**, 730–749.

- PUCCI, E. & SACCOMANDI, G. (1997). On universal relations in continuum mechanics. *Continuum Mech. Thermodyn.*, **9**, 61–72.
- QI, H.J. & BOYCE, M.C. (2004). Constitutive model for stretch-induced softening of the stress-stretch behavior of elastomeric materials. *J. Mech. Phys. Solids*, **52**, 2187–2205.
- QUIGLEY, C.J., MEAD, J. & JOHNSON, A.R. (1995). Large-strain Viscoelastic Constitutive Models For Rubber .2. Determination of Material Constants. *Rubber Chem. Technol.*, **68**, 230–247.
- QUINTANILLA, R. & SACCOMANDI, G. (2007). The Importance of the Compatibility of Non-linear Constitutive Theories With Their Linear Counterparts. *J. Appl. Mech.*, **74**, 455–460.
- RAJAGOPAL, K. & WINEMAN, A. (2008). A quasi-correspondence principle for Quasi-Linear viscoelastic solids. *Mech. Time-Depend. Mat.*, **12**, 1–14.
- RAMORINO, G., VETTURI, D., CAMBIAGHI, D., PEGORETTI, A. & RICCO, T. (2003). Developments in dynamic testing of rubber compounds: assessment of non-linear effects. *Polym. Test.*, **22**, 681–687.
- REICHERT, W.F., HOPFENMUELLER, M.K. & GORITZ, D. (1987). Volume change and gas transport at uniaxial deformation of filled natural rubber. *J. Mater. Sci.*, **22**, 3470–3476.
- RITTEL, D., LEE, S. & RAVICHANDRAN, G. (2002). A shear-compression specimen for large strain testing. *Exp. Mech.*, **42**, 58–64.
- RIVLIN, R. (2002). Frame Indifference and Relative Frame Indifference. *Math. Mech. Solids*, **10**, 145–154.
- RIVLIN, R. & ERICKSEN, J. (1955). Stress-deformation relations for isotropic materials. *J. Rational Mech. Anal.*, **4**, 323–425.
- RIVLIN, R. & SAUNDERS, D. (1952). The free energy of deformation for vulcanized rubber. *Trans. Faraday Soc.*, **48**, 200–206.
- RIVLIN, R.S. (2005). Some Thoughts on Frame Indifference. *Math. Mech. Solids*, **11**, 113.
- ROGERS, L. (1983). Operators and Fractional Derivatives for Viscoelastic Constitutive Equations. *J. Rheol.*, **27**, 351–372.
- ROLAND, C.M., MOTT, P.H. & HEINRICH, G. (1999). Elasticity of polydiene networks in tension and compression. *Comput. Theor. Polym. Sci.*, **9**, 197–202.
- RUDIN, W. (1976). *Principles of Mathematical Analysis*. McGraw-Hill, New York.
- SACCOMANDI, G. (2001). *Nonlinear Elasticity. Theory and Applications*, chap. 3, Universal Results in Finite Elasticity, 97–134. Cambridge University Press, Cambridge.
- SALVATORI, M.C. & SANCHINI, G. (2005). Finite amplitude transverse waves in materials with memory. *Int. J. Eng. Sci.*, **43**, 290–303.
- SANSOUR, C. (2008). On the physical assumptions underlying the volumetric-isochoric split and the case of anisotropy. *Eur. J. Mech. A. Solids*, **27**, 28.
- SASSO, M., PALMIERI, G., CHIAPPINI, G. & AMODIO, D. (2008). Characterization of hyperelastic rubber-like materials by biaxial and uniaxial stretching tests based on optical methods. *Polym. Test.*, **27**, 995–1004.

- SCHAPERLY, R. (1997). Nonlinear Viscoelastic and Viscoplastic Constitutive Equations Based on Thermodynamics. *Mech. Time-Depend. Mat.*, **1**, 209–240.
- SHAN, G.F., YANG, W., YANG, M.B., XIE, B.H., FENG, J.M. & FU, Q. (2007). Effect of temperature and strain rate on the tensile deformation of polyamide 6. *Polymer*, **48**, 2958–2968.
- SHIM, V.P.W., YANG, L.M., LIM, C.T. & LAW, P.H. (2004). A visco-hyperelastic constitutive model to characterize both tensile and compressive behavior of rubber. *J. Appl. Polym. Sci.*, **92**, 523–531.
- SIDOROFF, F. (1974). Nonlinear Viscoelastic Model with an Intermediate Configuration. *Journal Mécaniques*, **13**, 679–713.
- SIMO, J., TAYLOR, R. & PISTER, K. (1985). Variational and projection methods for the volume constraint in finite deformation elasto-plasticity. *Comput. Meth. Appl. Mech. Eng.*, **51**, 177–208.
- SIMO, J.C. (1987). On a fully three-dimensional finite-strain viscoelastic damage model: Formulation and computational aspects. *Comput. Meth. Appl. Mech. Eng.*, **60**, 153–173.
- SINGH, A., LAKES, R. & GUNASEKARAN, S. (2006). Viscoelastic characterization of selected foods over an extended frequency range. *Rheol. Acta*, **46**, 131–142.
- TRELOAR, L. (2005). *The Physics of Rubber Elasticity*. Clarendon Press, Oxford.
- TRUESDELL, C.A. & NOLL, W. (1965). *The Non-Linear Field Theories of Mechanics*. Springer, 3rd edn.
- TSCHOEGL, N. (1989). *The Phenomenological Theory of Linear Viscoelastic Behavior*. Springer-Verlag, Berlin.
- TVEDT, B. (2008). Quasilinear equations for viscoelasticity of strain-rate type. *Arch. Ration. Mech. Anal.*, **189**, 237–281.
- VAKADA, K.C. (2005). *Use of advanced material modeling techniques in large-scale simulations for highly deformable structures*. Master's thesis, University of Akron.
- VIDOLI, S. & SCIARRA, G. (2002). A model for crystal plasticity based on micro-slip descriptors. *Continuum Mech. Thermodyn.*, **14**, 425–435.
- VOINOVICH, P. (2010). Comment on paper "the bulk modulus and Poisson's ratio of "incompressible" materials" by P.H. Mott, J.R. Dorgan, C.M. Roland. *J. Sound Vib.*, **329**, 366–367.
- VOLTERRA, V. (1912). Sur les equations integro-differentielles et leurs applications. *Acta Math.*, **35**, 295–356.
- WANG, M.J. (1999). The role of filler networking in dynamic properties of filled rubber. *Rubber Chem. Technol.*, **72**, 430–448.
- WHITE, S.W., KIM, S.K., BAJAJ, A.K., DAVIES, P., SHOWERS, D.K. & LIEDTKE, P.E. (2000). Experimental techniques and identification of nonlinear and viscoelastic properties of flexible polyurethane foam. *Nonlinear Dyn.*, **22**, 281–313.
- WILLIAMS, M., LANDEL, R. & FERRY, J. (1955). The temperature dependence of relaxation mechanisms in amorphous polymers and other glass-forming liquids. *J. Am. Chem. Soc.*, **77**, 3701–3707.

- WINEMAN, A. (2009). Nonlinear Viscoelastic Solids—A Review. *Math. Mech. Solids*, **14**, 300–366.
- YANG, L.M. & SHIM, V.P.W. (2004). A visco-hyperelastic constitutive description of elastomeric foam. *Int. J. Impact Eng.*, **30**, 1099–1110.
- YANG, L.M., SHIM, V.P.W. & LIM, C.T. (2000). A visco-hyperelastic approach to modelling the constitutive behaviour of rubber. *Int. J. Impact Eng.*, **24**, 545–560.
- YEOH, O. & FLEMING, P. (1997). A new attempt to reconcile the statistical and phenomenological theories of rubber elasticity. *J. Polym. Sci. Pt. B-Polym. Phys.*, **35**, 1919–1931.
- YOSHIDA, J., ABE, M. & FUJINO, Y. (2004). Constitutive Model of High-Damping Rubber Materials. *J. Eng. Mech.*, **130**, 129–141.
- ZHAO, J., KNAUSS, W. & RAVICHANDRAN, G. (2009). A New Shear-Compression-Specimen for Determining Quasistatic and Dynamic Polymer Properties. *Exp. Mech.*, **49**, 427–436.

Acknowledgements

A number of individuals and organizations have made invaluable contributions to this thesis. I would firstly like to express my sincere gratitude to Prof Achille Paolone, whose guidance and encouragement were a constant source of inspiration. He gave me confidence and a high degree of freedom to carry out my research. I also would like to thank Dr Stefano Vidoli since many of the ideas presented in this work are the result of the pleasant and stimulating discussions I had with him. His outstanding insights have greatly inspired me.

I am also very grateful to Dr Fernando Baldoni, Dr Beatrice Mellara and the entire CAE group of the Bridgestone Technical Center Europe SpA for their kind cooperation and for supplying test specimens and laboratory support.

I wish to express my gratitude to my parents for their initial influence on and current support of my personal and academic advances. I am deeply thankful to Ida for her encouraging help, understanding and patience. I hope to be able to return to her all that she missed during the last months.

Finally, I gratefully acknowledge the Ceradini family contribution toward my PhD studies. I hope to have deserved their support.

Jacopo Ciambella

Roma, March 2010